NASA TECHNICAL MEMORANDUM

NASA TM X-71727

NASA TM X-71727

(NASA-TM-X-71727) CENTAUR STANDARD SHROUD (CSS) STATIC LIMIT LOAD STRUCTURAL TESTS (NASA) 232 p HC $7.50 CSCL 22B

N75-23669

Unclas
G3/18 21842

CENTAUR STANDARD SHROUD (CSS) STATIC LIMIT LOAD STRUCTURAL TESTS

by C. Eastwood
Lewis Research Center
Cleveland, Ohio 44135
April 1975

TABLE OF CONTENTS

ABBREVIATIONS

Cartridges	-	Electro Explosive Devices
CSS	-	Centaur Standard Shroud
FBR	-	Forward Bearing Reactor
FSR	-	Forward Seal Release
GDC	-	General Dynamics Convair Division
ISA	-	Interstage Adapter
LH_2	-	Liquid Hydrogen
LN_2	-	Liquid Nitrogen
LO_2	-	Liquid Oxygen
LMSC	-	Lockheed Missiles and Space Company, Inc.
MMC	-	Martin Marietta Corporation
^oF	-	Degrees Fahrenheit
#/in.	-	Pounds Per Inch

ORIGINAL PAGE IS
OF POOR QUALITY

I. PROGRAM SUMMARY

By C. W. Eastwood, G. S. Sarvay,
J. G. McArdle, and M. C. Seaver

SUMMARY

A jettisonable metallic shroud is utilized on the Titan/Centaur launch vehicle as a fairing to protect the payload and the second stage Centaur from aerodynamic and thermal environments during launch and ascent. A series of tests were conducted to verify the structural capabilities of the shroud and to evaluate the interaction of the shroud with the Centaur stage. A flight configured shroud and the structural and functional assemblies of the associated Centaur stage were subjected to a series of tests consisting of combinations of applied axial and shear loads to flight limit (design) values. Several of the tests included various thermal, pressure, and load conditions to verify localized strength capabilities of the shroud, to evaluate performance of subsystems, and to determine the aging affect on insulation system properties.

The test series verified the strength capabilities of the shroud and of all associated flight assemblies. Structural deflections of the complete specimen assembly were within the values predicted by design calculations. The tests also demonstrated that the shroud deflections would exceed the allowable limits unless load sharing members were connected between the shroud and the Centaur stage.

It was also demonstrated that local areas of the shroud are adequate for supporting the interface components, the Centaur subsystems are suitable for their required functions under simulated flight conditions, and that the shroud insulation effectiveness does not degrade significantly with age.

This test series of the shroud qualification program verified that the Titan/Centaur shroud, the Centaur interface components, and the subsystems are structurally qualified for flight.

INTRODUCTION

All spacecraft require some form of protection from weather and a thermally controlled environment during prelaunch operations. In addition, protection is required from aerodynamic and thermal environments during launch and ascent. These requirements are usually satisfied by a shroud or fairing attached to the forward end of the launch vehicle and enclosing the spacecraft. The shroud is jettisoned after the most adverse conditions are passed in the launch and ascent phase of flight.

In addition to spacecraft protection, launch vehicles utilizing cryogenic propellants require thermal insulation during prelaunch operations to prevent excessive propellant boiloff. Insulation is also required during ascent for protection from aerodynamic heating.

The Centaur upper stage vehicle, mated with the Titan IIID booster, was chosen to be the launch vehicle for the Viking spacecraft which is to orbit and soft land on the planet Mars in 1976. This Centaur vehicle is called the Centaur D-1T (reference 1).

The Centaur was the United States' first upper stage vehicle to use liquid hydrogen and liquid oxygen as propellants. As the upper stage for the Atlas Booster, this combination has been the launch vehicle for Surveyor, Mariner, Pioneer, OAO, and a series of communication satellites.

The D-1A Centaur upper stage vehicle, using the Atlas as the booster stage, utilizes several shroud designs for spacecraft protection dictated by spacecraft size and mission requirements. Thermal protection for the Centaur vehicle during prelaunch and ascent is provided by jettisonable insulation panels.

The Viking spacecraft requires a large diameter aeroshield. This meant an increased diameter shroud would be required for spacecraft enclosure. The larger diameter shroud would also be heavier than existing shrouds and aerodynamic loading during ascent would tax the strength of the Centaur. One possibility to enhance structural capability would be to make the Centaur tank heavier and redesign the present insulation panels to be capable of carrying structural loading. This, however, meant increased complexities and many modifications to existing designs.

Instead, a large shroud that would cover both the spacecraft and Centaur, and act as a structural member as well as incorporating insulation for Centaur's cryogenic propellant tanks, was conceived and studied. This was the design concept chosen and Lockheed Missiles and Space Company, Inc. (LMSC) was awarded the contract to design and build the shroud. This shroud has been designated the Centaur Standard Shroud (CSS).

A test program consisting of the following three major series of tests was conducted at the Lewis Research Center's Plum Brook Station to qualify the CSS for flight:

1. Cryogenic unlatch tests to qualify the CSS insulation, gas purges, and jettison systems under cryogenic conditions (references 2 and 3).

2. Structural tests to qualify the structural capabilities of the CSS, the interstage adapter (ISA), and the forward bearing reactor (FBR) struts.

3. Heated jettison tests at altitude conditions, to qualify the CSS jettison system operation after experiencing simulated aerodynamic heating during ascent.

This report presents the results of the structural test program that was completed in July 1973. The tests were performed with the active participation of General Dynamics Convair Division (GDC), the Centaur contractor; Lockheed Missiles and Space Company, Inc. (LMSC), the CSS contractor; and Martin Marietta Corporation (MMC), the Titan contractor. A test report has been prepared by each of the three contractors (references 4, 5, and 6) pertaining to the performance of the test specimen hardware furnished by them. Axial and shear loads, to limit load values, were applied to the CSS to simulate various critical flight inertial and aerodynamic loads. The values are shown in figure I-1. Axial loads are defined as loads acting aft to produce compression on the test specimen structures. Shear loads are defined as loads acting laterally to produce both shear and bending moments on the test specimen structures such that maximum compression is produced at a specified azimuth and maximum tension occurs diametrically opposite. In addition, for some tests, loads were also applied to the hydrogen vent fin and to the Centaur truss adapter, the forward seal was pressurized and released, and the Centaur was tanked with liquid nitrogen (LN_2) to obtain heat transfer data and to verify the performance of the FBR struts and forward seal releaser at cold temperature.

The purpose of this report is to provide a composite description of the CSS limit load structural tests. The report is separated into sections dealing with specific major components of flight hardware to assist the reader concerned with the performance of any one particular item. A description of the facility and the supporting test control and instrumentation systems is presented in Appendix A.

TEST HARDWARE CONFIGURATION

The test hardware for the CSS limit load structural tests consisted of the following major items and systems:

1. A CSS with all pertinent bolt-on hardware and the tank section insulation installed.

2. A Centaur flight-weight tank with stub adapter, equipment module, truss adapter, FBR system, forward seal and releaser system, aft seal, hydrogen vent disconnect system, and other hardware which interfaces with the CSS to configure the Centaur to a D-1T vehicle.

3. Centaur interstage adapter.

4. Titan skirt.

5. Test fixtures, structures, and load application systems.

6. Data acquisition, processing, recording, and display systems.

7. Test control, alarm, and abort systems.

The overall test configuration and assembly of this hardware in the Plum Brook B-3 facility is shown in figure I-2. Vehicle stations shown in the figure and referred to throughout this report are Centaur/CSS station designations. The interface of the Titan skirt and the ISA is Station 2127.43 and the forward terminus of the Centaur/CSS test assembly is Station 2882.25. The load application base and the lower distribution cylinder fixture supported the test specimen and reacted the test loads. At the juncture (Station 2608) of the conic portions of the biconic nose section of the CSS, the forward load distribution cylinder fixture was mounted on a test peculiar flanged ring. A forward load application fixture was mounted on the forward load distribution cylinder fixture. The axial load was applied to the shroud by fixture tare weight and by four hydraulic actuators acting through cables which were connected to load application fixtures at the top and bottom of the hardware stackup. Shear load was applied to the shroud by a hydraulic actuator connected through a whiffletree to a strap on the 15° CSS cone. Shear load was applied to the Centaur by a hydraulic actuator connected to a cylindrical fixture mounted on the truss adapter. The weight of this fixture could either be counterbalanced or used to apply axial load to the Centaur.

A brief description of the CSS, Centaur tank, interstage adapter, and Titan skirt follows. Detailed descriptions of each of the supporting systems can be found in the respective sections of this report.

Significant differences between the test hardware configuration and the flight hardware for the first Titan/Centaur flight (Proof Flight) are listed in Appendix B.

Centaur Standard Shroud (CSS)

The Centaur Standard Shroud (CSS) encloses both the Centaur and the spacecraft, and provides environmental protection for both while on the ground and in flight. The CSS general configuration is shown in figure I-3. The cylindrical portion of the CSS is 14 feet in diameter. Total CSS length is 58 feet. The payload section (forward of Station 2514.0) is of biconic configuration approximately 31 feet long. The nose dome is made from stainless steel, but was not installed for the structural tests. The two conical sections forward of Station 2680.66 are of magnesium semimonocoque construction reinforced by internal rings. The cylindrical section between the Stations 2514.00 and 2680.66 is of aluminum semi-monocoque construction with corrugated outer skin and smooth inner skin weld-bonded together and riveted to internal rings. Attached to the internal rings in the conical and cylindrical section are fiberglas insulation blankets. (These fiberglas blankets were not installed for these tests.)

The equipment section, from Station 2459.14 to Station 2514.00, allows access to hardware on the Centaur equipment module through doors in the CSS structure. This section is of the same construction as the cylindrical portion of the payload section.

The forward bearing reaction system between the CSS and the Centaur at Station 2459.14 reduces CSS/Centaur relative deflections through load sharing during launch and ascent. This reaction path is released in flight after maximum aerodynamic loading by a pyrotechnic system that severs the struts which retract to a stowed position.

The tank section of the CSS which encloses the Centaur LH_2 tank is also of aluminum semimonocoque, corrugated construction with reinforcing internal rings. The annular space between the CSS and the Centaur is isolated from the remainder of the CSS by flexible seals at Stations 2241.78 and 2459.14. This annular volume is purged with gaseous helium during prelaunch operations to prevent the formation of frozen air. Fiberglas insulation attached to internal rings in this section of the CSS provides insulation for the Centaur LH_2 tank.

The boattail section of the CSS aft of Station 2213.00 is of riveted aluminum ring-skin-stringer construction. It contains the aft circumferential separation joint, jettison hinges, and the interface to the Centaur interstage adapter.

The two halves of the CSS are joined along a longitudinal separation joint. Each half also is joined to the fixed aft part of the shroud along the circumferential separation joint at Station 2211.80.

At jettison, all separation joints are severed by a noncontaminating pyrotechnic system. Eight main springs mounted longitudinally at the aft end of the cylindrical tank section of the CSS force the two halves to rotate about hinges and jettison. Four smaller springs mounted laterally between the halves assist in the initial separation. Two hinges for each half are mounted at the aft circumferential separation plane. The aft conical boattail is bolted to the Centaur interstage adapter and is jettisoned with the Titan Stage.

Centaur Tank

The Centaur tank assembly used was a flight-weight tank of the "D" series configuration. The basic tank configuration and dimensions are shown in figure I-4. The tank assembly is made of type -301 stainless steel and is a completely monocoque structure requiring internal pressure for structural strength. An evacuated, double-walled bulkhead separates the forward liquid hydrogen tank from the aft liquid oxygen tank.

For these tests, the basic Centaur tank had the following major items of hardware and systems installed to configure it to the D-1T design:

1. Payload truss adapter.

2. Centaur D-1T equipment module and mass simulated electronic/avionic packages.

3. Centaur stub adapter.

4. Hydrogen tank flight vent disconnect system.

5. Forward and aft CSS to Centaur seals.

6. Forward seal releaser system.

7. Forward bearing reaction struts and separation/retract system.

Details and descriptions of each of these major items and systems can be found in other sections of this report.

Other Centaur D-1T systems not necessary for the conduct of the tests, such as propulsion, pneumatic, and propellant feed systems, were not installed.

Centaur Interstage Adapter

The Centaur interstage adapter is the structure that the Centaur and CSS are attached to at their aft support points. It provides the interface between the Centaur. CSS, and Titan skirt. Details of its construction can be found in Section II of this report. It is manufactured by General Dynamics Convair Division.

Titan Skirt

The Titan Skirt is a structural item providing an interface between the Centaur/CSS hardware and the Titan booster vehicle. It is manufactured by the Martin Marietta Corporation.

TEST OBJECTIVES

The limit load structural test program was a part of an overall CSS qualification test program, the objective of which was to qualify for flight the Centaur Standard Shroud and new Centaur systems for the Titan/Centaur D-1T launch vehicle. The general objectives of the structural tests were as follows:

1. Demonstrate the ability of the CSS, the Centaur structures, and the Titan skirt to withstand limit loads, both with and without the FBR struts connected.

2. Determine the lateral deflection of the CSS and the Centaur structures at limit loads, both with and without the FBR struts connected, and to verify payload to CSS and Centaur to CSS design clearances, under maximum differential deflection conditions.

3. Demonstrate that the FBR struts will release and retract properly while under simulated flight load.

4. Demonstrate the integrity of the forward purge gas seal under maximum flight annulus pressure and corresponding CSS/Centaur maximum differential deflection.

5. Determine the degradation, if any, of the CSS thermal insulation from aging during the four-month time lapse from the previous insulation evaluation performed in the cryogenic unlatch tests.

Specific objectives for each of the tests performed are given in the "Tests Performed" portion of this section.

TESTS PERFORMED

The tests were not performed chronologically in the same order as the numerical designation but, were arranged for structural strength considerations, optimum test setup, and schedule requirements. A summary of the actual chronological test sequence is given in Table I-1.

RESULTS AND CONCLUSIONS

The following is a summary of significant results and conclusions from the CSS Static Limit Load Structural Test Program. More detailed results and conclusions on specific components are included in the following sections of this report:

1. The test program has demonstrated that the Centaur D-1T and the CSS, as a combined structural system, is qualified for flight on the Titan/Centaur launch vehicle at loads up to limit loads.

2. No structural strength deficiencies or anomalies were observed during the tests.

3. Stress levels at limit loads are equal to or less than originally predicted.

4. The stiffness of the CSS boattail structure and the ISA/CSS interface ring was less than originally predicted. To prevent excessive CSS deflection at limit load, it is necessary to use the FBR struts to provide a lateral load transfer system between the CSS and Centaur.

5. The FBR system satisfactorily limited the relative deflection between the CSS and the Centaur and maintained the strut loads within design values.

6. The load distribution at the ISA/Titan skirt interface was satisfactory.

7. The forward purge gas seal, as modified, withstood the flight maximum purge gas pressure and the corresponding Centaur/CSS relative deflection.

8. Both the forward purge gas seal and the FBR struts released satisfactorily using the flight pyrotechnic systems at simulated flight pressure differential, temperature, and load conditions.

9. The CSS thermal insulation did not degrade during the four-month period between cryogenic boiloff tests.

TABLE I-I

Summary of Tests Performed

Test No.	Test Date	Principal Test Objective	Centaur Tanked	FBR Struts Connected	CSS Shear Load Azimuth Degrees	Max. CSS Shear Load, Pounds	Max. Payload Shear Load, Pounds	Total Axial Load at Station 2127 Pounds	Remarks
3L-25	4/11/73	Check out facility systems at 25% load.	No	No	150	8,040	N/A	50,320	Facility systems okay.
3L-25	4/11/73	Check out abort system at 25% load.			150	8,040		50,440	Abort system okay.
3L-50	4/13/73	Check out test monitoring system in control room at 50% load.			150	17,730		50,470	Test monitoring system okay.
3L	4/25/73	Verify strength of CSS hydrogen disconnect valve door reinforcement and equipment module doors at limit equivalent axial compressive load.			150	36,510		100,480	CSS reached limit equivalent axial compressive loading. Deflections were approximately 40% greater than expected.
4L	5/2/73	Same as Test 3L except in tensile loading.			330	36,910		43,320	CSS reached limit equivalent axial tensile loading.
2L-1	5/11/73	Verify strength of CSS hydrogen boost pump and electrical umbilical panel door reinforcements at limit equivalent axial tensile load.			270	36,920		43,340	CSS reached limit equivalent axial tensile loading.

TABLE I-1 (CONTINUED)

Test No.	Test Date	Principal Test Objective	Centaur Tanked	FBR Struts Connected	CSS Shear Load Azimuth Degrees	Max. CSS Shear Load, Pounds	Max. Payload Shear Load, Pounds	Total Axial Load at Station 2127 Pounds	Remarks
2L-1A	5/11/73	Determine effects of Centaur axial loading fixture counterbalance force.	No	No	270	27,880	N/A	44,270	Counterbalance force had negligible effect on the change in slope of shear load versus shroud deflection plot (see text for details).
1L-1	5/18/73	Determine CSS/Centaur load sharing characteristics, and measure spring rate of FBR system (original strut design).		Yes	90	11,440		44,270	Confirmed spring constants of attaching structures did not significantly affect the system spring rate. Also, more load than desired transferred to Centaur because CSS acts as a softer spring than originally expected (see Test 3L).

TABLE I-1 (CONTINUED)

Test No.	Test Date	Principal Test Objective	Centaur Tanked	FBR Struts Connected	CSS Shear Load Azimuth Degrees	Max. CSS Shear Load, Pounds	Max. Payload Shear Load, Pounds	Total Axial Load at Station 2127 Pounds	Remarks
1L-2	5/19/73	Verify CSS structural capability at H2 boost pump cutout and strength of electrical umbilical panel door reinforcement at limit equivalent axial compressive load. Demonstrate integrity of forward purge gas seal while deflected.	No	No	90	36,920	N/A	100,440	CSS reached limit equivalent axial compressive loading. Seal pulled out from under its restraining cable with 1.8 psig in the Centaur/CSS annulus and 28,080 pounds CSS shear load.
2L-2	5/23/73	Verify strength of hydrogen vent fin attachments.			N/A	N/A		N/A	Satisfactory results.
1L-3	6/4/73	Demonstrate capability of forward purge seal pressurized to limit condition.			90	None		100,420	Seal pulled out from under its restraining cable with 2.05 psig in the Centaur/CSS annulus with no CSS shear loads applied.
"Boil-off" Test	6/14/73	Obtain Centaur hydrogen tank heating rate data.	Yes	Yes	N/A	N/A		N/A	Boiloff data closely correlated to previous test data.

TABLE I-1 (CONTINUED)

Test No.	Test Date	Principal Test Objective	Centaur Tanked	FBR Struts Connected	CSS Shear Load Azimuth Degrees	Max. CSS Shear Load, Pounds	Max. Payload Shear Load, Pounds	Total Axial Load at Station 2127 Pounds	Remarks
7L-2	6/15/73	Verify FBR system capability and load distribution in CSS and Centaur at limit load.			90	36,480	8,010 @ 270° Azimuth	105,500 including 61,230 lbs., LN2 in Centaur, no hydraulic load.	Reached limit load in FBR system. Deflection and load sharing characteristics satisfactory and as expected.
7L-1	6/15/73	Simulate launch transient loading in FBR system.			N/A	N/A	9,890 @ 270° Azimuth		Satisfactory results.
7L-3	6/15/73	Demonstrate FBR strut separation at cold temperature.			90	15,100	N/A		Struts separated and retracted successfully.
7L-4	6/15/73	Determine payload branch deflection characteristics without FBR system.		No	N/A	N/A	8,880 @ 270° Azimuth.		

TABLE 1-1 (CONTINUED)

Test No.	Test Date	Principal Test Objective	Centaur Tanked	FBR Struts Connected	CSS Shear Load Azimuth Degrees	Max. CSS Shear Load, Pounds	Max. Payload Shear Load, Pounds	Total Axial Load at Station 2127 Pounds	Remarks
6L-1	6/28/73	Same as Test 7L-2 except at different load azimuth. Also pressure and load test of modified forward seal.	Yes	Yes	240	36,380	N/A	104,440 including 63,100 lbs., LN2 in Centaur, no hydraulic load.	Seal did not pull out from under its restraining cable with 3 psig Centaur/CSS annulus pressure.
6L-2	6/28/73	Same as Test 7L-3.			240	13,840			Struts separated and retracted successfully.
6L-3	6/28/73	Demonstrate forward purge gas seal release at cold temperature, with modified seal edge bead.			N/A	N/A			Seal released successfully. However, the lip of the seal was not completely pulled over the edge of seal ring by the spring loaded straps.
5L-2	6/28/73	Verify strength of cutouts at limit equivalent axial compressive load.	No	No	240	36,600		44,270	CSS and ISA reached limit equivalent axial tensile load.

TABLE I-1 (CONTINUED)

Test No.	Test Date	Principal Test Objective	Centaur Tanked	FBR Struts Connected	CSS Shear Load Azimuth Degrees	Max. CSS Shear Load, Pounds	Max. Payload Shear Load, Pounds	Total Axial Load at Station 2127 Pounds	Remarks
5L-1	7/2/73	Demonstrate integrity of forward purge seal with limit pressure and maximum deflection.	No	No	240	28,060	N/A	44,270	Seal did not pull out from under its restraining cable with 3.05 psig Centaur/CSS annulus pressure and 1.47" relative deflection between CSS and Centaur.
5L-3	7/2/73	Same as Test 6L-3, except at room temperature.			N/A	N/A			The test was successfully performed. The lip of the seal was pulled over the edge of seal ring by spring loaded straps.

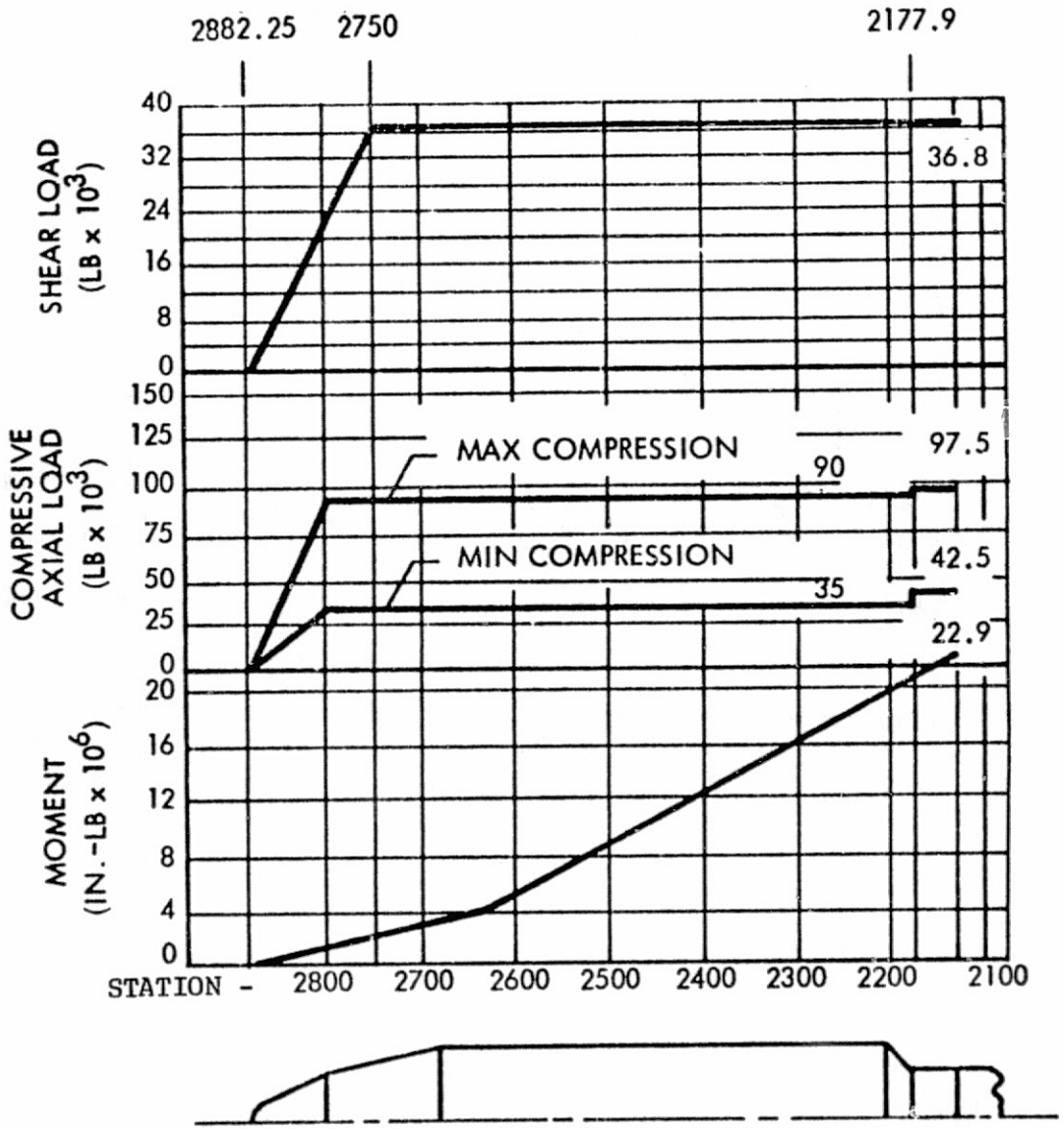

FIGURE I-1. CSS DESIGN LIMIT AXIAL, SHEAR, AND MOMENT LOADS

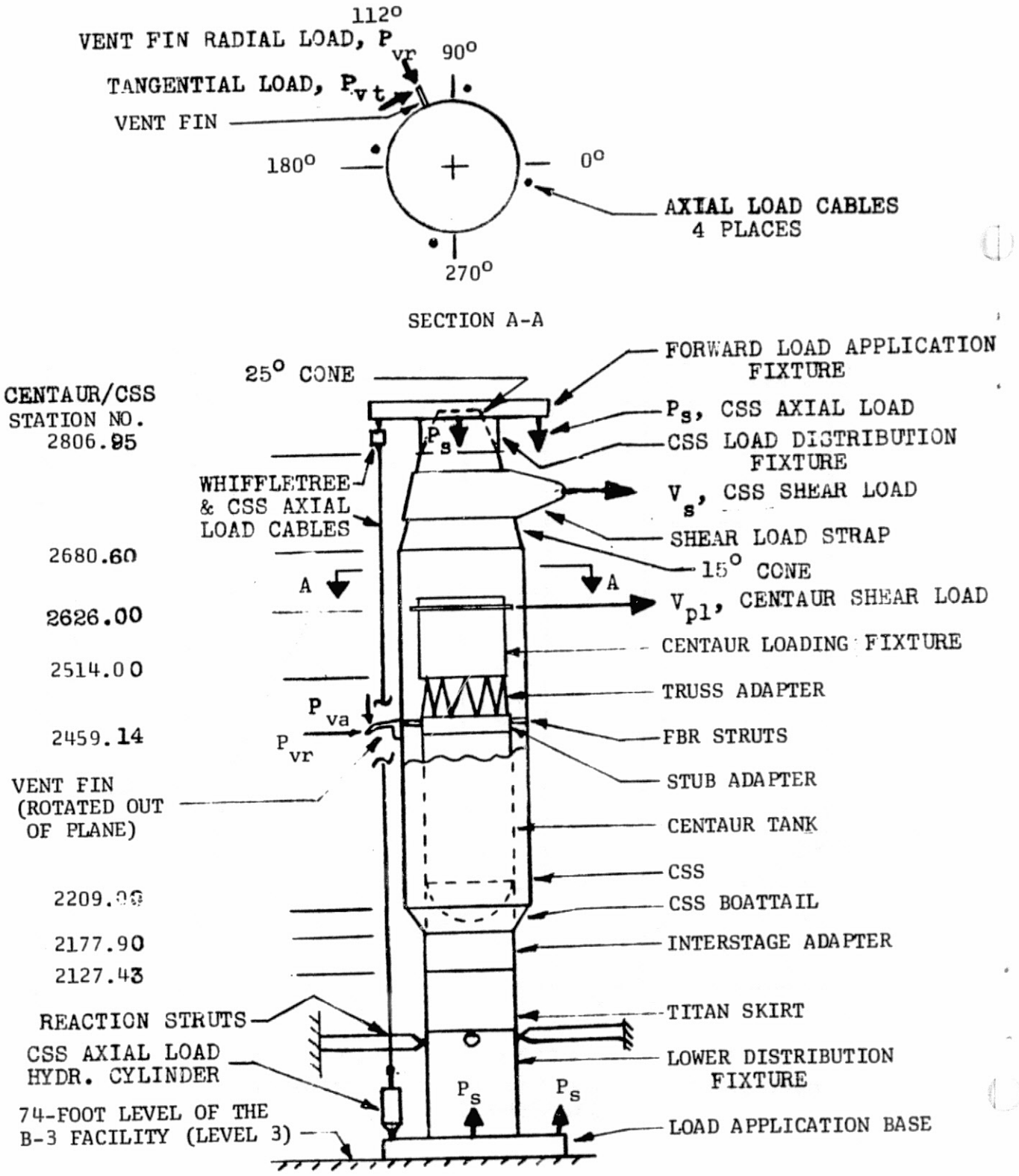

FIGURE I-2. TYPICAL TEST CONFIGURATION FOR CSS LIMIT LOAD TESTS

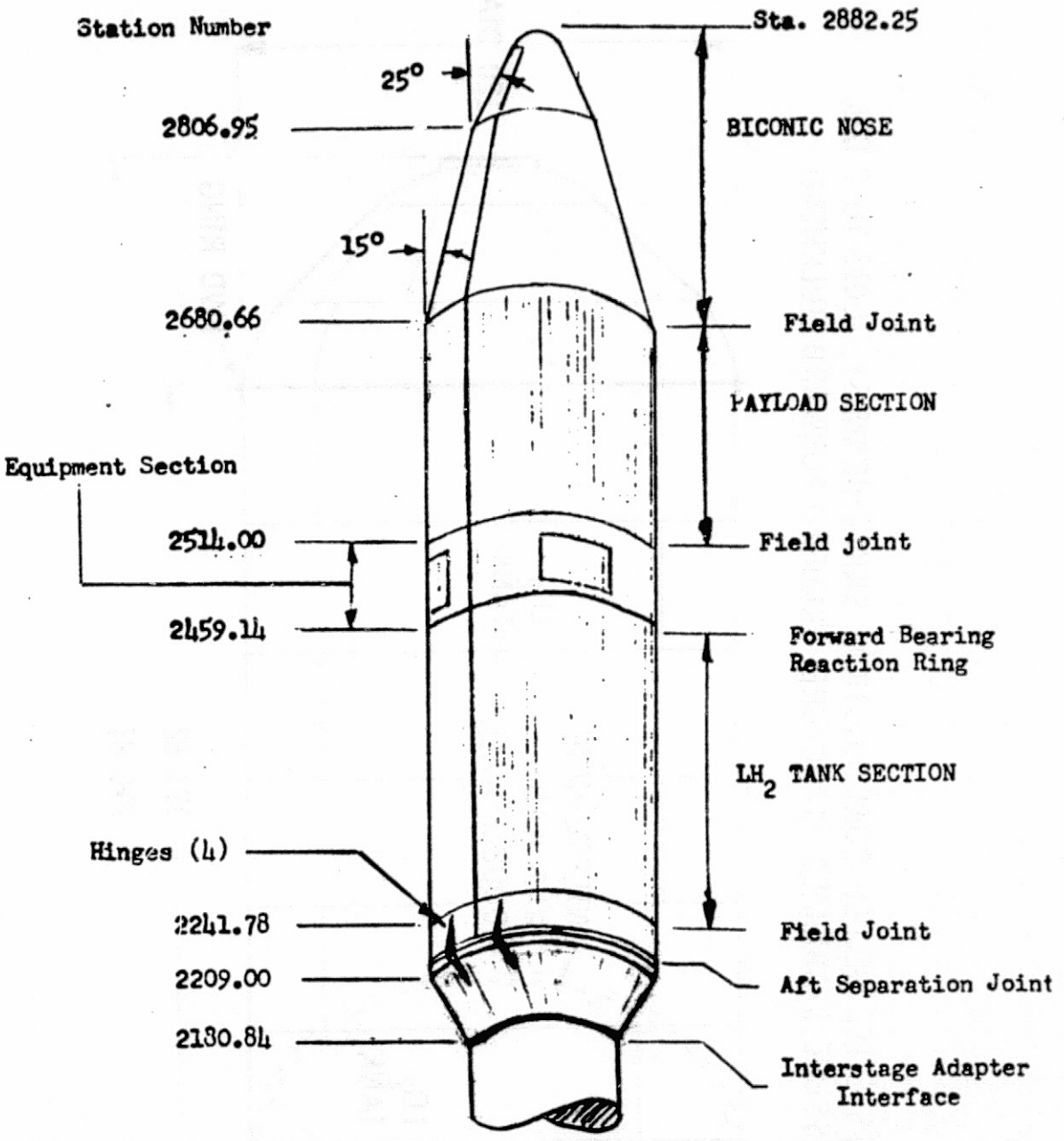

FIGURE I-3 CENTAUR STANDARD SHROUD (CSS) GENERAL CONFIGURATION

STAINLESS STEEL WELDED CONSTRUCTION; SKIN THICKNESS, 0.013 TO 0.026;
PRESSURE STABILIZED STRUCTURE; MODIFIED FORWARD BULKHEAD

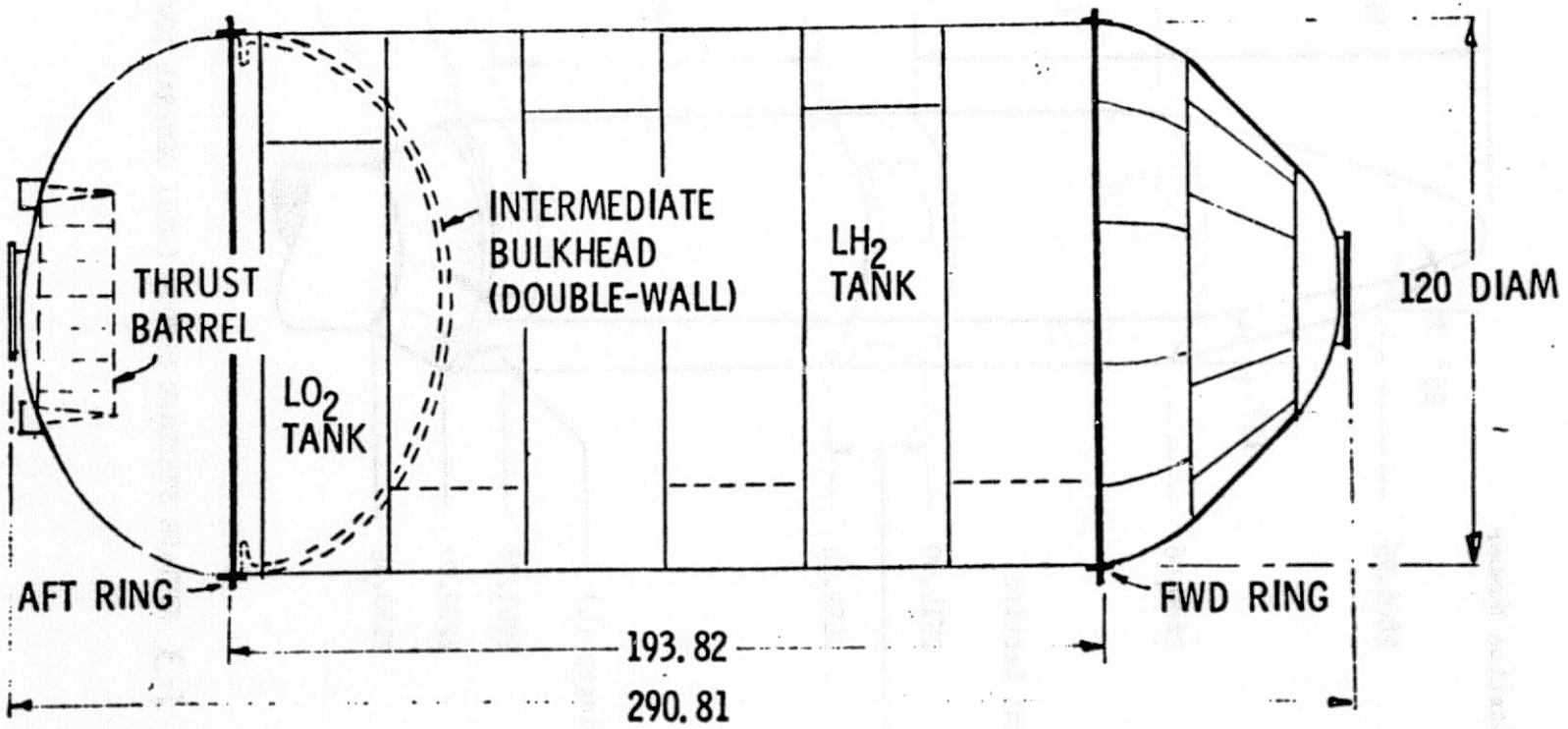

FIGURE I-4 CENTAUR PROPELLANT TANK CONFIGURATION

II CENTAUR STRUCTURES

By R. C. Edwards and R. T. Barrett

SUMMARY

The items of structural hardware which interface with the Centaur were subjected to loads during the limit loads tests. These items consisted of the ISA, the truss adapter, the stub adapter, and the equipment module. All the components withstood the loads satisfactorily without permanent deformation. The CSS support ring on the ISA deflected more than was expected. The thermal effects of LN_2 in the Centaur tanks were not detrimental to the stub adapter.

DESCRIPTION

Interstage Adapter

The D-1T ISA is a 113-inch long structural spacer between the forward end of the Titan skirt and the aft end of the Centaur vehicle. It also supports the CSS through an external ring flange at Station 2180.48. It is an all-aluminum sheet and stringer structure with 10 circular rings. There are 60 hat section stringers with return flanges on the aft end. Thirty-six internal longeron fittings are included in the aft bay of the ISA to match up with the Titan skirt 36 internal longerons. Each longeron has 2 bolts, for a total of 72 interface bolts. A bearing pad fits between the rings at each longeron connection to ensure controlled load distribution on the Titan skirt ring. Strain gages were installed on the shroud support ring, the structural maintenance access doors, and in areas adjacent to these doors, as well as on the longerons. For details of instrumentation, see reference 7. For each test, only the gages in the highest predicted load areas were monitored due to instrumentation limits.

Truss Adapter

The Centaur truss adapter is 120 inches in diameter and 49 inches in height. It consists of 24 aluminum tubular struts equally spaced around the circumference. The struts were attached to 12 fittings located on the aft end of the Centaur loading cylinder test fixture and to 12 fittings located on the forward end of the stub adapter. The wall thickness of the struts used in the test assembly were slightly below the design minimum value.

PRECEDING PAGE BLANK NOT FILMED

However, the assembly was not a qualification item in the test program and was not subjected to full limit load. It was primarily acting as a spacer to support the Centaur loading cylinder test fixture. Two strain gages were located at mid-height on each of four struts. Each pair of gages on a strut were located 180° apart on the radially inboard and outboard surfaces.

Stub Adapter

The stub adapter as used on the Titan/Centaur vehicle is a cylindrical structure 25 inches in height and 120 inches in diameter. The adapter consists of titanium skin and stringers reinforced by aluminum rings. Two axially oriented strain gages were located in the base of the stringers at 264° and 268° azimuths. Two pairs of back to back strain gage rosettes were located on the skin at 266° and two additional pairs of back to back rosettes were located at 180°.

Equipment Module

The Centaur equipment module is a truncated conical aluminum structure 30 inches in height. The diameter of the base, which is attached to the stub adapter, is 120 inches; the diameter of the forward end is 60 inches. The construction of the equipment module is skin/stringer with reinforcing rings. A pair of back to back strain gage rosettes was located on the skin near the base at 180°. Two axially oriented strain gages were located at the base of each stringer on either side of 180°.

TEST RESULTS

Interstage Adapter

Combined axial, bending, and shear loads were imposed on the ISA by the Centaur tank and the CSS. The recorded stresses were lower than expected.

The CSS boattail support ring outstanding leg was monitored to verify the assumptions used in its analysis. Comparisons of methods are shown in the Test 4L plots (figures II-1 and II-2). All stress plots for this ring (figures II-1 through II-5) show very low stresses (less than 12,000 psi versus a material yield allowable of 42,000 psi). The ring deflected more than was expected but was not damaged.

The axial component of the load in the CSS support ring diagonal leg closely approximates the applied axial equivalent load as shown in figures II-1 and II-2.

The use of the FBR struts did result in a reduction in stresses on the CSS support ring (figure II-5) but it was not possible to make a direct comparison, due to some inoperative strain gages on Test 1L-2.1.

The FBR system reduced the highest load seen at the CSS interface to a value significantly less than the load experienced during the structural testing without the FBR system installed. Thus, the ISA can safely sustain at least 125% of the limit load when the FBR system is installed.

The structural maintenance access doors distributed the load satisfactorily. The close proximity of these doors to the Titan/Centaur interface at Station 2127 created a requirement that they provide equal load distribution at the interface. To determine their effectiveness, the stringers on the structural doors and adjacent to the doors were monitored during Test 5L-2. Stringer 50, located on a structural door, indicated a stress of 17,300 psi compression. Stringer 51 adjacent to the door, indicated a stress of 19,270 psi compression, which shows the effectiveness of the structural door. A stringer gage on the opposite door showed a tension stress of 15,270 psi for this test.

Other gages were monitored on the ISA, and none indicated stresses above yield during any tests.

Truss Adapter

The Centaur truss adapter functioned as anticipated when subjected to 13,500 pounds of axial load and 10,000 pounds of lateral shear load with an associated bending moment. The lateral shear load was reacted primarily by truss struts located at 90^{o} to the line of action of shear load. The bending moment was reacted primarily by truss struts aligned with the line of action of the shear load. Very small values of strut bending were noted. The maximum compressive load imposed on a truss adapter strut was 4,500 pounds. This value is well within the allowable strut compressive load of 7,600 pounds.

Stub Adapter

The stub adapter was subjected to shear, axial, and bending loads applied through the FBR system and the truss adapter. The magnitude of the stresses in the stringers was small, indicating that the stub adapter satisfactorily distributes the concentrated loads from the truss adapter struts.

The magnitude of the skin panel shear and compression stresses appeared to be less than half the allowable shear buckling stress of 7,500 psi and the allowable compression buckling stress of 7,600 psi. The shear stress was linear for the full range of loading giving a further indication that the skin panels did not buckle. The skin bending stresses were also very small.

LN_2 was in the Centaur tanks during Tests 6L and 7L. The effect was to lower the stub adapter skin temperature to approximately $-60^{o}F$. There was no discernible effect on the adapter.

Equipment Module

Since the Centaur equipment module was not located in a direct load path, the applied test loads did not load the module to its full design strength. The recorded stresses were caused only by the deflection of the stub adapter. The axial and bending loads in the equipment module stringers were very small. The magnitudes of the maximum principal stresses and shearing stress in the module skin were not significant.

SUMMARY OF TEST RESULTS

The structural capability of the ISA was not degraded by the limit load tests. The structural maintenance doors in the ISA distributed loads satisfactorily and at no point were the loads above yield. The use of the FBR system reduces the loads in the ISA.

The truss adapter and stub adapter were found to be well within their structural capabilities. The loads were distributed uniformly and the use of cryogenics in the Centaur tanks had no deleterious effects.

The equipment module which was not tested to limit conditions was not loaded significantly through the stub adapter.

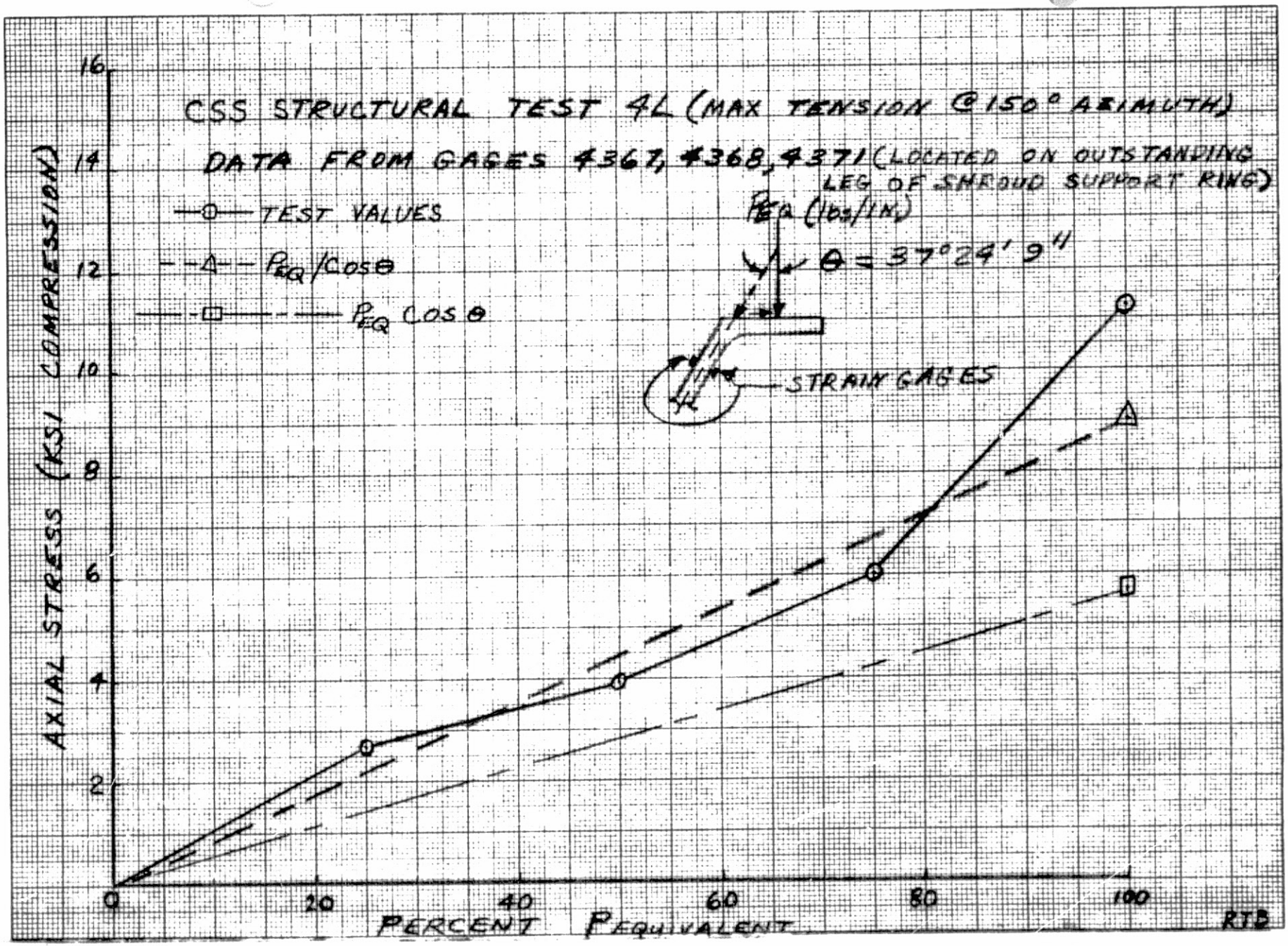

FIGURE II-1. ISA CSS SUPPORT RING - COMPARISON OF TEST 4L Vs. PREDICTED TEST STRESS.

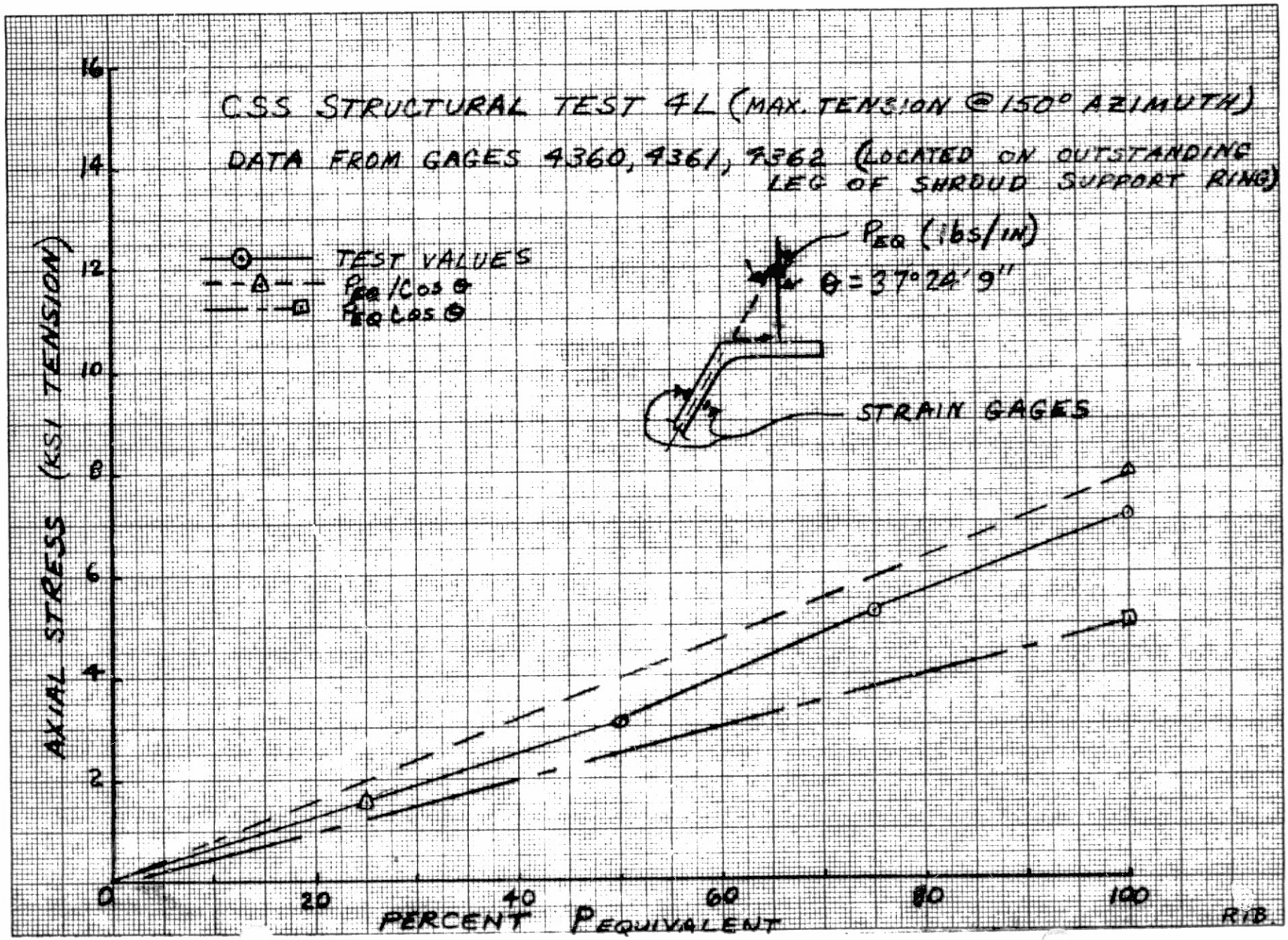

FIGURE II-2. ISA CSS SUPPORT RING: - COMPARISON OF TEST 4L Vs. PREDICTED TEST STRESS.

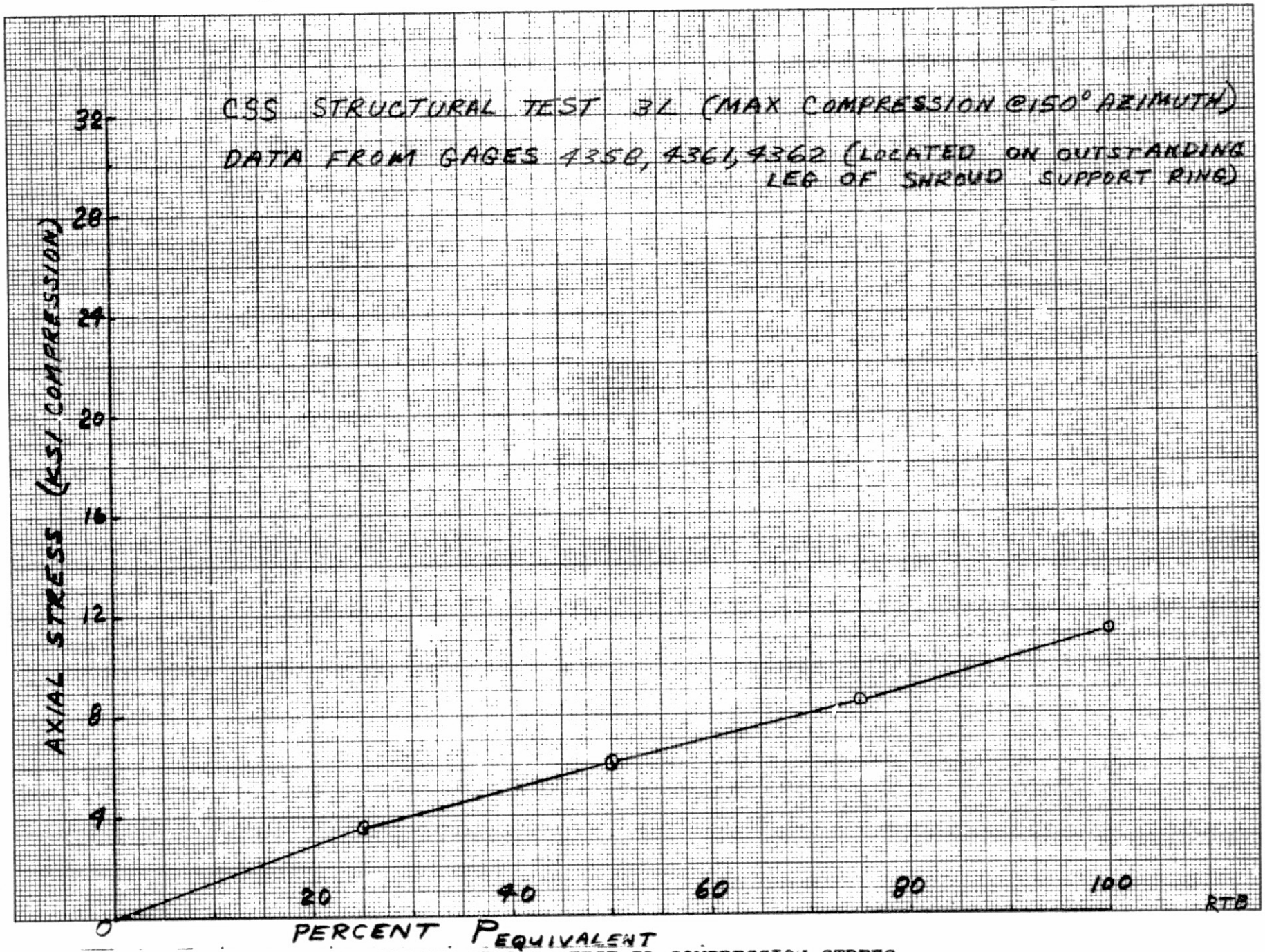

FIGURE II-3. ISA CSS SUPPORT RING: - TEST 3L COMPRESSION STRESS.

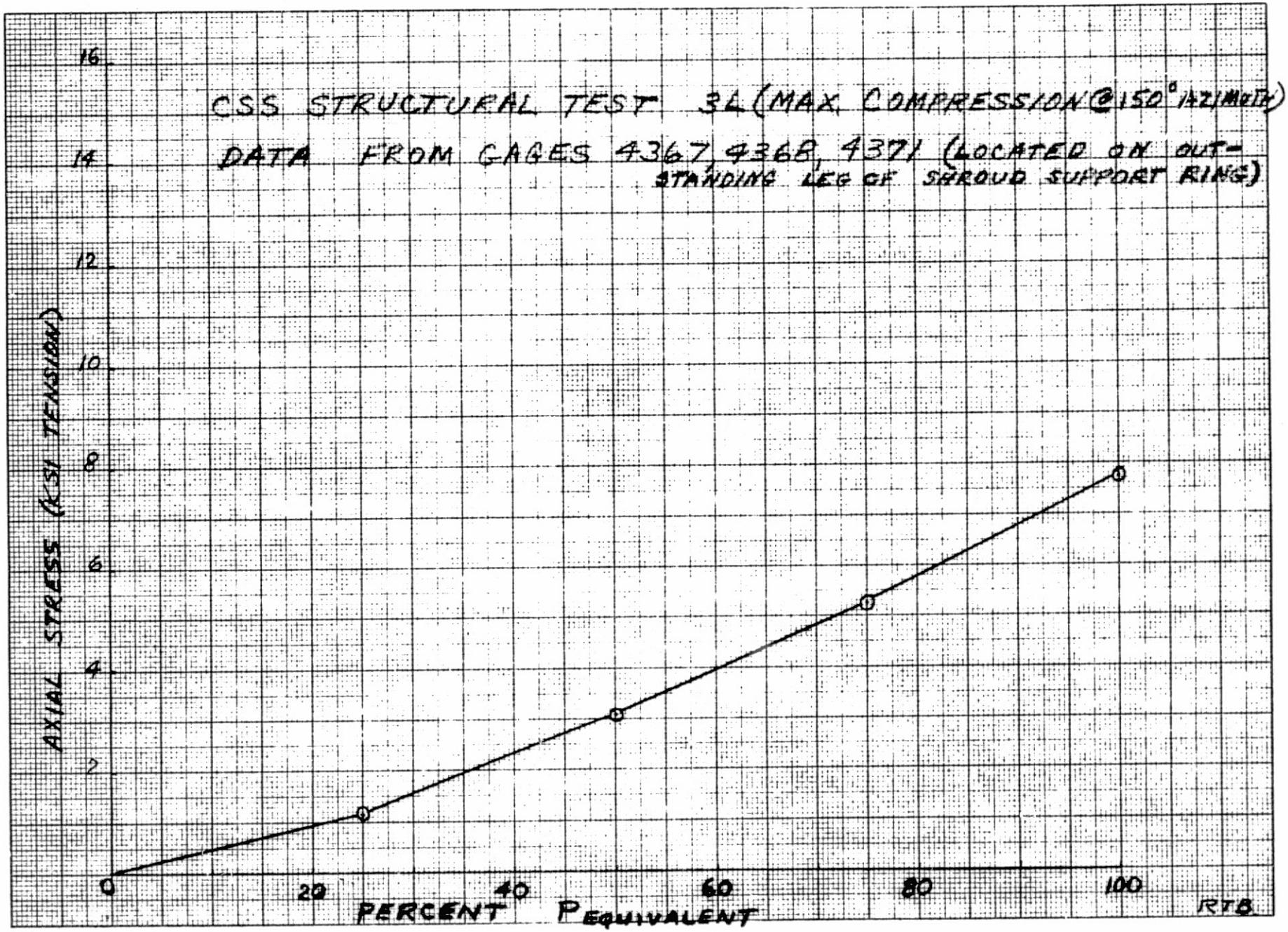

FIGURE II-4 ISA CSS SUPPORT RING: - TEST 3L TENSION STRESS.

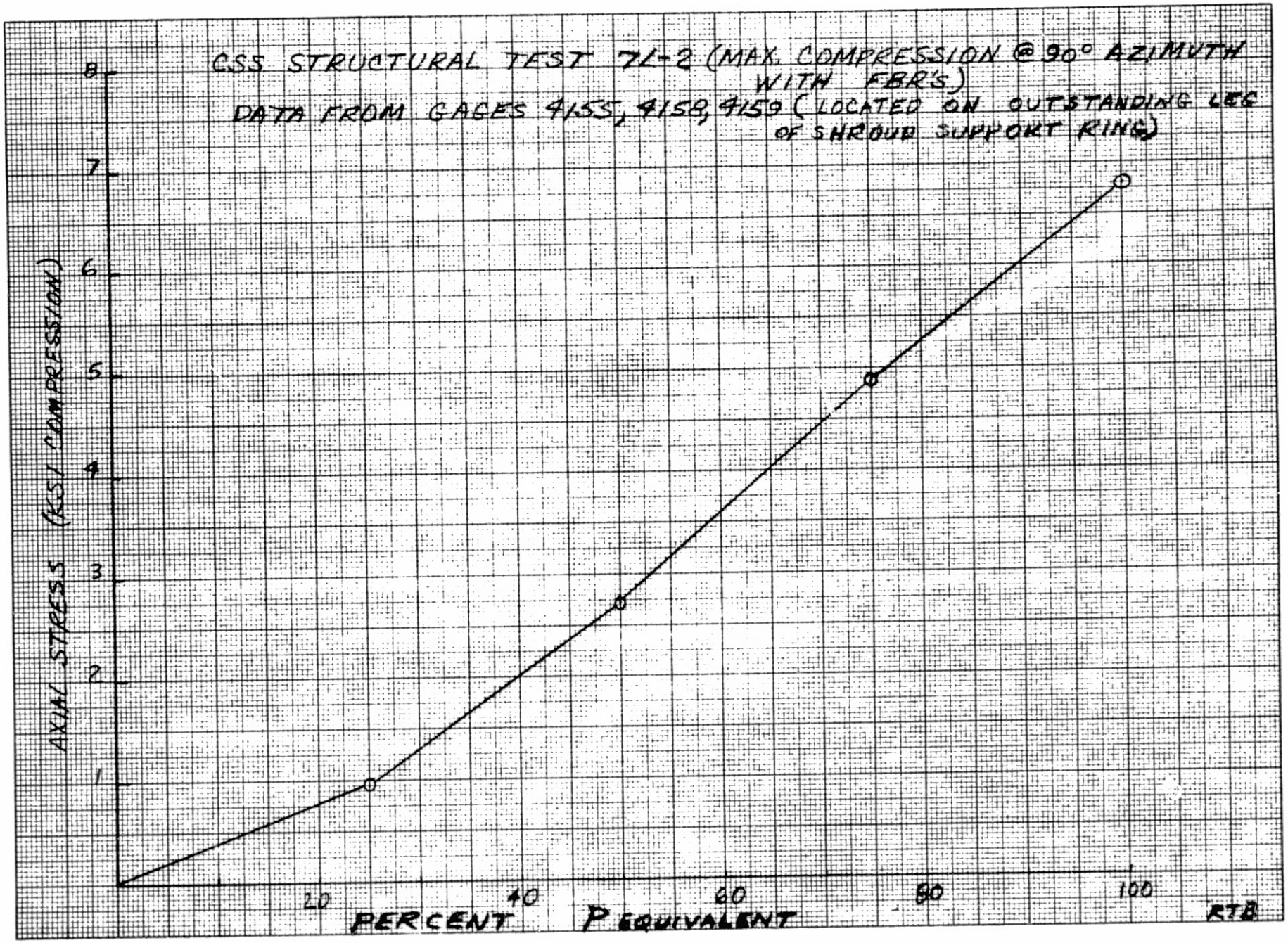

FIGURE II-5. ISA CSS SUPPORT RING: - TEST 7L-2 COMPRESSION STRESS.

III CSS/CENTAUR BOLT-ONS

By T. L. Seeholzer, W. A. Groesbeck, and H. M. Tang

SUMMARY

The following major CSS/Centaur bolt-ons were evaluated during the Structures Test:

1. Forward Bearing Reaction System (FBR).
2. Forward Seal and Release (FSR) System.
3. LH_2 Vent Disconnects.

The FBR system was successfully tested for adequate strength, proper stiffness, and separation function. Tests verified that installation of the FBR system was required to limit deflections between the CSS and Centaur to acceptable levels. Test data indicate that the FBR system can reliably sustain 125% of limit design load. Shock data were obtained during FBR separation. These data indicated shock levels would not adversely affect Centaur electronic equipment.

Forward seal structural adequacy and releaser system operation were verified under conditions of cryogenic temperatures, maximum delta pressure, and displacement associated with flight loads. Tests also substantiated that the LH_2 vent disconnects separate prematurely without the FBR system installed but operate satisfactorily when the FBR is used.

DESCRIPTION

Forward Bearing Reaction System

The CSS/Centaur FBR system provides load sharing and limits the relative deflection between the CSS and the Centaur vehicle during flight until the vehicle has passed through the period of significant aerodynamic loading (approximately 100 seconds after liftoff). The FBR system, located at Station 2460, consists of six spring loaded double action struts. The strut major structural components are aluminum. Previous component testing of the struts (reference 8) has shown structural capability to be in excess of 125% of limit load.

The basic strut system is illustrated in figures III-1 and III-2. The spring rate of the system must be compatible with the relative stiffnesses of the CSS and the Centaur in order to prevent overloading the Centaur and

PRECEDING PAGE BLANK NOT FILMED

maintain payload-to-CSS clearances at acceptable levels. Conical steel washers are utilized to produce the required spring rate in tension and compression. See Section VI for a discussion of stiffness properties. The initial strut design (30,000 #/inch) and the redesigned strut (6,500 #/inch) are shown in figure III-3.

Separation of the FBR is accomplished by redundant explosive bolts. Following bolt separation, the strut halves are retracted against the CSS by a spring loaded retractor and against the stub adapter by a tension spring (figure III-2). Explosive separation bolts are located as shown in figure III-3. Bolt separation is caused by actuation of two electro-explosive devices (cartridges). Firing of either cartridge will separate the bolts. Pressure produced by the cartridge is converted into a force by means of two pistons and a silicone rubber force amplifier. (See figures III-4 and III-5 for bolt and cartridge details.) The resultant force fractures the bolts in the grooved area. The bolt design has been successfully employed on the Atlas/Centaur vehicle for nose fairing separation.

Fifteen accelerometers were attached to the mass simulated electronic packages and to the FBR struts for Tests 6L-2 and 7L-3. The simulated packages were mounted on the Centaur equipment module. Figure III-6 shows the location of the accelerometers.

The accelerometers designated 900A through 914A had identical locations and orientations to those previously installed on Cryogenic Unlatch Test No. 1 (reference 4). Since there were no accelerometers attached to the R.F. disconnect panel for the previous Cryogenic Unlatch testing, accelerometers 954A and 955A were added to measure the response of the panel during FBR strut firing. See reference 7 for instrumentation details.

Forward Seal and Release System

The forward seal, illustrated in figure III-7, is located at Station 2454 between the CSS and Centaur stub adapter. The seal consists of a silicone rubberized dacron fabric attached to the stub adapter by bolts and retained on the CSS forward bulkhead by a cable and retaining mechanism. A 5/16-inch diameter segmented teflon bead on the outboard edge of the seal holds the seal under the cable. This bead was changed from 3/16-inch silicone rubber to 5/16-inch teflon after Structural Test 1L. See figure III-8 for bead details.

A redundant explosive bolt is employed to release the seal. This is the same bolt design used for the FBR separation (see figure III-4). Two bolts, one at each split line, are attached to the seal retaining cable as shown in figure III-7. When the bolts separate the cable tension is relaxed and the seal releases. Seal release assist retractors are located around the periphery of the seal to assist in raising the seal bead over the retainer lip. Two seal retractors are located at the LH_2 vent nozzles to insure seal retraction over the nozzles (figure III-9).

LH_2 Vent Fin Disconnect

The hydrogen vent disconnect is an extensible duct connection between the fixed vent nozzle on the tank and the vent fin inlet on the inside of the CSS. The function of the disconnect is to accommodate the differential motion between the tank and the CSS during prelaunch and boost flight phase, and to provide a release mechanism to disconnect the vent ducting from the fixed vent nozzles at CSS jettison. The vent fin disconnect configuration is illustrated in figure III-10. The design is a telescoping tube section with the inboard end attached to the vent nozzle and the outboard end attached to the CSS fitting by means of spherical ball joints. The disconnect mechanism is engaged by extension of the tubes to the full free length of travel as limited by internal stops. Release of the disconnect can be accomplished in one of two modes during CSS jettison. In the primary mode a continued pull on the disconnect ducting in the bottomed out condition (CSS rotating away from tank) shears two pins at the vent nozzle retainer assembly. Shearing the pins permits the inboard duct section to slide out and thereby release the latching lugs on the vent nozzle. The ducting then pulls clear of the vent nozzle. The secondary mode is used if the pins fail to shear. In this mode the continued outward pull on the disconnect forceably pulls the duct assembly off the nozzle by bending the latching lugs. The latching lugs are designed to bend in this manner at a load slightly above that required to shear the pins. The disconnect detailed design is shown in figure III-11.

TEST RESULTS

Forward Bearing Reaction

The FBR system, including the CSS and stub adapter attaching structures, was originally estimated to have a spring rate of 73,000 #/inch. The first test of the system for stiffness characteristics was performed in Test 1L-1. Test results, as shown in Table III-1, indicated the system spring rate was actually 81,000 #/inch. Since the combined spring rate of the FBR struts only was approximately 90,000 #/inch, the spring rate of the CSS and stub adapter attaching structure, K (Structure), was determined from:

$$\frac{1}{K(\text{System})} = \frac{1}{K(\text{Struts})} + \frac{1}{K(\text{Structure})}$$

K(Structure) was thus found to be equal to 800,000 #/inch.

The lower than expected stiffness of the CSS as determined from Tests 3L and 4L indicated that 81,000 #/inch in the FBR system would transfer unacceptably high loads into the Centaur vehicle. Consequently, it was necessary to reduce the system spring rate to 19,000 #/inch, which was

accomplished by changing the combined spring rate of the six FBR struts to 19,500 #/inch. Because of the geometric relationship shown in figure III-1, the equivalent spring rate for each strut was then 6,500 #/inch.

During Tests 7L-2 and 6L-1 the 19,000 #/inch FBR system was successfully tested. This system provided the proper stiffness between the CSS and the Centaur vehicle and also limited the CSS-to-payload deflection to acceptable values. Results of these tests on the FBR system are summarized in Table III-1.

The FBR system loads and the individual strut loads were determined by strain gages mounted inside the struts as shown in figure III-3. The FBR struts were individually calibrated to determine the load vs. strain relationship and to verify the strut spring rate of 6,500 #/inch. A typical spring rate calibration is shown in figure III-12. Maximum tension and compression strut loads during testing are listed in Table III-1. The individual struts were designed to 8,000 pounds limit load. This value was not exceeded during the test series. Post-test inspection verified that no damage or yielding occurred in any strut or attaching hardware during testing.

The FBR system total load at separation was 10,110 pounds for Test 6L-2 and 6,528 pounds for Test 7L-3. Figures III-13 and III-14 are plots of the envelopes of the acceleration responses for Tests 6L-2 and 7L-3. A comparison of these two plots with the previous Cryogenic Unlatch Test data has been made. For the frequencies above 200 Hz.. the shock responses of the packages were greater when the FBR struts were loaded. Figure III-15 shows the shock qualification specification for packages mounted on the Centaur equipment module. Comparing figures III-13 and III-14 with figure III-15, it is concluded that the shock responses when the FBR struts were loaded are well below the qualification level.

Separation of the FBR system, when subjected to expected flight loads, was evaluated in Tests 6L-2 and 7L-3. The results of these tests are listed in Table III-2. All struts separated properly and retracted normally. Post-test inspection verified all pyrotechnic cartridges fired. The maximum dynamic excursion of the CSS relative to the Centaur, following FBR separation, was 0.622 inches. This was within acceptable design limits.

Forward Seal and Release System

The pressure capability of the forward seal was tested in Tests 1L-2 and 1L-3. The original retaining bead failed to hold the 3 psi limit pressure during these tests. As a result, the seal was redesigned and successfully tested on 5L-1 and 6L-1. Test results are summarized in Table III-3. In Test 6L-1 the seal limit pressure capability was verified at a CSS/Centaur relative deflection produced by limit FBR system load of 20,000 pounds. In Test 5L-1 the seal limit pressure capability was verified at the maximum CSS/Centaur relative deflection

which would be produced by limit FBR load and worst case tolerance stackup. For this test the FBR struts were not connected in order that excessive loads would not be transmitted into the Centaur vehicle. During seal pressurization Test 6L-1, the forward seal retaining cable loads were monitored. Cable loads varied by 35 pounds, or less than 4% of the installation load. Figure III-16 shows the cable load fluctuation during Test 6L-1.

Due to the redesign of the forward seal bead for pressure capability, two tests (5L-3 and 6L-3) of the FBR system were conducted. These tests verified that the seal redesign did not adversely affect seal release. The two tests, conducted at LN_2 and ambient temperature conditions, were completely successful. In each test all explosive cartridges fired; the bolts separated and properly released the retaining cable. The assistor straps lifted the seal over the lip in local areas. LH_2 vent retractor straps successfully retracted the seal over the vent nozzles.

LH_2 Vent Fin Disconnect

The differential deflection between the CSS and the Centaur tank without the FBR installed was more than predicted. In one test the shroud deflection exceeded the extension capability of the disconnect resulting in release of the disconnect mechanism. The vent disconnect can extend to a maximum length of 17.19 inches between the centerline reference of the inner and outer spherical ball joints before engaging the disconnect release mechanism. During Test 2L-1, with limit load applied at the 270° azimuth, the disconnect extended length was just short of the limit stop at 17.14 inches. On Test 1L-2, with the limit load applied at 90° azimuth, the disconnect was extended to 17.59 inches. This travel resulted in the telescoping sections bottoming out, thereby actuating the release mechanism. A post-test inspection confirmed that the disconnect had released. The vent disconnect is located at azimuth 112°-30'. If the shear load had been applied at this azimuth, the local deflection of the CSS at the disconnect would have been even greater.

In tests conducted with the FBR struts in place the disconnects performed satisfactorily. At limit load conditions the maximum extension of the disconnect was approximately 0.1 inch from the normal position. Test results verified that the LH_2 vent disconnect design is adequate only with the FBR system installed.

SUMMARY OF TEST RESULTS

All CSS bolt-ons successfully withstood limit design loads imposed in the Structures Tests. However, both the FBR system and forward seal required design modifications as a result of these tests. The spring rate of the FBR system was changed from 73,000 #/inch to 19,000 #/inch, after Test 1L, to be compatible with the CSS stiffness. Tests 3L and 4L data verified the need for an FBR system. A 19,000 #/inch FBR system was successfully tested in Tests 6L and 7L.

Separation tests of the FBR struts under load verified the 19,000 #/inch spring rate system functioned properly. Test data at FBR separation (Tests 6L-2 and 7L-3) indicated shock levels did not exceed Centaur equipment qualification values.

Previous component testing of the individual FBR struts by the contractor (reference 8) verified the structural capability of the struts to be in excess of 125% of limit design loads. All stress levels monitored during the limit load test, with the FBR system installed, were well below predicted stress levels. It is concluded that the FBR system can reliably sustain 125% of limit design loads.

The original forward seal bead was redesigned to withstand 3 psi pressure as a result of initial testing. The new larger diameter seal bead was then successfully tested to 3 psi on Tests 5L and 6L. Separation tests of the forward seal releaser verified the redesigned seal bead did not adversely affect test results.

In the tests without the FBR system installed, the LH_2 disconnects separated prematurely. Following installation of the redesigned FBR system, the LH_2 vent disconnect stroke capability was shown to be adequate.

ORIGINAL PAGE IS
OF POOR QUALITY

TABLE III-1

Summary of FBR Load Tests

Test and Shear Azimuth	Calculated System K, Spring Rate (#/In.)	Actual System Spring Rate, K (#/In.)	Max. FBR System Load Lbs.	Max. CSS/ Centaur Defl. In.	Max. FBR Strut Load Lbs.	Applied Shroud Shear Load Lbs.	Applied Payload Shear Load Lbs.
1L-1 90°	73,000 (System) 30,000 (Per Strut)	81,000	8,800	.096	2,865 Ten. 2,876 Comp.	11,400	0
7L-2 0°	19,000 (System) 6,500 (Per Strut)	19,100	19,732	1.0267	6,493 Tens. 6,508 Comp.	36,680	8,010
6L-1 240°	19,000	19,000	21,057	1.124	6,926 Ten.	36,380	0

TABLE III-2

Summary of FBR Separation Tests

(19,000 #/In. System)

Test and Shear Azimuth	Conditions at Separation: Maximum FBR System Load Lbs.	Conditions at Separation: Maximum CSS/Centaur Defl.-In.	Conditions at Separation: Max. FBR Strut Loads Lbs.	Condition After Separation: Maximum Dynamic Excursion CSS/Centaur	Separation Results
7L-3 0° (LN_2)	6,528	.3030	2,264 Ten. 2,050 Comp.	.402	All cartridges fired, bolts separated, and struts retracted properly.
6L-2 240° (Amb.)	10,110	.5588	3,171 Ten. 3,061 Comp.	.622	All cartridges fired, bolts separated, and struts retracted properly.

TABLE III-3

Forward Seal Pressurization Tests

Seal Bead Configuration	Test and Shear Azimuth	Maximum Annulus Pressure - PSI	Maximum CSS/Centaur Deflection - Inches	Results
Original - 3/16" Diameter Silicone Rubber	1L-2 90°	1.80	1.60	Seal Bead Came Out From Under Cable
	1L-3 (No Shear)	2.05	0	Seal Bead Came Out From Under Cable
Existing - 5/16" Diameter Segmented Teflon Strung On 1/8" Diameter Silicone Rubber	6L-1 240° (With FBR)	2.99	1.12	Successful
	5L-1 240° (No FBR)	3.05	1.47	Successful

ORIGINAL PAGE IS
OF POOR QUALITY

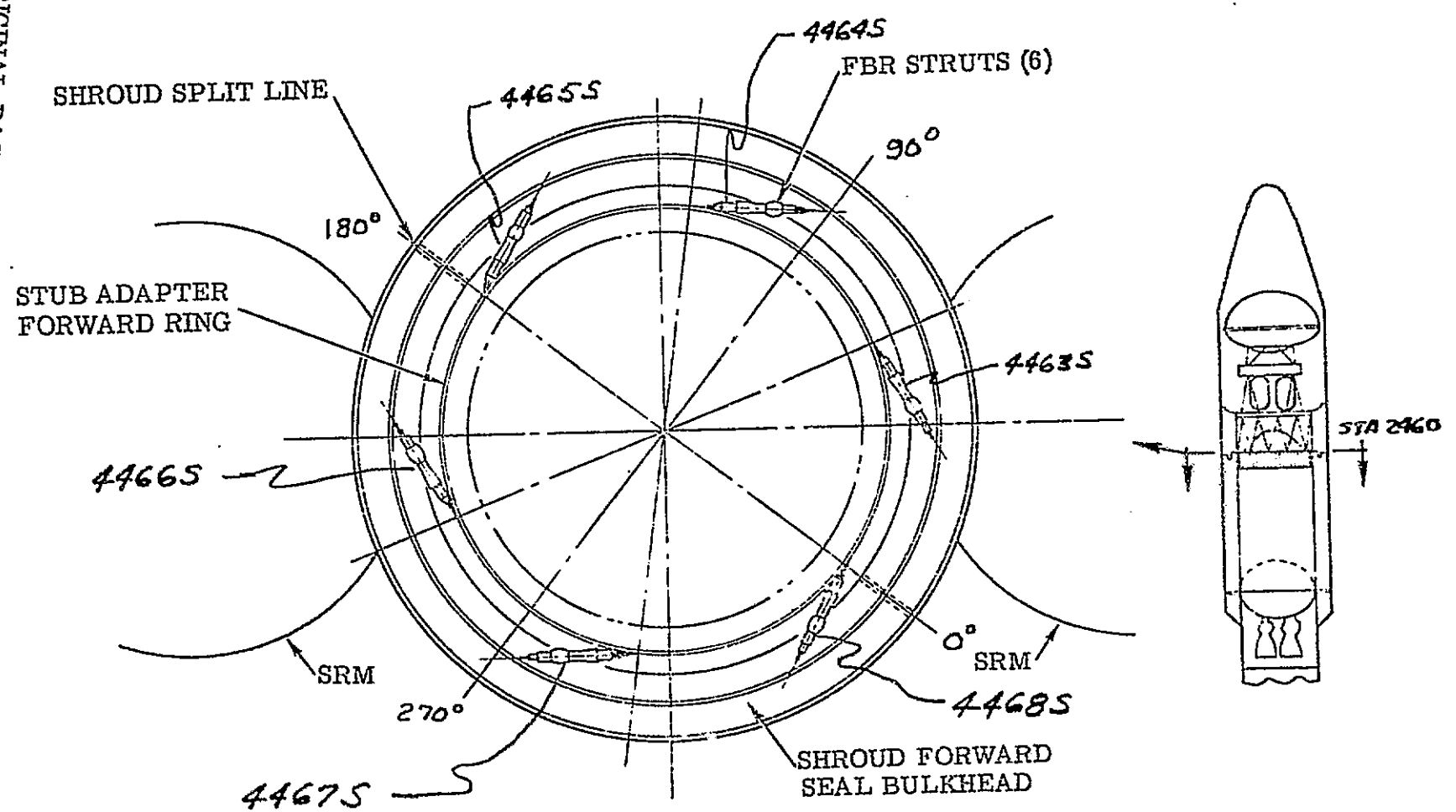

FIGURE III-1. FORWARD BEARING REACTOR SYSTEM.

ORIGINAL PAGE IS
OF POOR QUALITY.

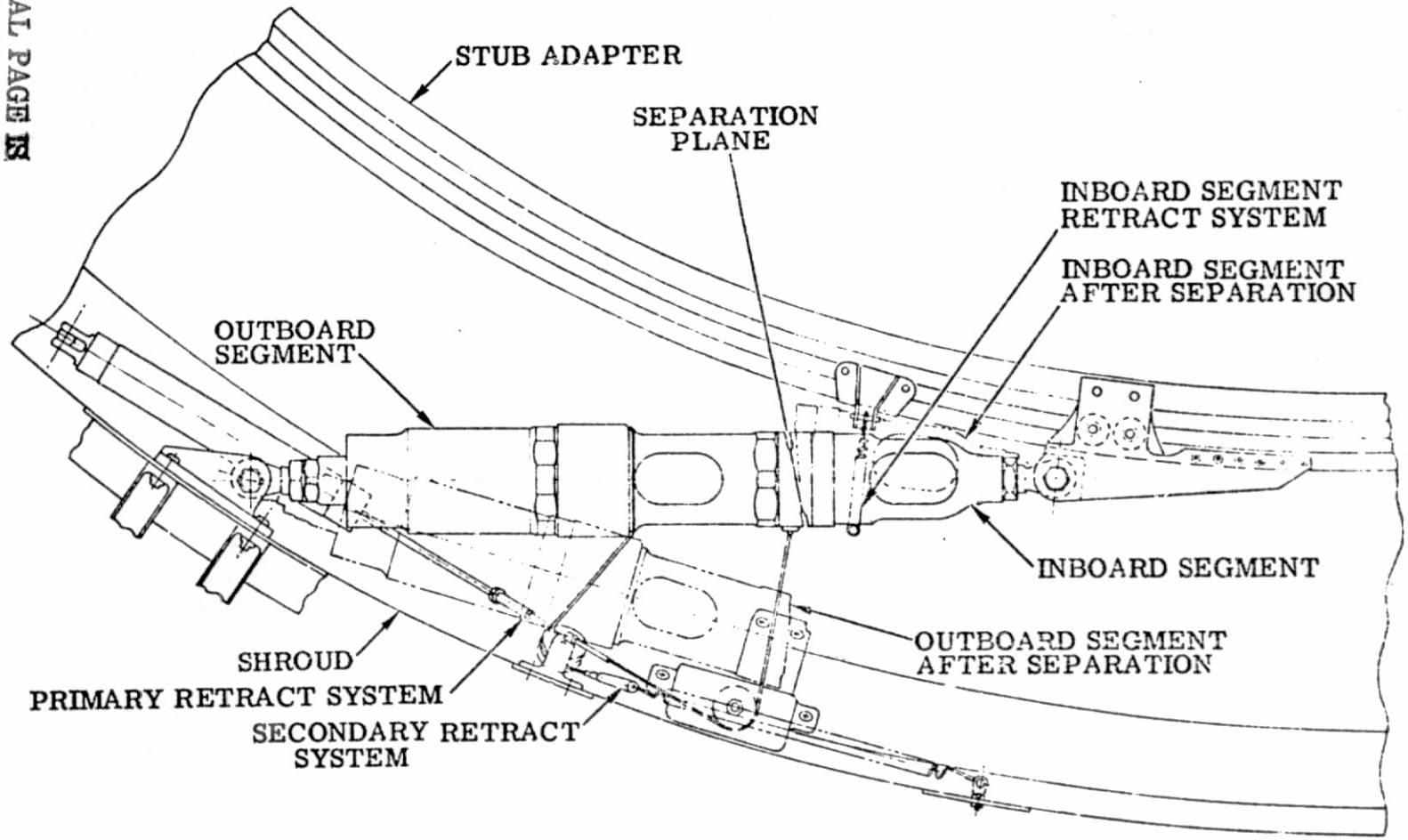

FIGURE III-2. FORWARD BEARING REACTOR STRUT INSTALLATION.

ORIGINAL PAGE IS
OF POOR QUALITY

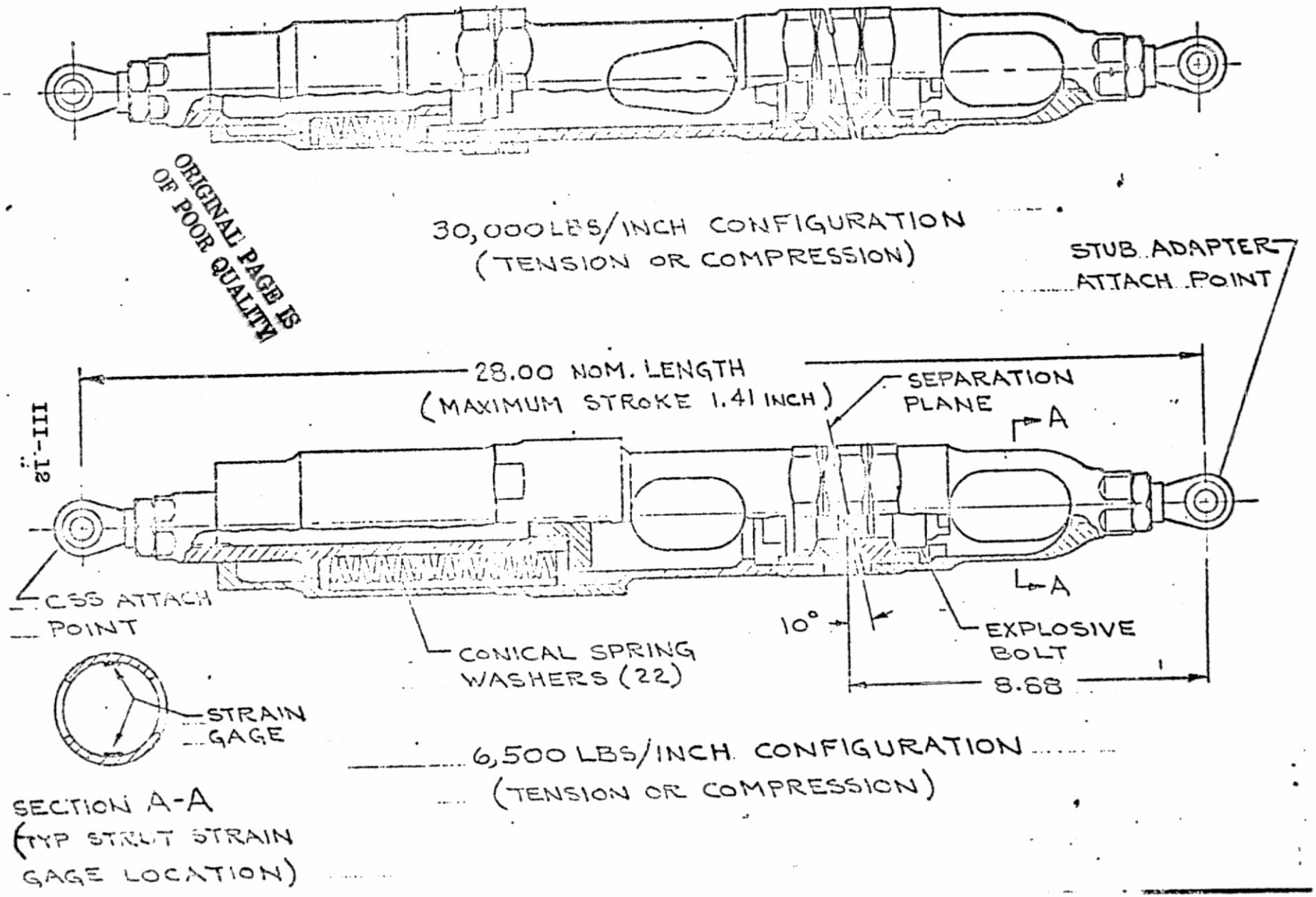

FIGURE III-3. FORWARD BEARING REACTOR STRUT.

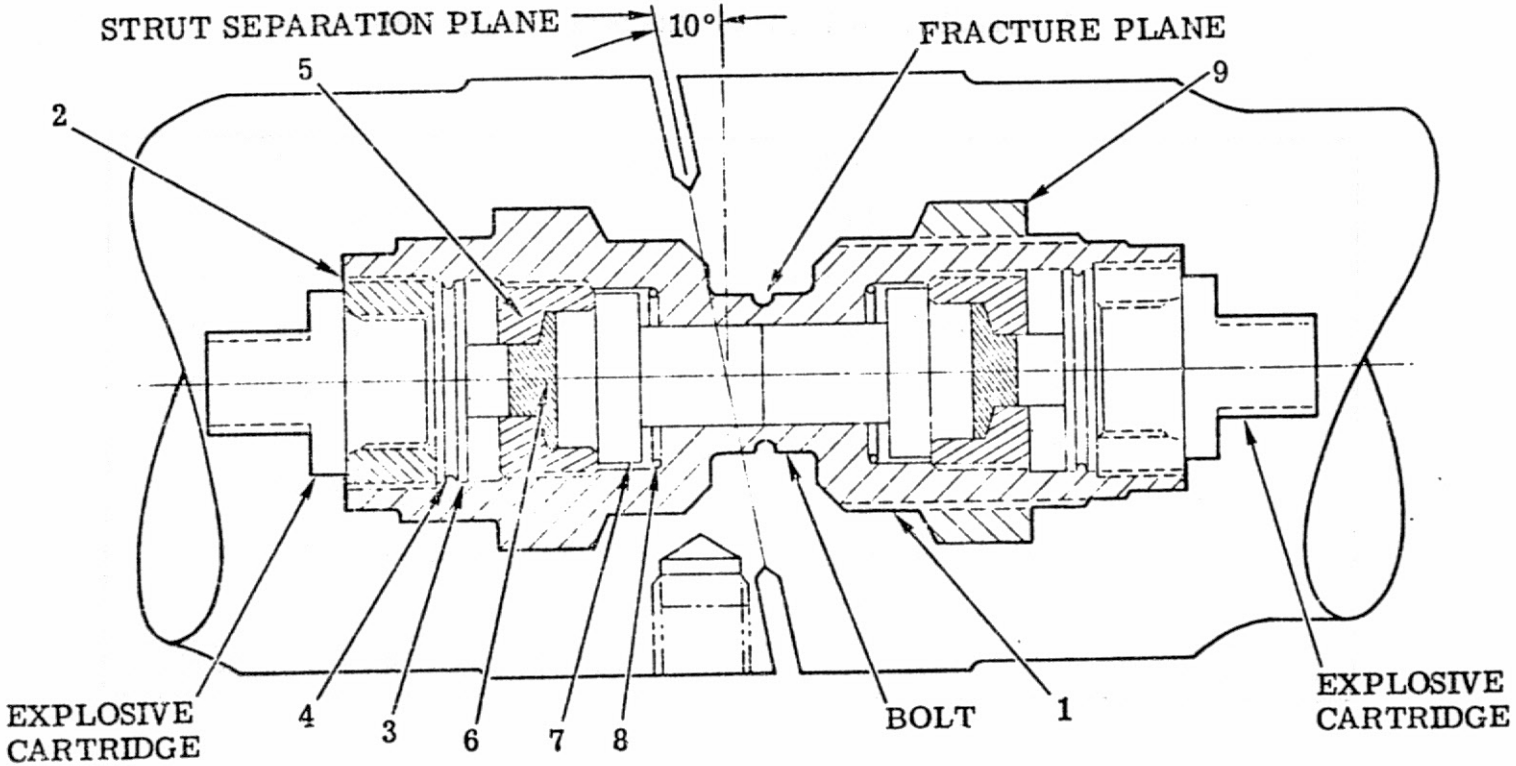

ITEM NO	NOMENCLATURE	MATERIAL	QTY/ BOLT
1	HOUSING	STEEL	1
2	RETAINER	MAR. STEEL	2
3	PISTON - PRIMARY	MAR. STEEL	2
4	O-RING	TEFLON	2
5	INSERT	MAR. STEEL	2

ITEM NO.	NOMENCLATURE	MATERIAL	QTY/ BOLT
6	COUPLER	SILICONE RUBBER	2
7	PISTON - SECONDARY	MAR. STEEL	2
8	RING	COPPER	2
9	NUT	4340 STEEL	1

FIGURE III-4. FBR & FORWARD SEAL SEPARATION BOLT ASSEMBLY.

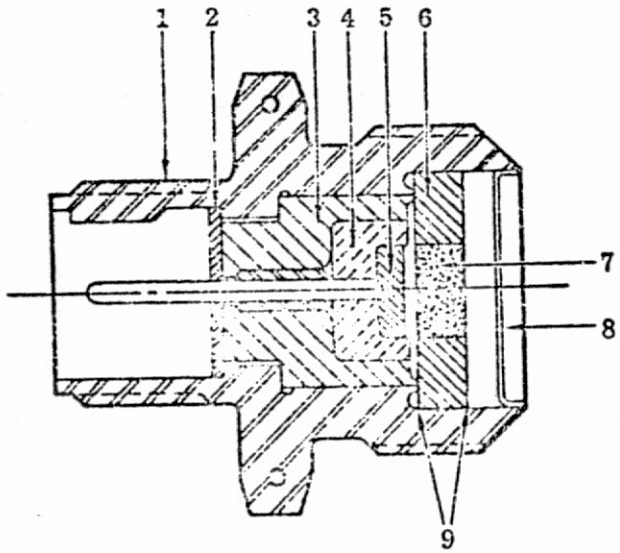

ITEM NO.	NOMENCLATURE	MATERIAL	QTY/CARTRIDGE
1	CARTRIDGE BODY	17-4PH CRES	1
2	RUBBER DISK, SEALING	SILICONE RUBBER	1
3	HEADER BODY ASSY.	304 CRES	1
4	CHARGE CUP	CERAMIC	1
5	INITIATION CHARGE	PYROTECHNIC	1
6	MAIN CHARGE PELLET	PYROTECHNIC	1
7	CORE CHARGE	PYROTECHNIC	1
8	CLOSURE CUP	347 CRES	1
9	EPOXY ON ISOMICA DISC	EPOXY	1

FIGURE III-5. ELECTRO EXPLOSIVE CARTRIDGE.

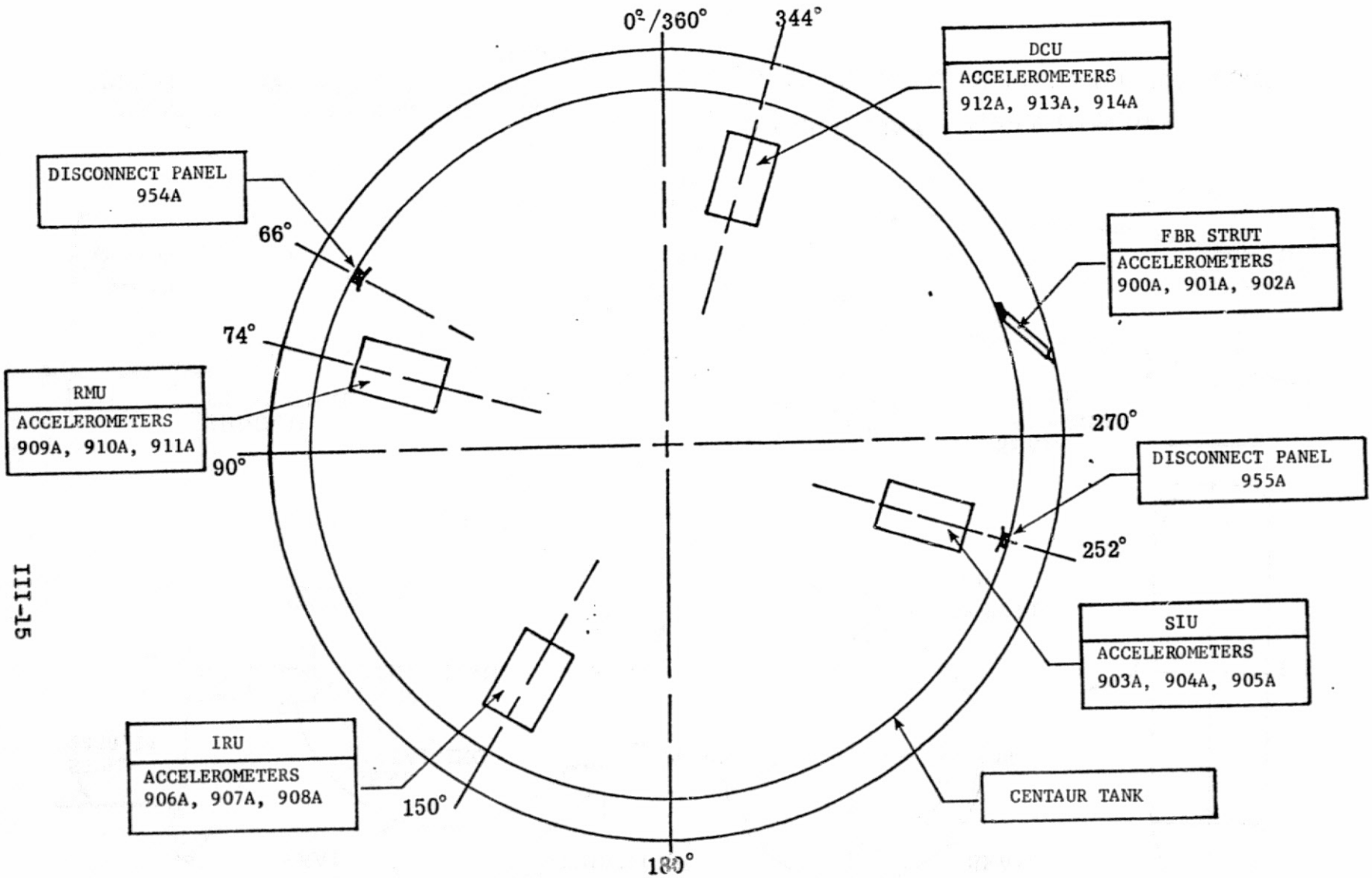

FIGURE III-6. LOCATION OF ACCELEROMETERS ON THE EQUIPMENT MODULE AND FBR STRUT.

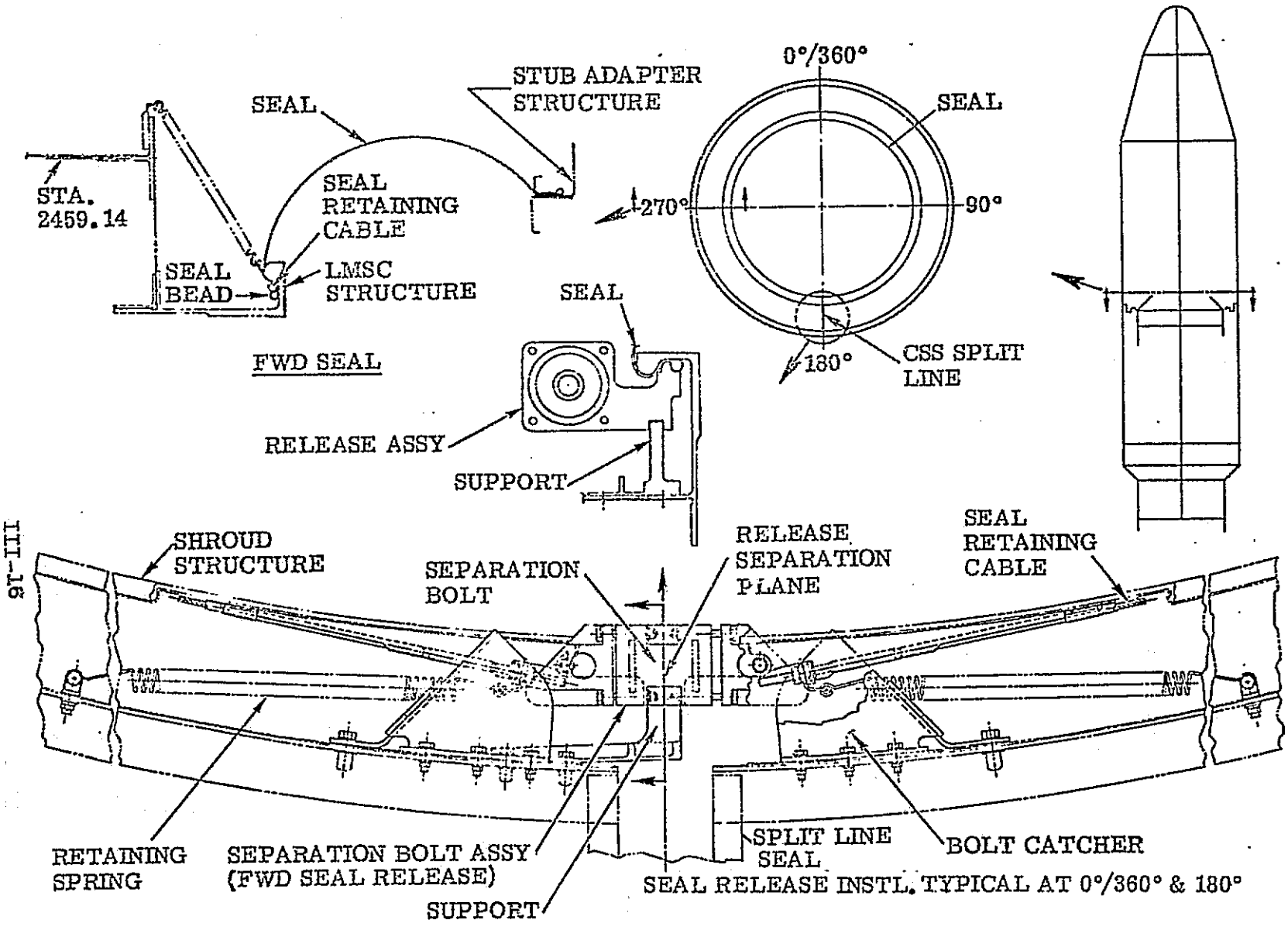

III-18

FIGURE III-7. FORWARD SEAL.

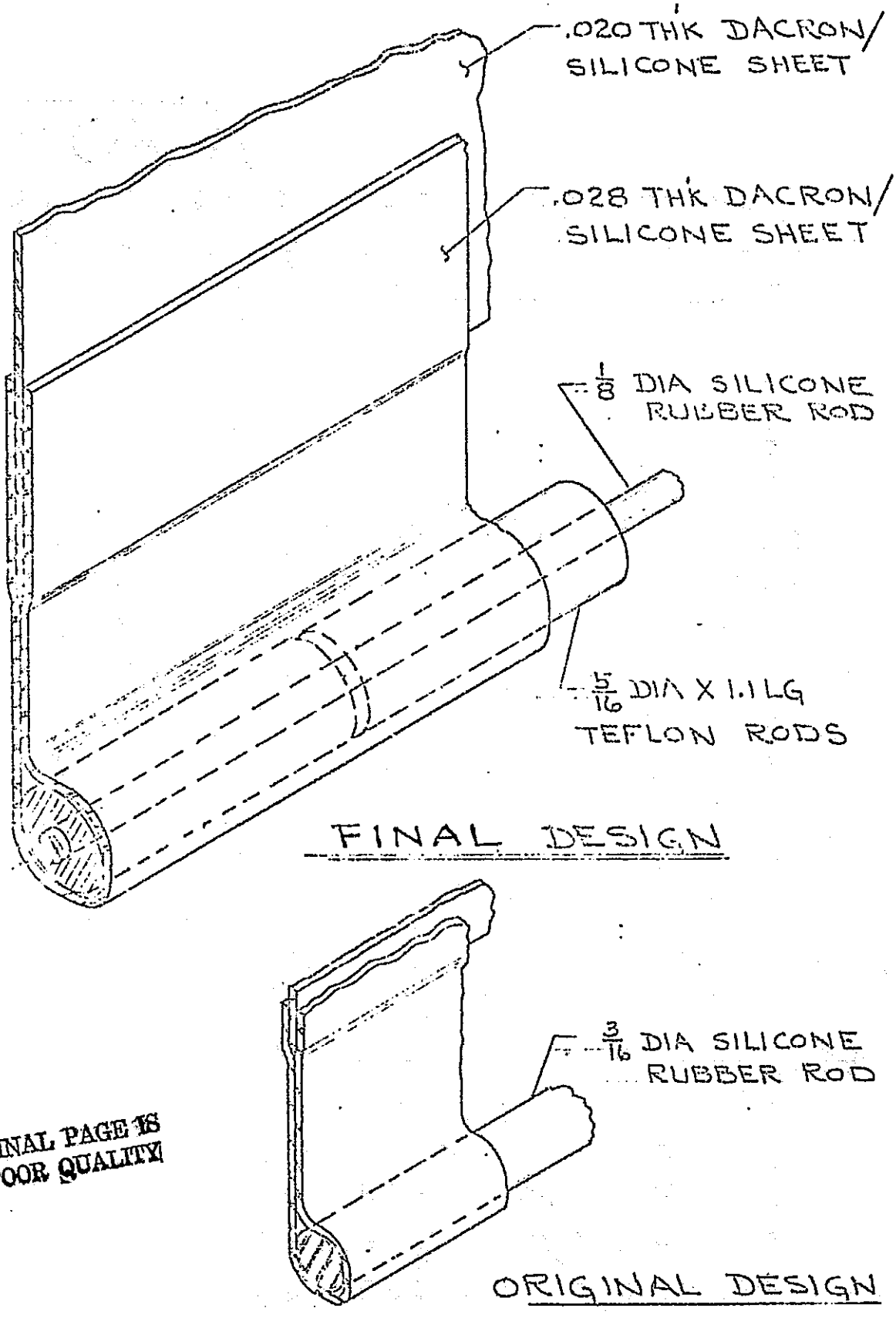

ORIGINAL PAGE IS OF POOR QUALITY

FIGURE III -8. FORWARD SEAL BEAD.

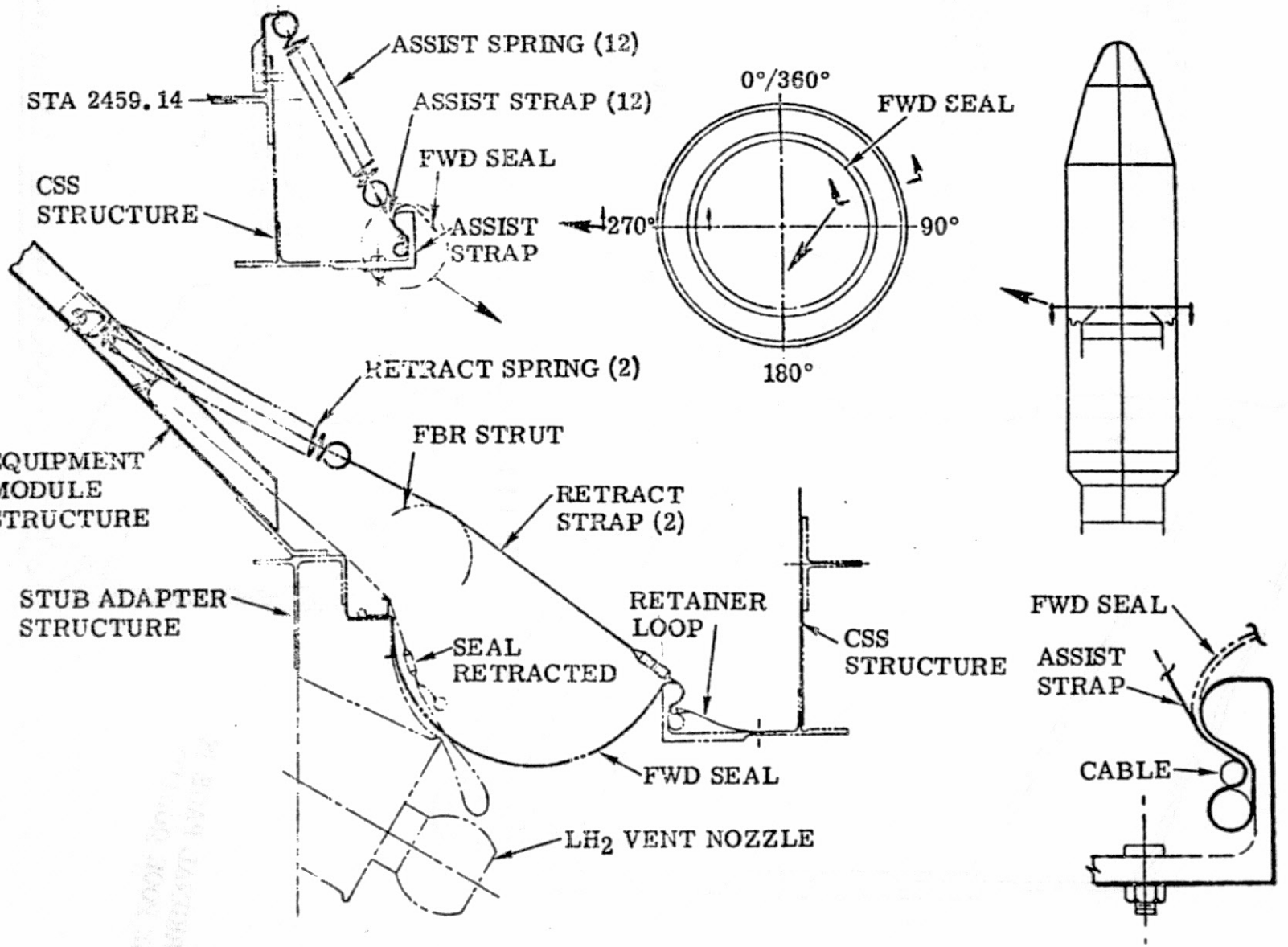

FIGURE III-9. FORWARD SEAL RELEASE ASSIST SYSTEM.

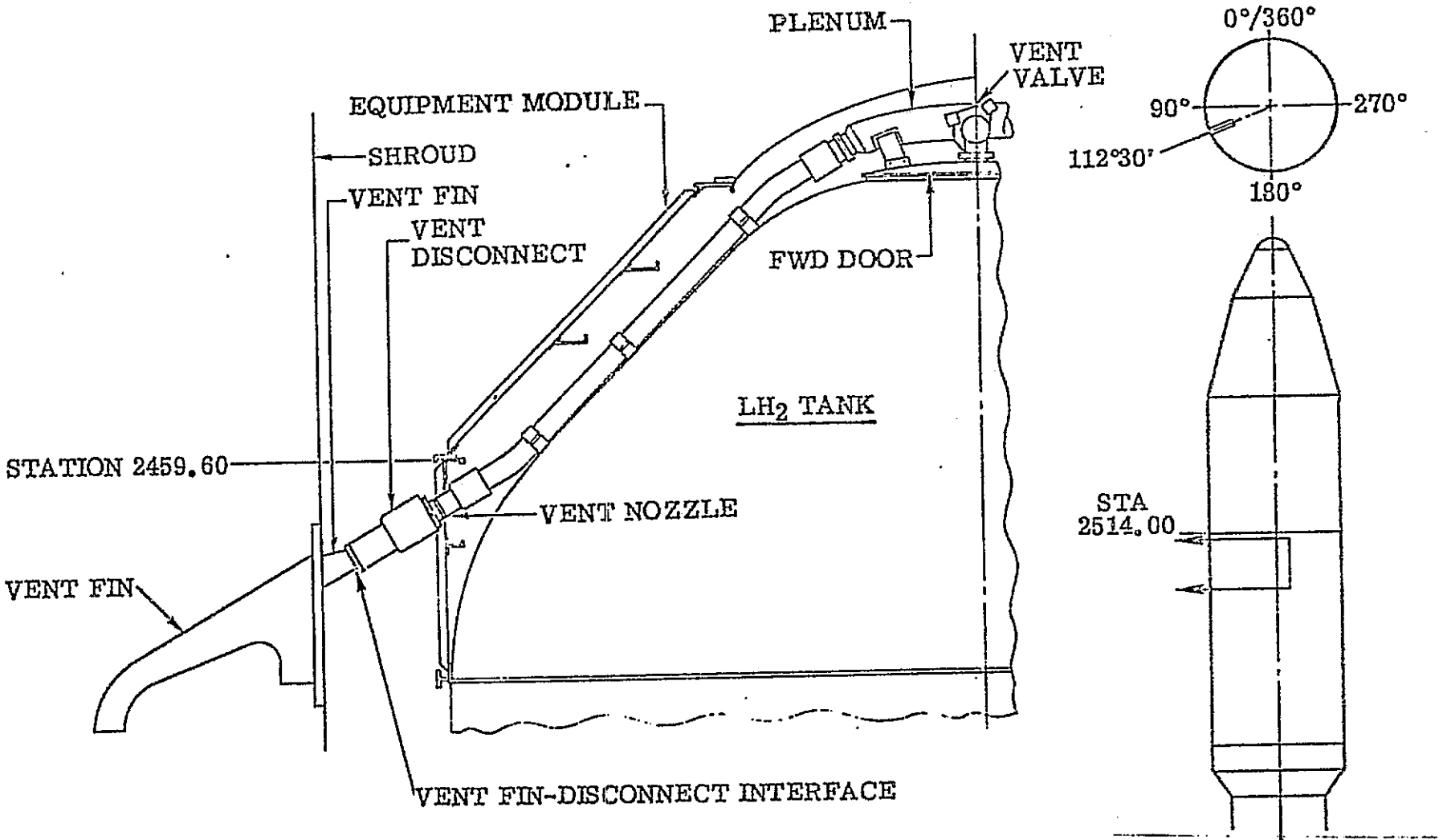

FIGURE III-10. LH_2 VENT DISCONNECT SYSTEM.

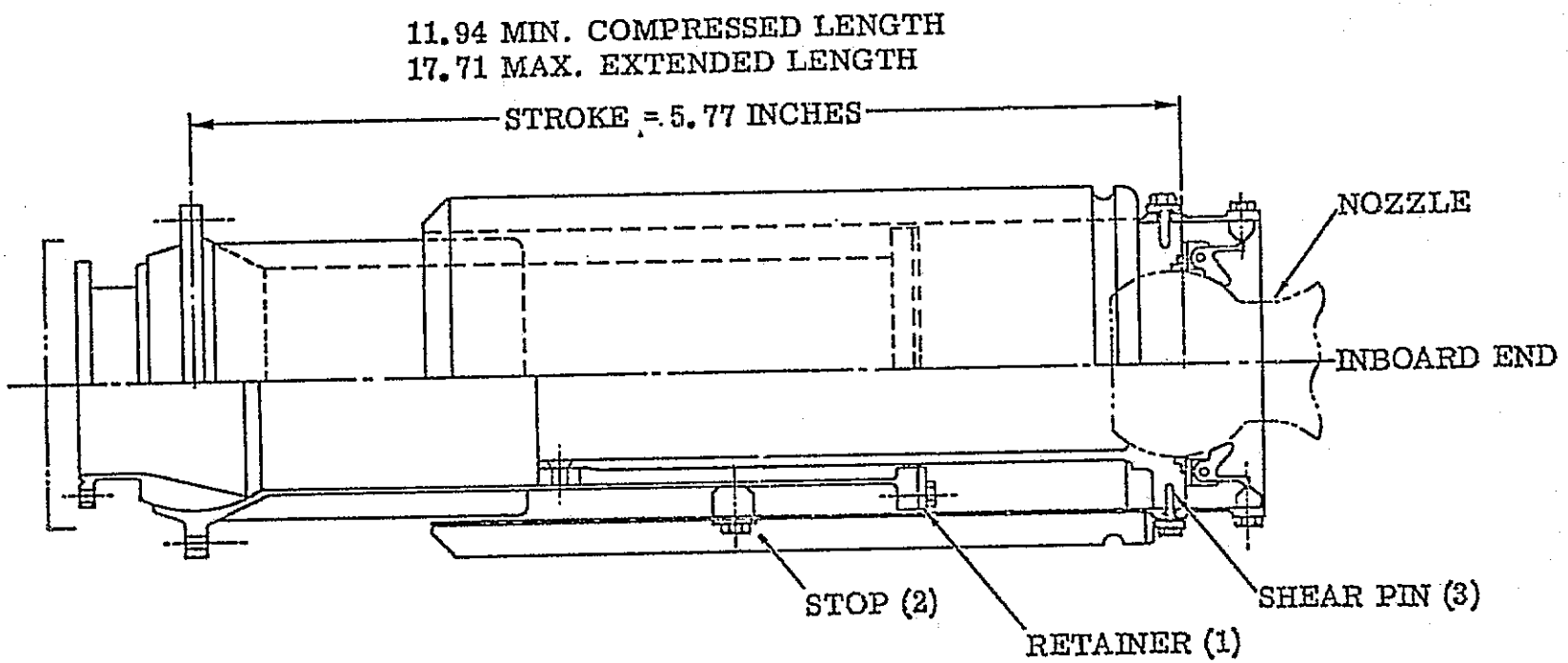

FIGURE III-11. LH_2 VENT DISCONNECT DETAILS.

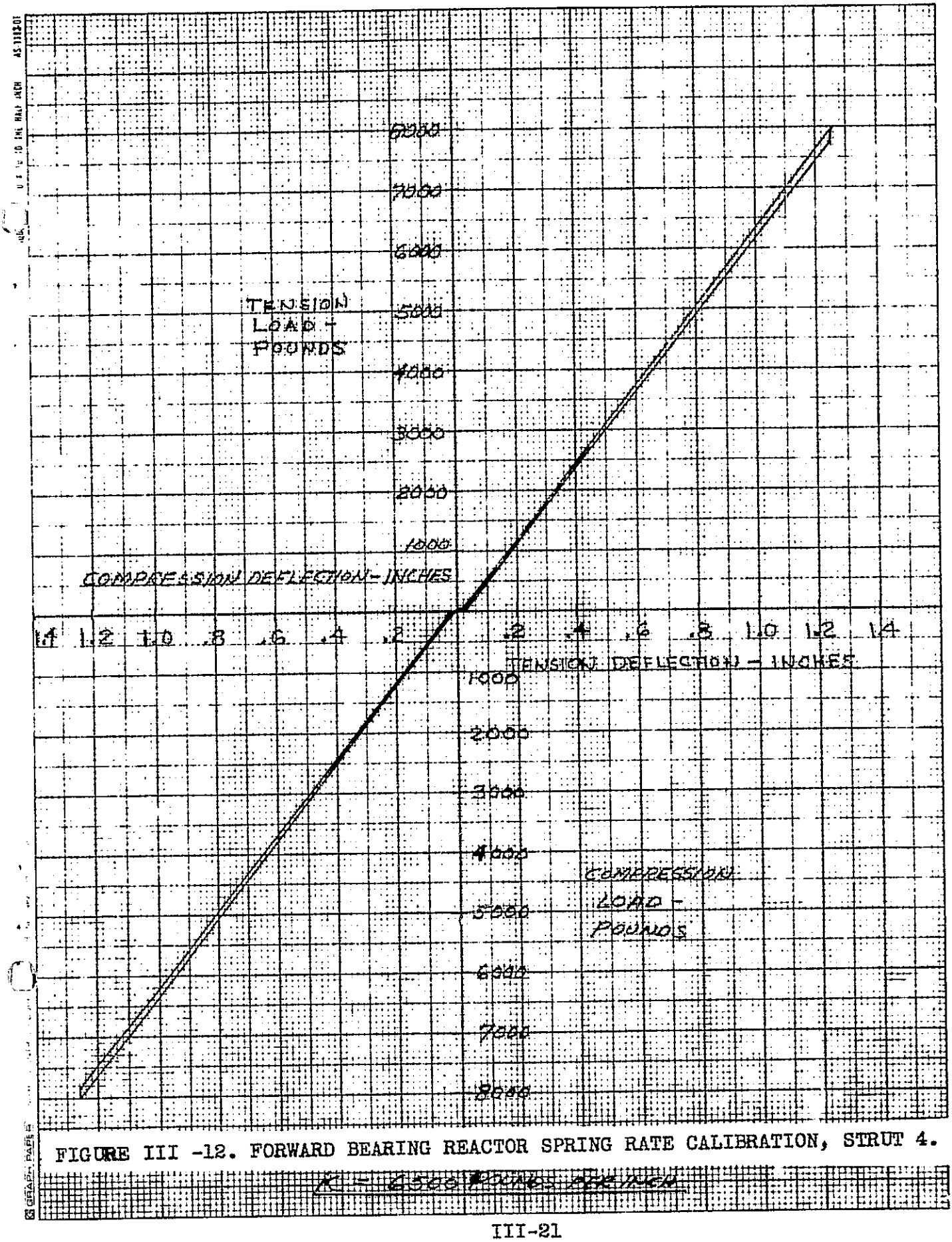

FIGURE III -12. FORWARD BEARING REACTOR SPRING RATE CALIBRATION, STRUT 4.

K = 6500 POUNDS PER INCH

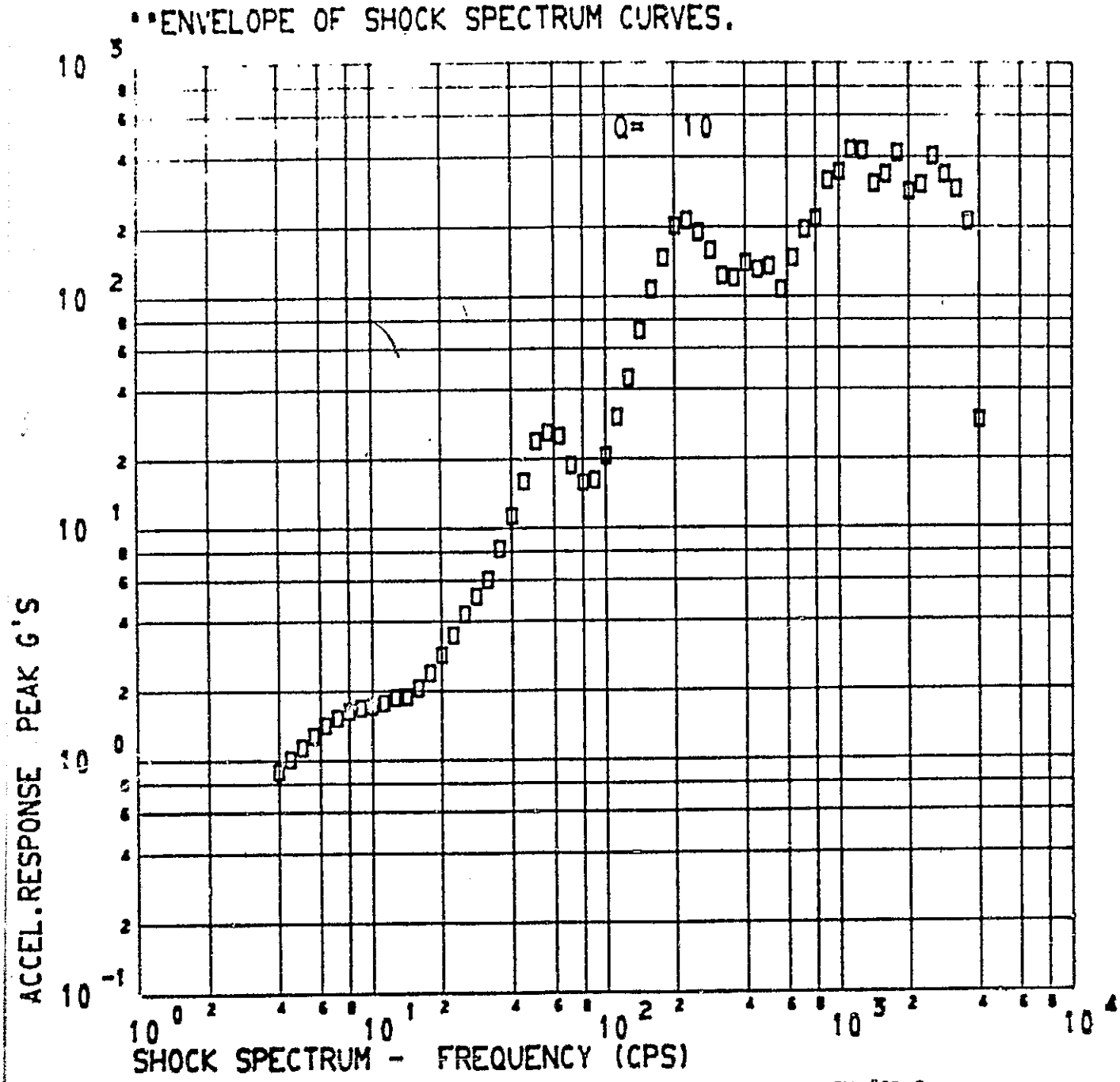

FIGURE III-13. FBR STRUT DISCONNECT. LIMIT LOAD STRUCTURAL TEST #6L-2.
PACKAGES MOUNTED ON CENTAUR EQUIPMENT MODULE

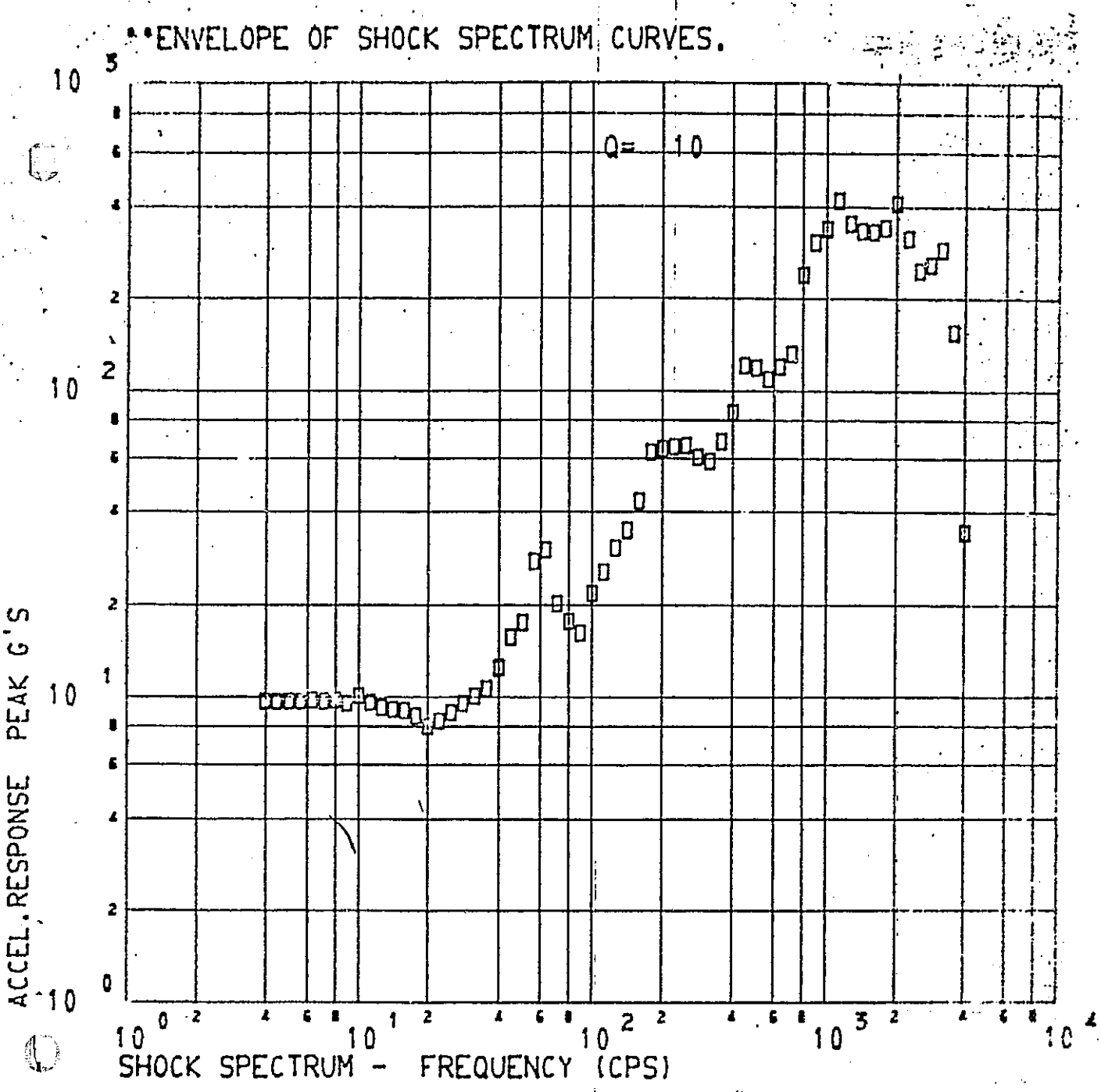

FIGURE III-14. FBR STRUT DISCONNECT. LIMIT LOAD STRUCTURAL TEST #7L-3. PACKAGES MOUNTED ON CENTAUR EQUIPMENT MODULE

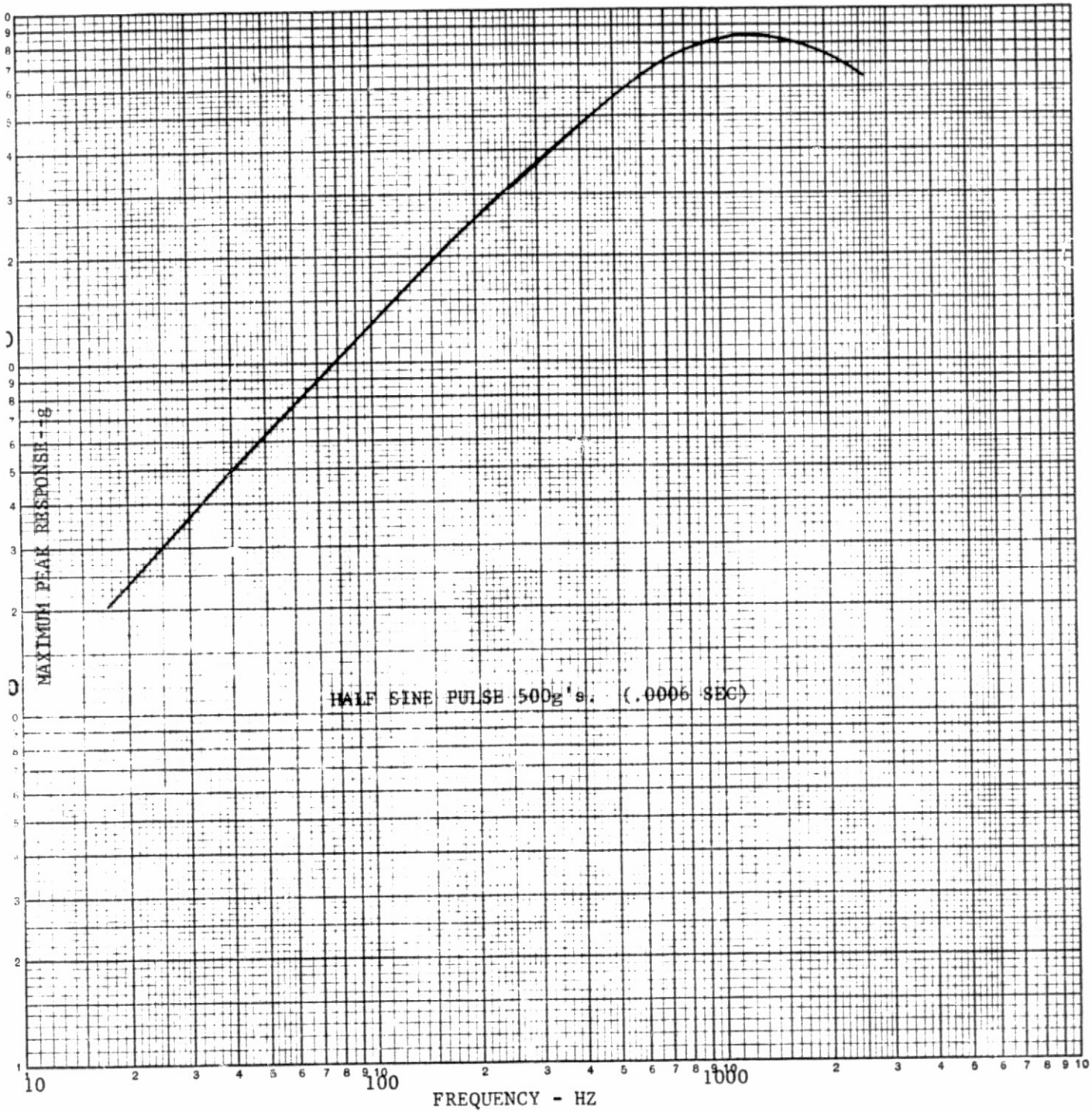

FIGURE III-15. SHOCK QUALIFICATION SPECIFICATION FOR PACKAGES MOUNTED ON THE CENTAUR EQUIPMENT MODULE

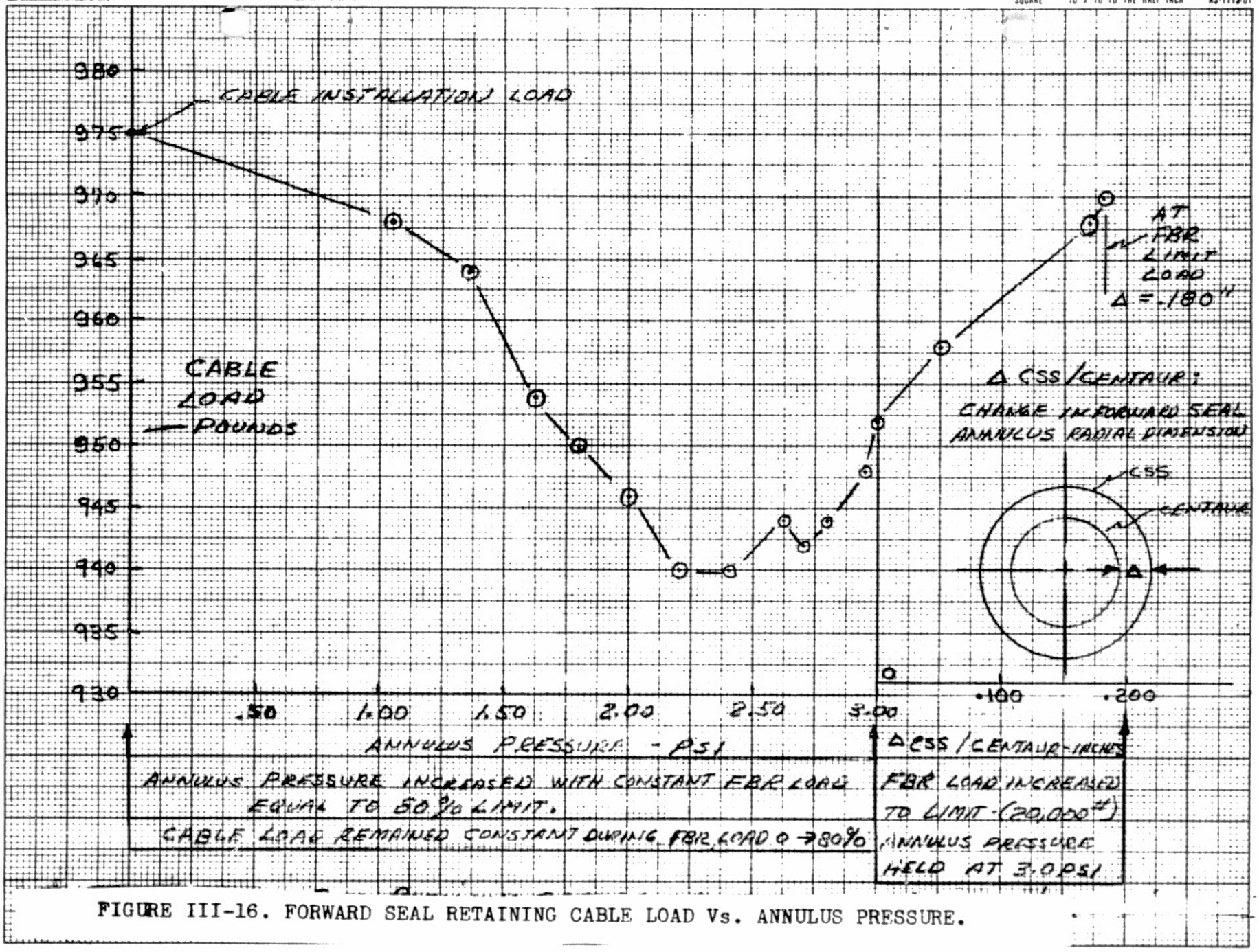

FIGURE III-16. FORWARD SEAL RETAINING CABLE LOAD Vs. ANNULUS PRESSURE.

IV TITAN SKIRT STRUCTURE

By R. W. York

SUMMARY

The loads applied during the limit load test program verified that the Titan skirt/ISA combination could sustain the design loads without permanent deformation. Stress levels recorded throughout the Titan skirt were less than limit values and, in general, as predicted. Load transfer across the Titan skirt/ISA interface was evenly distributed. Load distribution in the skirt aft of the ISA doors was essentially as predicted. All test objectives were accomplished without damage to the Titan skirt.

DESCRIPTION

The Titan skirt is the most forward section of the Titan vehicle. It is a 10-foot diameter, 76-inch long aluminum cylinder of ring reinforced skin and stringer construction. A Titan guidance equipment truss is mounted in the forward end of the structure. Details of the Titan skirt configuration are shown in figures IV-1 and IV-2.

The Titan skirt was mounted on the lower distribution cylinder fixture. Shimming and grouting were utilized as required to obtain 100% contact between the skirt and the lower distribution cylinder. The 132 bolts that fastened the Titan skirt mounting ring to the lower distribution cylinder were supplemented by 24 C-clamps placed two each in line with Titan stringers 1, 4, 7, 10, 13, 16, 19, 22, 25, 28, 31 and 34. The C-clamps were torqued to 100-150 ft.-lbs. and then fixed by welding the screw thread to the clamp body. They were substituted for bolts that were not installed. Following completion of Tests 3L, 4L, and 2L-1, but prior to Test 1L-1, the existing steel bolts and nuts at Station 2127 interface (Titan skirt/ISA) were replaced with flight-type bolts. This resulted from a flight hardware specification change to incorporate stress-corrosion resistant bolts.

The instrumentation on the Titan skirt is described in reference 7.

OBJECTIVES

As stated in Section I, the specific objective of the test program regarding the Titan skirt was to demonstrate its ability to withstand limit loads introduced through the CSS/Centaur structures. The design criteria of the CSS/Centaur structures were based on the Titan skirt

design limit capability of 864,000 pounds compression and 720,000 pounds tension equivalent axial limit load at Station 2127.43 (Titan skirt/ISA interface). Axial and shear test loads that were applied to the CSS/Centaur structures were selected to produce these equivalent axial loads at the Titan skirt forward Station 2127.43. Detailed objectives were to verify the structural capability of the Titan skirt and the load transfer distribution at the ISA interface for the equivalent axial limit loads at the following azimuths and conditions:

Test No.	Load	Azimuth
1L-2	Compression	90^{o}
2L-1	Tension	90^{o}
3L	Compression	150^{o}
4L	Tension	150^{o}
5L-2	Tension	60^{o}
6L-1	Compression	240^{o} LN_2 in Centaur
7L-2	Compression	90^{o} LN_2 in Centaur

TEST RESULTS

Test 1L-2 - The applied loads of 36,900 pounds shear and 100,400 pounds axial compression resulted in an equivalent axial load of 866,690 pounds compression at Station 2127. The design limit value at this interface is 864,000 pounds compression. The shear load was applied at 90^{o} azimuth (90^{o} to the CSS split line) and resulted in maximum compression loads being developed in Titan skirt stringers 14 and 15. The maximum compressive stresses resulting from bending moments induced on these stringers were lower than predicted indicating the ISA structure was stiffer than anticipated. The average stringer stress near the interface was 22,814 psi on stringer 14, and 24,461 psi on stringer 15. This indicates a relatively uniform load distribution across the interface as predicted. Stringer stress levels aft of the interface were generally lower than anticipated. No tensile stresses were measured during this test. See Table IV-1 for a summary of the data.

Test 2L-1 - The applied loads of 36,900 pounds shear and 43,400 pounds axial compression developed an equivalent axial load of 722,890 pounds tension at Station 2127. The design limit value in tension is 720,000 pounds. The shear load was applied at 270^{o} azimuth (90^{o} to CSS split line) and resulted in maximum tension loads being developed in Titan skirt stringers 14 and 15. Stringers 14 and 15 experienced maximum tensile stresses, near Station 2127. of 31, 913 psi and 35,329 psi, respectively. These values were higher than predicted and resulted from increased stringer bending moments. However, these values are well within the limit allowables. The average stringer tensile stress near the interface was 22,904 psi in stringer 14 and 24,705 psi in stringer 15. These values indicate essentially a uniform distribution of load. Tensile stresses were not recorded in the Titan structure aft of the interface.

ORIGINAL PAGE IS
OF POOR QUALITY

The compression stresses in stringers 32 and 33 (180° opposite stringers 14 and 15) were lower than experienced in Test 1L-2 because the axial compressive load requirements were lower. See Table IV-2 for a summary of the data.

Test 3L - The applied loads of 36,500 pounds shear and 100,500 pounds axial compression resulted in an equivalent axial load of 858,480 pounds compression at Station 2127. The shear load application at 150° azimuth (30° off the CSS split line) resulted in maximum compression loads being developed in Titan skirt stringers 20 and 21. The maximum compressive stress resulting from induced bending moments was 27,545 psi recorded on the outboard flange of stringer 20 near the interface. The same stringer experienced 17,248 psi compression stress on the inboard flange. Average stringer stresses near the interface were 22,396 psi on stringer 20, and 22,492 psi on stringer 21. These values indicate a uniform distribution of load across the interface. Compressive stresses aft of the interface were generally less than predicted. Maximum tensile stress of 28,157 psi was recorded on the inboard flange of stringer 3 (180° opposite the compression stringers) near the interface. This was approximately 10% higher than predicted but well within the limit allowables. See Table IV-3 for a summary of the data.

Test 4L - The applied loads of 36,900 pounds shear and 43,300 pounds axial compression resulted in an equivalent axial tension load of 722,990 pounds at Station 2127. The shear load was applied at 330° azimuth (30° off the CSS split line) and resulted in maximum tension loads being developed in Titan skirt stringers 20 and 21. Stringers 20 and 21 experienced maximum tensile stresses near the interface of 26,884 psi and 28,219 psi, respectively. These maximums were within 12% of the predicted values but well within the limit allowables. The average stringer tensile stress was 21,443 psi in stringer 20, and 21,640 psi in stringer 21. These values indicate essentially a uniform distribution of load. Tensile stresses aft of the interface followed the expected pattern of distribution. Stresses on the compression side of the Titan skirt were small and, in general, followed the predicted pattern. See Table IV-4 for a summary of the data.

Test 5L-2 - The applied loads of 36,600 pounds shear and 44,300 pounds axial compression resulted in an equivalent axial tension load of 715,760 pounds at Station 2127. The shear load was applied at 240° azimuth (60° off the CSS split line) and resulted in average compression loads of 22,182 psi in stringer 29, 21,349 psi in stringer 30, and 20,301 psi in stringer 31. This indicates a uniform distribution of load across the interface. Tensile stresses were not recorded during this test. See Table IV-5 for a summary of the data.

Test 6L-1 - The applied loads of 36,400 pounds shear and 107,400 pounds axial compression resulted in an equivalent axial load of 862,830 pounds compression at Station 2127. The shear load was applied at 240° azimuth (60° off the CSS split line). This resulted in maximum compression loads being developed in Titan skirt stringers 29, 30, and 31. Stringers

ORIGINAL PAGE IS
OF POOR QUALITY

29 and 30 are in line with the ISA access door immediately forward of Station 2127. The influence of this access door on load distribution across Station 2127 was determined to be negligible. The average compressive stress level across the three stringers was 22,798 psi at stringer 29, 21,765 psi at stringer 30, and 21,226 psi at stringer 31. No tensile stresses were recorded during this test. The Centaur tanks contained LN_2 during this test. The presence of LN_2 did not appear to affect the Titan structure. Approximate temperatures experienced were 20°F at the interface and 40°F at the base of the Titan skirt. The load level achieved during this test represents 99.9% of design limit equivalent axial load. Structural constraints in the ISA and the CSS prevented attainment of 100% design limit load in the Titan skirt. See Table IV-6 for a summary of the data.

Test 7L - The applied loads of 36,500 pounds shear and 105,500 pounds axial compression resulted in an equivalent axial load of 863,480 pounds compression at Station 2127. The shear load was applied at 90° azimuth (90° to CSS split line). This resulted in maximum compression loads being developed in Titan skirt stringers 14 and 15. Maximum compressive stresses recorded in these stringers near the interface were lower than predicted. The variation of cross-sectional stress level in either stringer was not as great as predicted indicating the ISA structure was stiffer than anticipated and transferred a smaller stringer bending moment across the interface. The average compressive stress level across the two stringers near the interface was 20,455 psi at stringer 14, and 22,527 psi at stringer 15. This indicates essentially a uniform distribution of load across the interface. The Centaur tanks contained LN_2 during this test. The presence of LN_2 did not appear to affect the Titan structure. Tensile stresses were not recorded during this test. The load level achieved during this test represents 99.9% of design limit equivalent axial load. Structural constraints in the ISA and the CSS prevented attainment of 100% design limit load in the Titan skirt. See Table IV-7 for a summary of the data.

SUMMARY OF TEST RESULTS

The loads applied during the test program confirmed that the Titan skirt structure, when mated to a Centaur ISA, is capable of sustaining design limit loads without permanent deformation when the Centaur stage is at either cryogenic or ambient temperature conditions. The tests further demonstrated that the ISA hardware effectively transferred load in a uniform manner across the Titan/Centaur interface to the Titan skirt. Longitudinal stringer loads experienced by the Titan skirt aft of cutouts or doors in the ISA were determined to be within analytically predicted values.

TABLE IV-1

TEST DATA SUMMARY - TEST NO. 1L-2

Maximum Applied Shear Load Vs = 36,900 Lbs.
Maximum Applied Axial Load Pax = 100,400 lbs. Compression

Gage No.	Inches Aft of Station 2127.43	MMC Stringer No.	Direction	Maximum Predicted Value PSI	Maximum Test Value PSI	Remarks
4190S	4.0	15	Axial	-13500	-19052	
4191S	"	15	"	-13500	-19731	
4192S	"	15	"	-36000	-29531	
4193S	17.38	15	"	-24000	-20502	
4194S	"	15	"	-24000	-21643	
4195S	"	15	"	-32000	-29993	
4196S	33.35	15	"	-40000	-23831	
4197S	"	15	"	-40000	-24263	
4198S	"	15	"	-24000	-22013	
4199S	65.90	15	"	-13500	-18772	
4200S	"	15	"	-13500	-19582	
4201S	4.0	14	"	-13500	-21458	
4202S	"	14	"	-36000	-24170	
4203S	17.38	14	"	-24000	-16554	
4204S	17.38	14	"	-32000	-25434	
4205S	33.35	14	"	-40000	-20224	
4206S	"	14	"	-40000	-20841	
4207S	"	14	"	-24000	-23122	

TABLE IV-2

TEST DATA SUMMARY - TEST NO. 2L-1

Maximum Applied Shear Load Vs = 36,900 Lbs.
Maximum Applied Axial Load Pax = 43,400 lbs. Compression

Gage No.	Inches Aft of Station 2127.43	MMC Stringer No.	Direction	Maximum Predicted Value PSI	Maximum Test Value PSI	Remarks
4190S	4.0	15	Axial	25000	35329	
4192S	4.0	15	"	25000	14081	
4201S	4.0	14	"	25000	31912	
4202S	4.0	14	"	25000	13895	
4232S	17.38	33	"	-20000	-23092	
4233S	"	33	"	-20000	-23461	
4234S	"	33	"	-26500	-1422	Out
4235S	33.35	33	"	-33500	-23893	
4236S	"	33	"	-33500	-23215	
4237S	"	33	"	-20000	-23924	
4238S	65.9	33	"	-12000	-19489	
4239S	"	33	"	-12000	-17838	
4240S	17.38	32	"	-20000	-20841	
4241S	"	32	"	-20000	-21211	
4242S	"	32	"	-26500	-24972	
4243S	33.35	32	"	-33500	-20995	
4244S	"	32	"	-33500	-21303	
4245S	"	32	"	-20000	-24263	

TABLE IV-3

TEST DATA SUMMARY - TEST NO. 3L

Maximum Applied Shear Load Vs = 36,500 Lbs.
Maximum Applied Axial Load Pax = 100,500 Lbs. Compression

Gage No.	Inches Aft of Station 2127.43	MMC Stringer No.	Direction	Maximum Predicted Value PSI	Maximum Test Value PSI	Remarks
4389					8252	
4390S					12915	
4391S	4.0	20	Axial	-13500	-17248	
4392S	4.0	20	"	-36000	-27545	
4393S	17.38	20	"	-24000	-17125	
4394S	"	20	"	-24000	-17510	
4395S	"	20	"	-32000	-21473	
4396S	33.4	20	"	-40000	-4605	Out
4397S	"	20	"	-40000	-20933	
4398S	"	20	"	-24000	-21720	
4399S	4.0	3	"	25000	28157	
4400S	4.0	3	"	25000	16110	
4401S	17.4	3	"	25000	20790	
4402S	"	3	"	-	20278	
4403S	"	3	"	25000	16420	
4404S	33.4	3	"	-	15924	
4405S	"	3	"	-	371	Out
4406S	"	3	"	-	18000	
4529S	9.0	21	"	-13500	-19191	
4530S	"	21	"	-13500	-20158	
4531S	"	21	"	-36000	-25310	
4532S	17.4	21	"	-24000	-24602	
4533S	"	21	"	-24000	-24454	
4534S	"	21	"	-32000	-24802	
4535S	33.4	21	"	-40000	-26019	
4536S	"	21	"	-40000	-25684	
4537S	"	21	"	-24000	-24864	
4538S	65.9	21	"	-13500	-16794	
4539S	65.9	21	"	-13500	-16685	

TABLE IV-4

TEST DATA SUMMARY - TEST NO. 4L

Maximum Applied Shear Load Vs = 36,900 Lbs.
Maximum Applied Axial Load Pax = 43,300 Lbs. Compression

Gage No.	Inches Aft of Station 2127.43	MMC Stringer No.	Direction	Maximum Predicted Value PSI	Maximum Test Value PSI	Remarks
4391S	4.0	20	Axial	25000	26885	
4392S	4.0	20	"	25000	16002	
4393S	17.4	20	"	NA	20092	
4394S	"	20	"	NA	20154	
4395S	"	20	"	NA	17241	
4396S	33.4	20	"	NA	3556	Out
4397S	"	20	"	NA	16404	
4398S	"	20	"	NA	19627	
4399S	4.0	3	"	-12000	-16739	
4400S	"	3	"	-32000	-22198	
4401S	17.4	3	"	-20000	-23000	
4402S	"	3	"	-20000	-22722	
4403S	"	3	"	-26500	-25434	
4404S	33.4	3	"	-32000	-22259	
4405S	"	3	"	-32000	-896	Out
4406S	"	3	"	-20000	-27929	
4529S	9.0	21	"	25000	28219	
4530S	"	21	"	25000	27964	
4531S	"	21	"	25000	15189	
4532S	17.4	21	"	NA	24992	
4535S	"	21	"	NA	24862	
4534S	"	21	"	NA	13554	
4535S	33.4	21	"	NA	22976	
4536S	"	21	"	NA	22137	
4537S	"	21	"	NA	12842	
4538S	65.9	21	"	15000	14219	
4539S	"	21	"	15000	14063	

TABLE IV-5

TEST DATA SUMMARY - TEST NO. 5L-2

Maximum Applied Shear Load Vs = 36,600 Lbs.
Maximum Applied Axial Load Pax = 44,300 Lbs. Compression

Gage No.	Inches Aft of Station 2127.43	MMC Stringer No.	Direction	Maximum Predicted Value PSI	Maximum Test Value PSI	Remarks
4451S	17.4	29	Axial	-24000	-20995	
4453S	17.4	29	"	-32000	-23369	
4454S	17.4	30	"	-24000	-20563	
4456S	17.4	30	"	-32000	-22136	
4457S	17.4	31	"	-24000	-20312	
4459S	17.4	31	"	-32000	-20471	

TABLE IV-6

TEST DATA SUMMARY - TEST NO. 6L-1

Maximum Applied Shear Load Vs = 36,400 Lbs.
Maximum Applied Axial Load Pax = 107,400 Lbs. Compression

Gage No.	Inches Aft of Station 2127.43	MMC Stringer No.	Direction	Maximum Predicted Value PSI	Maximum Test Value PSI	Remarks
4451S	17.4	29	Axial	-24000	-21519S	
4453S	17.4	29	"	-32000	-24078S	
4454S	17.4	30	"	-24000	-20409	
4456S	17.4	30	"	-32000	-23122	
4457S	17.4	31	"	-24000	-20378	
4459S	17.4	31	"	-32000	-22074	

TABLE IV-7

TEST DATA SUMMARY - TEST NO. 7L-2

Maximum Applied Shear Load Vs = 36,500 Lbs.
Maximum Applied Axial Load Pax = 105,500 Lbs. Compression

Gage No.	Inches Aft of Station 2127.43	MMC Stringer No.	Direction	Maximum Predicted Value PSI	Maximum Test Value PSI	Remarks
4190S	4.0	15	Axial	-13600	-17664	
4191S	4.0	15	"	-13600	-18250	
4192S	4.0	15	"	-36000	-27098	
4193S	17.4	15	"	-24000	-19854	
4194S	17.4	15	"	-24000	-19885	
4195S	17.4	15	"	-32000	-27128	
4196S	33.4	15	"	-40000	-21242	
4197S	33.4	15	"	-40000	-21550	
4198S	33.4	15	"	-24000	-20748	
4199S	65.9	15	"	-13600	-16093	
4200S	65.9	15	"	-13600	-17184	
4201S	4.0	14	"	-13600	-20008	
4202S	4.0	14	"	-36000	-20903	
4203S	17.4	14	"	-24000	-14024	
4204S	17.4	14	"	-32000	-23061	
4205S	33.4	14	"	-40000	-16739	
4206S	33.4	14	"	-40000	-20163	
4207S	33.4	14	"	-24000	-24201	

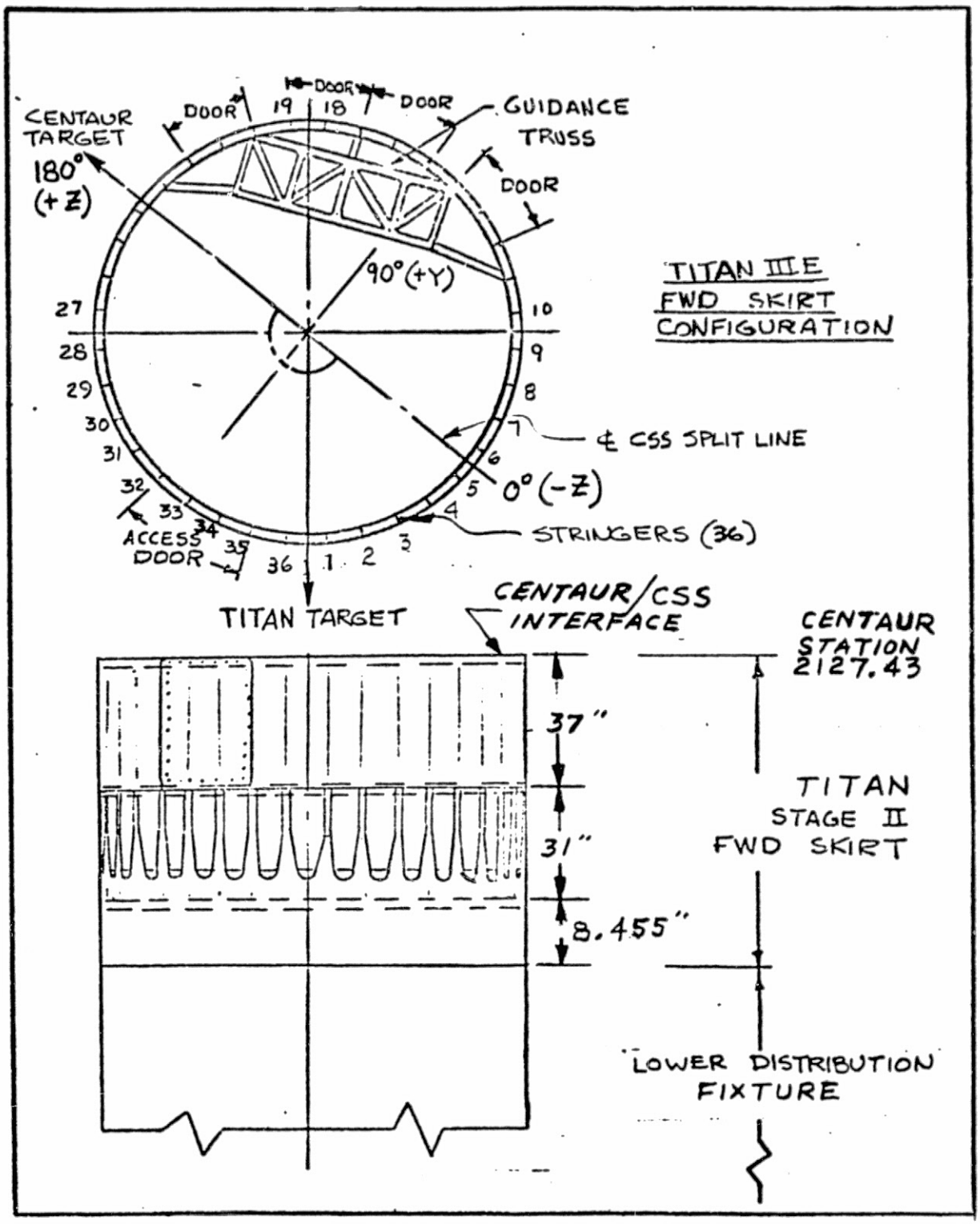

Figure IV-1. Titan Skirt Configuration

ORIGINAL PAGE IS
OF POOR QUALITY

ORIGINAL PAGE IS
OF POOR QUALITY

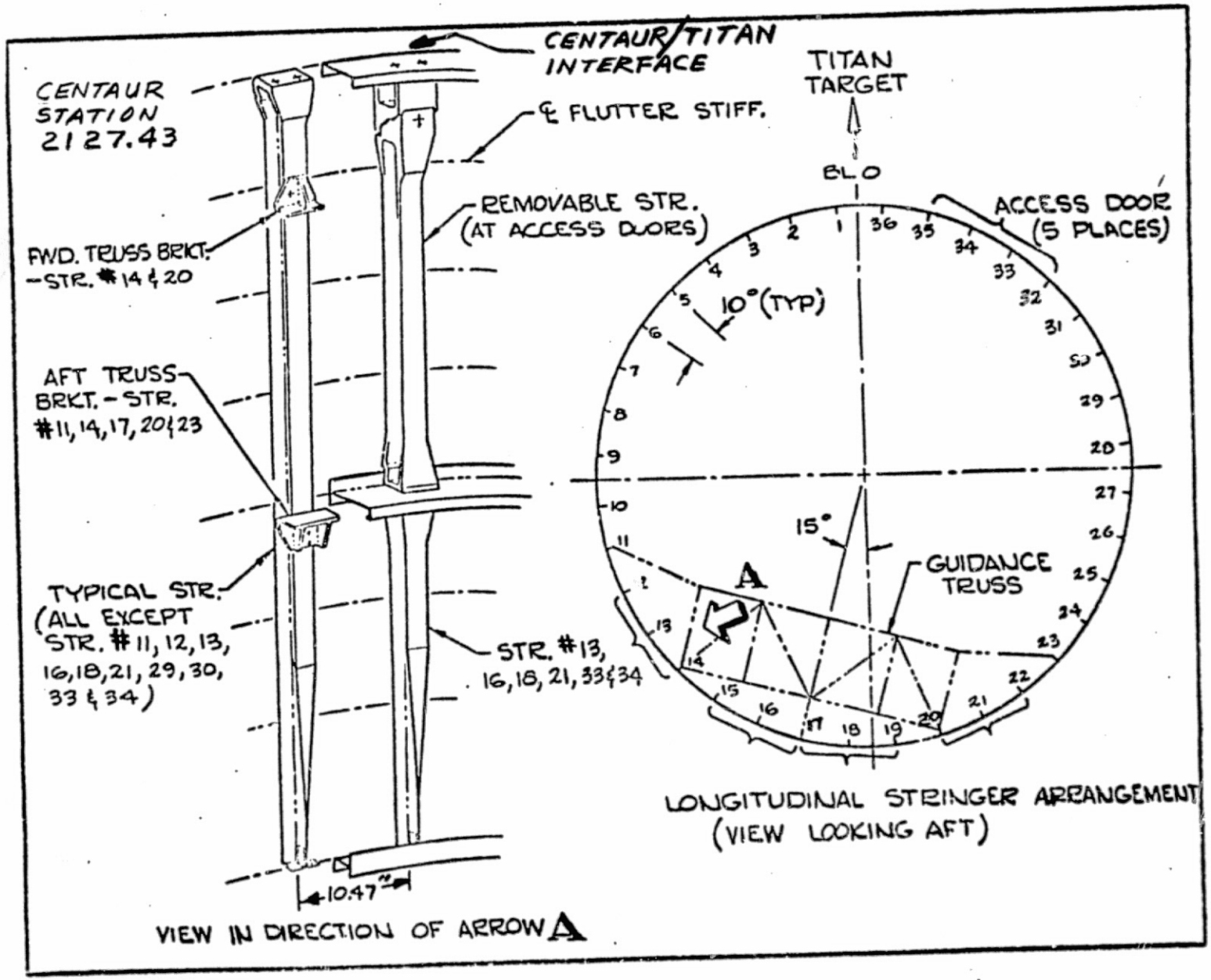

Figure IV-2. Titan Stringer Detail

V CENTAUR STANDARD SHROUD STRUCTURAL STRENGTH

By K. I. Davidson and George S. Sarvay

SUMMARY

The CSS limit load structural tests demonstrated the ability of the CSS to withstand a series of design limit loading conditions which were applied at various shroud azimuths. Also, the tests determined the effectiveness of the FBR system in sharing loads between the CSS and the Centaur vehicle. All test objectives were achieved and no structural deficiencies were noted. In general, the results of the strain gage data were in good agreement with predicted stress levels. The tests demonstrated that the highest stress regions in the CSS occurred in the ring components adjacent to the circumferential separation joint. These areas are the most critical CSS structural regions, but the stress levels are safely below the allowable limits. The results of the testing indicated that the stiffness of the boattail structure is less than predicted, thereby requiring the use of the FBR system. Various tests were performed to evaluate the interaction effects of the FBR system. In general, stress data comparisons indicate that the CSS stress levels aft of the FBR system are lower with the FBR system connected than when it is not. Refer to Sections III and VI for further discussion on the FBR system.

DESCRIPTION

The CSS structural configuration used during the tests is illustrated in figure V-1. The shroud enclosed the entire Centaur vehicle and was mounted at its aft end (Station 2180.48) to the ISA. The overall height of the CSS test specimen structure was approximately 687 inches, while its major diameter was 168 inches. The figure also shows the various sections of the shroud and the separation planes. The nose cone section is a biconic configuration with a 25 degree half angle forward cone and a 15 degree half angle aft cone. The biconic skin is fabricated from magnesium-thorium sheets which are reinforced by internal rings (figure V-2). The 24-inch radius stainless steel nose cone dome structure was not installed during the static loads tests.

The 168-inch diameter cylindrical portion of the CSS is constructed of an aluminum skin which is strengthened by external longitudinal corrugated stiffeners as shown in figure V-3. The sheets are joined together by a process which utilizes a combination of spot welding and aluminum epoxy adhesive bonding. The shell is internally stiffened by three-inch deep zee rings which are spaced approximately 15 inches apart. The rings are attached by conventional rivet construction.

The cylindrical portion of the CSS is mated to the 120-inch diameter ISA by a conical transition boattail section which has a re-entrance half angle of approximately 37.4 degrees. This structure provides the load path for transferring the axial loads and bending moments from the CSS into the vehicle at the ISA. The construction utilized in this region of the CSS is a riveted ring, hat section stringer stiffened aluminum conical shell. The details of the construction are shown in figure V-4.

To facilitate the fabrication, assembly, and shipping of the CSS segments, four field joints, as shown in figure V-1, are provided. The details of the type of joint used at the four locations are shown in figures V-2, V-4, and V-5.

The Centaur vehicle access requirements through the CSS are shown in the flat pattern of figure V-6. The structural doors are identified by shaded areas while the remaining openings are hinged to allow for umbilical access to the Centaur vehicle. The structural doors are designed to take the flight loads while the hinged doors are not load carrying members. However, the structure around the hinged door openings is reinforced to insure structural integrity of the CSS.

Figure V-7 illustrates a typical cross section of the structural components of the longitudinal and circumferential separation joints. The joints are designed for the maximum combination of external flight loads and internal compartment pressure loads.

The structural arrangement of the hinge brackets, which are located at the base of the CSS between the aft field and interface joints, is illustrated in figure V-8. A pair of hinges is located on each half of the CSS. The forward hinge fitting jettisons with the CSS while the aft hinge fitting and support structure remain with the vehicle. The functions of the hinges are to control the pivot and release action of each CSS half. During the launch phase of flight the upper and lower hinge fittings are not in contract. Loads therefore are not transferred through the hinge fittings until the time of CSS jettison.

The eight longitudinal thruster springs, which provide the main jettison force, are located at the base of the CSS between the aft field joint and the circumferential separation plane (figure V-9). The springs are loaded after installation of the CSS on the vehicle and the force is stored until the separation joints are severed. Consequently, the structure adjacent to the springs is designed for both stored spring and flight aerodynamic loads.

An external vent fin used to vent gaseous hydrogen (LH_2) from the Centaur vehicle is mounted on the CSS. The vent fin structure location is shown in figures V-1 and V-6 and its configuration is shown in figure V-10. The CSS hardware used to mount the vent fin is designed to withstand the external flight loads and cryogenic environment.

ORIGINAL PAGE IS
OF POOR QUALITY

Strain gage instrumentation on the CSS structural components was available in all tests. Approximately 190 measurements were provided for Tests 1L and 2L while Tests 3L and 4L had approximately 160 measurements. The strain gages were generally located in regions of expected low margins of safety or in those areas where analytical predictions are difficult because of the complex nature of the load paths which result from highly redundant structure. In addition to uniaxial gages, a large portion of the gages were located in a back-to-back pair configuration to measure axial loading as well as bending effects. Typical strain gage installations are shown in figures V-11 and V-12. See reference 7 for more detailed instrumentation information.

TEST RESULTS

The following subsections delineate, in chronological sequence, the general requirements and results for each test condition. Reference 7 contains greater detail of the test requirements.

Test 3L - The shear load was applied in the 150° azimuth concurrently with the maximum axial compressive loads. This condition subjected the CSS to maximum limit equivalent axial compressive loads in the following regions:

1. Hydrogen disconnect valve cutout and reinforcement (150° azimuth at Station 2265).

2. Equipment module door (135° azimuth at Station 2478).

3. T-0 umbilical chute cutout and reinforcement (151° azimuth at Station 2197).

4. Circumferential separation joint structure adjacent to the detonator block opening (180° azimuth at Station 2211).

The test load levels were successfully achieved after several preliminary loadings were performed at lower levels to settle out the hardware. All structural hardware withstood the loads without damage. The post-test inspection indicated that the soft aluminum washers which are used under fasteners at the field joints (Stations 2241.78 and 2514) were deformed at various azimuth locations. Since the discrepancy was random, it was concluded that the deformations were the result of the bolt preload operation. These washers were changed to steel for the flight vehicle. Bolt torque readings were taken after each series of tests and those which were deficient were retorqued to proper specification limits.

The LH_2 fill and drain valve cutout (Item 12 in figure V-6) had strain gages located on the door longerons and doublers. These gages are identified as numbers 4292 through 4301. The predicted and actual values

ORIGINAL PAGE IS OF POOR QUALITY

for these instruments are shown in Table V-1. A comparison of this information shows that the actual stresses were below the predicted values for this test except for gages 4293, 4298, 4300, and 4301 located on the longerons. These had greater local bending effects than had been anticipated. However, the stress levels were below design allowables and no structural damage was observed.

The equipment module access doors (Item 1-2 shown in figure V-6) and payload pick-up arm doors (Item 1-6 in figure V-6) were instrumented with strain gages on the door longerons, skin, and stiffeners. The gages used to investigate the equipment module doors are numbers 4260 through 4273 while those for payload pick-up arm doors are identified as numbers 4246 through 4253 and 4256 and 4257. The stress levels for the equipment module doors show excellent agreement with analytical predictions as shown in Table V-1A. Gage 4266 was slightly above the predicted value. Some of the actual stress levels for the payload pick-up arm doors exceeded predictions by more than 25 percent, as indicated in Table V-1A. This increase can be attributed to a different load distribution in the redundant structure than had originally been assumed. However, a review of the data indicates the stress levels are low and below the design allowables.

The Station 2209 ring-circumferential separation joint region was instrumented by a combination of hoop and back-to-back axial gages. The gages were clustered in the shear load azimuth region as well as around detonator block openings. The actual test stress values and calculated axial and bending stress effects are shown in Tables V-1A and V-1B. A comparison of the circumferential gages, which were located on the Station 2209 ring shows that the hoop stresses in the 150° to 180° azimuth region were higher than predicted. This increase can be attributed to the reduced circumferential shell stiffness in the region of the T-4 panel and detonator block openings. The axial and bending stress effects show that the circumferential separation joint has higher peak load concentrations at the compression azimuth than at the tension azimuth. Also, the data indicates that the stresses, in general, were greatest in the 150° to 180° azimuth region of the Station 2209 ring.

Test 4L - This test was performed by applying the shear load at the 330° azimuth concurrently with minimum axial compressive loads. The 330° direction was chosen to apply maximum limit equivalent axial tensile loads to the structural components indicated in the subsection "Test 3L" and, in addition, the following tension-critical components:

1. Field joints and longeron bathtub fittings.

2. Boattail structure (in hoop compression which results from tensile meridional loads).

The desired test loads were achieved after the second loading attempt. The tension-critical structural components withstood the loads without any damage. The summary of stresses is shown in Table V-2. They are all below allowable levels. The comments for the remaining hardware are similar to those stated in the subsection "Test 3L".

Test 2L-1 - The shear load was applied at the 270° azimuth concurrently with the minimum axial compressive loads. This condition subjected the shroud to maximum limit equivalent axial tension loads in the following regions:

1. Hydrogen boost pump door and reinforcement (90° azimuth at Stations 2197 and 2227).

2. Electrical umbilical cutouts and reinforcement (90° azimuth at Station 2468).

3. Circumferential joint structure located between Stations 2209 and 2214.

4. Tension-critical components (field joints and longeron bathtub fittings).

5. Boattail structure in hoop compression which results from tensile meridional loads.

The hydrogen boost pump door (Item 15 in figure V-6) had strain gages mounted on the door stiffeners, skin and adjacent reinforced structure and longerons. These gages are identified as numbers 4068 through 4088. As indicated in Table V-3, predicted values for the hydrogen boost pump doors were not available. However, the actual stress levels achieved during the test were quite small and no structural anomalies were noted.

The electrical umbilical panel door (Item 2 in figure V-6) was instrumented by strain gages located on the longerons and doublers. The gages are listed in Table V-3 and are identified as numbers 4023 through 4031. The data show that the reinforcement longerons located on each side of the electrical umbilical panel door are of similar values indicating that the load path is approximately symmetric about the opening. The stress intensity in the center longeron is approximately of the same level as the outer component. However, since the cross sectional area of the center longeron is larger than the other two adjacent stiffening members, a greater portion of the peak load is carried by the center structural member.

A combination of hoop and back-to-back axial strain gages was mounted on the Station 2209 ring circumferential separation joint region. The gages were located in the 90° and 270° shear load azimuth region. The test stress values and calculated axial and bending stress effects are shown in Tables V-3 and V-3B. A comparison of the axial and bending stress results reveals that the 90 degree azimuth of the ring is less sensitive to peak load concentrations compared to the 270° azimuth region. The stress intensity in the hardware located on either side of the 90°/270° shear load azimuth is greater than the values on the maximum load line, indicating that the peak load concentrations are greater in these regions. These higher peak values can be attributed to the increased stiffness of the upper and lower hinge bracket longerons.

Test 1L-2 - The original requirements for this test were to apply the shear load in the 90° azimuth concurrently with the shroud maximum axial compressive loads. This condition subjected Items 1, 2, and 3 in the subsection "Test 2L-1" to maximum limit equivalent axial compressive loads. The test procedure was modified to include an additional combined CSS/Centaur annulus pressure and relative motion test for the forward seal. The desired CSS test loads were achieved after the forward seal had separated prematurely at a lower annulus pressure level. Strain gage data did not reveal any loading anomalies and the post-test inspection of the shroud did not indicate any structural deficiencies.

A summary of stress levels for this test is shown in Table V-4. In general, the comments stated in the subsection "Test 2L-1" can also be applied for this test.

Test 2L-2 - The vent fin loads (axial, radial, tangential) were applied simultaneously during this test. These loads subjected the vent fin attachment and CSS backup hardware to their maximum limit design loads. The tests were successfully performed to the desired load levels and no structural anomalies were observed. The CSS structure, which was located behind the fin vent structure, had strain gages (back-to-back) located on the ring segments and longitudinal longerons. A summary of the predicted and actual test values is shown in Table V-5. A comparison of stress levels does not indicate complete correlation between predicted and actual values. However, the actual stresses achieved during the test were low in magnitude, indicating that the CSS vent fin backup structure is lightly loaded for the design conditions.

Test 7L-2 - This test was performed to evaluate the interaction effects due to an installed FBR system. Various combinations of fixture axial loads, 90° azimuth CSS shear loads, and 270° azimuth payload shear loads were applied. The primary objectives of the test were:

1. Determine the load distribution within the FBR system when the CSS maximum design shear load is applied.

2. Verify the structural integrity of the CSS and FBR system.

3. Evaluate spring rates of the CSS and FBR system when subjected to limit design loads.

A secondary objective of the test was the correlation of CSS stress levels with those obtained without an FBR system.

The comparison can be determined by referring to Table V-6. In general, the stress levels in the CSS structure aft of the FBR system were lower than those obtained during Test 1L-2. Summaries of the stress levels are listed in Tables V-7 and V-8.

Other Test Conditions - The primary objectives of the remaining tests, identified at the beginning of this section and described in Summary Section,

were the evaluation and verification of the structural and functional capability of other (non-CSS) hardware. Consequently, the CSS hardware stress levels will not be discussed except to state that the magnitudes were lower than those described in the previous subsections. The strain gage instrument characteristics and the CSS stress levels for these tests are summarized in Tables V-9, V-10, V-11, V-12 and V-13.

SUMMARY OF TEST RESULTS

The CSS structure successfully demonstrated the ability to withstand various combinations of design limit loads. The test objectives were successfully achieved with no structural deficiencies observed. The boattail structural stiffness was less than predicted.

Post-test inspection indicated that the soft aluminum washers which are located at the flanged field joints (Stations 2241 and 2514) were deformed. As a consequence, the aluminum washers were changed to steel for flight vehicles.

Stress levels in various door and cutout reinforcements were, in general, low and below the allowable design values.

The stress levels in the Station 2209 ring peaked highest adjacent to the detonator block openings and in the 150^{o} to 180^{o} azimuth region. These areas of the CSS were the most highly stressed regions; however, the stresses were below the allowable design values.

The vent fin attachment and CSS backup structure successfully withstood a combination of three simultaneously applied maximum limit design loads. The stress levels achieved during the test were very low indicating that the CSS vent fin backup structure is lightly loaded.

Various load tests were performed to evaluate the interaction effects of the FBR system on CSS and Centaur structures. The results confirmed that stress levels in the CSS aft of the FBR are lower when the FBR system is used, as expected.

TABLE V-IA
STRESS RESULTS FOR TEST 3L

GAGE NO.	STATION	AZIMUTH DEG.	COMPONENT	DIRECTION	PREDICTED VALUE (PSI) MAXIMUM STRESS	TEST VALUE (PSI) MAXIMUM STREEE	TYPE GAGE INSTALL. SEE FIG. V-11.
4246	2505.1	142.	D STIF	AX	- 2900.	- 3807.	9
4247	2505.1	142.	D STIF	"	- 2900.	2685.	8
4248	2504.9	137.	D SKIN	"	- 3500.	- 4730.	10
4249	2504.9	137.	D SKIN	"	- 3500.	- 5154.	11
4250	2504.9	134.	D STIF	"	- 3500.	- 3759.	9
4251	2504.9	134.	D STIF	"	- 3500.	375.	8
4252	2505.4	157.	LONG	"	- 5670.	- 6011.	7
4253	2505.4	157.	LONG	"	- 3240.	- 4409.	6
4254	2505.3	151.	CORR	"	- 7100.	- 7850.	12
4255	2505.3	151.	CORR	"	- 7100.	- 9079.	13
4256	2505.1	128.	D STIF	"	- 2900.	- 3838.	9
4257	2505.1	128.	D STIF	"	- 2900.	2154.	8
4258	2487.5	152.	LONG	"	- 6950.	- 5975.	2
4259	2487.5	152.	LONG	"	- 7720.	- 6539.	1
4260	2487.6	144.	CORR	"	- 8830.	- 3680.	12
4261	2487.6	144.	CORR	"	- 8830.	- 5460.	13
4262	2477.2	144.	CORR	"	- 9120.	- 6838.	12
4263	2477.2	144.	CORR	"	- 9120.	- 5357.	13
4264	2477.2	133.	CORR	"	- 6950.	- 6704.	12
4265	2477.2	133.	CORR	"	- 6950.	- 5549.	13
4266	2477.2	120.	CORR	"	- 6100.	- 6898.	12
4267	2477.2	120.	CORR	"	- 6100.	- 4254.	13
4268	2468.9	158.	LONG	"	- 6440.	- 4296.	2
4269	2468.9	158.	LONG	"	- 8070.	- 6079.	1
4270	2468.8	152.	LONG	"	- 6960.	- 5897.	2
4271	2468.8	152.	LONG	"	- 7770.	- 6618.	1
4272	2468.9	144.	CORR	"	- 9300.	- 3338.	12
4273	2468.9	144.	CORR	"	- 9300.	- 7946.	13
4274	2454.5	158.	LONG	"	-10040.	- 4306.	2
4275	2454.5	158.	LONG	"	-10320.	- 4328.	1
4276	2454.1	151.	LONG	"	- 4930.	- 2497.	2
4277	2454.1	151.	LONG	"	- 7760.	- 7998.	1
4278	2451.5	133.	LONG	"	- 460.	- 1280.	5
4279	2451.5	133.	LONG	"	- 6510.	- 3980.	4
4280	2446.4	165.	D STIF	"	- 4100.	- 2338.	9

TABLE V-1A
STRESS RESULTS FOR TEST 3L (CONTINUED)

GAGE NO.	STATION	AZIMUTH DEG.	COMPONENT	DIRECTION	PREDICTED VALUE (PSI) MAXIMUM STRESS	TEST VALUE (PSI) MAXIMUM STRESS	TYPE GAGE INSTALL. SEE FIG. V-11.
4281	2446.4	165.	D. STIF	AX	- 4100.	--	8
4282	2446.4	163.8	D SKIN	"	- 4100.	- 2911.	10
4283	2446.4	163.8	D SKIN	"	- 4100.	- 3533.	11
4284	2446.5	125.	D STIF	"	- 2940.	- 2385.	9
4285	2446.5	125.	D STIF	"	- 2940.	--	8
4286	2429.3	151.	LONG	"	- 8160.	- 9061.	7
4287	2429.3	151.	LONG	"	- 4750.	- 5648.	6
4288	2428.8	133.	LONG	"	- 3680.	--	5
4289	2428.8	133.	LONG	"	- 6650.	- 6777.	4
4290	2414.3	158.	LONG	"	- 9720.	- 9683.	7
4291	2414.3	158.	LONG	"	- 5310.	- 6229.	6
4292	2294.7	142.	LONG	"	- 5870.	- 2044.	5
4293	2294.7	142.	LONG	"	- 7760.	- 8046.	4
4294	2276.4	143.8	DBLR	"	-10200.	- 6196.	10
4295	2265.3	162.	LONG	"	- 7780.	- 6443.	2
4296	2265.3	162.	LONG	"	-10530.	-10531.	1
4297	2265.3	141.	LONG	"	- 6080.	- 2885.	2
4298	2265.3	141.	LONG	"	-11200.	-13086.	1
4299	2254.7	143.8	DBLR	"	- 8040.	- 6269.	10
4300	2249.0	141.	LONG	"	- 4430.	- 6287.	2
4301	2249.0	141.	LONG	"	- 7040.	- 7855.	1
4302	2234.9	171.	LONG	"	1960.	1678.	5
4303	2234.9	171.	LONG	"	- 7620.	-10377.	4
4304	2234.4	165.	D STIF	"	- 6250.	- 4959.	9
4305	2234.4	165.	D STIF	"	- 6250.	3887.	8
4306	2234.4	157.	LONG	"	820.	1889.	5
4307	2234.4	157.	LONG	"	- 9070.	- 7982.	4
4308	2228.1	171.	LONG	"	1390.	--	5
4309	2228.1	171.	LONG	"	- 9940.	-10060.	4
4310	2227.0	165.	D STIF	"	- 5780.	- 4470.	9
4311	2227.0	165.	D STIF	"	- 5780.	1264.	8
4312	2219.6	157.	LONG	"	- 1070.	- 1982.	5
4313	2219.6	157.	LONG	"	- 9640.	- 4991.	4
4314	2220.1	142.	LONG	"	- 440.	- 5304.	5
4315	2220.1	142.	LONG	"	-14700.	- 5591.	4
4316	2220.4	171.	LONG	"	210.	--	5

TABLE V-1A
STRESS RESULTS FOR TEST 3L (CONTINUED)

GAGE NO.	STATION	AZIMUTH DEG.	COMPONENT	DIRECTION	PREDICTED VALUE (PSI) MAXIMUM STRESS	TEST VALUE (PSI) MAXIMUM STRESS	TYPE GAGE INSTALL. SEE FIG. V-11.
4317	2220.4	171.	LONG	AX	- 8820.	- 8934.	4
4318	2202.8	142.	LONG	AX	- 6900.	- 3214.	2
4319	2201.	142.	LONG	AX	- 9540.	-10988.	1
4320	2202.6	160.	LONG	AX	- 5450.	--	2
4321	2200.7	160.	LONG	AX	-11370.	-12763.	1
4322	2202.4	174.	LONG	AX	960.	4402.	2
4323	2200.6	174.	LONG	AX	-11550.	-11856.	1
4324	2185.9	160.	LONG	AX	-13430.	- 3947.	5
4325	2185.	160.	LONG	AX	- 6710.	-12455.	4
4326	2213.	161.1	RING	AX	-64000.	-53077.	22
4327	2213.	161.1	RING	AX	49000.	43042.	23
4328	2211.6	161.1	S-Z	AX	- 6700.	6644.	20
4329	2211.6	161.1	S-Z	AX	- 6700.	- 5088.	21
4330	2209.	144.1	RING	AX	19500.	30954.	25
4331	2209.	144.1	RING	AX	-31500.	--	26
4332	2210.	144.1	RING	CIR	12400.	18658.	27
4333	2210.	144.1	RING	CIR	12400.	20487.	30
4334	2209.	161.3	RING	AX	19500.	35449.	25
4335	2209.	161.3	RING	AX	-31500.	--	26
4336	2210.	161.3	RING	CIR	12700.	21332.	27
4337	2210.	161.3	RING	CIR	12700.	19100.	30
4338	2209.	161.3	RING	CIR	12700.	19080.	24
4339	NO GAGE						
4340	2213.	341.1	RING	AX	43000.	32216.	22
4341	2213.	341.1	RING	AX	-33000.	-20361.	23
4342	2211.6	341.1	S-Z	AX	4600.	1389.	20
4343	2211.6	341.1	S-Z	AX	4600.	4187.	21
4344	2209.	341.3	RING	AX	-13890.	-22536.	25
4345	2209.	341.3	RING	AX	21750.	- 5884.	26
4346	2210.	341.3	RING	CIR	- 8400.	-10742.	27
4347	2210.	341.3	RING	CIR	- 8400.	-12160.	30
4348	2209.	341.3	RING	CIR	- 8400.	- 9782.	29
4349	2209.	341.3	RING	CIR	- 8400.	- 8643.	28
4350	2209.	323.4	RING	AX	-13890.	-13159.	25
4351	2209.	323.4	RING	AX	21750.	30692.	26
4352	2210.	323.4	RING	CIR	- 8400.	-11041.	27
4353	2210.	323.4	RING	CIR	- 8400.	-11561.	30

TABLE V-1A

STRESS RESULTS FOR TEST 3L (CONTINUED)

GAGE NO.	STATION	AZIMUTH DEG.	COMPONENT	DIRECTION	PREDICTED VALUE (PSI) MAXIMUM STRESS	TEST VALUE (PSI) MAXIMUM STRESS	TYPE GAGE INSTALL. SEE FIG. V-11.
4603	2210.	103.	HNGF	AX	0	1,721.	31
4649	2210.	77.	HNGF	AX	0	- 1,931.	31
4654	2210.	283.	HNGF	AX	0	- 2,603.	31
4659	2210.	257.	HNGF	AX	0	- 1,050.	31
4664	2209.	171.0	RING	CIR	13,900.	23,866.	24
4665	2209.	171.0	RING	CIR	13,900.	15,383.	28
4666	2209.	171.0	RING	AX	18,000.	33,030.	25
4667	2209.	171.0	RING	AX	-30,000.	--	26
4668	2209.	172.3	RING	CIR	14,630.	26,040.	24
4669	2209.	172.3	RING	CIR	14,630.	17,311.	28
4670	2209.	172.3	RING	AX	18,000.	25,899.	25
4671	2209.	172.3	RING	AX	-30,000.	-58,922.	26
4672	2209.	173.5	RING	CIR	15,350.	24,430.	24
4673	2209.	173.5	RING	CIR	15,350.	18,015.	28
4674	2209.	173.5	RING	AX	18,000.	14,198.	25
4675	2209.	173.5	RING	AX	-30,000.	-49,493.	26
4676	2209.	186.5	RING	CIR	13,780.	25,778.	24
4677	2209.	186.5	RING	CIR	13,780.	16,086.	28
4678	2209.	186.5	RING	AX	16,500.	10,303.	25
4679	2209.	186.5	RING	AX	-26,500.	-40,405.	26
4695	2187.	77.	HNGL	AX	- 3,570.	- 5,293.	18
4696	2187.	257.	HNGL	AX	7,160.	3,465.	18
4697	2187.	283.	HNGL	AX	4,330.	4,691.	18
4698	2187.	103.	HNGL	AX	- 6,700.	-11,730.	18
4901	2294.	24.	CORR	AX	3,700.	3,395.	12
4902	2294.	114.	CORR	AX	-10,600.	- 8,617.	12
4903	2294.	204.	CORR	AX	- 8,300.	- 6,597.	12
4904	2294.	294.	CORR	AX	5,970.	5,071.	12

TABLE V-1A
STRESS RESULTS FOR TEST 3L (CONCLUDED)

GAGE NO.	STATION	AZIMUTH DEG.	COMPONENT	DIRECTION	PREDICTED VALUE (PSI) Maximum Stress	TEST VALUE (PSI) Maximum Stress	TYPE GAGE INSTALL. See Fig. V-11.
4909	2209.	6.5	RING	AX	-11290.	- 4343.	25
4910	2209.	6.5	RING	AX	17240.	--	26
4911	2209.	6.5	RING	CIR	- 8490.	-16653.	24
4912	2209.	6.5	RING	CIR	- 8490.	-11980.	28
4913	2209.	353.5	RING	AX	-12810.	- 4724.	25
4914	2209.	353.5	RING	AX	19860.	28355.	26
4915	2209.	353.5	RING	CIR	-10000.	-18568.	24
4916	2209.	353.5	RING	CIR	-10000.	-12999.	28
4917	2339.	141.2	CORR	AX	-15700.	-13533.	13
4918	2339.	141.2	CORR	AX	-15700.	-10083.	12

Symbols for hardware components strain gaged:

D STIF - door stiffener
LONG - longeron
CORR - skin corrugation
D SKIN - door skin
DBLR - doubler
S-Z - super zip doubler at separation joint
HNGF - hinge fitting
HNGL - hinge longeron

Symbols for direction (orientation) of strain gage mounting:

AX - axial
CIR - cicumferential

TABLE V-1B

STATION 2209 CIRCUMFERENTIAL JOINT STRESSES FOR TEST 3L

GAGE NUMBER	AZIMUTH DEG.	ORIENT	TYPE GAGE INSTAL REF. FIG. V-11.	TEST VALUE (PSI) MAX. DATA	STRESS CORRECTION (PSI) POISSON EFFECT	TOTAL STRESS (PSI) MAX.	AXIAL STRESS EFFECT (PSI)	BENDING STRESS EFFECT (PSI)
4332	144.	CIR	27	18658.	6219.			
4330	"	AX	25	30954.		37173.		
4331	"	AX	26	--		--		
4337	161.	CIR	30	19100.	6367.			
4334	"	AX	25	35449.		41816.		
4335	"	AX	26	--		--		
4664	171.	CIR	24	23866.	7955.			
4666	"	AX	25	33030.		40985.		
4667	"	AX	26	--		--		
4668	172.	CIR	24	26040.	8680.			
4670	"	AX	25	25899.		34579.	-7831.	±42410.
4671	"	AX	26	-58922.		-50242.		
4672	173.	CIR	24	24430.	8143.			
4674	"	AX	25	14198.		22341.	-9504.	±31845.
4675	"	AX	26	-49493.		-41350.		
4676	186.	CIR	24	25778.	8593.			
4678	"	AX	25	10303.		18896.	-6458.	±25354.
4679	"	AX	26	-40405.		-31812.		
4352	323.	CIR	27	-11041.	-3680.			
4350	"	AX	25	-13159.		-16839.	5086.	±21925.
4351	"	AX	26	30692.		27012.		
4346	341.	CIR	27	-10742.	-3581.			
4344	"	AX	25	-22536.				
4345	"	AX	26	-5884.				
4915	353.	CIR	24	-18568.	-6189.			
4913	"	AX	25	- 4724.		-10913.	5626.	±16539.
4914	"	AX	26	28355.		22166.		
4911	6.	CIR	24	-16653.	-5551.			
4909	"	AX	25	-4343.		-9894.		
4910	"	AX	26	--		--		

TABLE V-1B

STATION 2209 CIRCUMFERENTIAL JOINT STRESSES FOR TEST 4L

GAGE NUMBER	AZIMUTH DEG.	ORIENT	TYPE GAGE INSTAL SEE FIG. V-11.	TEST VALUE (PSI) MAX. DATA	STRESS CORRECTION (PSI) POISSON EFFECT	TOTAL STRESS (PSI) MAX.	AXIAL STRESS EFFECT (PSI)	BENDING STRESS EFFECT (PSI)
4332	144.	CIR	27	-14477.	-4826.			
4330	"	AX	25	-24330.		-29156.	10898.	±40054.
4331	"	AX	26	55779.		50953.		
4337	161.	CIR	30	-18788.	-6263.			
4334	"	AX	25	-28075.		-34338.	6920.	±41258.
4335	"	AX	26	50442.		48179.		
4664	171.	CIR	24	-17670.	-5890.			
4666	"	AX	25	-22576.		-28066.	6523.	±34989.
4667	"	AX	26	47402.		41512.		
4668	172.	CIR	24	-19785.	-6595.			
4670	"	AX	25	-16473.		-23068.	7152.	±30220.
4671	"	AX	26	43967.		37372.		
4672	173.	CIR	24	-18389.	-6130.			
4674	"	AX	25	-8043.		-14173.	8844.	±23017.
4675	"	AX	26	37991.		31861.		
4676	186.	CIR	24	-21340.	-7113.			
4678	"	AX	25	-7204.		-14317.	4490.	±18807.
4679	"	AX	26	30410.		23297.		
4352	323.	CIR	27	16327.	5442.			
4350	"	AX	25	25738.		31180.	-5563.	±36743.
4351	"	AX	26	-47748.		-42306.		
4346	341.	CIR	27	16367.	5456.			
4344	"	AX	25	33513.				
4345	"	AX	26	3966.				
4915	353.	CIR	24	24611.	8204.			
4913	"	AX	25	7437.		15641.	-6839.	±22470.
4914	"	AX	26	-37504.		-29300.		
4911	6.	CIR	24	23645.	7882.			
4909	"	AX	25	7374.		15256.	-5732.	±20988.
4910	"	AX	26	-34602.		-26720.		

ORIGINAL PAGE IS
OF POOR QUALITY

TABLE V-1B

STATION 2209 CIRCUMFERENTIAL JOINT STRESSES FOR TEST 2L-1

GAGE NUMBER	AZIMUTH DEG.	ORIENT	TYPE GAGE INSTAL SEE FIG. V-11.	TEST VALUE (PSI) MAX. DATA	STRESS CORRECTION (PSI) POISSON EFFECT	TOTAL STRESS (PSI) MAX.	AXIAL STRESS EFFECT (PSI)	BENDING STRESS EFFECT (PSI)
4119	74.2	CIR	27	-10202.	-3401.			
4122	"	AX	25	--		--		
4123	"	AX	26	22438.		19037.		
4125	90.	CIR	27	-7643.	-2548.			
4128	"	AX	25	-14557.		-17105.	3667.	±20771.
4129	"	AX	26	26986.		24438.		
4131	105.	CIR	27	-9762.	-3254.			
4133	"	AX	25	--		--		
4134	"	AX	26	21955.		18701.		
4139	254.	CIR	27	12792.	4264.			
4142	"	AX	25	7374.		11638.	-7340.	±18978.
4143	"	AX	26	-30583.		-26319.		
4145	270.	CIR	27	9541.	3180.			
4148	"	AX	25	12230.		15410.	-2372.	±17782.
4149	"	AX	26	-23334.		-20154.		
4151	286.	CIR	27	11226.	3742.			
4153	"	AX	25	5770.		9512.	-5478.	14990.
4154	"	AX	26	-24211.		-20469.		

ORIGINAL PAGE IS
OF POOR QUALITY

TABLE V-1B

STATION 2209 CIRCUMFERENTIAL JOINT STRESSES FOR TEST IL-2.1

GAGE NUMBER	AZIMUTH DEG.	ORIENT	TYPE GAGE INSTAL SEE FIG. V-11.	TEST VALUE (PSI) MAX. DATA	STRESS CORRECTION (PSI) POISSON EFFECT	TOTAL STRESS (PSI) MAX.	AXIAL STRESS EFFECT (PSI)	BENDING STRESS EFFECT (PSI)
4119	74.2	CIR	27	13394.	4465.			
4122	"	AX	25	3005.		7470.	-7393.	±14863.
4123	"	AX	26	-26721.		-22256.		
4125	90.	CIR	27	10022.	3341.			
4128	"	AX	25	18577.		21918.	-4293.	±26211.
4129	"	AX	26	-33846.		-30505.		
4131	105.	CIR	27	13635.	4545.			
4133	"	AX	25	3045.		7590.	-8527.	±16162.
4134	"	AX	26	-29190.		-24645.		
4139	254.	CIR	27	-10642.	-3547.			
4142	"	AX	25	-5564.		-9111.	6741.	±15852.
4143	"	AX	26	26140.		22593.		
4145	270.	CIR	27	-8723.	-2908.			
4148	"	AX	25	-10362.		-13270.	2507.	±15777.
4149	"	AX	26	21191.		18283.		
4151	286.	CIR	27	-9001.	-3001.			
4153	"	AX	25	-1562.		-4563.	5346.	± 9909.
4154	"	AX	26	18256.		15255.		

Symbols for orientation of strain gage mounts:

AX - axial

CIR - circumferential

Axial stress calculated from:

$$\sigma_a = (\sigma_{in} + \sigma_{out})/2$$

$$\sigma_b = \pm|(\sigma_{in} - \sigma_{out})|/2$$

where, σ_{in} = total stress from axial inboard gage.

σ_{out} = total stress from axial outboard gage.

TABLE V-2
STRESS RESULTS FOR TEST 4L

GAGE NO.	STATION	AZIMUTH DEG.	COMPONENT	DIRECTION	PREDICTED VALUE (PSI) MAX. STRESS	TEST VALUE (PSI) MAX. STREE	TYPE GAGE INSTALL. SEE FIG. V-11.
4246	2505.1	142.	D STIF	AX	1710.	2307.	9
4247	2505.1	142.	D STIF	↑	1710.	- 671.	8
4248	2504.9	137.	D SKIN		2060.	2275.	10
4249	↕	137.	D SKIN		2060.	2548.	11
4250		134.	D STIF		2060.	2086.	9
4251	2504.9	134.	D STIF		2060.	--	8
4252	2505.4	157.	LONG		3340.	3348.	7
4253	2505.4	157.	LONG		1910.	2818.	6
4254	2505.3	151.	CORR.		4190.	4890.	12
4255	2505.3	151.	CORR.		4190.	5420.	13
4256	2505.1	128.	D STIF		1710.	2181.	9
4257	2505.1	128.	D STIF		1710.	--	8
4258	2487.5	152.	LONG		4230.	3497.	2
4259	2487.5	152.	LONG		4720.	4606.	1
4260	2487.6	144.	CORR.		5400.	2653.	12
4261	2487.6	144.	CORR.		5400.	3534.	13
4262	2477.2	144.	↕		5620.	4324.	12
4263	↕	144.			5620.	3797.	13
4264		133.			4230.	3817.	12
4265		133.			4230.	3741.	13
4266		120.			3540.	3846.	12
4267	2477.2	120.	CORR.		3540.	2592.	13
4268	2468.9	158.	LONG		4030.	2792.	2
4269	2468.9	158.	↕		5040.	4129.	1
4270	2468.8	152.			4350.	3247.	2
4271	2468.8	152.	LONG		4860.	4574.	1
4272	2468.9	144.	CORR.		5810.	2952.	12
4273	2468.9	144.	CORR.		5810.	5155.	13
4274	2454.5	158.	LONG		6490.	2435.	2
4275	2454.5	158.	↕		6670.	2939.	1
4276	2454.1	151.			3160.	1467.	2
4277	2454.1	151.			4980.	5845.	1
4278	2451.5	133.			300.	793.	5
4279	2451.5	133.	LONG	↓	5500.	3034.	4
4280	2446.4	165.	D STIF	AX	2640.	1327.	9

TABLE V-2

STRESS RESULTS FOR TEST 4L (CONTINUED)

GAGE NO.	STATION	AZIMUTH DEG.	COMPONENT	DIRECTION	PREDICTED VALUE (PSI) MAX. STRESS	TEST VALUE (PSI) MAX. STRESS	TYPE GAGE INSTALL. SEE FIG. V-11.
4281	2446.4	165.	D STIF	AX	2640.	--	8
4282	2446.4	163.8	D SKIN	↑	2640.	1577.	10
4283	2446.4	163.8	D SKIN		2640.	1985.	11
4284	2446.5	"	D STIF		1820.	1759.	9
4285	2446.5	125.	D STIF		1820.	884.	8
4286	2429.3	151.	LONG		5480.	6140.	7
4287	2429.3	151.	↑		3190.	4319.	6
4288	2428.8	133.	↓		2610.	--	5
4289	2428.8	133.	LONG		4490.	4924.	4
4290	2414.3	158.	DBLR		6640.	6203.	7
4291	2414.3	158.	LONG		3630.	4864.	6
4292	2294.7	142.	↑		4410.	1935.	5
4293	2294.7	142.	↓		5830.	6449.	4
4294	2276.4	143.8	LONG		7740.	4713.	10
4295	2265.3	162.	DBLR		5940.	4996.	2
4296	2265.3	162.	LONG		8050.	7271.	1
4297	2265.3	141.	↑		4650.	3075.	2
4298	2265.3	141.	↓		8560.	10276.	1
4299	2254.7	143.8	LONG		6170.	5420.	10
4300	2249.0	141.	DBLR		3410.	4801.	2
4301	2249.0	141.	LONG		5420.	6926.	1
4302	2234.9	171.	↑		-1520.	-1409.	5
4303	2234.9	171.	↓		5910.	7212.	4
4304	2234.4	165.	LONG		4850.	3827.	9
4305	↑	165.	D STIF		4850.	-1685.	8
4306	↓	157.	D STIF		- 640.	-1748.	5
4307	2234.4	157.	LONG		7030.	6163.	4
4308	2228.1	171.	↑		-1080.	--	5
4309	2228.1	171.	↓		7730.	6322.	4
4310	2227.0	165.	LONG		4500.	3413.	9
4311	2227.0	165.	D STIF		4500.	936.	8
4312	2219.6	157.	D STIF		840.	1097.	5
4313	2219.6	157.	LONG		7530.	3729.	4
4314	2220.1	142.	↑		340.	3434.	5
4315	2220.1	142.	↓	↓	11480.	4709.	4
4316	2220.4	171.	LONG	AX	- 165.	888.	5

TABLE V-2
STRESS RESULTS FOR TEST 4L (CONTINUED)

GAGE NO.	STATION	AZIMUTH DEG.	COMPONENT	DIRECTION	PREDICTED VALUE (PSI) MAX. STRESS	TEST VALUE (PSI) MAX. STRESS	TYPE GAGE INSTALL. SEE FIG. V-11.
4317	2220.4	171.	LONG	AX	6890.	6608.	4
4318	2202.8	142.	LONG	↑	5450.	4215.	2
4319	2201.	142.	↑	↑	7540.	9738.	1
4320	2202.6	160.	↑	↑	4310.	2841.	2
4321	2200.7	160.	↑	↑	8910.	9770.	1
4322	2202.4	174.	↑	↑	- 760.	--	2
4323	2200.6	174.	↑	↑	9130.	10181.	1
4324	2185.9	160.	↑	↑	10890.	2092.	5
4325	2185.	160.	LONG	↑	5440.	10371.	4
4326	2213.	161.1	RING	↑	49940.	35214.	22
4327	2213.	161.1	RING	↑	-38240.	-21763.	23
4328	2211.6	161.1	S-Z	↑	5230.	2437.	20
4329	2211.6	161.1	S-Z	↓	5230.	5677.	21
4330	2209.	144.1	RING	↓	-13500.	-24330.	25
4331	2209.	↑	↑	AX	23000.	55779.	26
4332	2210.	↓	↑	CIR	- 9690.	-14477.	27
4333	2210.	144.1	↑	CIR	- 9690.	-15994.	30
4334	2209.	161.3	↑	AX	-13500.	-28075.	25
4335	2209.	↑	↑	AX	23000.	54442.	26
4336	2210.	↓	↑	CIR	- 9910.	-14636.	27
4337	2210.	↓	↑	CIR	- 9910.	-18788.	30
4338	2209.	161.3	RING	CIR	- 9910.	-15635.	24
4339	NO GAGE						
4340	2213.	341.1	RING	AX	-56550.	-46702.	22
4341	2213.	341.1	RING	↑	43400.	36835.	23
4342	2211.6	341.1	S-Z	↑	- 6050.	6370.	20
4343	2211.6	341.1	S-Z	↓	- 6050.	- 4344.	21
4344	2209.	341.3	RING	↓	17500.	33513.	25
4345	2209.	341.3	↑	AX	-29000.	3966.	26
4346	2210.	341.3	↑	CIR	11020.	16367.	27
4347	2210.	341.3	↑	↑	11020.	16929.	30
4348	2209.	341.3	↑	↓	11020.	14439.	29
4349	2209.	341.3	↑	CIR	11020.	12832.	28
4350	2209.	323.4	↑	AX	17500.	25738.	25
4351	2209.	323.4	↑	AX	-29000.	-47748.	26
4352	2210.	323.4	↑	CIR	11020.	16327.	27
4353	2210.	323.4	RING	CIR	11020.	16769.	30

TABLE V-2
STRESS RESULTS FOR TEST 4L (CONTINUED)

GAGE NO.	STATION	AZIMUTH DEG.	COMPONENT	DIRECTION	PREDICTED VALUE (PSI) MAX. STRESS	TEST VALUE (PSI) MAX. STRESS	TYPE GAGE INSTALL. SEE FIG. V-11.
4603	2210.	103.	HNGF	AX	0	-12132.	31
4649	↑	77.	↑		0	--	31
4654	↓	283.	↓		0	902.	31
4659	2210.	257.	HNGF	AX	0	1092.	31
4664	2209.	171.0	RING	CIR	-10620.	-17670.	24
4665	↑	↑	↑	CIR	-10620.	- 7855.	28
4666	↓	↓	↓	AX	-12500.	-22576.	25
4667		171.0		AX	21000.	47402.	26
4668		172.3		CIR	-11160.	-19785.	24
4669		↑		CIR	-11160.	- 8923.	28
4670		↓		AX	-12500.	-16473.	25
4671		172.3		AX	21000.	43967.	26
4672		173.5		CIR	-11680.	-18389.	24
4673		↑		CIR	-11680.	- 8441.	28
4674		↓		AX	-12500.	- 8043.	25
4675		173.5		AX	21000.	37991.	26
4676		186.5		CIR	-10120.	-21340.	24
4677		↑		CIR	-10120.	- 9203.	28
4678		↓		AX	-11000.	- 7204.	25
4679	2209.	186.5	RING	AX	18000.	30410.	26
4695	2187.	77.	HNGL	AX	1900.	3221.	18
4696	↑	257.	↑		- 2820.	- 6714.	18
4697	↓	283.	↓		- 5980.	- 6654.	18
4698	2187.	103.	HNGL	AX	5050.	8446.	18
4901	2294.	24.	CORR.	AX	- 6900.	- 5399.	12
4902	↑	114.	↑		7390.	6184.	12
4903	↓	204.	↓		5100.	4218.	12
4904	2294.	294.	CORR.	AX	- 9170.	- 7650.	12

TABLE V-2
STRESS RESULTS FOR TEST 4L (CONCLUDED)

GAGE NO.	STATION	AZIMUTH DEG.	COMPONENT	DIRECTION	PREDICTED VALUE (PSI) MAX. STRESS	TEST VALUE (PSI) MAX. STRESS	TYPE GAGE INSTALL. SEE FIG. V-11.
4904	2209.	6.5	RING	AX	14500.	7374.	25
4910	↑	↑	↑	AX	-24000.	-34602.	26
4911		↓		CIR	12150.	23645.	24
4912		6.5		CIR	12150.	14680.	28
4913		353.5	↓	AX	16500.	7437.	25
4914		↑		AX	-26500.	-37504.	26
4915		↓		CIR	13630.	24611.	24
4916	2209.	353.5	RING	CIR	13630.	16407.	28
4917	2339.	141.2	CORR.	AX	11400.	9694.	13
4918	2339.	141.2	CORR.	AX	11400.	8769.	12

See figure V-1A for symbol list.

TABLE V-3
STRESS RESULTS FOR TEST 2L

GAGE NO.	STATION	AZIMUTH DEG.	COMPONENT	DIRECTION	PREDICTED VALUE (PSI)	TEST VALUE FOR TEST NO. 2L-1 (PSI)	TEST VALUE FOR TEST NO. 2L-1A (PSI)	TYPE GAGE INSTALL. SEE FIG. V-11.
4001	2520.	88.	CORR.	AX	5900.	358.	1819.	12
4002	2520.	88.	CORR.	AX	5900.	5892.	4801.	13
4003	2519.7	87.	CORR.	AX	5690.	4065.	4684.	14
4004	2519.7	87.	CORR.	AX	5690.	5715.	4654.	15
4005	2520.	84.	CORR.	AX	5470.	--	1640.	12
4006	2520.	84.	CORR.	AX	5470.	4890.	3800.	13
4007	2520.	80.	CORR.	AX	5420.	--	1491.	12
4008	2520.	80.	CORR.	AX	5420.	5008.	3880.	13
4009	2505.5	89.	LONG	AX	3030.	3122.	2373.	5
4010	2505.5	89.	LONG	AX	3030.	3653.	2986.	4
4011	2505.5	88.	CORR.	AX	4010.	5636.	2355.	12
4012	2505.5	88.	CORR.	AX	4010.	3564.	2955.	13
4013	2505.9	71.	LONG	AX	4690.	3153.	2279.	5
4014	2505.9	71.	LONG	AX	4690.	3666.	2939.	4
4015	2490.4	89.	LONG	AX	--	3840.	2903.	2
4016	2490.4	89.	LONG	AX	--	3494.	2763.	1
4017	2490.4	88.	CORR.	AX	--	6859.	3459.	12
4018	2490.4	88.	CORR.	AX	--	4684.	3417.	13
4019	2490.3	71.	LONG	AX	--	1498.	1186.	5
4020	2490.3	71.	LONG	AX	--	3090	2364.	4
4021	2490.4	68.	LONG	AX	--	2529.	1935.	2
4022	2490.4	68.	LONG	AX	--	4034.	3113.	1
4023	2478.	88.7	DBLR	AX	--	7749.	3770.	10
4024	2468.8	106.	LONG	AX	--	2966.	2248.	2
4025	2468.8	106.	LONG	AX	--	5654.	3780.	1
4026	2468.9	88.7	DBLR	AX	--	--	- 324.	10
4027	2468.9	89.	LONG	AX	2230.	1686.	1530.	--
4028	2468.9	89.	LONG	AX	6910.	5714.	3372.	--
4029	2469.4	71.1	DBLR	AX	--	4359.	2857.	10
4030	2469.4	71.	LONG	AX	--	1217.	1030.	--
4031	2469.4	71.	LONG	AX	--	5686.	3684.	--
4032	2453.5	89.	LONG	AX	--	5402.	3903.	2
4033	2453.5	89.	LONG	AX	--	5845.	4542.	1
4034	2453.3	88.	CORR.	AX	--	6442	4711.	12
4035	2453.3	88.	CORR	AX	--	6923.	4949.	13

TABLE V-3
STRESS RESULTS FOR TEST 2L (CONTINUED)

GAGE NO.	STATION	AZIMUTH DEG.	COMPONENT	DIRECTION	PREDICTED VALUE (PSI)	TEST VALUE FOR TEST NO. 2L-1 (PSI)	TEST VALUE FOR TEST NO. 2L-1A (PSI)	TYPE GAGE INSTALL. SEE FIG. V-11.
4036	2453.3	84.	CORR	AX	--	2415.	1819.	12
4037	2453.3	84.	CORR	AX	--	5302.	4330.	13
4038	2440.3	106.	LONG	AX	--	1588.	1334.	3
4039	2440.4	106.	LONG	AX	--	2668.	2033.	1
4040	2441.7	89.	LONG	AX	4470.	4340.	3309.	2
4041	2441.7	89.	LONG	AX	5420.	4320.	3526.	1
4042	2441.5	71.	LONG	AX	--	--	656.	--
4043	2441.5	71.	LONG	AX	--	--	- 316.	--
4044	2429.1	89.	LONG	AX	--	1093.	968.	5
4045	2429.1	89.	LONG	AX	--	7307.	5813.	4
4046	2414.2	89.	LONG	AX	6450.	7013.	5330.	7
4047	2414.2	89.	LONG	AX	4440.	5300.	3952.	6
4048	2414.2	88.	CORR	AX	--	5845.	4503.	12
4049	2414.2	88.	CORR	AX	--	6894.	5420.	13
4050	2384.8	89.	CORR	AX	9890.	9134.	7130.	14
4051	2384.8	89.	CORR	AX	9890.	8427.	6570.	15
4052	2384.8	87.	CORR	AX	9890.	7934.	6173.	12
4053	2384.8	87.	CORR	AX	9890.	8662.	6717.	13
4054	2279.3	82.	CORR	AX	9630.	8680.	7068.	12
4055	2279.3	82.	CORR	AX	9630.	--	--	13
4056	2279.3	79.	CORR	AX	9630.	8680.	6650.	12
4057	2279.3	79.	CORR	AX	9630.	8633.	6717.	13
4058	2279.3	75.	CORR	AX	9630.	8650.	6859.	12
4059	2279.3	75.	CORR	AX	9630.	9046.	7041.	13
4060	2249.5	102.	LONG	AX	5320.	6680.	5457.	7
4061	2249.5	102.	LONG	AX	2550.	980.	858.	6
4062	2249.5	89.	CORR	AX	--	8515.	6923.	14
4063	2249.5	89.	CORR	AX	--	-2208.	1031.	15
4064	2249.5	90.	CORR	AX	--	2653.	2147.	12
4065	2249.5	90.	CORR	AX	--	8603.	7012.	13
4066	2249.5	79.	LONG	AX	--	6889.	6113.	7
4067	2249.5	79.	LONG	AX	--	--	- 429.	6
4068	2233.5	104.	LONG	AX	--	2810.	2497.	2
4069	2233.5	104.	LONG	AX	--	6543.	4836.	1
4070	2234.	104.	HNGL	AX	--	6920.	6314.	19

TABLE V-3

STRESS RESULTS FOR TEST 2L (CONTINUED)

GAGE NO.	STATION	AZIMUTH DEG.	COMPONENT	DIRECTION	PREDICTED VALUE (PSI)	TEST VALUE FOR TEST NO. 2L-1 (PSI)	TEST VALUE FOR TEST NO. 2L-1A (PSI)	TYPE GAGE INSTALL. SEE FIG. V-11.
4071	2234.	104.	HNGL	AX	--	3892.	3546.	17
4072	2234.	104.	HNGL	AX	--	3287.	1989.	16
4073	2225.9	104.	LONG	AX	--	3747.	3497.	2
4074	2225.9	104.	LONG	AX	--	4267.	3034.	1
4075	2227.	104.	HNGL	AX	--	4325.	4671.	19
4076	2227.	104.	HNGL	AX	--	6055.	4152.	16
4077	2227.	101.	D STIF	AX	--	3255.	2497.	9
4078	2227.	101.	D STIF	AX	--	2529.	1811.	8
4079	2227.	99.1	D SKIN	AX	--	3185.	2396.	11
4080	2227.	99.1	D SKIN	AX	--	3883.	3094.	10
4081	2227.	91.4	D SKIN	AX	--	4642.	3701.	11
4082	2227.	91.4	D SKIN	AX	--	4885.	3823.	10
4083	2227.	90.	D STIF	AX	--	3382.	2086.	9
4084	2227.	90.	D STIF	AX	--	--	--	8
4085	2225.9	77.	LONG	AX	--	2622.	2622.	2
4086	2225.9	77.	LONG	AX	--	5974.	3951.	1
4087	2227.	77.	HNGL	AX	--	3979.	6660.	19
4088	2227.	77.	HNGL	AX	--	4238.	2681.	16
4089	2220.6	104.	LONG	AX	--	2341.	2185.	2
4090	2220.6	104.	LONG	AX	--	4931.	3887.	1
4091	2221.0	104.	HNGL	AX	--	--	3373.	19
4092	2221.0	104.	HNGL	AX	--	4757.	3719.	16
4093	2202.4	103.	HNGL	AX	--	8580.	6250.	19
4094	2202.4	103.	HNGL	AX	--	-1347.	-1041.	16
4095	2204.7	90.	D SKIN	CIR	-2640.	-8157.	-6657.	10
4096	2204.7	84.9	D SKIN	CIR	-2640.	-6004.	-5080.	10
4097	2204.7	79.8	D SKIN	CIR	-2640.	-4388.	-3657.	10
4098	2195.8	99.	D STIF	AX	--	--	1593.	8
4099	2195.8	99.	D STIF	AX	--	4838.	4217.	9
4100	2195.8	86.	D STIF	AX	--	949.	827.	8
4101	2195.8	86.	D STIF	AX	--	5551.	4528.	9
4102	2195.8	84.8	D SKIN	AX	--	6864.	6010.	10
4103	2195.8	84.8	D SKIN	AX	--	9193.	7247.	11
4104	2192.4	103.	HNGL	AX	--	9592.	6802.	19
4105	2192.4	103.	HNGL	AX	--	1899.	2328.	16

TABLE V-3

STRESS RESULTS FOR TEST 2L (CONTINUED)

GAGE NO.	STATION	AZIMUTH DEG.	COMPONENT	DIRECTION	PREDICTED VALUE (PSI)	TEST VALUE FOR TEST NO. 2L-1 (PSI)	TEST VALUE FOR TEST NO. 2L-1A (PSI)	TYPE GAGE INSTALL. SEE FIG. V-11.
4106	2192.4	77.	HNGL	AX	--	10910.	8089.	19
4107	2192.4	77.	HNGL	AX	--	2726.	1930.	16
4108	2185.	103.	HNGL	AX	--	10765.	8251.	19
4109	2185.	103.	HNGL	AX	--	9592.	8181.	16
4110	2185.	90.	SKIN	CIR	--	11374.	8595.	11
4111	2185.	84.9	SKIN	CIR	--	12146.	9521.	11
4112	2185.	86.	STRG	AX	--	--	--	--
4113	2185.	86.	STRG	AX	--	7010.	6048.	--
4114	2185.	79.8	SKIN	CIR	--	32845.	27962.	11
4115	2213.	74.6	RING	AX	49949.	1248.	1529.	22
4116	2211.6	74.6	S-Z	AX	5230.	- 9930.	-11857.	20
4117	2213.	74.6	RING	AX	-38240.	--	--	23
4118	2211.6	74.6	S-Z	AX	5230.	-33689.	-27970.	21
4119	2210.	74.2	RING	CIR	-8350.	-10202.	- 7683.	27
4120	2210.	74.2	RING	CIR	-8350.	- 4323.	- 3563.	30
4121	2209.	74.2	RING	CIR	-8350.	-13279.	- 9982.	24
4122	2209.	74.2	RING	AX	-13500.	--	- 1361.	25
4123	2209.	74.2	RING	AX	23000.	22438.	17291.	26
4124	2208.	74.2	RING	CIR	-8350.	- 8723.	- 7324.	28
4125	2210.	90.	RING	CIR	-8350.	- 7643.	- 6244.	27
4126	2210.	90.	RING	CIR	-8350.	- 5964.	- 5084.	30
4127	2209.	90.	RING	CIR	-8350.	- 4964.	- 4163.	24
4128	2209.	90.	RING	AX	-13500.	-14557.	-11361.	25
4129	2209.	90.	RING	AX	23000.	26986.	21151.	26
4130	2208.	90.	RING	CIR	-8350.	- 9163.	- 7124.	28
4131	2210.	105.4	RING	CIR	-8350.	- 9762.	- 7324.	27
4132	2210.	105.4	RING	CIR	-8350.	- 4603.	- 4003.	30
4133	2209.	105.4	RING	AX	-13500.	--	- 400.	25
4134	2209.	105.4	RING	AX	23000.	21955.	16849.	26
4135	2213.	254.6	RING	AX	-56580.	-33689.	-27970.	22
4136	2211.6	254.6	S-Z	AX	-6050.	- 1408.	- 604.	20
4137	2213	254.6	RING	AX	43400.	13217.	12006.	23
4138	2211.6	254.6	S-Z	AX	-6050.	- 1127.	- 684.	21
4139	2210.	254.4	RING	CIR	9600.	12792.	10062.	27
4140	2210.	254.4	RING	CIR	9600.	8056.	5931.	30

TABLE V-3

STRESS RESULTS FOR TEST 2L (CONTINUED)

GAGE NO.	STATION	AZIMUTH DEG.	COMPONENT	DIRECTION	PREDICTED VALUE (PSI)	TEST VALUE FOR TEST NO. 2L-1 (PSI)	TEST VALUE FOR TEST NO. 2L-1A (PSI)	TYPE GAGE INSTALL. SEE FIG. V-11.
4141	2209.	254.4	RING	CIR	9600.	13716.	10785.	24
4142	2209.	254.4	RING	AX	17500.	7374.	7575.	25
4143	2209.	254.4	RING	AX	-29000.	-30583.	-23653.	26
4144	2208.	254.4	RING	CIR	9600.	12190.	9260.	28
4145	2210.	270.	RING	CIR	9600.	9541.	7735.	27
4146	2210.	270.	RING	CIR	9600.	6452.	4688.	30
4147	2209.	270.	RING	CIR	9600.	10263.	8096.	24
4148	2209.	270.	RING	AX	17500.	12230.	9059.	25
4149	2209.	270.	RING	AX	-29000.	-23334.	-17989.	26
4150	2208.	270.	RING	CIR	9600.	12591.	9581.	28
4151	2210.	285.7	RING	CIR	9600.	11226.	8377.	27
4152	2210.	285.7	RING	CIR	9600.	6011.	4848.	30
4153	2209.	285.7	RING	AX	17500.	5770.	4407.	25
4154	2209.	285.7	RING	AX	-29000.	-24211.	-18628.	26
4208	2453.3	113.	CORR	AX	--	1222.	656.	12
4209	2453.3	113.	CORR	AX	--	3534	2074	13
4210	2444.5	114.	RING	CIR	--	--	--	--
4211	2443.6	114.	RING	CIR	--	--	--	--
4212	2444.5	114.	RING	CIR	--	--	-501.	--
4213	NO GAGE							
4214	2440.6	117.	LONG	AX	--	1302.	984.	3
4215	2440.1	117.	LONG	AX	--	4892.	3271.	1
4216	NO GAGE							
4217	NO GAGE							
4218	2431.	112.8	DBLR	AX	--	1266.	1031.	15
4219	2431.	117.	LONG	AX	--	1124.	1217.	2
4220	2431.	117.	LONG	AX	--	2795.	2604.	1
4221	2425.	112.8	DBLR	AX	--	2032.	1561.	15
4222	2431.	106.	LONG	AX	--	812.	905.	2
4223	2431.	106.	LONG	AX	--	2986.	2255.	1
4224	2435.3	114.	RING	CIR	--	--	--	--
4225	2435.3	114.	RING	CIR	--	--	--	--
4226	2435.3	112.	RING	CIR	--	--	--	--
4227	2435.3	112.	RING	CIR	--	--	--	--
4228	2399.3	113.	CORR	AX	--	8053.	6173.	12
4229	2399.3	113.	CORR	AX	--	7041.	5479.	13

TABLE V-3
STRESS RESULTS FOR TEST 2L (CONCLUDED)

GAGE NO.	STATION	AZIMUTH DEG.	COMPONENT	DIRECTION	PREDICTED VALUE (PSI)	TEST VALUE FOR TEST NO. 2L-1 (PSI)	TEST VALUE FOR TEST NO. 2L-1A (PSI)	TYPE GAGE INSTALL. SEE FIG. V-11.
4603	2210.	103.	HNGF	AX	0	- 3190.	-1679.	31
4649	2210.	77.	HNGF	AX	0	- 3526.	-1595.	31
4654	2210.	283.	HNGF	AX	0	1679.	1008.	31
4659	2210.	257.	HNGF	AX	0	- 924.	-1511.	31
4695	2187	77.	HNGL	AX	--	11264.	8719.	18
4696	2187	257.	HNGL	AX	--	-11368.	-8346.	18
4697	2187	283.	HNGL	AX	--	-10008.	-7802.	18
4698	2187	103.	HNGL	AX	--	11597.	8689.	18
4901	2294	24.	CORR	AX	3310.	3689.	3074.	12
4902	2294	114.	CORR	AX	8450.	10461.	8267.	12
4903	2294	204.	CORR	AX	-5060.	- 5337.	-3955.	12
4904	2294	294.	CORR	AX	-10200.	-10630.	-8252.	12

See figure V-1A for symbol list.

TABLE V-4

STRESS RESULTS FOR TEST 1L

GAGE NO.	STATION	AZIMUTH DEG.	COMPONENT	DIRECTION	PREDICTED VALUE (PSI)	TEST VALUE FOR TEST NO. 1L-2.1 (PSI)	TEST VALUE FOR TEST NO. 1L-1.2 (PSI)	TYPE GAGE INSTALL. SEE FIG V-11.
4001	2520.	88.	CORR.	AX	-10140.	-1252.	- 805.	12
4002	2520.	88.	↑	↑	-10140.	-9858.	-2679.	13
4003	2519.7	87.			- 9780.	-8829.	-2532.	14
4004	2519.7	87.			- 9780.	-9593.	-2414.	15
4005	2520.	84.			- 9400.	- 805.	- 626.	12
4006	2520.	84.			- 9400.	-8270.	-2179.	13
4007	2520.	80.			- 9310.	- 775.	- 537.	12
4008	2520.	80.	CORR.		- 9310.	-8123.	-2149.	13
4009	2505.5	89.	LONG		- 5140.	-4587.	-1248.	5
4010	2505.5	89.	LONG		- 5140.	-5873.	-1651.	4
4011	2505.5	88.	CORR.		- 6800.	-4112.	-1162.	12
4012	2505.5	88.	CORR.		- 6800.	-5740.	-1590.	13
4013	2505.9	71.	LONG		- 7950.	-5024.	-1561.	5
4014	2505.9	71.	LONG		- 7950.	-6191.	-1548.	4
4015	2490.4	89.	LONG		--	-6365.	-1654.	2
4016	2490.4	89.	LONG		--	-4889.	-1365.	1
4017	2490.4	88.	CORR.		--	-6227.	-1610.	12
4018	2490.4	88.	CORR.		--	-7093.	-1767.	13
4019	2490.3	71.	LONG		--	-2590.	- 687.	5
4020	2490.3	71.	LONG		--	-5199.	-1229.	4
4021	2490.4	68.	LONG		--	-3932.	- 999.	2
4022	2490.4	68.	LONG		--	-6539.	-1588.	1
4023	2478.	88.7	DBLR		--	-6358.	-1560.	10
4024	2468.8	106.	LONG		--	-4805.	- 999.	2
4025	2468.8	106.	LONG		--	-8633.	-2096.	1
4026	2468.9	88.7	DBLR		--	-8593.	-2002.	10
4027	2468.9	89.	LONG		- 3520.	-3339.	- 687.	--
4028	2468.9	89.	LONG		-10920.	-9140.	-1904.	--
4029	2469.4	71.1	DBLR		--	-6593.	-1296.	10
4030	2469.4	71.	LONG		--	-3027.	- 655.	--
4031	2469.4	71.	LONG		--	-8220.	-1937.	--
4032	2453.5	89.	LONG		--	-9919.	-1592.	2
4033	2453.5	89.	LONG		--	-8474.	-2191.	1
4034	2453.3	88.	CORR.		--	-8907.	-2116.	12
4035	2453.3	88.	CORR.	AX	--	-9887.	-1943.	13

TABLE V-4
(STRESS RESULTS FOR TEST 1L (CONTINUED)

GAGE NO.	STATION	AZIMUTH DEG.	COMPONENT	DIRECTION	PREDICTED VALUE (PSI)	TEST VALUE FOR TEST NO. 1L-2.1 (PSI)	TEST VALUE FOR TEST NO. 1L-1.2 (PSI)	TYPE GAGE INSTALL. SEE FIG. V-11.
4036	2453.3	84.	CORR.	AX	--	- 2116.	- 507.	12
4037	2453.3	84.	CORR.		NOT USED		--	13
4038	2440.3	106.	LONG		NOT USED		--	3
4039	2440.4	106.	LONG		--	- 3810.	- 953.	1
4040	2441.7	89.			- 6750.	- 6895.	-1561.	2
4041	2441.7	89.			- 8190.	- 6063.	-1683.	1
4042	2441.5	71.			--	- 1592.	- 375.	--
4043	2441.5	71.			NOT USED		--	--
4044	2429.1	89.			--	- 1498.	- 437.	5
4045	2429.1	89.			--	- 9679.	-2508.	4
4046	2414.2	89.			- 9450.	- 9839.	-2399.	7
4047	2414.2	89.	LONG		- 6510.	- 6734.	-1592.	6
4048	2414.2	88.	CORR.		--	- 8074.	-1908.	12
4049	2414.2	88.			--	-10064.	-2385.	13
4050	2384.8	89.			-14150.	-12563.	-2826.	14
4051	2384.8	89.			-14150.	-12151.	-2709.	15
4052	2384.8	87.			-14150.	-10069.	-2355.	12
4053	2384.8	87.			-14150.	-12151.	-2709.	13
4054	2279.3	82.			-12800.	-10307.	-2206.	12
4055	2279.3	82.			NOT USED		--	13
4056	2279.3	79.			-12800.	- 9949.	-2146.	12
4057	2279.3	79.			-12800.	-11475.	-2296.	13
4058	2279.3	75.			-12800.	- 9979.	-2116.	12
4059	2279.3	75.	CORR.		-12800.	-11710.	-2355.	13
4060	2249.5	102.	LONG		- 6910.	- 8282.	-1729.	7
4061	2249.5	102.	LONG		- 3310.	2818.	--	6
4062	2249.5	89.	CORR.		--	-12328.	-2385.	14
4063	2249.5	89.			NOT USED		--	15
4064	2249.5	90.			--	1342.	- 328.	12
4065	2249.5	90.	CORR.		--	--	--	13
4066	2249.5	79.	LONG		--	- 7716.	-1818.	7
4067	2249.5	79.			--	4381.	368.	6
4068	2233.5	104.			--	- 2871.	- 812.	2
4069	2233.5	104.	LONG		--	- 9978.	-1453.	1
4070	2234.	104.	HNGL	AX	--	- 6572.	-1903.	19

TABLE V-4
STRESS RESULTS FOR TEST 1L (CONTINUED)

GAGE NO.	STATION	AZIMUTH DEG.	COMPONENT	DIRECTION	PREDICTED VALUE (PSI)	TEST VALUE FOR TEST NO. 1L-2.1 (PSI)	TEST VALUE FOR TEST NO. 1L-1.2 (PSI)	TYPE GAGE INSTALL. SEE FIG V-11.
4071	2234.	104.	HNGL	AX	--	- 4324.	- 778.	17
4072	2234.	↑	HNGL	↑	--	- 6226.	605.	16
4073	2225.9	↕	LONG	↕	--	- 4712.	-1061.	2
4074	2225.9	↕	LONG	↕	--	- 5591.	-1011.	1
4075	2227.	↓	HNGL	↕	--	- 2594.	-1730.	19
4076	↑	104.	HNGL	↕	--	-16426.	--	16
4077	↕	101.	D STIF	↕	--	- 4012.	- 790.	9
4078	↕	101.	D STIF	↕	--	- 3557.	- 593.	8
4079	↕	99.1	D SKIN	↕	--	- 3790.	- 819.	11
4080	↕	99.1	D SKIN	↕	--	- 4578.	- 940.	10
4081	↕	91.4	D SKIN	↕	--	- 5063.	-1092.	11
4082	↕	91.4	D SKIN	↕	--	- 5730.	-1183.	10
4083	↓	90.	D STIF	↕	--	- 3285.	- 664.	9
4084	2227.	90.	D STIF	↕	--	- 1529.	- 156.	8
4085	2225.9	77.	LONG	↕	--	- 3214.	- 749.	2
4086	2225.9	77.	LONG	↕	--	- 6917.	-1232.	1
4087	2227.	77.	HNGL	↕	--	--	-1903.	19
4088	2227.	77.	HNGL	↕	--	-16771.	- 692.	16
4089	2220.6	104.	LONG	↕	--	- 2559.	- 624.	2
4090	2220.6	104.	LONG	↕	--	- 7011.	-1137.	1
4091	2221.0	104.	HNGL	↕	--	--	-1557.	19
4092	2221.0	104.	HNGL	↕	--	-12537.	--	16
4093	2202.4	103.	HNGL	↓	--	-11567.	-1929.	19
4094	2202.4	103.	HNGL	AX	--	--	--	16
4095	2204.7	90.	D SKIN	CIR	3500.	--	--	10
4096	2204.7	84.9	D SKIN	CIR	3500.	7477.	1502.	10
4097	2204.7	79.8	D SKIN	CIR	3500.	3929.	924.	10
4098	2195.8	99.	D STIF	AX	--	--	- 582.	8
4099	↑	99.	D STIF	↑	--	- 5733.	-1209.	9
4100	↕	86.	D STIF	↕	--	1899.	--	8
4101	↕	86.	D STIF	↕	--	- 7034.	-1302.	9
4102	↓	84.8	D SKIN	↕	--	-10240.	-1855.	10
4103	2195.8	84.8	D SKIN	↕	--	-11210.	-2061.	11
4104	2192.4	103.	HNGL	↓	--	-10619.	-2021.	19
4105	2192.4	103.	HNGL	AX	--	- 2511.	-1102.	16

TABLE V-4
STRESS RESULTS FOR TEST 1L (CONTINUED)

GAGE NO.	STATION	AZIMUTH DEG.	COMPONENT	DIRECTION	PREDICTED VALUE (PSI)	TEST VALUE FOR TEST NO. 1L-2.1 (PSI)	TEST VALUE FOR TEST NO. 1L-1.2 (PSI)	TYPE GAGE INSTALL. SEE FIG V-11.
4106	2192.4	77.	HNGL	AX	--	-13249.	-2021.	19
4107	2192.4	77.	↕		--	- 4898.	-1102.	16
4108	2185.	103.			--	-14062.	-2449.	19
4109	↑	103.	HNGL	AX	--	- 6490.	-2694.	16
4110		90.	SKIN	CIR	--	-17605.	-2194.	11
4111		84.9	SKIN	CIR	--	-18602.	-3003.	11
4112		86.	STRG	AX	--	4901.	--	--
4113	↓	86.	STRG	AX	--	- 9450.	-1860.	--
4114	2185.	79.8	SKIN	CIR	--	-17374.	-2310.	11
4115	2213.	74.6	RING	AX	-64000.	-34009.	-8926.	22
4116	2211.6	↑	S-Z	↑	- 6700.	- 2695.	--	20
4117	2213.	↕	RING	↕	49000.	12854.	4670.	23
4118	2211.6	74.6	S-Z	AX	- 6700.	- 1489.	- 724.	21
4119	2210.	74.2	RING	CIR	10700.	13394.	2323.	27
4120	2210.	74.2	↑	CIR	10700.	6653.	1282.	30
4121	2209.	74.2		CIR	10700.	15965.	2924.	24
4122	2209.	74.2		AX	19500.	3005.	441.	25
4123	2209.	74.2		AX	-31500.	-26721.	-5044.	26
4124	2208.	74.2		CIR	10700.	12190.	2283.	28
4125	2210.	90.		↑	10700.	10022.	1883.	27
4126	2210.	↑		↕	10700.	8859.	1682.	30
4127	2209.			CIR	10700.	7374.	1442.	24
4128	2209.			AX	19500.	18577.	4087.	25
4129	2209.			AX	-31500.	-33846.	-7284.	26
4130	2208.	90.		CIR	10700.	14037.	2604.	28
4131	2210.	105.4		CIR	10700.	13635.	2363.	27
4132	2210.	↑		CIR	10700.	6131.	1282.	30
4133	2209.	↕		AX	19500.	3045.	--	25
4134	2209.	105.4		AX	-31500.	-29190.	-5604.	26
4135	2213.	254.6	RING	↑	43000.	36106.	6523.	22
4136	2211.6	↑	S-Z		4600.	2254.	- 322.	20
4137	2213.	↕	RING		-33000.	-11937.	-3540.	23
4138	2211.6	254.6	S-Z	AX	4600.	1529.	443.	21
4139	2210.	254.4	RING	CIR	- 7300.	-10642.	-1121.	27
4140	2210.	254.4	RING	CIR	- 7300.	- 3403.	- 801.	30

TABLE V-4
STRESS RESULTS FOR TEST 1L (CONTINUED)

GAGE NO.	STATION	AZIMUTH DEG.	COMPONENT	DIRECTION	PREDICTED VALUE (PSI)	TEST VALUE FOR TEST NO. 1L-2.1 (PSI)	TEST VALUE FOR TEST NO. 1L-1.2 (PSI)	TYPE GAGE INSTALL. SEE FIG V-11.
4141	2209.	254.4	RING	CIR	- 7300.	-12480.	-1722.	24
4142	2209.	254.4	↑	AX	-11000.	- 5564.	-1001.	25
4143	2209.	254.4	↑	AX	20000.	26140.	3285.	26
4144	2208.	254.4	↑	CIR	- 7300.	- 6564.	-1402.	28
4145	2210.	270.	↑		- 7300.	- 8723.	-1161.	27
4146	2210.	↑	↑		- 7300.	- 2843.	- 561.	30
4147	2209.	↕	↑	CIR	- 7300.	- 9842.	-1602.	24
4148	2209.	↕	↑	AX	-11000.	-10362.	-1442.	25
4149	2209.	↓	↑	AX	20000.	21191.	2844.	26
4150	2208.	270.	↑	CIR	- 7300.	- 7763.	-1522.	28
4151	2210.	285.7	↑	CIR	- 7300.	- 9003.	-1241.	27
4152	2210.	↑	↑	CIR	- 7300.	- 3363.	- 601.	30
4153	2209.	↓	↓	AX	-11000.	- 1562.	--	25
4154	2209.	285.7	RING	AX	20000.	18256.	2724.	26
4208	2453.3	113.	CORR.	AX	--	- 1431.	--	12
4209	2453.3	113.	CORR.	AX	--	- 4651.	-1237.	13
4210	2444.5	114.	RING	CIR	N O T U S E D		--	--
4211	2443.6	114.	RING	CIR	--	--	--	--
4212	2444.5	114.	RING	CIR	--	1425.	--	--
4213	N O G A G E		--	---	--	--	--	--
4214	2440.6	117.	LONG	AX	--	- 1937.	- 635.	3
4215	2440.1	117.	LONG	AX	--	- 7808.	-1556.	1
4216	N O G A G E		--	---	--	--	--	--
4217	N O G A G E		--	---	--	--	--	--
4218	2431.	112.8	DBLR	AX	--	- 2591.	- 471.	15
4219	2431.	117.	LONG	AX	--	- 1935.	- 749.	2
4220	2431.	117.	LONG	AX	--	- 4889.	-1111.	1
4221	2425.	112.8	DBLR	AX	--	- 3621.	- 795.	15
4222	2431.	106.	LONG	AX	--	- 1217.	- 499.	2
4223	2431.	106.	LONG	AX	--	- 4032.	-1111.	1
4224	2435.3	114.	RING	CIR	--	--	--	--
4225		114.	RING	CIR	--	--	--	--
4226		112.	RING	CIR	--	--	--	--
4227	2435.3	112.	RING	CIR	--	--	--	--
4228	2399.3	113.	CORR.	AX	--	-11765.	-2802.	12
4229	2399.3	113.	CORR.	AX	--	- 8976.	-2296.	13

TABLE V-4
STRESS RESULTS FOR TEST 1L (CONCLUDED)

GAGE NO.	STATION	AZIMUTH DEG.	COMPONENT	DIRECTION	PREDICTED VALUE (PSI)	TEST VALUE FOR TEST NO. 1L-2.1 (PSI)	TEST VALUE FOR TEST NO. 1L-1.2 (PSI)	TYPE GAGE INSTALL. SEE FIG V-11.
4603	2210.	103.	HNGF	AX	0	--	--	31
4649	2210.	77.	↑		0	- 2748.	- 550.	31
4654	↑	283.	↓		0	- 7473.	- 769.	31
4659	2210.	257.	HNGF	AX	0	- 5715.	- 330.	31
4695	2187	77.	HNGL	AX	--	-20401.	-3379.	18
4969	|	257.	↑		--	12329.	1932.	18
4697	|	283.	↓		--	12289.	1932.	18
4698	2187	103.	HNGL	AX	--	-19399.	-3460.	18
4901	2294.	24.	CORR.	AX	- 6400.	- 6488.	-1306.	12
4902	|	114.	↑		-11620.	-13427.	-2688.	12
4903	|	204.	↓		1890.	2306.	423.	12
4904	2294.	294.	CORR.	AX	7030.	8690.	1614.	12

See figure V-1A for symbol list.

TABLE V-5

STRESS RESULTS FOR TEST 2L-2

GAGE NO.	STATION	AZIMUTH DEG.	COMPONENT	DIRECTION	PREDICTED VALUE (PSI)	TEST VALUE FOR TEST NO. 2L-2.P (PSI)	TYPE GAGE INSTALL. SEE FIG. V-11.
4024.	2468.8	106.	LONG	AX		1217.	2
4025	2468.8	106.	LONG	AX			1
4038	2440.3	106.	LONG	AX	-9400	-11233.	3
4039	2440.4	106.	LONG	AX	-720		1
4060	2249.5	102.	LONG	AX			7
4061	2249.5	102.	LONG	AX			6
4068	2233.5	104.	LONG	AX		-156.	2
4069	2233.5	104.	LONG	AX		-221.	1
4070	2234.	104.	HNGL	AX		-259.	19
4071	2234.	104.	HNGL	AX		-173.	17
4072	2234.	104.	HNGL	AX		86.	16
4073	NOT USED						
4074	2225.9	104,	LONG	AX		-158.	1
4075	2227.	104.	HNGL			-173.	19
4076	2227.	104.	HNGL				16
4077		101.	D STIF			-95.	9
4078		101.	D STIF			-31.	8
4079		99.1	D SKIN			-91.	11
4080	2227.	99.1	D SKIN	AX		-30.	10
4089	2220.6	104.	LONG	AX		-94.	2
4090	2220.6	104.	LONG			-221.	1
4091	2221.0	104.	HNGL			-86.	19
4092	2221.0	104.	HNGL				16
4093	2202.4	103.	HNGL				19
4094	2202.4	103.	HNGL	AX		306.	16
4098	2195.8	99.	D STIF	AX		-122.	8
4099	2195.8	99.	D STIF	AX		-186.	9
4104	2192.4	103.	HNGL	AX		-214.	19
4105	2192.4	103.	HNGL	AX		-276.	16
4108	2185.	103.	HNGL	AX		-341.	19
4109	2185.	103.	HNGL	AX		-521.	16
4131	2210.	105.4	RING	CIR		401.	27
4133	2209.	105.4	RING	AX		160.	25
4210	2444.5	114.	RING	CIR	4690	2554.	-
4211	2443.6	114.	RING	CIR	-4790	5240.	-
4212	2444.5	114.	RING	CIR	-6580	-9118.	-
4213	NO GAGE						

TABLE V-5.

STRESS RESULTS FOR TEST 2L-2 (CONCLUDED)

GAGE NO.	STATION	AZIMUTH DEG.	COMPONENT	DIRECTION	PREDICTED VALUE (PSI)	TEST VALUE FOR TEST NO. 2L-2.P (PSI)	TYPE GAGE INSTALL. SEE FIG. V-11.
4214	2440.6	117.	LONG	AX	-9400	-3810.	3
4215	2440.1	117.	LONG	AX	-720	-1492.	1
4216	NO GAGE						
4217	NO GAGE						
4218	2431.	112.8	DBLR	AX		1767.	15
4219	2431.	117.	LONG		5030	7495.	2
4220	2431.	117.	LONG		-1790	-3841.	1
4221	2425.	112.8	DBLR			2562.	15
4222	2431.	106.	LONG		-10,830	-6490.	2
4223	2431.	106.	LONG	AX	-1740	-349.	1
4224	2435.3	114.	RING	CIR	-9490	680.	-
4225		114.			22,170	2040.	-
4226		112.			-3250	-7251.	-
4227	2435.3	112.	RING	CIR	-3250	8502.	-
4698	2187.	103.	HNGL	AX		-333.	18
4902	2294.	114.	CORR	AX		-538.	12

See figure V-1A for symbol list.

TABLE V-6

STRESS COMPARISONS OF TESTS 1L AND 7L
(WITH AND WITHOUT FBR)

GAGE NO.	STATION	AZIMUTH DEG.	COMPONENT	DIRECTION	PREDICTED VALUE 1 L (PSI)	TEST VALUE W/O FBR 1L-2.1 (PSI)	TEST VALUE W/FBR 7L-2 213L=0 (PSI)	TEST VALUE W/FBR 7L-2 213L=MAX. (PSI)
4001	2520.	88.	CORR	AX	-10140.	-1252.	-	-
4002		88.			-10140.	-9858.	-3974.	-6740.
4003		87.			-9780.	-8829.	1384.	-6122.
4004		87.			-9780.	-9595.	-3768.	-6446.
4005		84.			-9400.	-805.	-	-
4006		84.			-9400.	-8270.	-3268.	-5593.
4007		80.			-9310.	-775.	-	-
4008	2520.	80.	CORR	AX	-9310.	-8123.	-3180.	-5446.
4023	2478	89	DBLR	AX	-	-6358.	-2355.	-4004.
4027	2469	89	LONG	AX	-3520.	-3339.	-531.	-1248.
4028	2469	89	LONG	AX	-10920.	-9140.	-5398.	-7394.
4032	2453.5	89.	LONG	AX	-	-9910.	1093.	-312.
4033		89.	LONG		-	-8474.	-1111.	-3651.
4034		88.	CORR		-	-8907.	-6466.	-7180.
4035	2453.5	88.	CORR	AX	-	-9887.	560.	-1413.
4052	2384.8	87.	CORR	AX	-14150.	-10069.	-3785.	-6257.
4053	2384.8	87.			-14150.	-12151.	-3592.	-6652.
4054	2279.3	82.			-12800.	-10307.	-3755.	-6257.
4055		82.			-	-	-	-
4056		79.			-12800.	-9949.	-3964.	-6406.
4057		79.			-12800.	-11475.	-3356.	-6211.
4058		75.			-12800.	-9979.	-3517.	-6019.
4059	2279.3	75.	CORR		-12800.	-11710.	-4092.	-6917.
4060	2249.5	102.	LONG		-6910.	-8282.	-3815.	-5989.
4061		102.	LONG		-3310.	2818.	980.	980.
4062		89.	CORR		-	-12328.	-3709.	-6446.
4063		89.			-	-	-	-
4064		90.			-	1342.	89.	-89.
4065		90.	CORR		-	-	-3503.	-6740.
4066		79.	LONG		-	-7716.	-3189.	-5513.
4067	2249.5	79.	LONG	AX	-	4381.	-	-
4104	2192.4	103.	HNGL	AX	-	-10619.	-4684.	-6857.
4105		103.			-	-2511.	-1562.	-1929.
4106		77.			-	-13249.	-4929.	-7101.
4107	2192.4	77.	HNGL	AX	-	-4898.	-1745.	-2143.

TABLE V-6 (CONCLUDED)

STRESS COMPARISONS OF TESTS 1L AND 7L
(WITH AND WITHOUT FBR)

GAGE NO.	STATION	AZIMUTH DEG.	COMPONENT	DIRECTION	PREDICTED VALUE 1L (PSI)	TEST VALUE W/O FBR 1L-2.1 (PSI)	TEST VALUE W/FBR 7L-2 213L=0 (PSI)	TEST VALUE W/FBR 7L-2 213L=MAX. (PSI)
4111	2185.	84.9	SKIN	CIR	-	-18602.	-7119.	-10693.
4112		86.	STRG	AX	-	4901.	1501.	2450.
4113		86.	STRG	AX	-	-9450.	-3069.	-5485.
4114	2185.	79.8	SKIN	CIR	-	-17374.	-5734.	-9272.
4119	2210.	74.2	RING	CIR	10700.	13394.	4367.	6452.
4120	2210.			CIR	10700.	6653.	2564.	3966.
4122	2209.			AX	19500.	3005.	2323.	2804.
4123	2209.	74.2	RING	AX	-31500.	-26721.	-12280.	-17351.
4131	2210.	105.4	RING	CIR	10700.	13635.	5329.	7856.
4132	2210.			CIR	10700.	6131.	3125.	4728.
4133	2209.			AX	19500.	3045.	1963.	2684.
4134	2209.	105.4	RING	AX	-31500.	-29190.	-12759.	-18788.
4139	2210.	254.4	RING	CIR	-7300.	-10642.	-6724.	-9363.
4140	2210.			CIR	-7300.	-3403.	-1762.	-3203.
4142	2209.			AX	-11000.	-5564.	-3963.	-5444.
4143	2209.	254.4	RING	AX	20000.	26140.	13796.	20547.
4151	2210.	285.7	RING	CIR	-7300.	-9003.	-4724.	-7124.
4152	2210.			CIR	-7300.	-3363.	-1281.	-2562.
4153	2209.			AX	-11000.	-1562.	-2322.	-2322.
4154	2209.	285.7	RING	AX	20000.	18256.	9501.	14599.
4603	2210.	103.	HNGF	AX	0	-	-2099.	-1679.
4649		77.			0	-2748.	-4366.	-4617.
4654		283.			0	-7473.	-5037.	-6632.
4659	2210.	257.	HNGF	AX	0	-5715.	-4114.	-5205.
4695	2187	77.	HNGL	AX	-	-20401.	-6140.	-8860.
4696		257.			-	12329.	4389.	6932.
4697		283.				12289.	4328.	6871.
4698	2187	103.	HNGL	AX	-	-19399.	-6321.	-9072.
4901	2294	24.	CORR	AX	-6400.	-6488.	-2051.	-3033.
4902		114.			-11620.	-13427.	-4909.	-7246.
4903		204.			1890.	2306.	-116.	1040.
4904	2294	294.	CORR	AX	7030.	8690.	3265.	5693.

See figure V-1A for symbol list.

TABLE V-7

STRESS RESULTS FOR TEST 7L-2 (WITHOUT PAYLOAD SHEAR)

GAGE NO.	STATION	AZIMUTH DEG.	COMPONENT	DIRECTION	PREDICTED VALUE (PSI)	TEST VALUE (PSI)	TYPE GAGE INSTALL. SEE FIG V-11.
4001	2520.	88.	Corr.	AX		--	12
4002	↑	88.	↑	↑		-3974.	13
4003		87.				1384.	14
4004		87.				-3768.	15
4005		84.				--	12
4006		85.				-3268.	13
4007	↓	80.	↓	↓		--	12
4008	2520.	80.	Corr.	AX		-3180.	13
4023	2478	89	Dblr.	AX		-2355.	10
4027	2469	89	Long.	AX		- 531.	-
4028	2469	89	Long.	AX		-5398.	-
4032	2453.5	89.	Long.	AX		1093.	2
4033	↑	89.	Long.	↑		-1111.	1
4034		88.	Corr.			-6466.	12
4035	2453.5	88.	Corr.	AX		560.	13
4052	2384.8	87.	Corr.	AX		-3785.	12
4053	2384.8	87.	↑	↑		-3592.	13
4054	2279.3	82.				-3755.	12
4055	↑	82.				--	13
4056		79.				-3964.	12
4057		79.				-3356.	13
4058	↓	75.	↓			-3517.	12
4059	2279.3	75.	Corr.			-4092.	13
4060	2249.5	102.	Long.			-3815.	7
4061	↑	102.	Long.			980.	6
4062		89.	Corr.			-3709.	14
4063		89.	↑			--	15
4064		90.				89.	12
4065		90.	Corr.			-3503.	13
4066	↓	79.	Long.	↓		-3189.	7
4067	2249.5	79.	Long.	AX		--	6
4104	2192.4	103.	Hngl.	AX		-4684.	19
4105	↑	103.	↑			-1562.	16
4106		77.				-4929.	19
4107	2192.4	77.	Hngl.	AX		-1745.	16
4111	2185.	84.9	Skin	CIR		-7119.	11
4112	↑	86.	Strg.	AX		1501.	-
4113	↓	86.	Strg.	AX		-3069.	-

TABLE V-7 (CONCLUDED)

STRESS RESULTS FOR TEST 7L-2 (WITHOUT PAYLOAD SHEAR) (CONCLUDED)

GAGE NO.	STATION	AZIMUTH DEG.	COMPONENT	DIRECTION	PREDICTED VALUE (PSI)	TEST VALUE (PSI)	TYPE GAGE INSTALL. SEE FIG. V-11.
4114	2185.	79.8	Skin	CIR		-5734.	11
4119	2210.	74.2	Ring	CIR		4367.	27
4120	2210	↑	↑	CIR		2564.	30
4122	2209.	↓	↓	AX		2323.	25
4123	2209.	74.2	Ring	AX		-12280.	26
4131	2210.	105.4	Ring	CIR		5329.	27
4132	2210.	↑	↑	CIR		3125.	30
4133	2209.	↓	↓	AX		1963.	25
4134	2209.	105.4	Ring	AX		-12759.	26
4139	2210.	254.4	Ring	CIR		-6724.	27
4140	2210.	↑	↑	CIR		-1762.	30
4142	2209.	↓	↓	AX		-3963.	25
4143	2209.	254.4	Ring	AX		13796.	26
4151	2210.	285.7	Ring	CIR		-4724.	27
4152	2210.	↑	↑	CIR		-1281.	30
4153	2209.	↓	↓	AX		-2322.	25
4154	2209.	285.7	Ring	AX		9501.	26
4603	2210.	103.	Hngf.	AX	0	-2099.	31
4649	↑	77.	↑	↕	0	-4366.	31
4654	↓	283.	↓	↕	0	-5037.	31
4659	2210.	257.	Hngf.	AX	0	-4114.	31
4695	2187	77.	Hngl.	AX		-6140.	18
4696	↑	257.	↑	↕		4389.	18
4697	↓	283.	↓	↕		4328.	18
4698	2187	103.	Hngl.	AX		-6321.	18
4901	2294	24.	Corr.	AX		-2051.	12
4902	↑	114.	↓	↕		-4909.	12
4903	↓	204.	↑	↕		- 116.	12
4904	2294	294.	Corr.	AX		3265.	12

See figure V-1A for symbol list.

TABLE V-8

STRESS RESULTS FOR TEST 7L-2 (WITH MAXIMUM PAYLOAD SHEAR)

GAGE NO.	STATION	AZIMUTH DEG.	COMPONENT	DIRECTION	PREDICTED VALUE (PSI)	TEST VALUE (PSI)	TYPE GAGE INSTALL. SEE FIG. V-11.
4001	2520.	88.	Corr.	AX		--	12
4002	↑	88.	↑	↑		-6740.	13
4003		87.				-6122.	14
4004		87.				-6446.	15
4005		84.				--	12
4006		84.				-5593.	13
4007	↓	80.	↓	↓		--	12
4008	2520.	80.	Corr.	AX		-5446.	13
4023	2478	89	Dblr.	AX		-4004.	10
4027	2469	89	Long.	AX		-1248.	-
4028	2469	89	Long.	AX		-7394.	-
4032	2453.5	89.	Long.	AX		- 312.	2
4033	↑	89.	Long.	↑		-3651.	1
4034		88.	Corr.			-7180.	12
4035	2453.5	88.	Corr.	AX		-1413.	13
4052	2384.8	87.	Corr.	AX		-6257.	12
4053	2384.8	87.	↑	↑		-6652.	13
4054	2279.3	82.				-6257.	12
4055	↑	82.				--	13
4056		79.				-6406.	12
4057		79.				-6211.	13
4058	↓	75.	↓	↓		-6019.	12
4059	2279.3	75.	Corr.			-6917.	13
4060	2249.5	102.	Long.			-5989.	7
4061	↑	102.	Long.			980.	6
4062		89.	Corr.			-6446.	14
4063		89.	↑			--	15
4064		90.				- 89.	12
4065		90.	Corr.			-6740.	13
4066	↓	79.	Long.	↓		-5513.	7
4067	2249.5	79.	Long.	AX		--	6
4104	2192.4	103.	Hngl.	AX		-6857.	19
4105	↑	103.	↑	↑		-1929.	16
4106		77.				-7101.	19
4107	2192.4	77.	Hngl.	AX		-2143.	16

TABLE V-8

STRESS RESULTS FOR TEST 7L-2 (WITH MAXIMUM PAYLOAD SHEAR) (CONCLUDED)

GAGE	STATION	AZIMUTH DEG.	COMPONENT	DIRECTION	PREDICTED VALUE (PSI)	TEST VALUE (PSI)	TYPE GAGE INSTALL. SEE FIG. V-11.
4111	2185.	84.9	Skin	CIR		-10693.	11
4112	↑	86.	Strg.	AX		2450.	-
4113	↓	86.	Strg.	AX		-5485.	-
4114	2185.	79.8	Skin	CIR		-9272.	11
4119	2210.	74.2	Ring	CIR		6452.	27
4120	2210	↑	↑	CIR		3966.	30
4122	2209.	↓	↓	AX		2804.	25
4123	2209.	74.2	Ring	AX		-17351.	26
4131	2210.	105.4	Ring	CIR		7856.	27
4132	2210.	↑	↑	CIR		4728.	30
4133	2209.	↓	↓	AX		2684.	25
4134	2209.	105.4	Ring	AX		-18788.	26
4139	2210.	254.4	Ring	CIR		-9363.	27
4140	2210.	↑	↑	CIR		-3203.	30
4142	2209.	↓	↓	AX		-5444.	25
4143	2209.	254.4	Ring	AX		20547.	26
4151	2210.	285.7	Ring	CIR		-7124.	27
4152	2210.	↑	↑	CIR		-2562.	30
4153	2209.	↓	↓	AX		-2322.	25
4154	2209.	285.7	Ring	AX		14599.	26
4603	2210.	103.	Hngf.	AX	0	-1679.	31
4649	↑	77.	↑		0	-4617.	31
4654	↓	283.	↓		0	-6632.	31
4659	2210.	257.	Hngf.	AX	0	-5205.	31
4695	2187	77.	Hngl.	AX		-8860.	18
4696	↑	257.	↑			6932.	18
4697	↓	283.	↓			6871.	18
4698	2187	103.	Hngl.	AX		-9072.	18
4901	2294	24.	Corr.	AX		-3003.	12
4902	↑	114.	↑			-7246.	12
4903	↓	204.	↓			1040.	12
4904	2294	294.	Corr.	AX		5693.	12

See figure V-1A for symbol list.

TABLE V-9
STRESS RESULTS FOR TEST 5L-2

GAGE NO.	STATION	AZIMUTH DEG.	COMPONENT	DIRECTION	PREDICTED VALUE (PSI)	TEST VALUE (PSI)	TYPE GAGE INSTALL. SEE FIG. V-11.
4135	2213	254.	RING	AX		-32410.	22
4137	2213	254.	RING	AX		11321.	23
4139	2210	254.	RING	CIR		11146.	27
4142	2209	254.	RING	AX		6412.	25
4143	2209	254.	RING	AX		-29708.	26
4409	2220.9	237.	LONG	AX		--	5
4410	2220.9	237.	LONG	AX		- 5496.	4
4413	2192.2	238.	D STIF	AX		1717.	8
4414	2192.2	238.	D STIF	AX		- 4899.	9
4695	2187	77.	HNGL	AX		12749.	18
4696	2187	257.	HNGL	AX		- 9192.	18
4697	2187	283.	HNGL	AX		- 9041	18
4698	2187	103.	HNGL	AX		9385.	18
4901	2294	24.	CORR	AX		5693.	12
4902	2294	114.	CORR	AX		4825.	12
4903	2294	204.	CORR	AX		- 8112.	12
4904	2294	294.	CORR	AX		- 5919.	12

See figure V-1A for symbol list.

TABLE V-10

STRESS RESULTS FOR TEST 6L-1A

GAGE NO.	STATION	AZIMUTH DEG.	COMPONENT	DIRECTION	PREDICTED VALUE (PSI)	TEST VALUE (PSI)	TYPE GAGE INSTALL. SEE FIG. V-11.
4135	2213	254.	RING	AX		-22525.	22
4137	2213	254.	RING	AX		8619.	23
4139	2210	254.	RING	CIR		5530.	27
4142	2209	254.	RING	AX		2363.	25
4143	2209	254.	RING	AX		-19186.	26
4409	2220.9	237.	LONG	AX		--	5
4410	2220.9	237.	LONG	AX		- 5212.	4
4413	2192.2	238.	D STIF	AX		--	8
4414	2192.2	238.	D STIF	AX		- 2871.	9
4695	2187	77.	HNGL	AX		8383.	18
4696	2187	257.	HNGL	AX		- 6230.	18
4697	2187	283.	HNGL	AX		- 6109.	18
4698	2187	103.	HNGL	AX		641[illegible].	18
4901	2294	24.	CORR	AX		4103.	12
4902	2294	114.	CORR	AX		3178.	12
4903	2294	204.	CORR	AX		- 6208.	12
4904	2294	294.	CORR	AX		- 4187.	12

See figure V-1A for symbol list.

TABLE V-11
STRESS RESULTS FOR TEST 6L-1B

GAGE NO.	STATION	AZIMUTH DEG.	COMPONENT	DIRECTION	PREDICTED VALUE (PSI)	TEST VALUE (PSI)	TYPE GAGE INSTALL. SEE FIG. V-11.
4135	2213	254.	RING	AX		-23126.	22
4137	2213	254.	RING	AX		9345.	23
4139	2210	254.	RING	CIR		5570.	27
4142	2209	254.	RING	AX		2484.	25
4143	2209	254.	RING	AX		-20343.	26
4409	2220.9	237.	LONG	AX		--	5
4410	2220.9	237.	LONG	AX		- 5528.	4
4413	2192.2	238.	D STIF	AX		531.	8
4414	2192.2	238.	D STIF	AX		- 2933.	9
4695	2187	77.	HNGL	AX		8416.	18
4696	2187	257.	HNGL	AX		- 6502.	18
4697	2187	283.	HNGL	AX		- 6351.	18
4698	2187	103.	HNGL	AX		6266.	18
4901	2294	24.	CORR	AX		5172.	12
4902	2294	114.	CORR	AX		4739.	12
4903	2294	204.	CORR	AX		- 6034.	12
4904	2294	294.	CORR	AX		- 3754.	12

See figure V-1A for symbol list.

TABLE V-12

STRESS RESULTS FOR TEST 7L-1 (WITH MAXIMUM PAYLOAD SHEAR)

GAGE NO.	STATION	AZIMUTH DEG.	COMPONENT	DIRECTION	PREDICTED VALUE (PSI)	TEST VALUE (PSI)	TYPE GAGE INSTALL. SEE FIG. V-11.
4001	2520.	88.	Corr.	AX		--	12
4002	↑	88.	↑	↑		-1001.	13
4003		87.				--	14
4004		87.				-854.	15
4005		84.				--	12
4006		84.				-736.	13
4007	↓	80.	↓	↓		--	12
4008	2520.	80.	Corr.	AX		-766.	13
4023	2478	89	Dblr.	AX		-618.	10
4027	2469	89	Long.	AX		--	-
4028	2469	89	Long.	AX		-2653	-
4032	2453.5	89.	Long.	AX		3309.	2
4033	↑	89.	Long.	↑		1493.	1
4034	↓	88.	Corr.	↓		-1580.	12
4035	2453.5	88.	Corr.	AX		3358.	13
4052	2384.8	87.	Corr.	AX		-388.	12
4053	2384.8	87.	↑	↑		471.	13
4054	2279.3	82.				-447.	12
4055	↑	82.				--	13
4056		79.				-626.	12
4057		79.				324	13
4058	↓	75.	↓	↓		-417.	12
4059	2279.3	75.	Corr.			-206.	13
4060	2249.5	102.	Long.			-715.	7
4061	↑	102.	Long.			--	6
4062		89.	Corr.			--	14
4063		89.	↑			--	15
4064		90.				--	12
4065		90.	Corr.			795.	13
4066	↓	79.	Long.	↓		-388.	7
4067	2249.5	79.	Long.	AX		--	6
4104	2192.4	103.	Hngl.	AX		-1102.	19
4105	↑	103.	↑	↑		--	16
4106		77.				--	19
4107	2192.4	77.	Hngl.	AX		--	16
4111	2185.	84.9	Skin	CIR		-1194.	11
4112	↑	86.	Strg.	AX		--	-
4113	↓	86.	Strg.	AX		--	-
4114	2185.	79.8	Skin	CIR		-809.	11

TABLE V-12

STRESS RESULTS FOR TEST 7L-1 (WITH MAXIMUM PAYLOAD SHEAR) (CONCLUDED)

GAGE NO.	STATION	AZIMUTH DEG.	COMPONENT	DIRECTION	PREDICTED VALUE (PSI)	TEST VALUE (PSI)	TYPE GAGE INSTALL. SEE FIG. V-11
4119	2210.	74.2	Ring	CIR		801.	27
4120	2210	↕	↕	CIR		481.	30
4122	2209.			AX		--	25
4123	2209.	74.2	Ring	AX		--	26
4131	2210.	105.4	Ring	CIR		--	27
4132	2210.	↕	↕	CIR		481.	30
4133	2209.			AX		--	25
4134	2209.	105.4	Ring	AX		-2883.	26
4139	2210.	254.4	Ring	CIR		-1962.	27
4140	2210.	↕	↕	CIR		240.	30
4142	2209.			AX		-1241.	25
4143	2209.	254.4	Ring	AX		1242.	26
4151	2210.	285.7	Ring	CIR		-1121.	27
4152	2210.	↕	↕	CIR		441.	30
4153	2209.			AX		-1922.	25
4154	2209.	285.7	Ring	AX		1362.	26
4603	2210.	103.	Hngf.	AX	0	-2435.	31
4649	↕	77.	↕	↕	0	-2435.	31
4654		283.			0	-2855.	31
4659	2210.	257.	Hngf.	AX	0	-2687.	31
4695	2187	77.	Hngl.	AX		-1240.	18
4696	↕	257.	↕	↕		333.	18
4697		283.				272.	18
4698	2187	103.	Hngl.	AX		- 998.	18
4901	2294	24.	Corr.	AX		- 722.	12
4902	↕	114.	↕	↕		-1473.	12
4903		205.				-1329.	12
4904	2294	294.	Corr.	AX		376.	12

See figure V-1A for symbol list.

TABLE V.-13

STRESS RESULTS FOR ROSETTE GAGES:

4680, 4681, AND 4682

STATION: 2185

COMPONENT: SKIN

AZIMUTH: 140 DEG.

TEST	TEST MAXIMUM VALUE (PSI)	TEST MINIMUM VALUE (PSI)	TEST SHEAR VALUE (PSI)
3L	625	-14,853	7739
4L	10,952	1419	4766

STRESS RESULTS FOR ROSETTE GAGES:

4683, 4684, AND 4685

STATION: 2185

COMPONENT: SKIN

AZIMUTH: 143 DEG

TEST	TEST MAXIMUM VALUE (PSI)	TEST MINIMUM VALUE (PSI)	TEST SHEAR VALUE (PSI)
1L-1.2	237	-1292	765
1L-2.1	2,346	-6436	4391
2L-1	7,056	-4343	5700
2L-1A	4,828	-3120	3974
3L	4,756	-13099	8928
4L	11,141	-877	6009
5L-2	8,060	-8676	8368
6L-1A	7,638	-2704	5171
6L-1B	7,751	-2583	5167

TABLE V -13 (CONTINUED)

STRESS RESULTS FOR ROSETTE GAGES:

4686, 4687, AND 4688

STATION: 2185

COMPONENT: SKIN

AZIMUTH: 143 DEG.

TEST	TEST MAXIMUM VALUE (PSI)	TEST MINIMUM VALUE (PSI)	TEST SHEAR VALUE (PSI)
1L-1.2	-58	-938	440
1L-2.1	-437	-4797	2180
2L-1	3728	-2414	3071
2L-1A	2607	-1730	2169
3L	-3582	-14,647	5532
4L	13,004	2131	5436

STRESS RESULTS FOR ROSETTE GAGES:

4689, 4690, AND 4691

STATION: 2185

COMPONENT: SKIN

AZIMUTH: 147 DEG.

TEST	TEST MAXIMUM VALUE (PSI)	TEST MINIMUM VALUE (PSI)	TEST SHEAR VALUE (PSI)
3L	511	-11,693	6102
4L	9244	1253	3996

TABLE V-13 (CONCLUDED)

STRESS RESULTS FOR ROSETTE GAGES:

4692, 4693, AND 4694

STATION: 2185

COMPONENT: SKIN

AZIMUTH: 151 DEG

TEST	TEST MAXIMUM VALUE (PSI)	TEST MINIMUM VALUE (PSI)	TEST SHEAR VALUE (PSI)
3L	-901	-10,579	4839
4L	6912	3111	1901
5L-2	14,310	-14,375	14,342
6L-1A	9100	-9406	9253
6L-1B	9160	-9232	9196

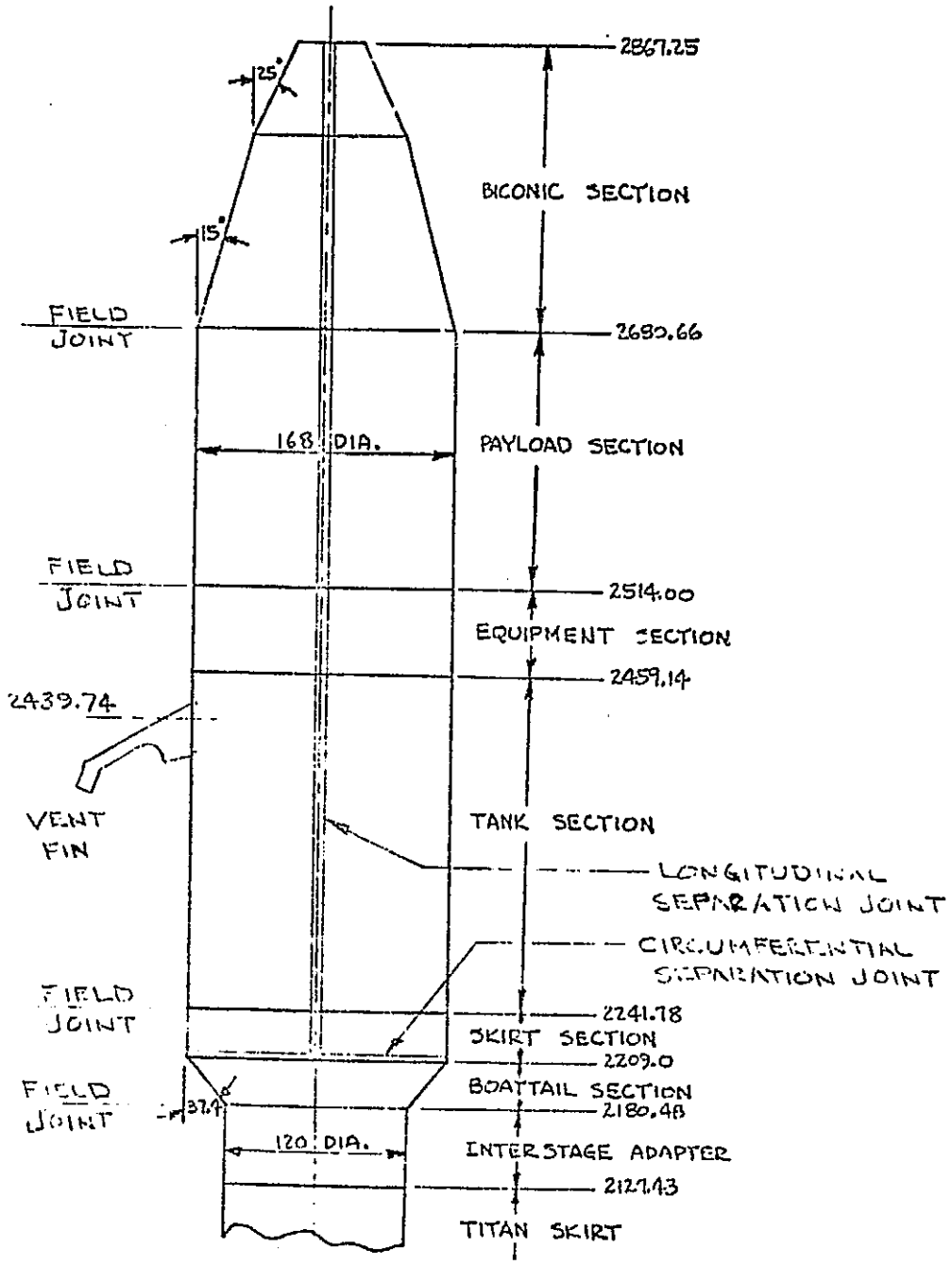

FIGURE V-1. CENTAUR STANDARD SHROUD (CSS) CONFIGURATION.

ORIGINAL PAGE IS
OF POOR QUALITY

ORIGINAL PAGE IS
OF POOR QUALITY

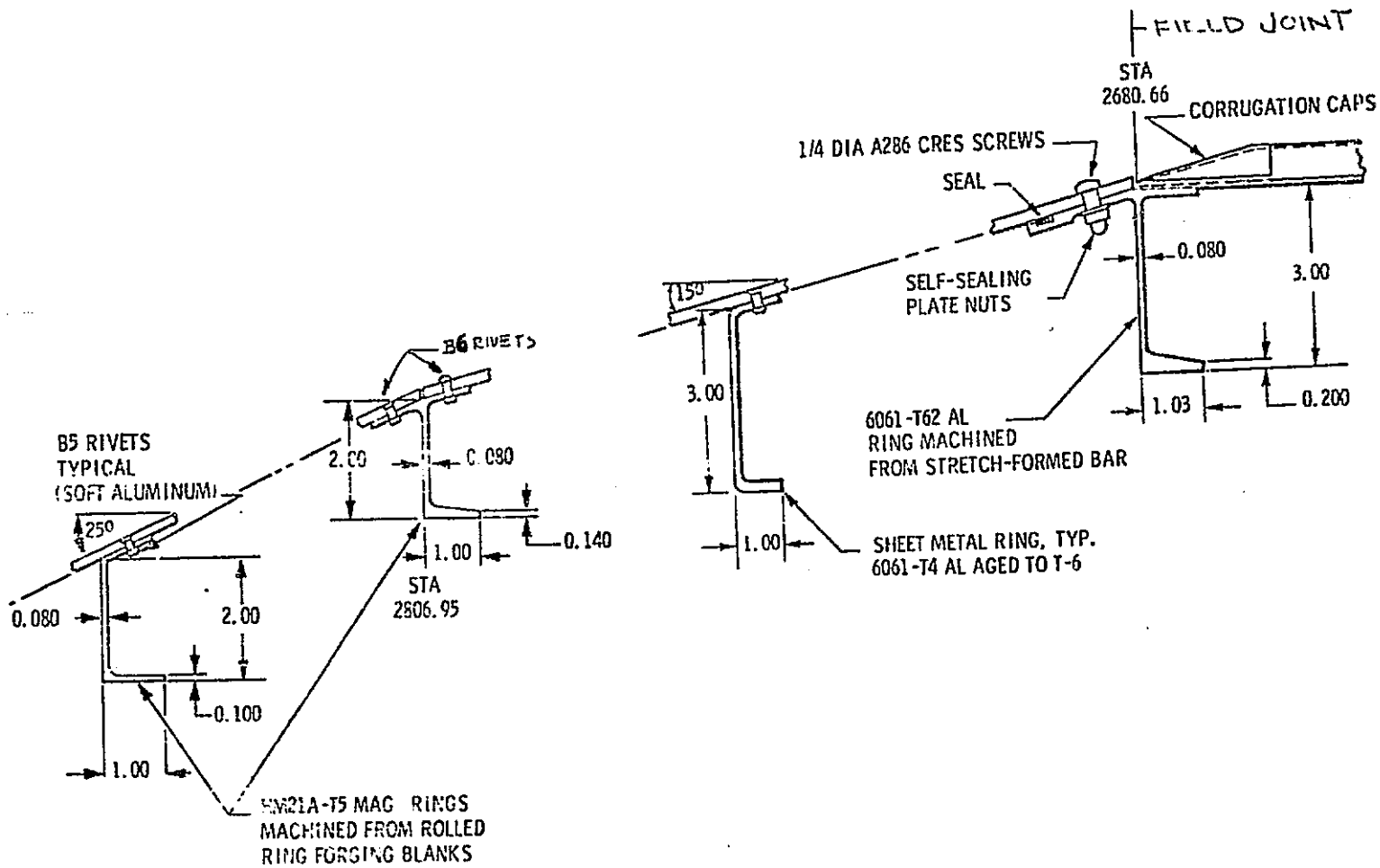

FIGURE V-2. NOSE CONE RING DETAILS.

LOCATION (STA)	SKIN	CORRUGATION
2680.66 - 2514.00	0.032	0.020
2514.00 - 2458.10	0.040	0.025
2458.10 - 2316.78	0.032	0.020
2316.78 - 2241.78	0.040	0.025
2241.78 - 2209.00	0.050	0.032
2209.00 - 2180.48	0.080	0.040

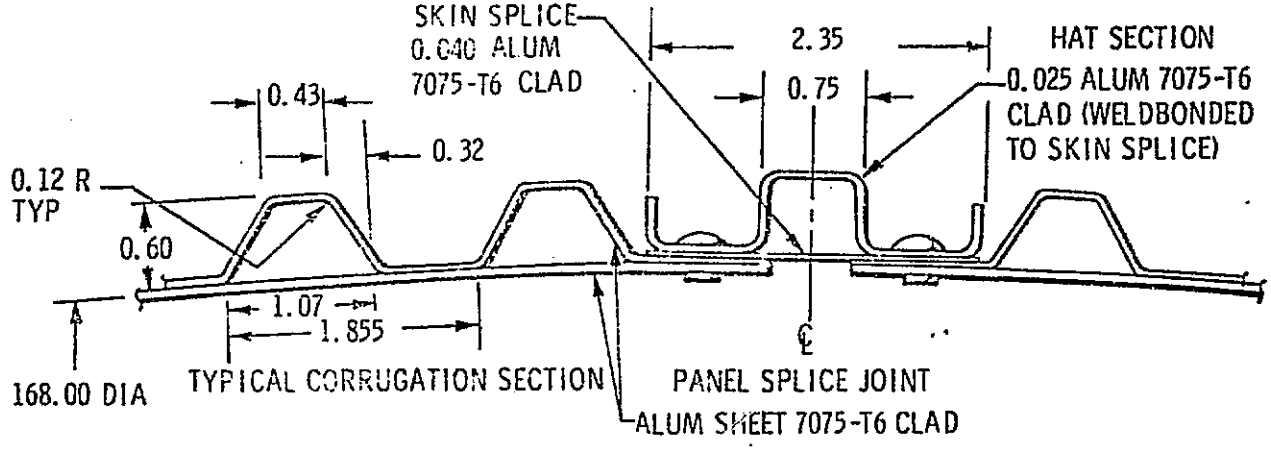

FIGURE V-3. PANEL DETAILS.

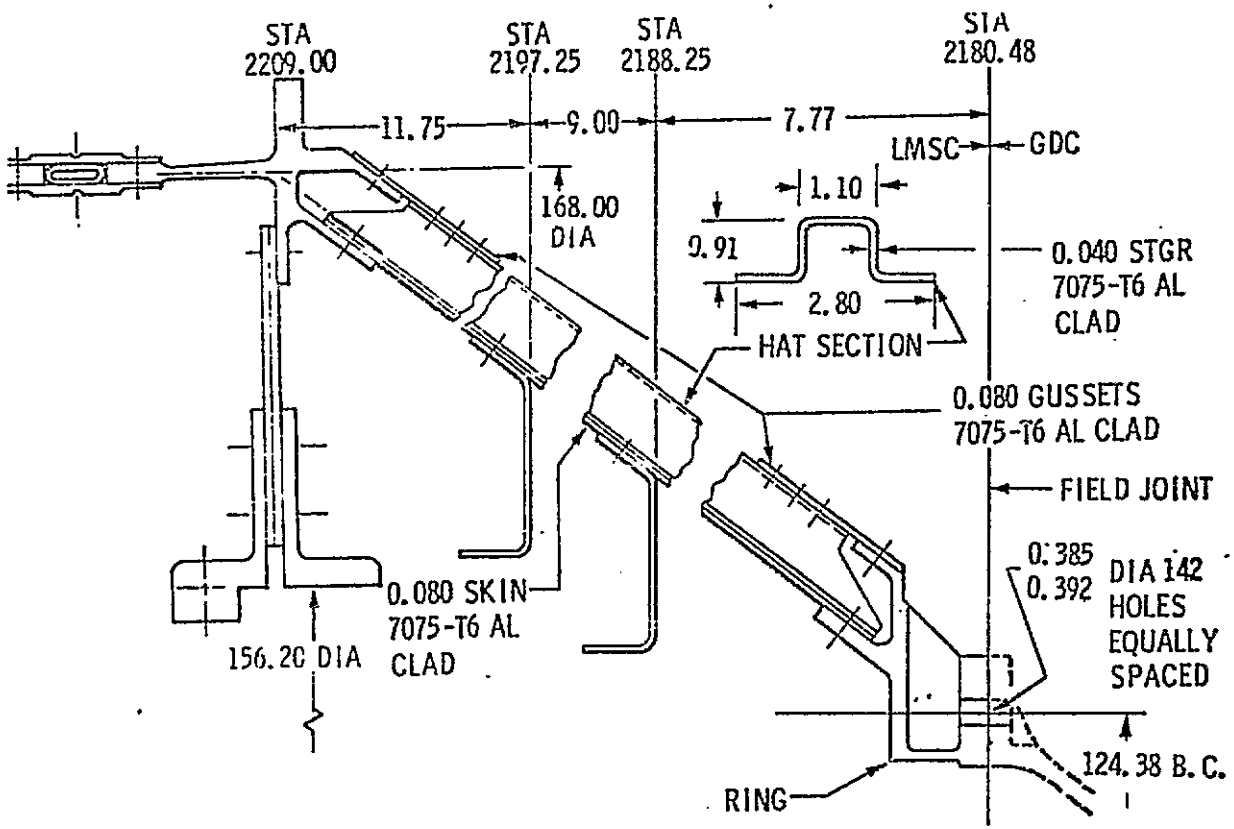

FIGURE V-4. BOATTAIL INTERFACE STRUCTURE.

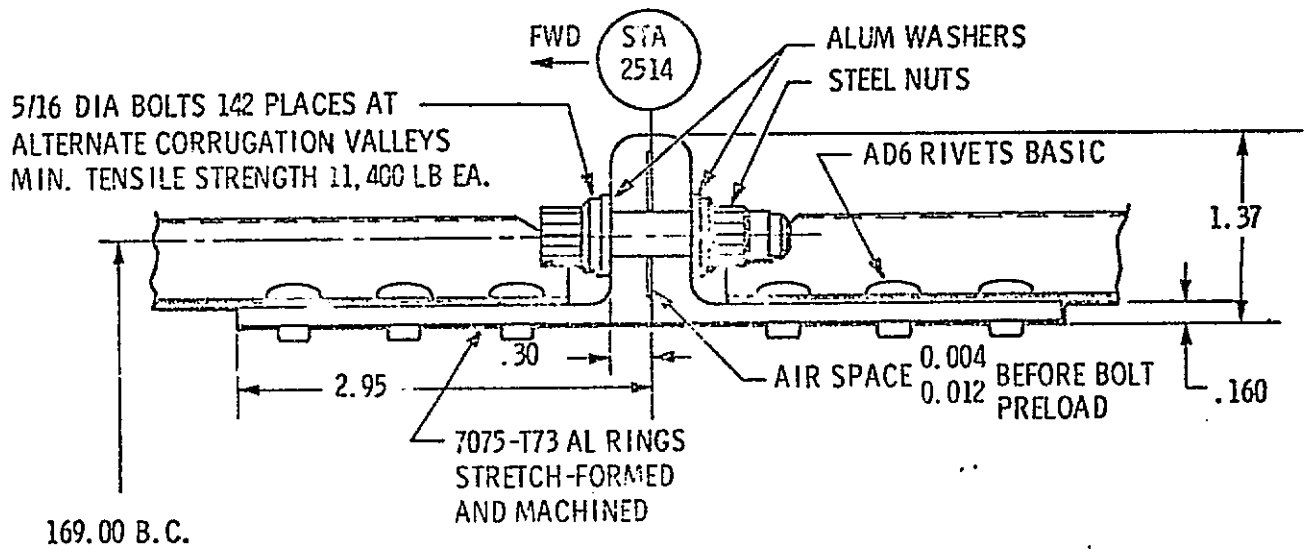

FIGURE V-5. CYLINDRICAL SECTION FIELD JOINT DETAILS.

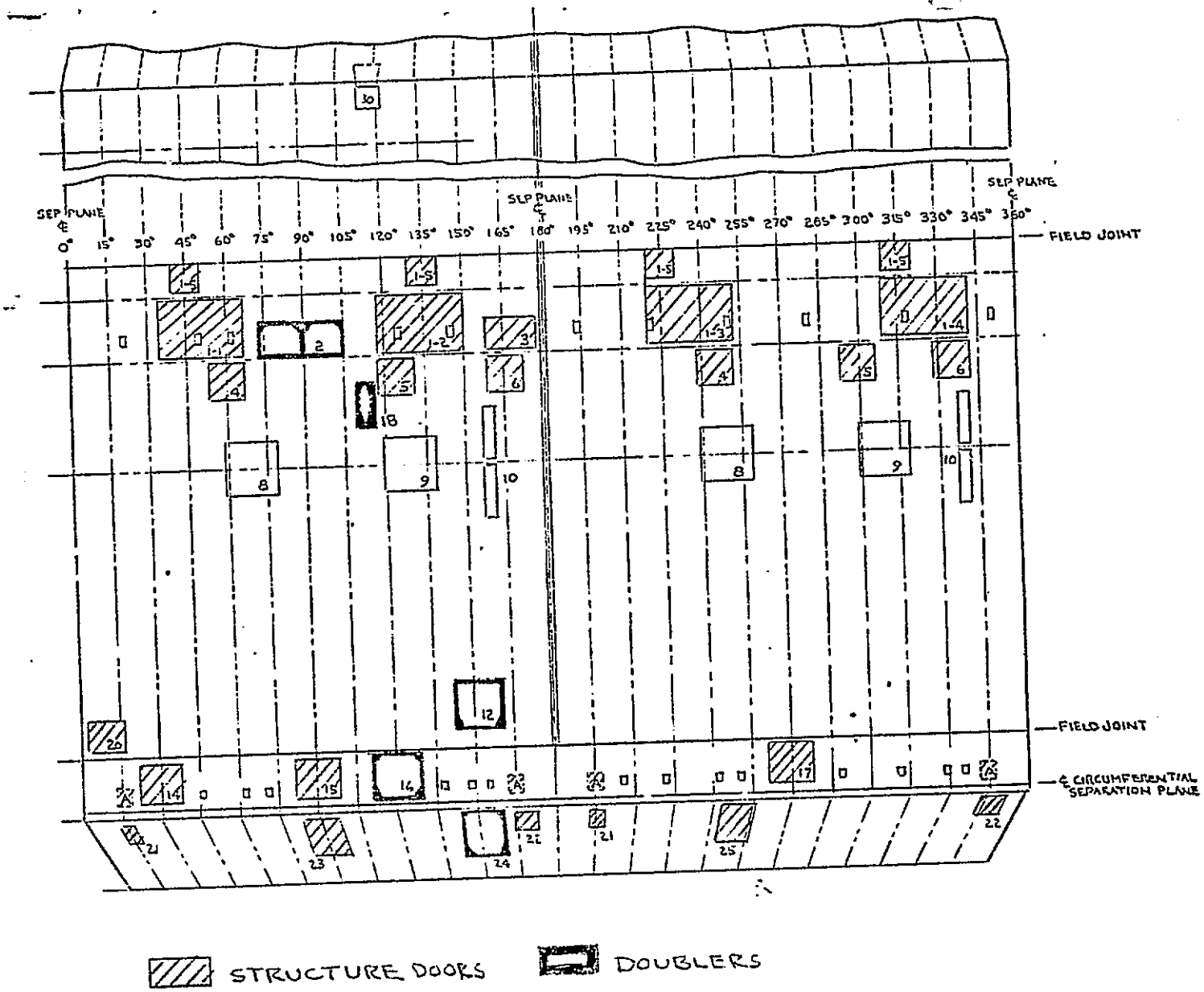

FIGURE V-6. CENTAUR VEHICLE ACCESS REQUIREMENTS.

DOOR NO.	ACCESS TO:
1-1	EQUIPMENT MODULE - QUAD 1
1-2	" " - QUAD 2
1-3	" " - QUAD 3
1-4	" " - QUAD 4
1-5	PAYLOAD PICK UP ARM DOORS
2	ELECTRICAL UMBILICAL PANEL CHUTE
3	AIR CONDITIONING INLET & IRU LINE OF SIGHT
4	RSC ANTENNA
5	"S" BAND ANTENNA & BALANCED VENT
6	"C" BAND ANTENNA
8	RSC ANTENNA & GROUND PLANE - SHROUD MOUNT
9	"S" BAND ANTENNA & GROUND PLANE - SHROUD MOUNT
10	"C" BAND ANTENNA & FAIRING - SHROUD MOUNT
12	LH_2 FILL & DRAIN VALVE CHUTE & DOOR
14	ATTITUDE & ULLAGE MOTORS
15	BOOST PUMP
16	LO_2 FILL & DRAIN VALVE CHUTE & DOOR
17	SHAPED CHARGE DET, MOTORS, DIAPHRAGM SEAL
18	H_2 VENT FIN MOUNTING
20	VEHICLE DESTRUCT UNIT
21	ATTITUDE CONTROL MOTOR EXHAUST
22	" " " "
23	SHAPED CHARGE DET & BOOST PUMP EXHAUST
24	T-4 UMBILICAL PANEL CHUTE & DOOR
25	H_2O_2 BOTTLE
30	PAYLOAD AIR CONDITIONING INLET
A	SPRING LOCKING DOOR

FIGURE V-6. CENTAUR VEHICLE ACCESS REQUIREMENTS (CONCLUDED)

ORIGINAL PAGE IS
OF POOR QUALITY

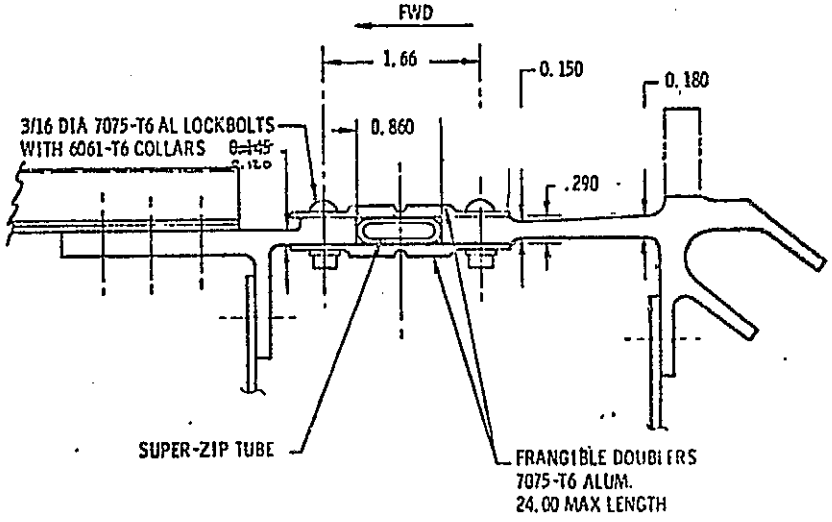

CIRCUMFERENTIAL JOINT

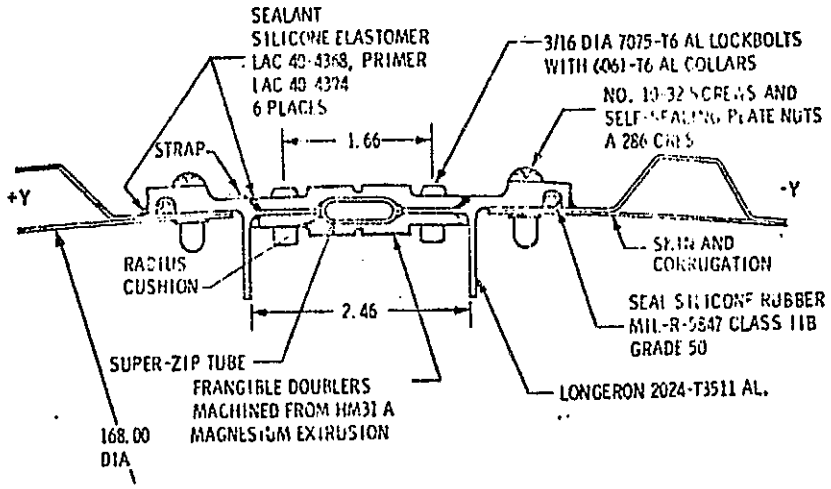

LONGITUDINAL JOINT

FIGURE V-7. SEPARATION JOINT DETAILS.

ORIGINAL PAGE IS
OF POOR QUALITY

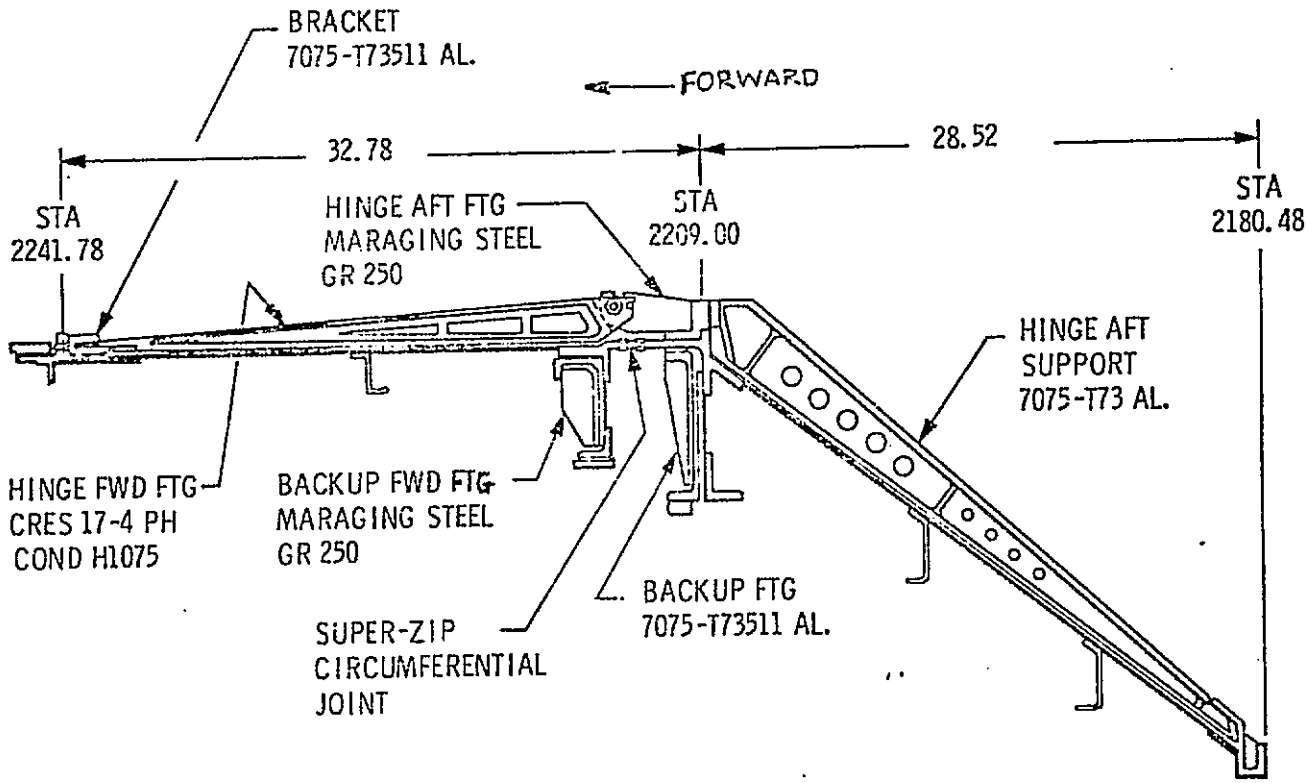

FIGURE V-8. HINGE STRUCTURE ARRANGEMENT.

ORIGINAL PAGE IS
OF POOR QUALITY

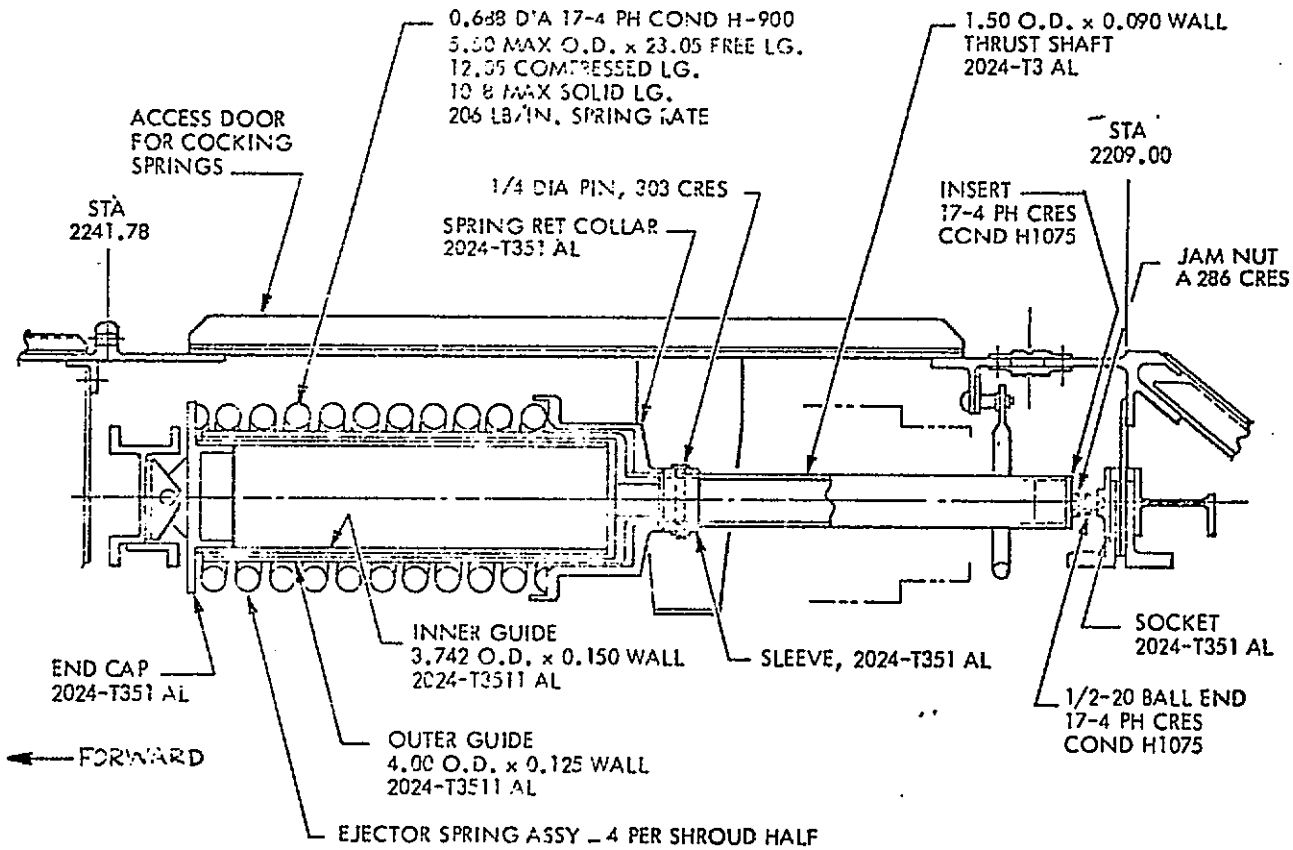

FIGURE V-9. THRUSTER SPRING SYSTEM.

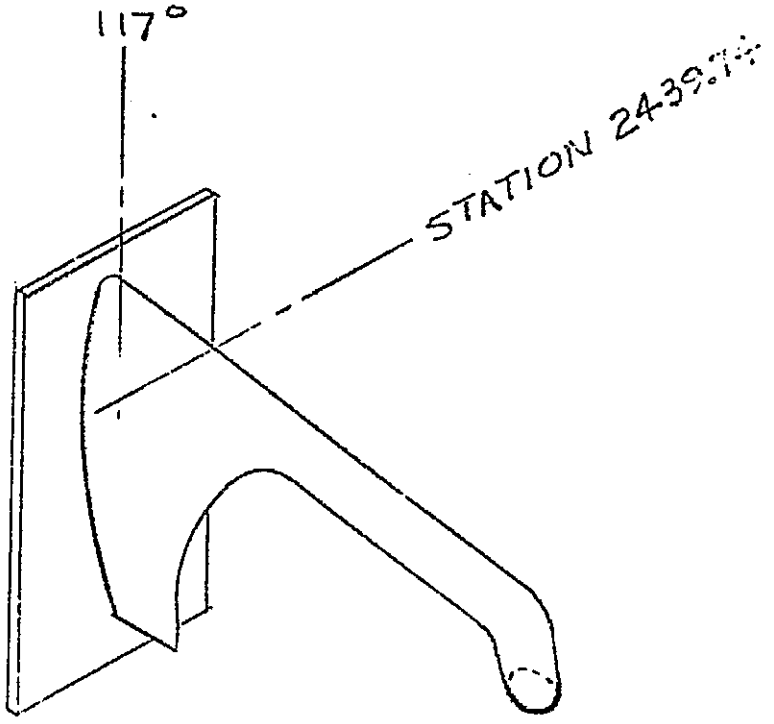

FIGURE V-10. LH_2 VENT FIN STRUCTURE.

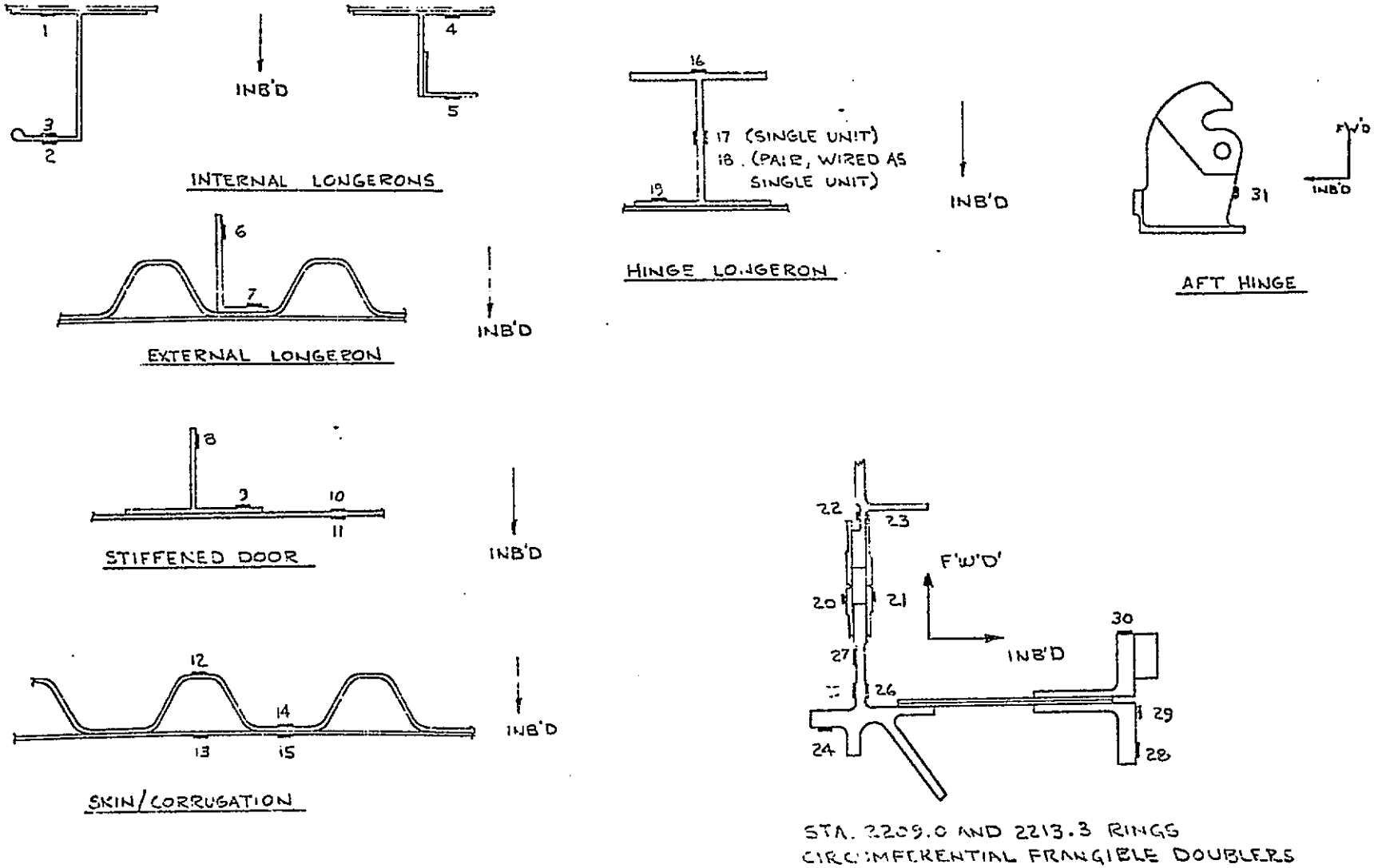

FIGURE V-11. STRAIN GAGE INSTALLATION LOCATIONS.

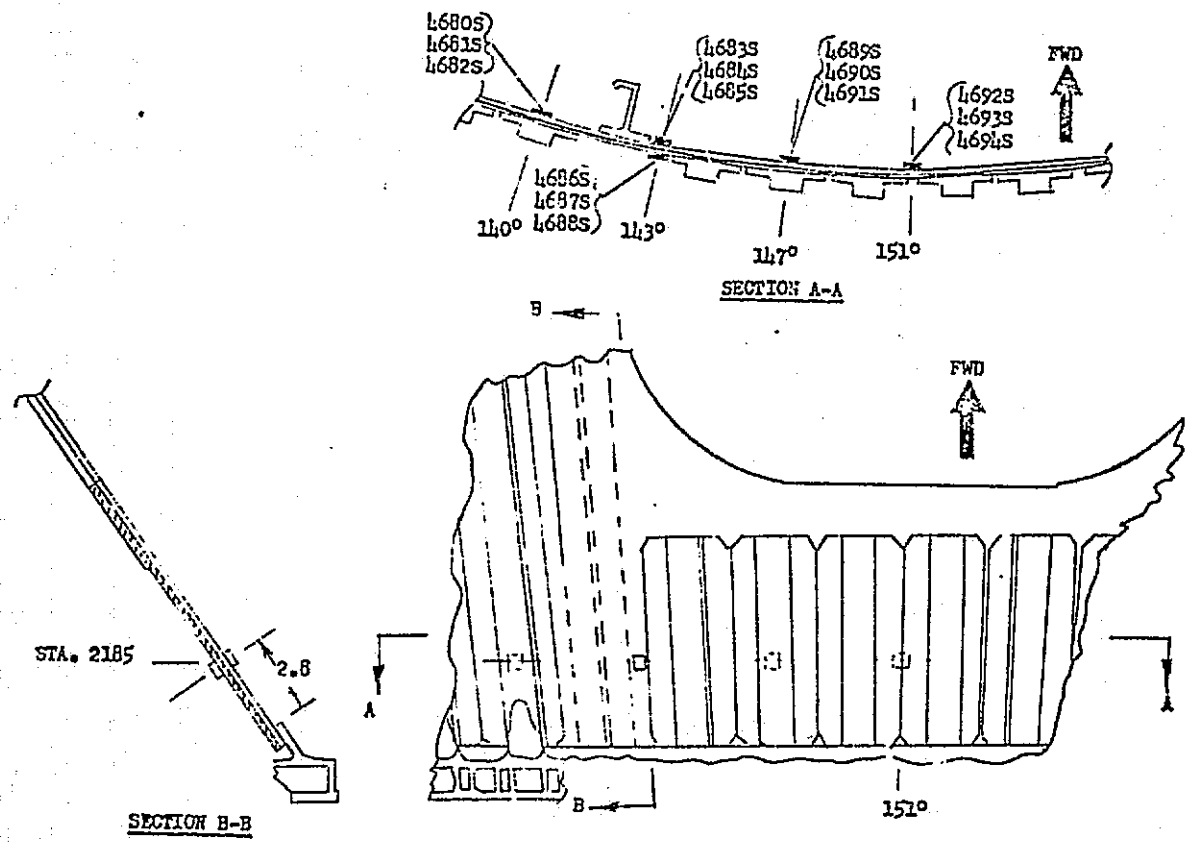

FIGURE V-12. ROSETTE STRAIN GAGE LOCATIONS ON BOATTAIL.

VI STIFFNESS PROPERTIES

By R. P. Miller and T. F. Niezgoda

SUMMARY

Stiffness properties were determined for: (1) the CSS both with and without the FBR in place, (2) the FBR system, and (3) the Centaur, ISA, and Titan skirt. Data were acquired that indicated that the CSS and its attachment to the ISA exhibited less stiffness than the analytical model had predicted. The deviations from expected values were primarily in the aft portion of the boattail, and in the interstage structure. The larger than expected CSS deflections resulted in excessive clearance loss between the CSS and Centaur; this necessitated the use of the FBR system which reduced the clearance loss to acceptable values. Revisions were made to the analytical model to take the test findings into account.

TEST CONFIGURATION

The Titan skirt, ISA, Centaur vehicle, and the CSS were mounted as shown in figure I-2. The entire test specimen assembly was mounted to and cantilevered from a relatively stiff cylindrical steel base. The steel base cylinder was restrained in the tower by shear ties to the main tower structural members. The tower structure was reinforced by cross bracing in the section where the base cylinder was attached to increase load capability and to stiffen the base of the test setup.

The CSS and Centaur were loaded by axial and lateral loads which resulted in the desired shear loads, axial loads, and moment distribution over the entire test specimen. The load application systems are described in Appendix B.

String type deflectometers were used to obtain deflection data. A schematic of the general instrumentation setup is shown in figure VI-1. This figure represents the basic instrumentation plan for each test azimuth. A definition of the deflectometer locations for each test is contained in reference 7. The deflectometer locations were specified to provide data to define (1) lateral displacement of the test structure to allow accurate determination of the deflected shape, (2) axial deflection and rotation of cross sectional planes, (3) radial displacement to define distortion or out of roundness of the cylindrical shells, (4) relative motion between CSS and Centaur, (5) FBR spring rate, and (6) both plane rotation and lateral motion of the base cylinder to isolate the effect of the test fixture from the test specimen. The instrumentation was located in a manner that allowed definition of the individual stiffness characteristics

ORIGINAL PAGE IS OF POOR QUALITY

of the different sections of the test specimen assembly, such as Titan skirt, ISA, boattail, CSS, and Centaur. All lateral deflectometers were referenced to the tower structure. The axial and plane rotation instrumentation was referenced to the forward end of the base cylinder except for those instruments monitoring the motion of the base cylinder. These motions were referenced to the tower structure. To assure that the tower provided a stable reference, and to allow for corrections if required in the event of tower motion from wind or test loads, a laser reference was established. Throughout testing the tower motions were of negligible amplitude.

Relative motion between the Centaur and the CSS was measured by instrumentation as illustrated in Figure VI-2. At the FBR location the desired measurement accuracy required to define the FBR spring rate was achieved by utilizing six deflectometers. The average reading of two instruments A and B, oriented tangentially from the CSS neutral axis, provided CSS displacement. The displacement of the Centaur was determined by combining the output from the four deflectometers C, D, E, F. By computing the difference in displacements of the CSS and Centaur neutral axes, the deflection of the total FBR system was obtained with most of the local effects eliminated. The FBR load was determined from the calibrated strain gaged FBR struts.

The deflectometer outputs were monitored and recorded as described in Appendix B. A Cathode Ray Tube (CRT) allowed direct observations of such parameters as cross-sectional plane rotations, average outputs from tangential deflectometers, FBR deflections, and system loads. The displays were updated every 2 seconds. In addition to digital displays a video "Bar Chart" was utilized to monitor all critical channels. This device provided instantaneous assessment as to the linearity of the relationship between load and deflection and indications of any yielding occurring in the test structures.

RESULTS AND DISCUSSION

The tests were conducted in a chronological sequence dictated by structural strength considerations. Each test provided deflection data that further defined the stiffness characteristics of the overall structure so that the final definition of structural stiffness properties evolved throughout the test series. The results are discussed first from a general test series view followed by a presentation and discussion of each test in chronological order.

All deflection data reported herein is presented with the plane rotation and translational effects of the test fixture base cylinder removed. The aft joint of the Titan skirt was of a nonflight type design and the effect of the rotation of this joint has also been removed from the data. Thus, the deflections described are of the test specimen fixed to a rigid base at Station 2050 (aft end of Titan skirt).

The test results indicate that the CSS and its attachment to the ISA exhibit less stiffness than the analytical model (Appendix C) predicts (see figure VI-3). This deviation from expected values exists primarily in the aft boattail section of the CSS and the ISA. This results in lateral deflections of the CSS at Station 2680 that exceed expected values by 46% to 80% depending upon shear azimuth and the extent of "exercising" that the structure was exposed to prior to collecting test data. Revisions were made to the analytical model of the boattail section of the CSS following Tests 3L and 1L-2. See figure VI-4. The larger than expected CSS deflections results in excessive clearance loss between the CSS and Centaur and necessitates the use of the FBR system to limit relative motion. Further tests were conducted that defined the stiffness characteristics of the CSS, FBR, and Centaur system. The results of these tests verified the stiffness of the FBR system to be 19,000 lbs./in. as expected, and demonstrated that the relative motion between the CSS and Centaur under limit load with the FBR system installed, is held to an acceptable value (see Section III for a description of the FBR system).

The lateral deflection of the composite CSS, FBR, and Centaur system is compared to predicted values based upon revised boattail stiffnesses in figures VI-5 and VI-6.

In tests where the Centaur vehicle was subjected to lateral loads it exhibited stiffness properties approximately 14% less than expected. See figures VI-7 and VI-8.

Throughout testing the deflection data for the Titan skirt and the aft section of the ISA indicated close agreement with expected values.

The test series yielded data that indicates a non-linear relationship between lateral load and lateral deflection. This non-linear characteristic is attributed to slippage within riveted joints as friction is overcome with applied load.

Two revised analytical boattail stiffness models were developed to define the flexibility of the CSS (Appendix C). Revision I is based upon the nominal test data for a load up to 25% of limit. Revision II is based upon the test deflection at 100% of limit load for Test 1L-2 which provided the maximum lateral deflection. A comparison of test data and predicted values from the revised analytical models is shown in figures VI-4, VI-5, VI-6, VI-9, and VI-10.

Test 3L - The first test of the series, 3L, applied the shear load in the 150 degree azimuth. Prior to Test 3L several loadings below 50% were applied in order to check out test equipment. As a result, the structure was exercised in the 150 degree azimuth and all slack was removed from test fixtures and test specimen joints.

Figures VI-11 through VI-14 present lateral deflection versus shear load for Stations 2680 (forward end of CSS), 2209 (forward end of boattail), 2180 (aft end of boattail), and 2127 (forward end of Titan skirt). The

ORIGINAL PAGE IS
OF POOR QUALITY

deflection versus load relationship for each station is compared to expected values. The expected values are based upon the analytical stiffness model in Appendix C. The figures indicate the deflection of the test stackup was greater than expected by 36% at Station 2680, 25% at Station 2209, 12% at Station 2180 and less than 1% difference at Station 2127. The load versus deflection curves show some non-linearity throughout the loading. This is attributed to friction being overcome within the riveted and bolted connections within the test structure and results in some residual deformation when all loads are removed. At a point where the shear load reaches approximately 8000 pounds the curves show a pronounced change in slope. This point in the load-deflection curves coincides with the application of axial load. However, this same change in the slope was indicated by data from Test 2L-1A when no axial load was present at the 8000-pound shear load point (see figure VI-15). Assessment of this anomaly indicates that the test structure undergoes a change in stiffness at approximately 25% of limit shear load.

Instrumentation located at the bolted circumferential joints of the test structure to measure joint gapping indicates that discernible gapping of the joints began at approximately 25% of limit load. While the quantitative values of the gapping measurements are small and limited to local areas, their occurrence coincides with the point of change in the overall structural stiffness. It is believed the change in stiffness is produced by distortion of the bolted circumferential joints as shear load is applied, and by the overcoming of frictional forces in connections throughout the test structure.

Figure VI-3 shows the lateral deflection versus station for limit load and compares the measured to the expected profile. This figure indicates that the major deviation from expected deflection occurs forward of Station 2177. The relative deflection between the Centaur and CSS is shown to be 2.1 inches at the LH_2 vent (Station 2440) and 4.1 inches at the Viking bioshield location (Station 2672). These measured relative displacements compare to analytically predicted values of 1.25 and 2.5 inches respectively.

The rotations of cross-sectional planes at limit load are presented in figure VI-16 and are compared to predicted values. The data indicates that the actual rotations forward of Station 2177 exceeded the predicted by a significant amount. The change in rotation between Stations 2209 and 2680 was as expected. Figure VI-16 illustrates that measured rotation of the total structure exceeded predicted values due to causes primarily in the boattail section between Stations 2177 and 2209.

Figure VI-17 presents the measured deflected profile of the CSS at limit load compared to the predicted profile. At Station 2680 the measured deflection was 46% greater than predicted.

Figure VI-18 shows the shear load versus deflection relationship for the CSS at Station 2460 independent of the displacements, rotation, and translation below Station 2177. The test data are compared with predicted values which were made using the original CSS stiffness model and also with computed values incorporating revisions to the boattail stiffness based upon Test 3L data (Revision 1). (See Appendix C).

Figure VI-9 compares the deflected profile of the CSS to computed values from the original stiffness model and the revised (Revision 1) model. The data in figures VI-18 and VI-7 indicates that the flexibility of the CSS, exhibited in Test 3L. can be adequately defined analytically by a revision to the boattail portion of the stiffness model only.

Test 4L - Test 4L duplicated Test 3L except that the shear load was oriented in the 330 degree azimuth, or 180 degrees from the Test 3L shear azimuth. The axial load for Test 4L was reduced. The deflection data from Test 4L indicated approximately the same results as Test 3L and the same comments apply. Figures VI-19, VI-20, VI-21, and VI-22 present the shear versus lateral deflection at Stations 2680, 2209, 2180, and 2127, respectively. Figure VI-23 presents the deflected profile of the entire structure at limit load. Figure VI-24 presents rotation of cross sectional planes versus station for limit load. The deflected profile of the CSS at limit load, independent of the rest of the test structure, is presented in figure VI-25. For both Tests 3L and 4L the test structure had been exercised by shear loadings up to 50% of limit load to remove slack in the test fixtures prior to collecting data.

Test 2L - Following Test 4L the shear load was positioned to the 270 degree azimuth for Tests 2L-1 and 2L-1A. For Test 2L-1 no exercise loading was applied to the structure before testing. The resulting data indicated that lateral deflections of the test stackup were approximately 7% greater than those observed in the previous tests. Figures VI-26. VI-27, VI-28, and VI-29 present the shear load versus deflection at Stations 2680, 2209, 2180, and 2127, respectively. Figure VI-30 shows the deflected profile for Test 2L-1 at limit load. Figure VI-31 presents the plane rotation versus station.

A comparison of the rotation data from Test 2L-1 with Test 4L and Test 3L indicates that the rotation in the boattail section between Stations 2180 and 2209 is approximately 10% greater for 2L-1 than for the other two tests at limit load.

Figure VI-32 shows the deflected profile at limit load of the CSS only. The deflection of the CSS in Test 2L-1 was about 10% greater than observed in the previous tests.

Test 2L-1A was performed following Test 2L-1 and thus the results from 2L-1A were obtained after the structure had been exercised to limit load. In Test 2L-1A the shear loading was limited to 80% of the limit load and no axial load was applied.

Figure VI-15 shows the shear load versus lateral deflection of the CSS at Station 2460 for Tests 2L-1 and 2L-1A. This data represents the displacement relative to Station 2177 of the CSS only. The deflection of the unexercised structure in Test 2L-1 is seen to be 8% greater than the exercised structure in Test 2L-1A at 28,000-pound shear load. The change in slope at approximately 8,000 pound shear load can be observed in the data from both tests.

Test 1L - For Tests 1L-1, 1L-2 and 1L-3 the shear load was applied in the 90 degree azimuth. Test 1L-1 was conducted to verify the spring rate of the FBR system which was designed to have a nominal 73,000 lb./in. value. The results of this test are presented and discussed in Section III. Figure VI-33 shows the deflected profile for Test 1L-1.

After completion of Test 1L-1, the FBR was removed and the structure loaded to limit load in Test 1L-2. Figures VI-34, VI-35, VI-36, and VI-37 show the shear load versus deflection for Stations 2680, 2209, 2180, and 2127, respectively. The deflection of the CSS in Test 1L-2 was approximately 80% greater than predicted and exceeded previous results by nearly 30%, as shown in figure VI-38 which compares the CSS deflection for Tests 3L, 4L, 2L-1 and 1L-2. Figure VI-39 shows the deflected profile of the test stackup at limit load. Figure VI-40 presents the cross sectional plane rotation versus station for limit load. The data indicate that the increased deflection resulted from an increase in rotation at Station 2209. The rotation in 1L-2 between Station 2180 and 2209 exceeded that of Test 3L by 30%. Figure VI-41 shows the deflected profile of the CSS relative to Station 2177.

The increased deflections in Test 1L-2 are attributed to the structure having been loaded in the opposite direction in Test 2L. At the completion of the 2L tests the structure was left in a fully exercised condition with most of the internal frictional restraints removed. This effect is demonstrated by the increased linearity of the data from Test 2L-1A when compared to Test 2L-1 (see figure VI-15). Relatively large residual displacement was evident when the loads were removed, as shown in figure VI-34. Approximately one inch of residual displacement was indicated at Station 2680 for the total test stackup. In figure VI-39, it is shown that the relative displacement between the CSS and Centaur is 2.5 inches at Station 2460 and 5.0 inches at Station 2672.

The residual displacements observed in the CSS after completion of each test are summarized in Table VI-1. The tests are listed in order of their completion. The data in the table indicate that the CSS acquires less residual displacement when exercised or loaded repeatedly in the same azimuth, indicating a tightening of the structural connections and on-coming frictional force. Tests 2L-1 and 2L-1A applied shear in an azimuth not previously loaded. The sum of residual displacement from the two tests was 0.27 inches. When the shear load was next applied in the opposite direction (90°) in Tests 1L-1 and 1L-2 the total residual displacement was 0.56 inches, or approximately twice the amount indicated in the 2L series. These data indicate that the CSS acquires a residual displacement of approximately 0.27 inches, referenced from the unloaded position, when limit shear load is applied.

Based upon the information from Tests 3L, 4L, 2L and 1L-2, it was determined that the stiffness of the CSS without the FBR system installed would not adequately restrict the relative motion between the CSS and the Centaur at limit load. The allowable clearance was determined to be violated at the LH_2 vent disconnect, the forward seal, and the Viking bioshield. Using the test results, corrections were made to the analytical

ORIGINAL PAGE IS
OF POOR QUALITY

stiffness model of the boattail section. Two revisions were made. The first, Revision I, was based upon data from Test 3L and the second, Revision II, was based upon data from Test 1L-2. The analytical stiffness model and revisions are presented in Appendix C. Figure VI-9 compares analytical values of CSS deflection using Revision I with Test 3L data. Figure VI-10 compares analytical values using Revision II with Test 1L-2 data. Good agreement is evident in both cases.

Using the Revision I CSS analytical model, a study was made to determine the stiffness required for the FBR system that would (1) limit the relative displacement between the CSS and Centaur to acceptable values, and (2) prevent the Centaur vehicle from being overloaded. The results of the analysis indicated the optimum spring rate for the FBR system to be approximately 20,000 pounds per inch (see Section III).

Tests 7L, 6L, and 5L Series - Tests 7L-2 and 6L-1 were conducted with an FBR system nominally designed to have a spring rate of 19,000 lb./in. installed between the CSS and Centaur. The tests were similar except that in Test 7L-2 the shear azimuth was at 90 degrees and the structure had been previously exercised in this direction in Test 1L-2. The shear azimuth for 6L-1 was at 240 degrees without previous exercising in this direction.

Figure VI-5 compares the deflected profile of the test stackup for Test 7L-2 with analytical values obtained using both Revisions I and II for the boattail stiffness. The test data show good agreement with the Revision I analytical values. The measured FBR load was 17,200 pounds compared to an analytical value of 18,000 pounds for Revision I and 22,050 pounds for Revision II. Figure VI-42 compares measured FBR load versus CSS shear load with analytical values. The test data indicates that the FBR system load in Test 7L-2 was less than the predicted values based upon Revision I while the measured FBR system load in Test 6L-1 shows good agreement with predicted values based upon Revision II. Figure VI-7 shows the measured Centaur lateral deflection versus FBR load in Test 7L-2. The data represent the Centaur and ISA lateral deflections relative to Station 2177. The data indicate that the stiffness is non-linear at smaller loads and that the structure is approximately 14% less stiff in the linear portion than predicted. Figure VI-8 shows the deflected profile of the Centaur with a 16,300 pound FBR load in Test 7L-2. The data in figure VI-8 indicate that the lower than expected Centaur stiffness is attributable to the ISA between Stations 2177 and 2141.

The measured deflected profile of the entire test structure is compared to analytically predicted values in figure VI-6. The comparison shows that the measured deflections slightly exceeded the expected values for Revision II. The measured FBR load was 21,000 pounds compared to computed values of 18,800 for Revision I and 22,050 pounds for Revision II. From the preceding data it can be observed that the unexercised structure in Test 6L-1 yielded larger deflections and larger FBR loads than did the exercised structures in Test 7L-2.

ORIGINAL PAGE IS
OF POOR QUALITY

In Test 7L-3 the FBR system was released while loaded at 6,600 pounds. For this portion of the test, shear load was applied to the CSS until the FBR load reached 6,600 pounds. At this point the position of the CSS was maintained with the shear load actuator, and the FBR system was released. The static deflection and dynamic response of the Centaur at Station 2626 is shown in figure VI-43. It should be mentioned that the dynamic response observed in this is not directly applicable to the flight condition because of the non-flight configured test fixture mounted on the Centaur and because the CSS was restrained in its deflected position by the shear load actuator. In Test 6L-2 the FBR was successfully released while loaded at 10,000 pounds and exhibited response similar to Test 7L-3 results as shown in figure VI-44. Test 5L-2 loaded the test structure to limit load in the 240 degree azimuth, the same as in Test 6L-1 except that the FBR system was not installed. The data from this test indicated deflection characteristics similar to Tests 3L, 4L and 2L-1.

For each test, data were obtained to define radial distortion of the circular, cross section at several locations such as Stations 2460, 2209, 2180, and 2127. The data indicated that the out of roundness, as defined by a change in cross sectional diameter, did not exceed one-tenth of an inch for any test.

The axial stiffnesses for all tests were similar resulting in the following axial spring rates:

Titan Skirt	4.3×10^6 lbs./in.
ISA between Stations 2180 and 2127	8.0×10^6 lbs./in.
CSS boattail only	3.3×10^6 lbs./in.
Total CSS, including boattail Stations 2680 to 2180	0.73×10^6 lbs./in.

The CSS, ISA, and Titan skirt combined axial spring rate was 0.50×10^6 lbs./in.

A summary plot of the shear load versus lateral displacement of the CSS relative to Station 2177 is compared in figure VI-4 with values determined by stiffness models evolved throughout the test program.

SUMMARY OF RESULTS

The stiffness of the CSS boattail and its attachment to the ISA is 40 to 80% less than predicted, depending upon azimuth and previous loadings.

The stiffness as indicated in the tests without the FBR system, would result in unacceptable clearance loss between the Centaur and the CSS at Station 2460 (LH_2 vent disconnect) and Station 2676 (Viking bioshield). The clearance loss is maintained at an acceptable value with incorporation at Station 2460 of an FBR system with a spring rate of 19,000 lbs./in.

The spring rate of the FBR system as tested is 19,000 lbs./in. With this spring rate, the CSS can sustain limit load without overloading the Centaur vehicle.

The Centaur vehicle exhibited a stiffness approximately 14% less than predicted. The Titan skirt and aft section of the ISA (aft of Station 2177) exhibited expected and repeatable stiffness properties.

While the stiffness of the CSS varied from test to test, the analytical stiffness model, revised to satisfy Test 3L data (Revision I), adequately defines the CSS stiffness up to 30% of limit load. This analytical model is considered suitable for use in determining transient type loads and deflections. The analytical model, revised to satisfy Test 3L-2 data (Revision II), provides a conservative representation of the CSS stiffness for use in determining quasi-static type loads and deflections.

TABLE VI-1

Test	Azimuth	CSS Station 2460 Residual Displacement	Comments
3L-50%	150°	.008"	Exercised to 25% 2 or 3 times.
3L-100%	150°	.094	Exercised in 3L-50%.
4L-100%	330°	.159	Exercised to 25%.
2L-1	270°	.194	Not exercised. Pulled from Zero Position.
2L-1A	270°	.080	Exercised in 2L-1 Maximum Shear of 28K.
1L-1	90°	.047	Not exercised, 73^{K}FBR Maximum CSS Shear of 11.44K.
1L-2	90°	.513	Exercised in 1L-1.
7L-1	270°	Not applicable due to residual load remaining in FBR system.	20^{K}FBR installed.
7L-2	90°		20^{K}FBR installed.
6L-1	250°		20^{K}FBR installed.
6L-1A	250°		20^{K}FBR installed.
5L-2	250°	.150	No FBR, exercised in Test 6L-1 and 6L-1A.

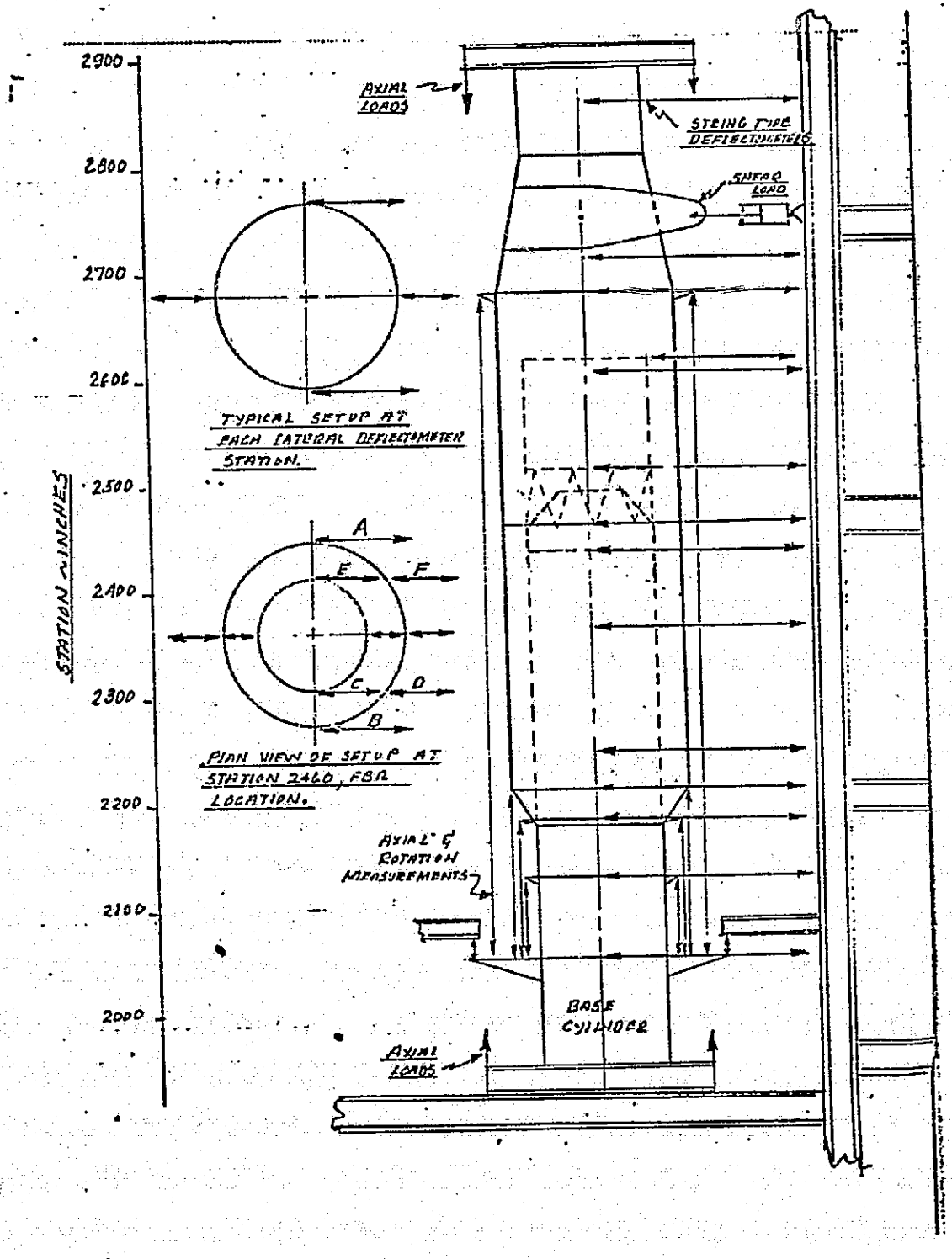

FIGURE VI-1. BASIC INSTRUMENTATION ARRANGEMENT FOR DEFLECTION MEASUREMENTS.

ORIGINAL PAGE IS
OF POOR QUALITY

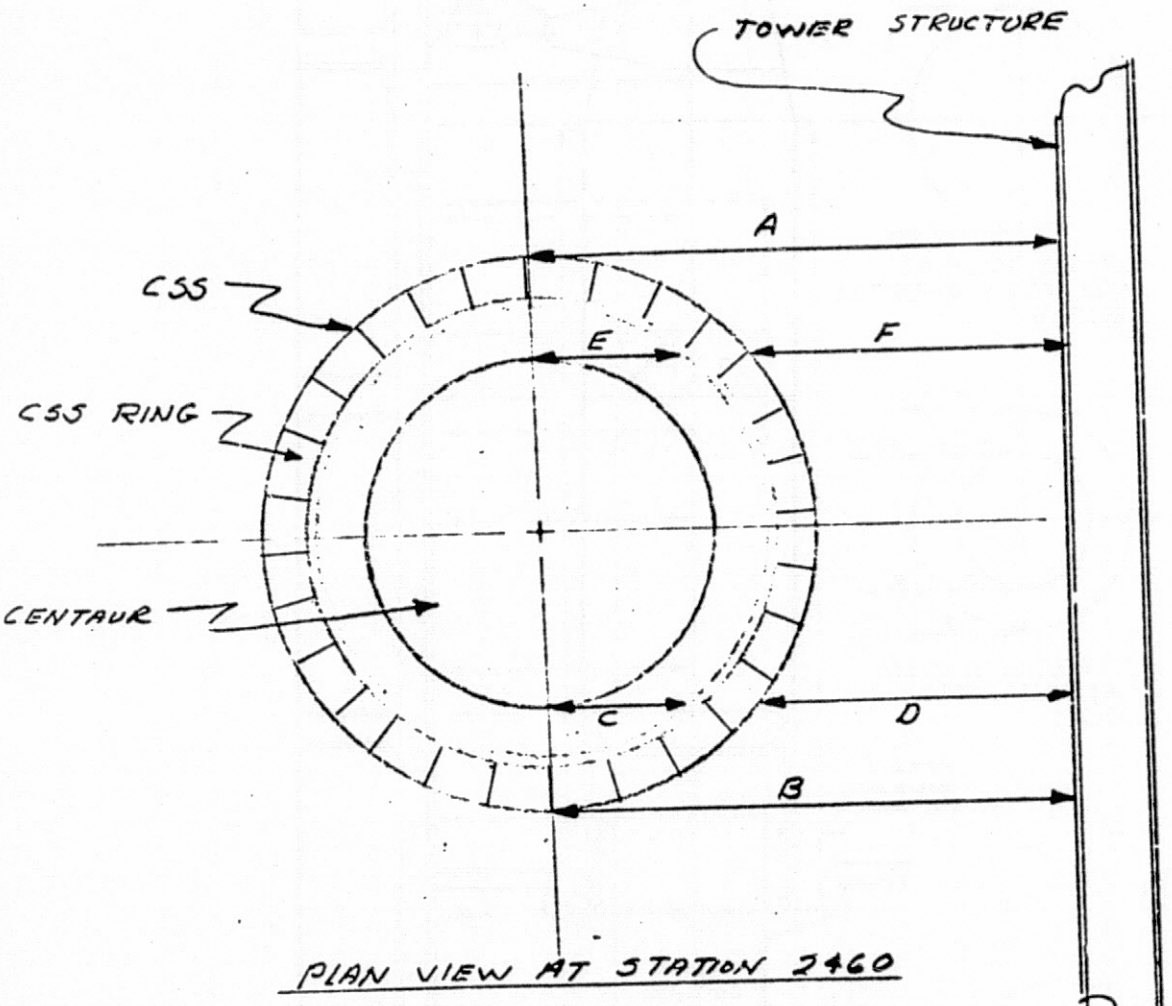

FIGURE VI-2. DEFLECTION INSTRUMENTATION AT FBR LOCATION.

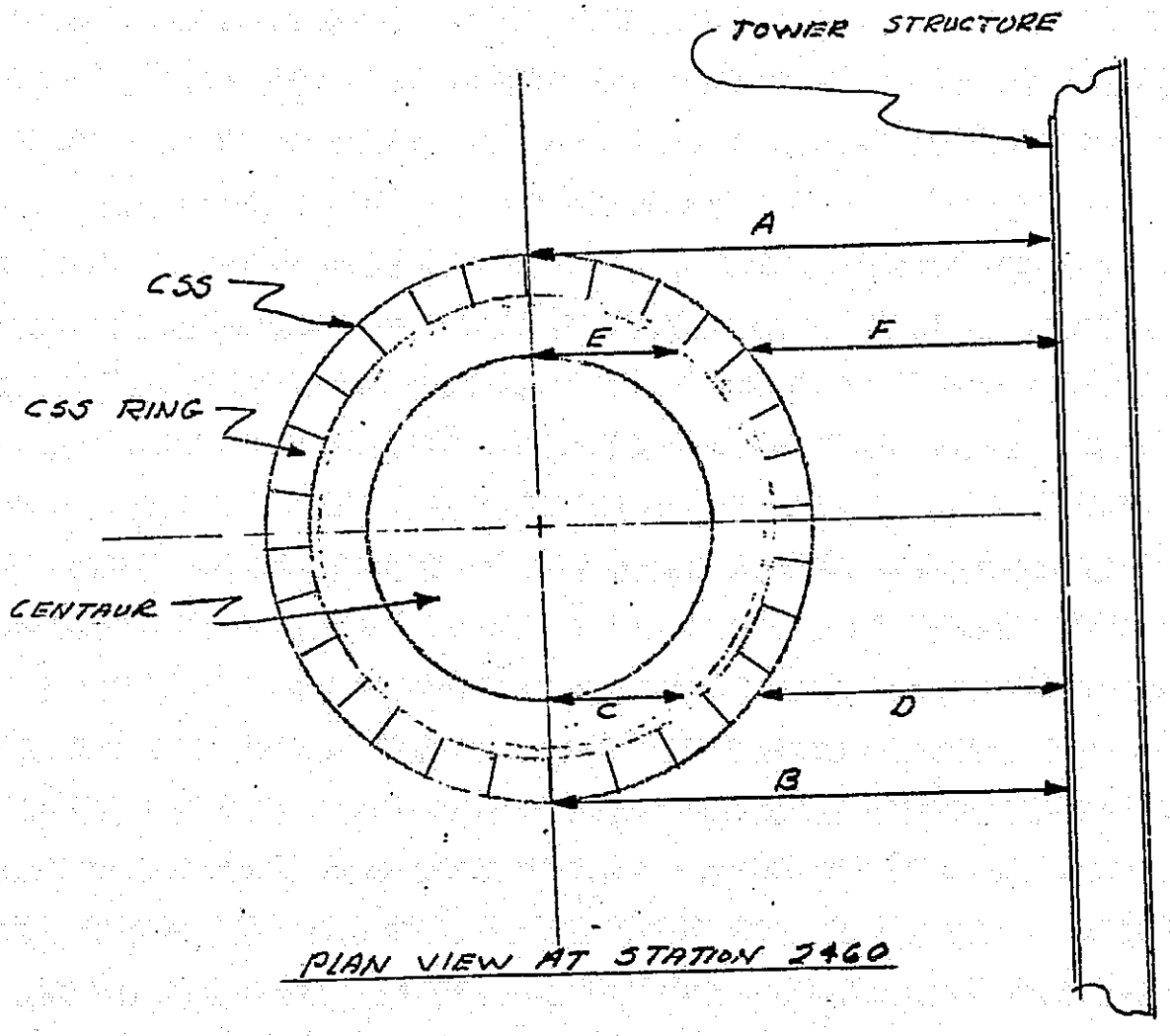

FIGURE VI-2. DEFLECTION INSTRUMENTATION AT FBR LOCATION.

ORIGINAL PAGE IS
OF POOR QUALITY

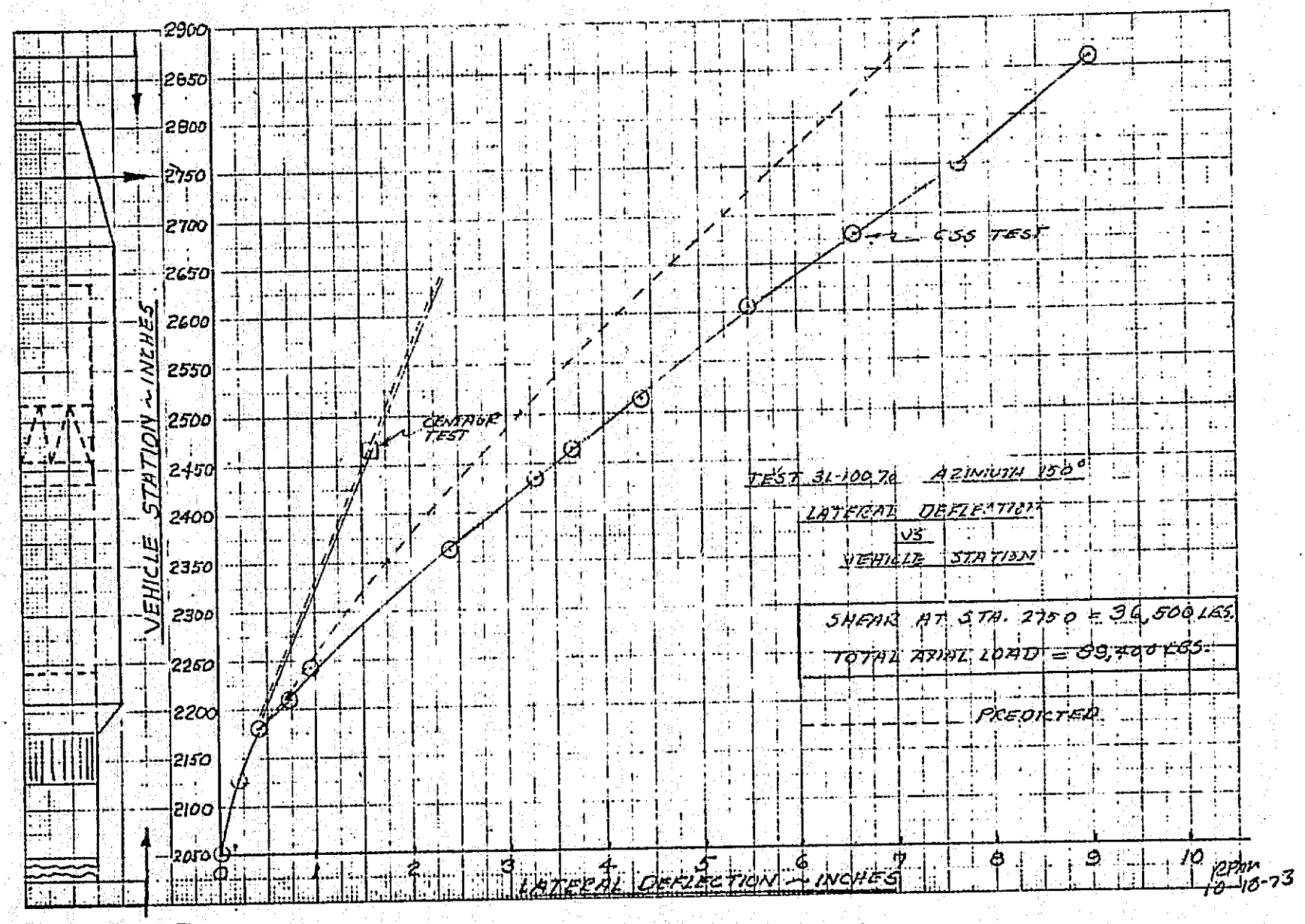

FIGURE VI-3. LATERAL DEFLECTION Vs. STATION.

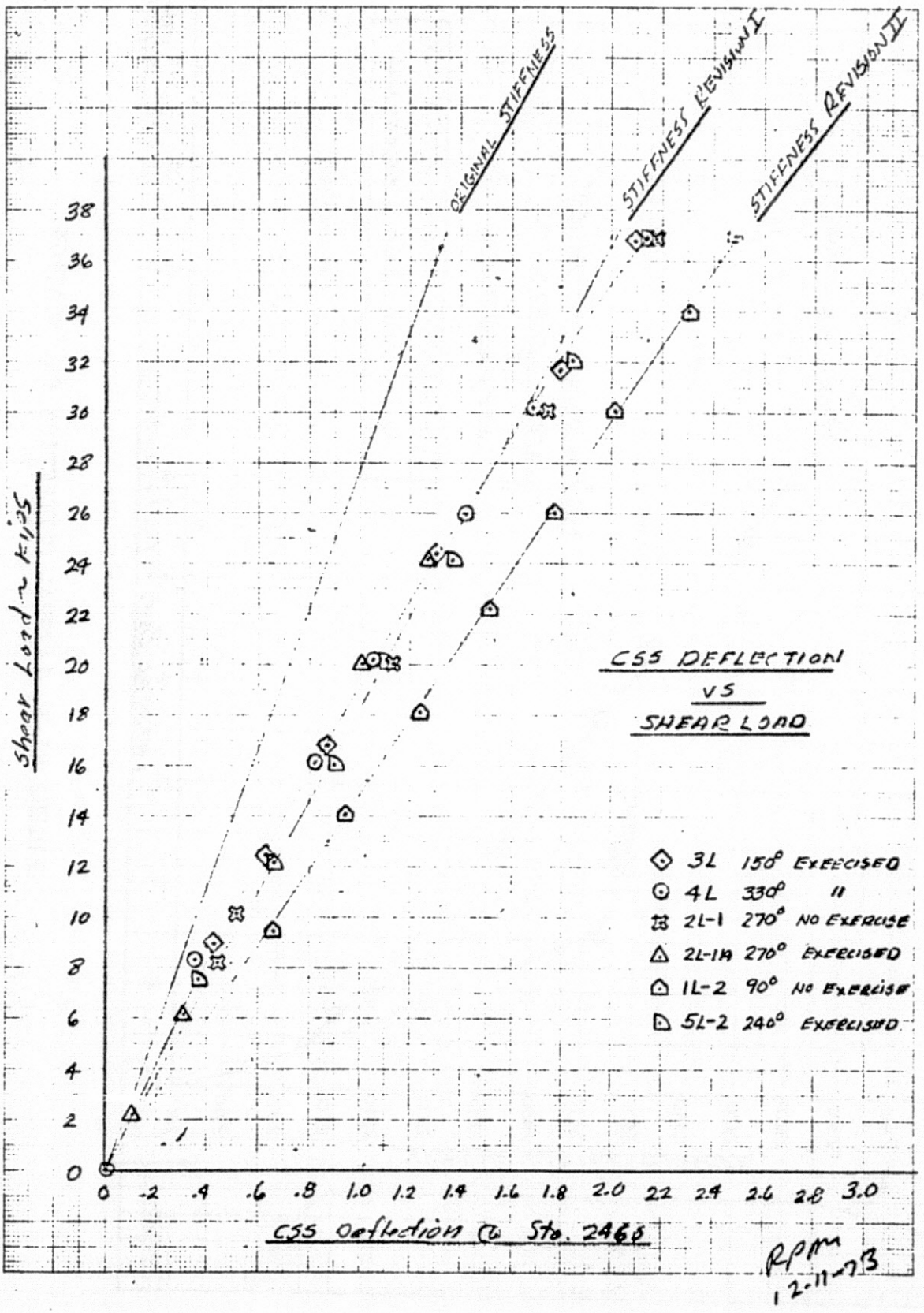

FIGURE VI-4. SUMMARY CSS DEFLECTION Vs. SHEAR LOAD.

ORIGINAL PAGE IS
OF POOR QUALITY

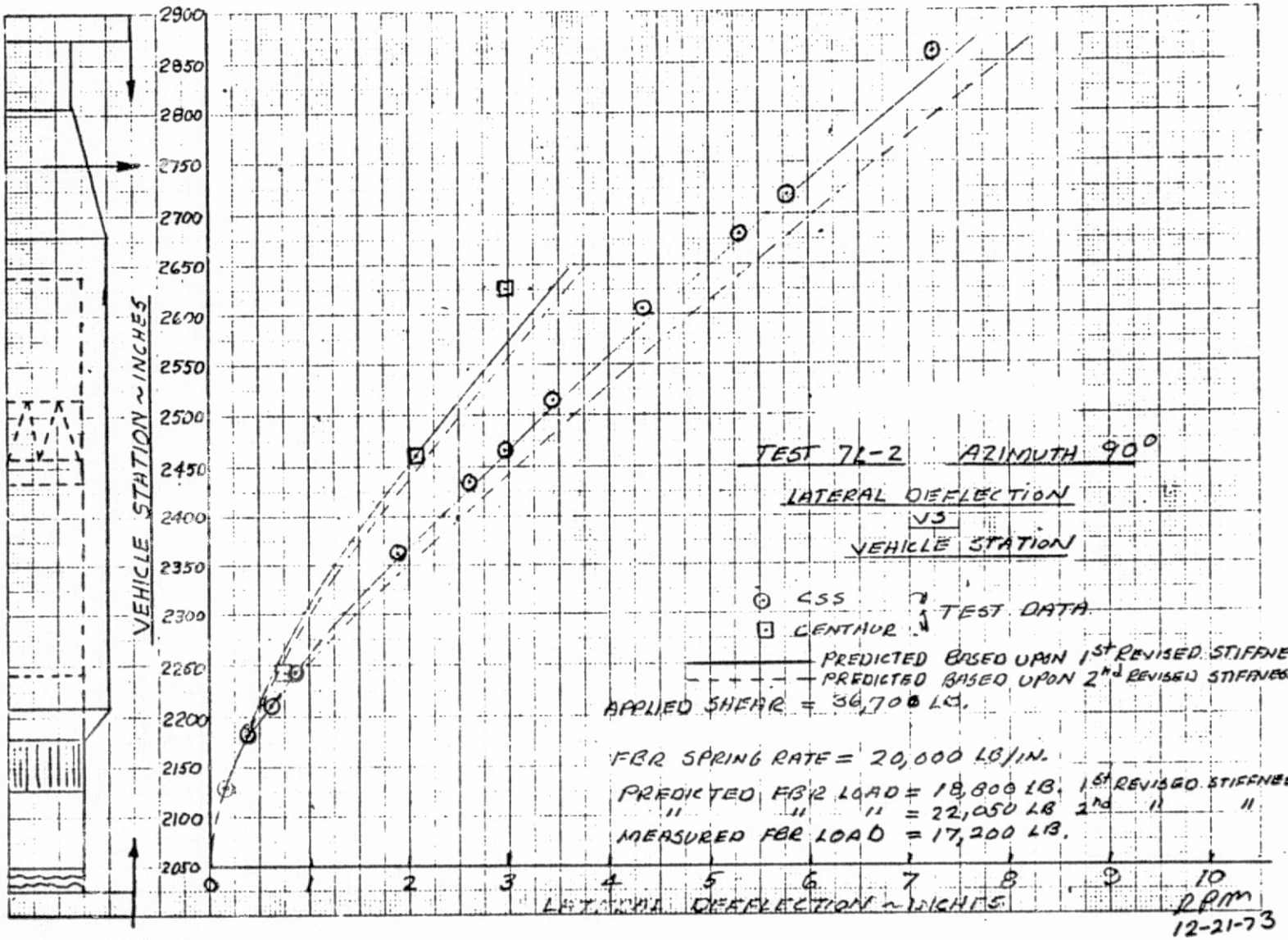

FIGURE VI-5. LATERAL DEFLECTION Vs. STATION

"Page missing from available version"

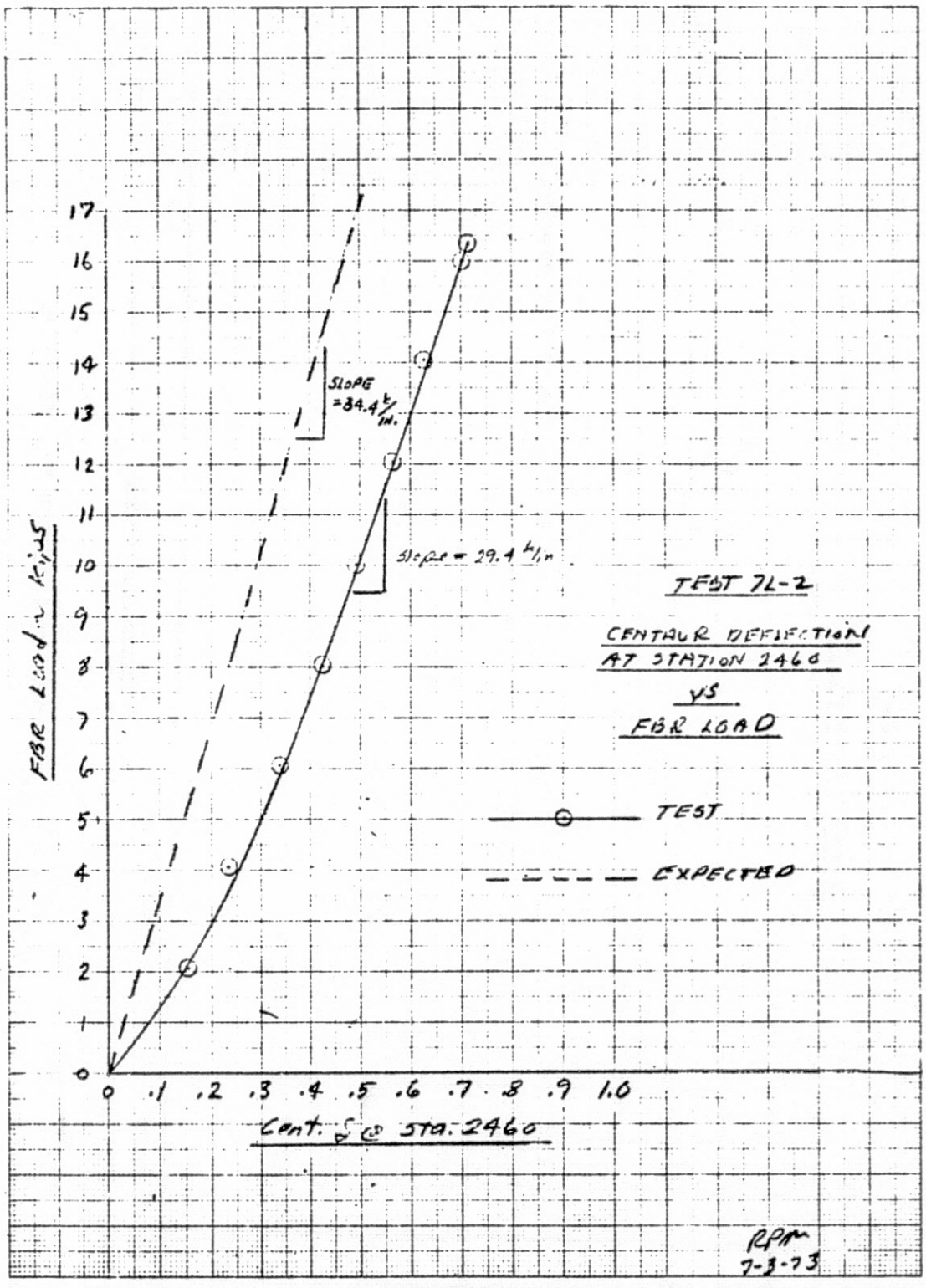

FIGURE VI-7. CENTAUR DEFLECTION Vs. FBR LOAD

ORIGINAL PAGE IS
OF POOR QUALITY

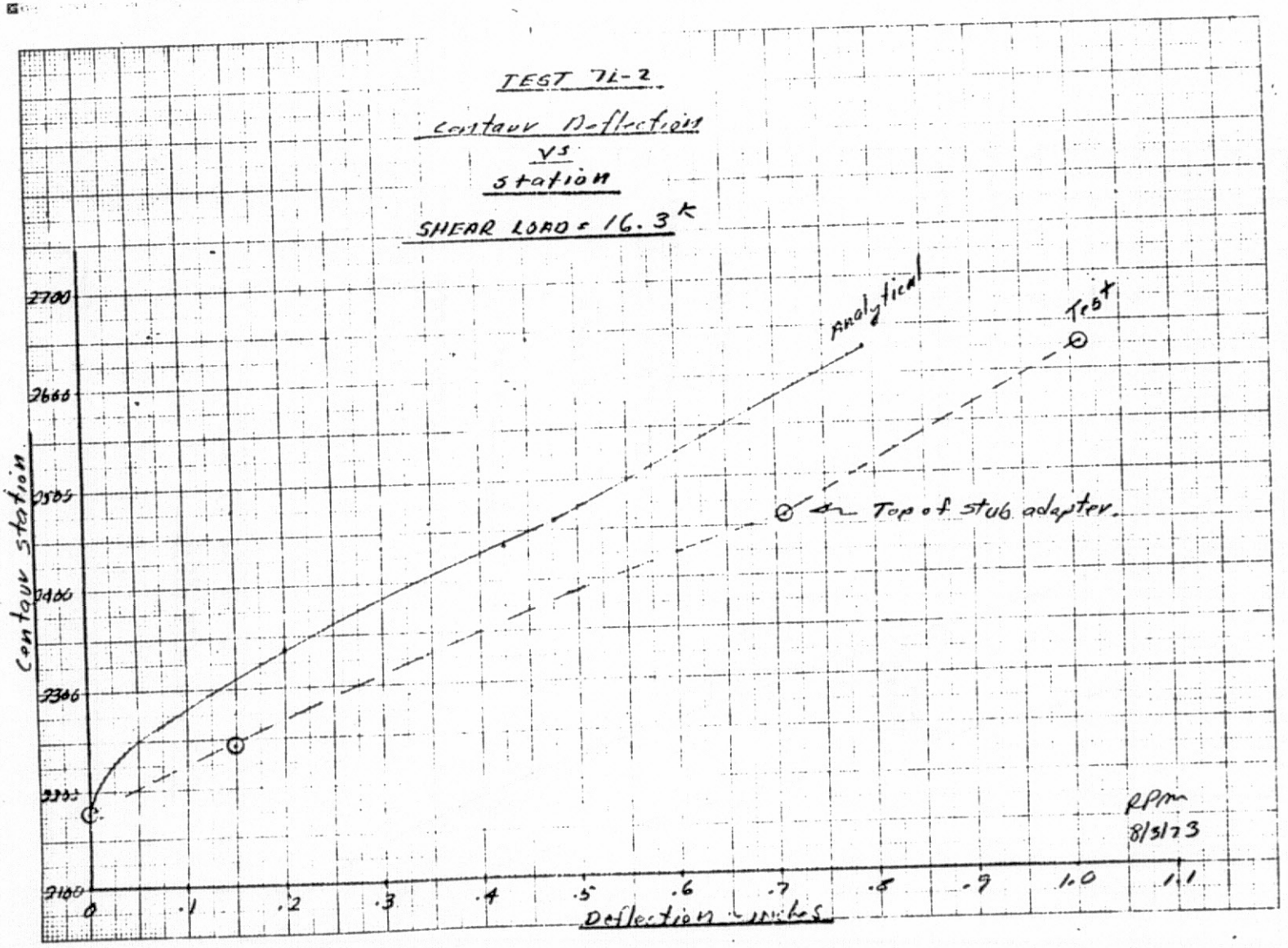

FIGURE VI-8. CENTAUR DEFLECTION Vs. STATION.

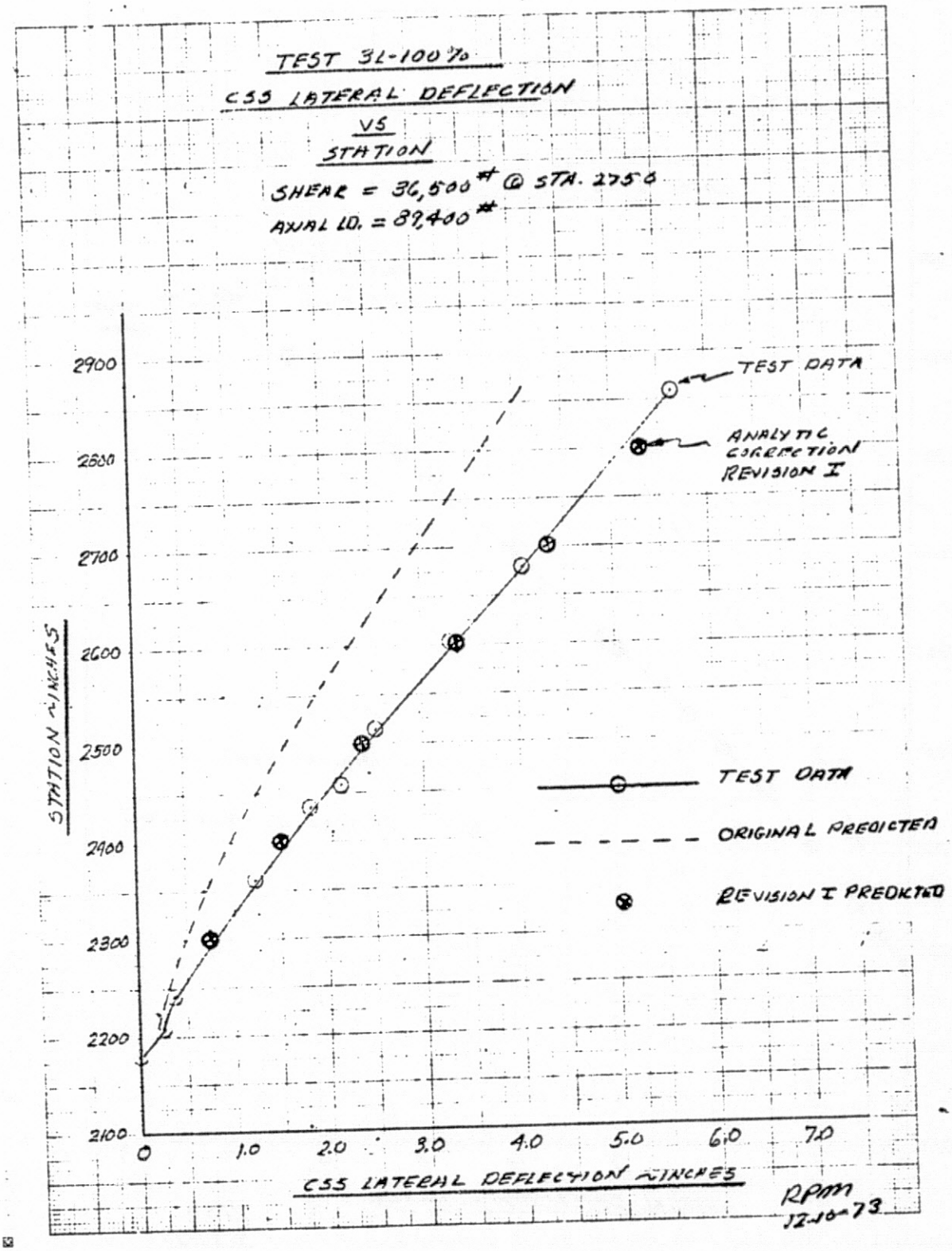

FIGURE VI-9. CSS DEFLECTION Vs. STATION

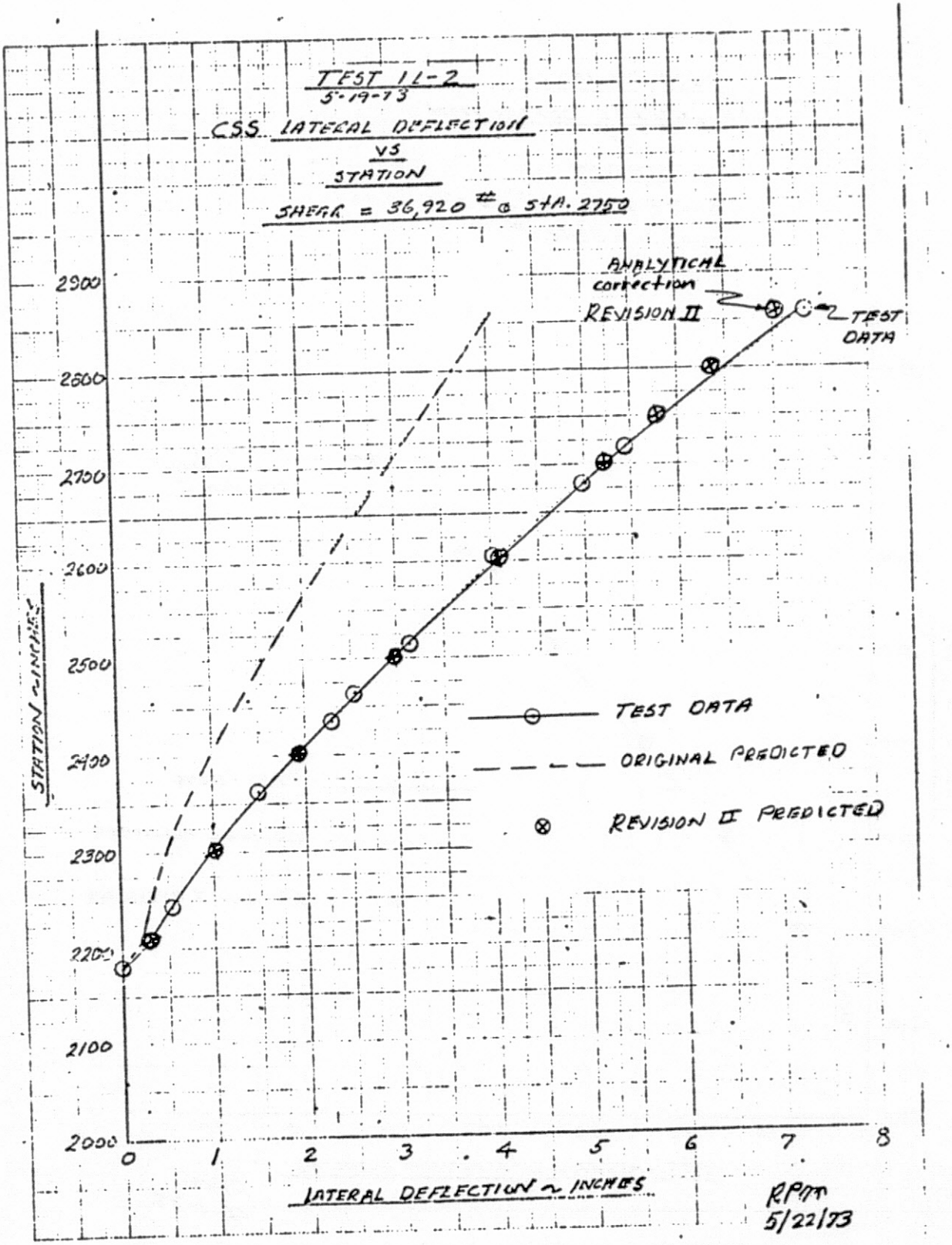

FIGURE VI-10. CSS DEFLECTION Vs. STATION

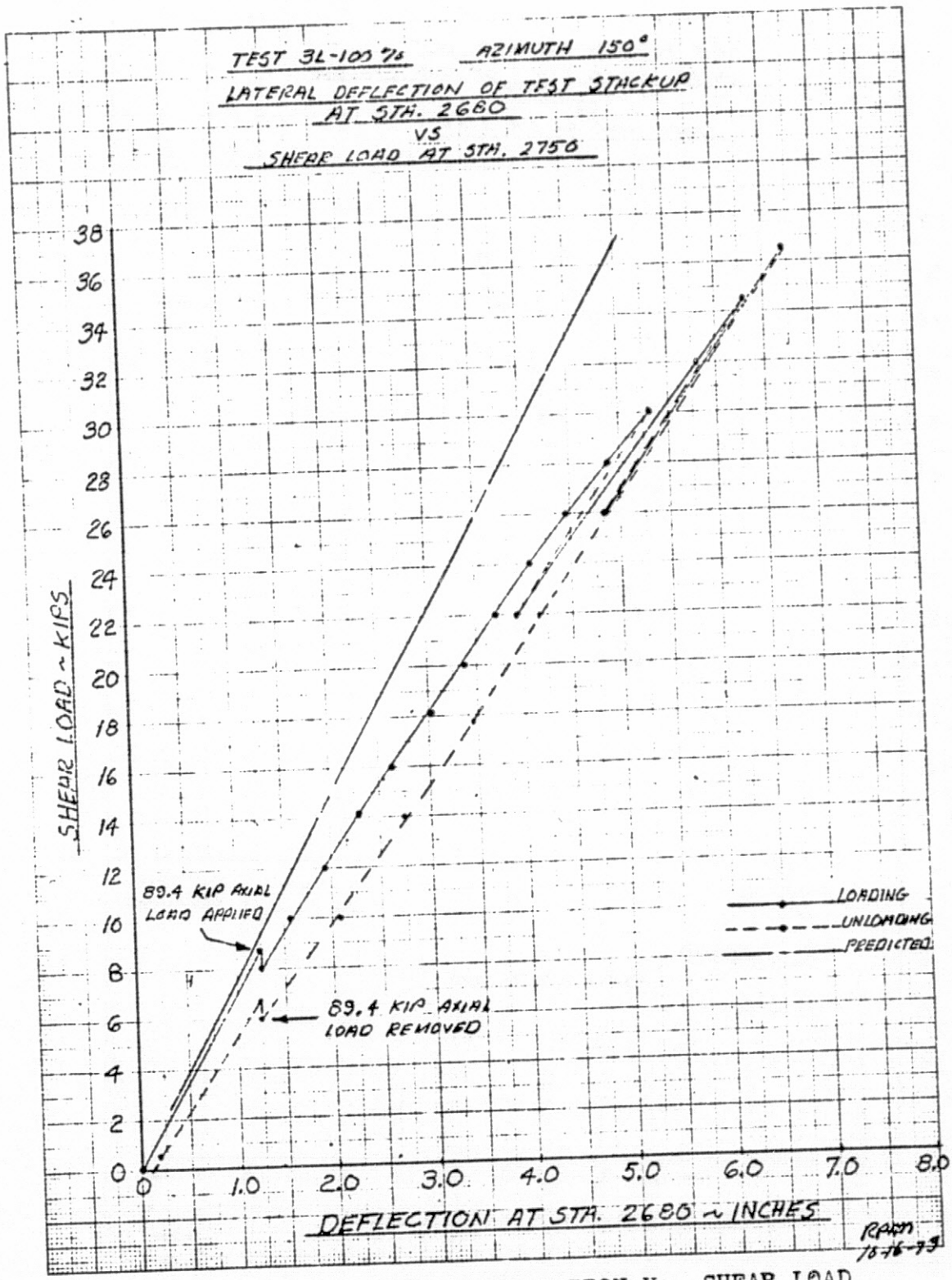

FIGURE VI-11. LATERAL DEFLECTION Vs. SHEAR LOAD

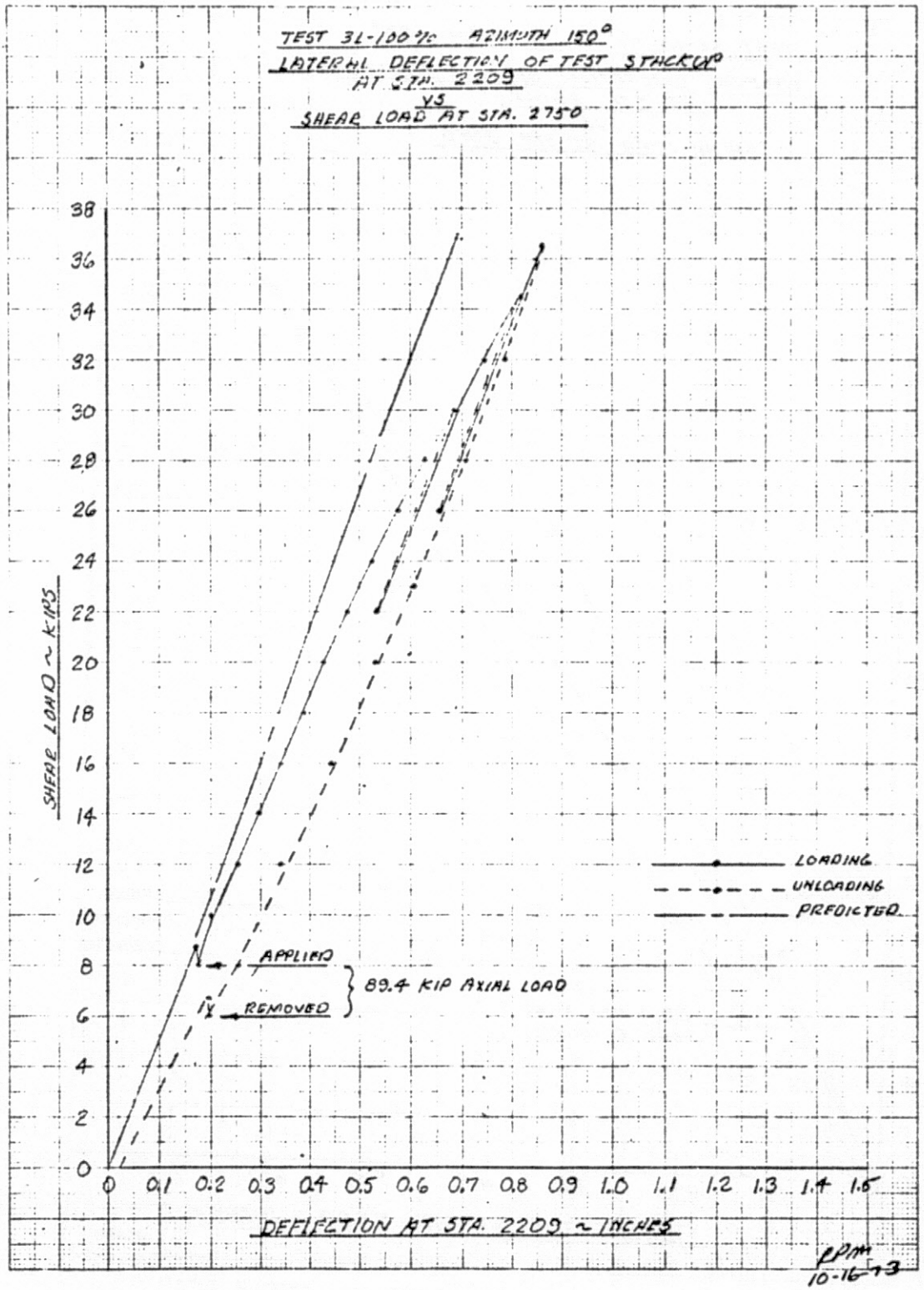

FIGURE VI-12. LATERAL DEFLECTION Vs. SHFAR LOAD

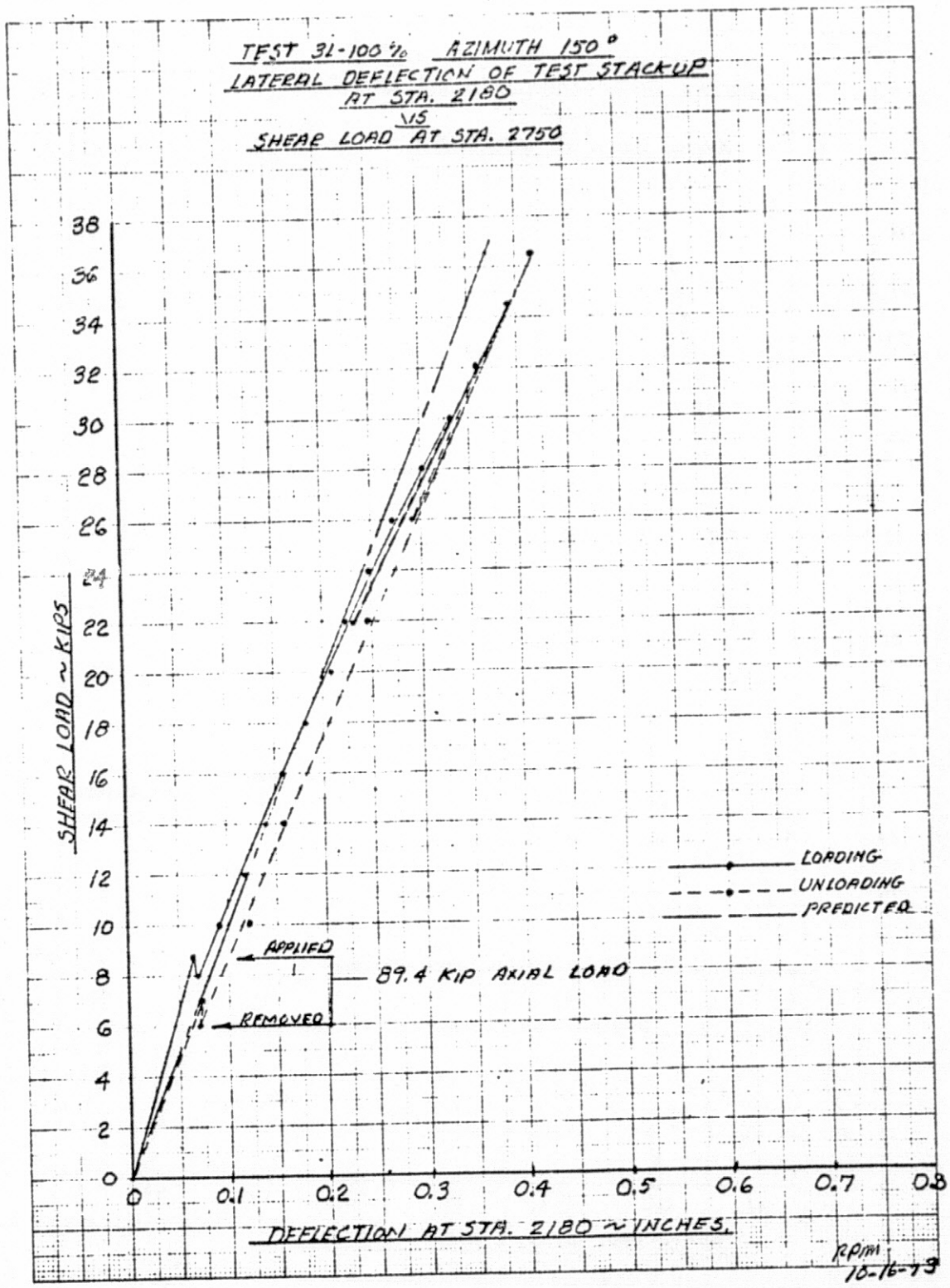

FIGURE VI-13. LATERAL DEFLECTION Vs. SHEAR LOAD

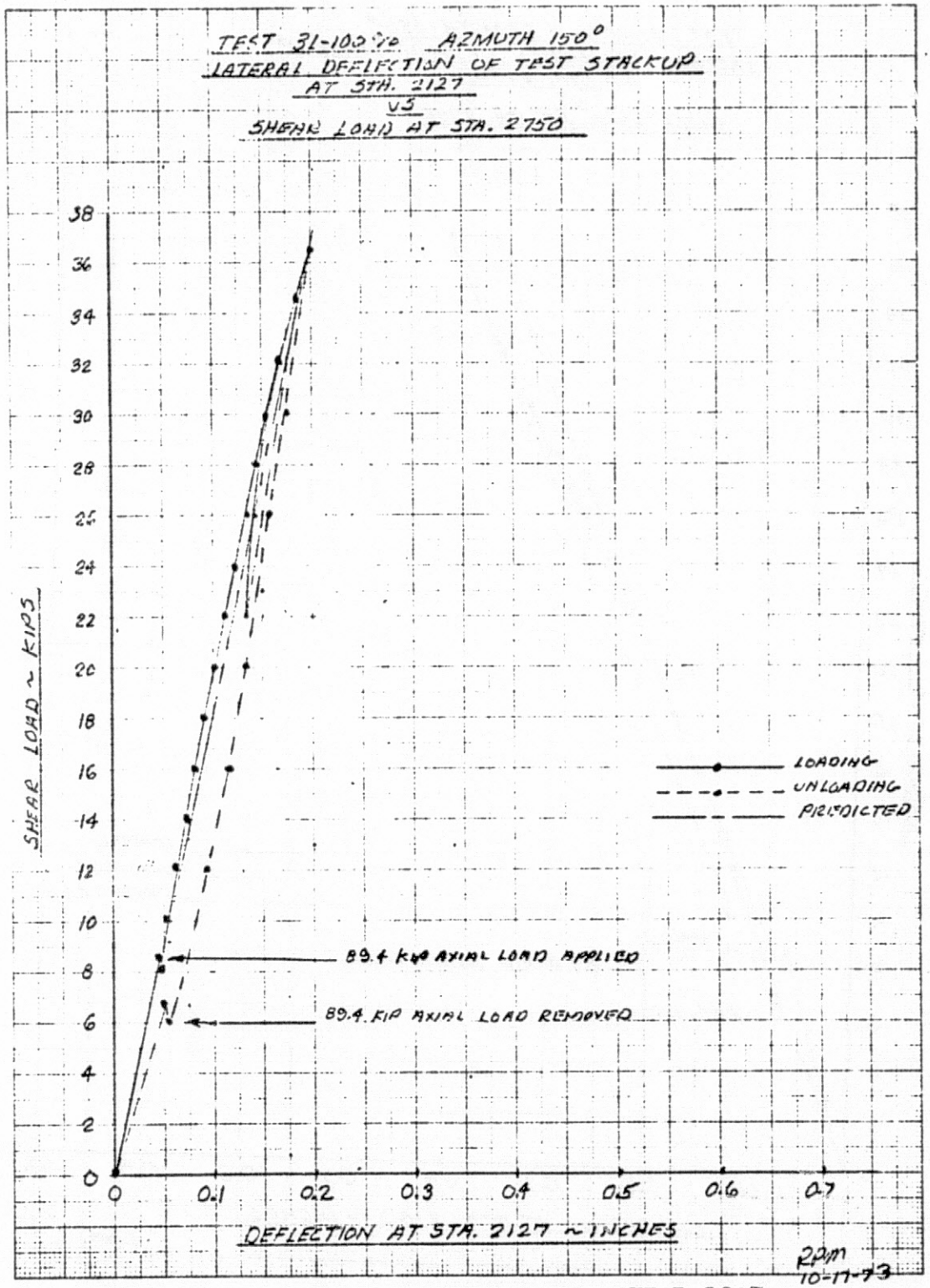

FIGURE VI-14. LATERAL DEFLECTION Vs. SHEAR LOAD.

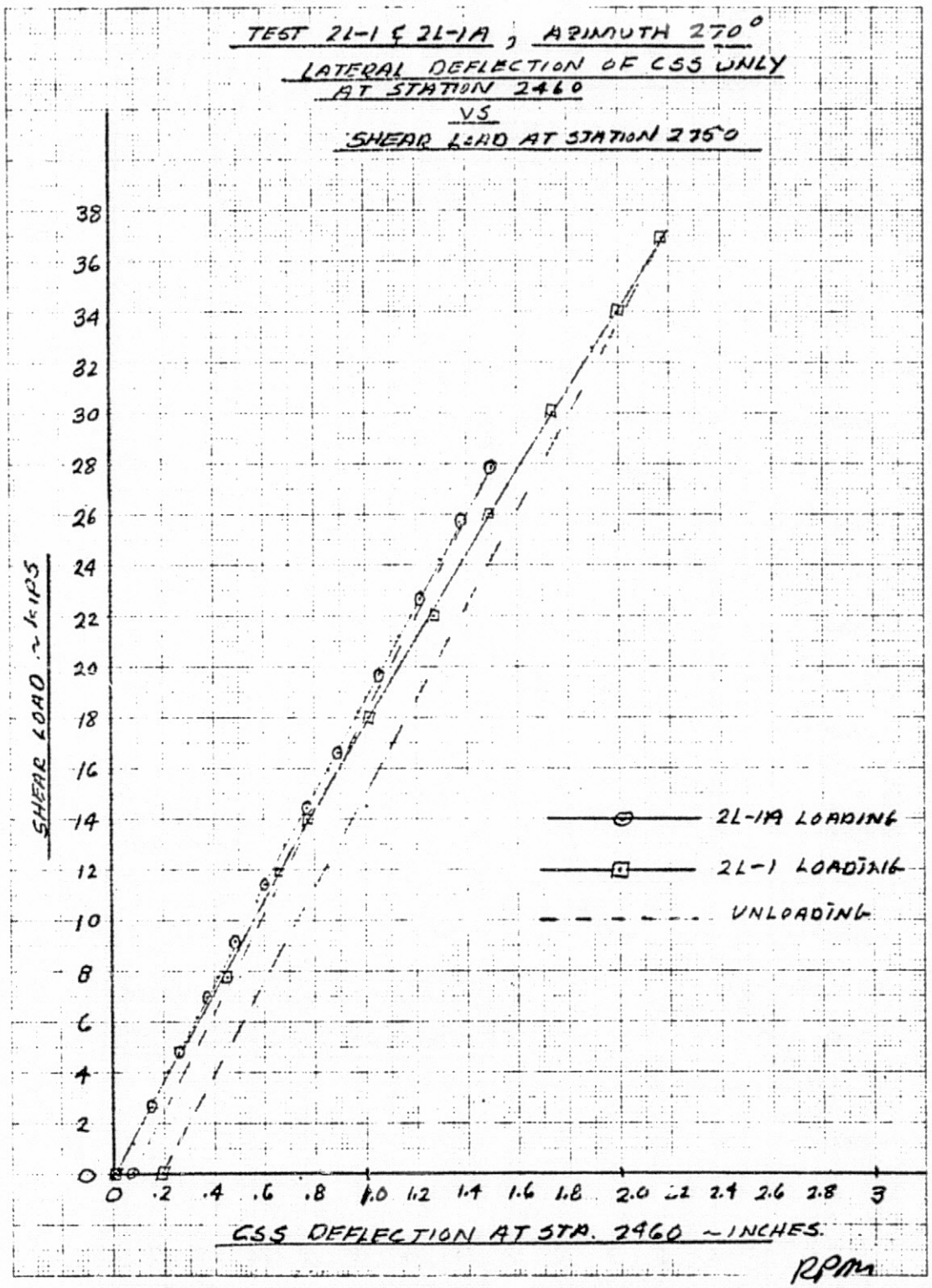

FIGURE VI-15. LATERAL DEFLECTION Vs. SHEAR LOAD.

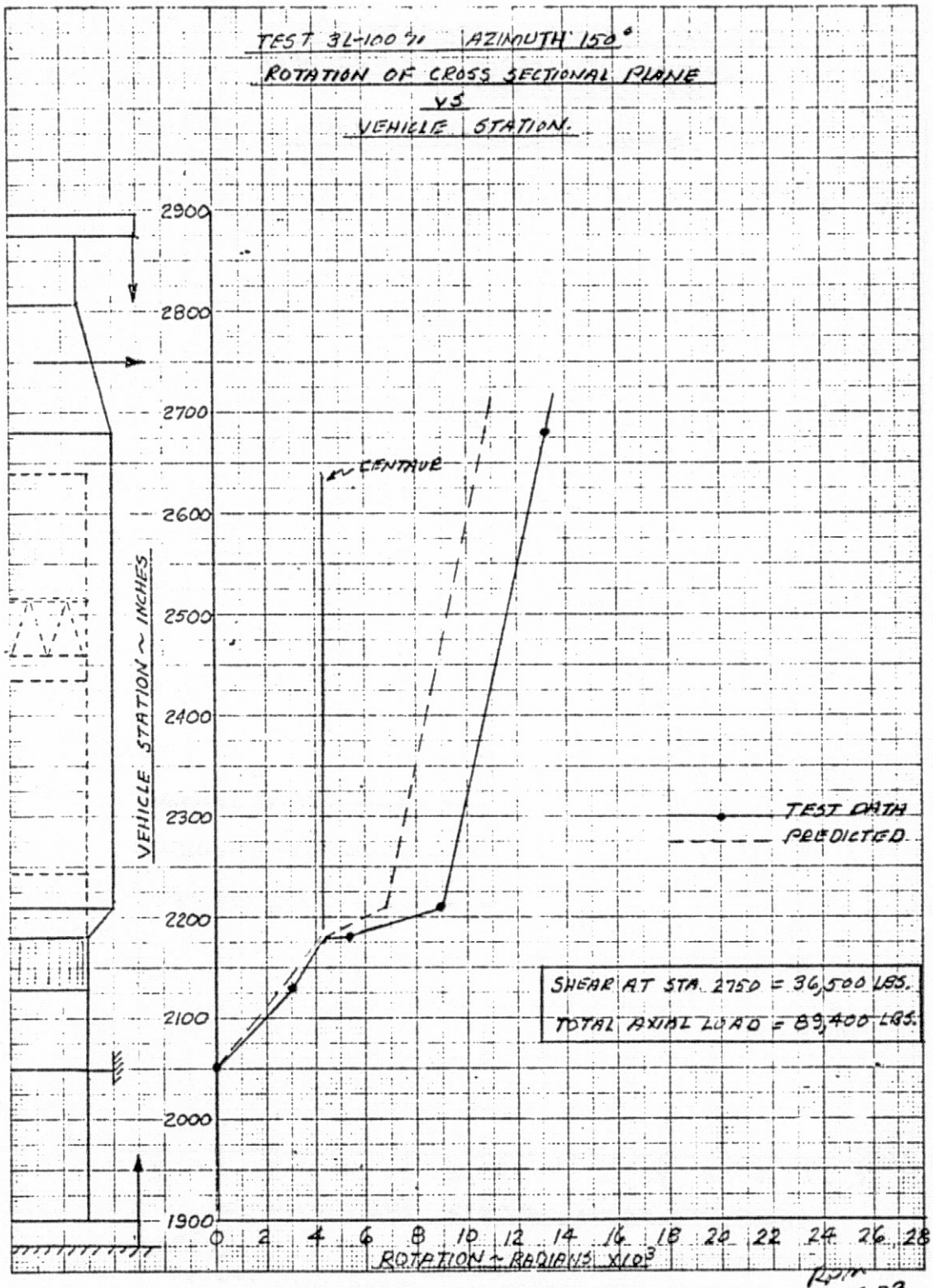

FIGURE VI-16. BENDING ROTATION Vs. STATION.

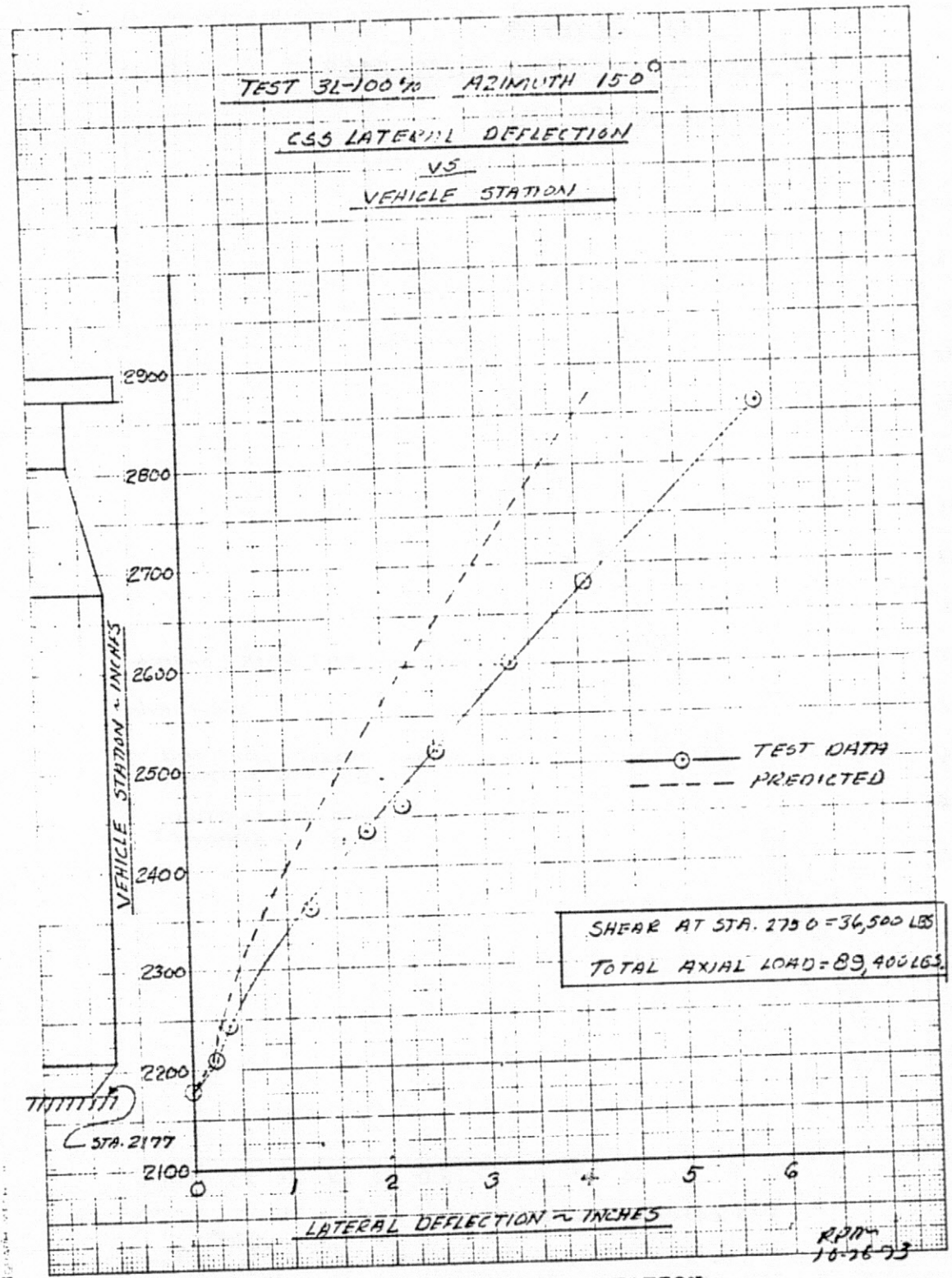

FIGURE VI-17. CSS DEFLECTION Vs. STATION.

ORIGINAL PAGE IS
OF POOR QUALITY

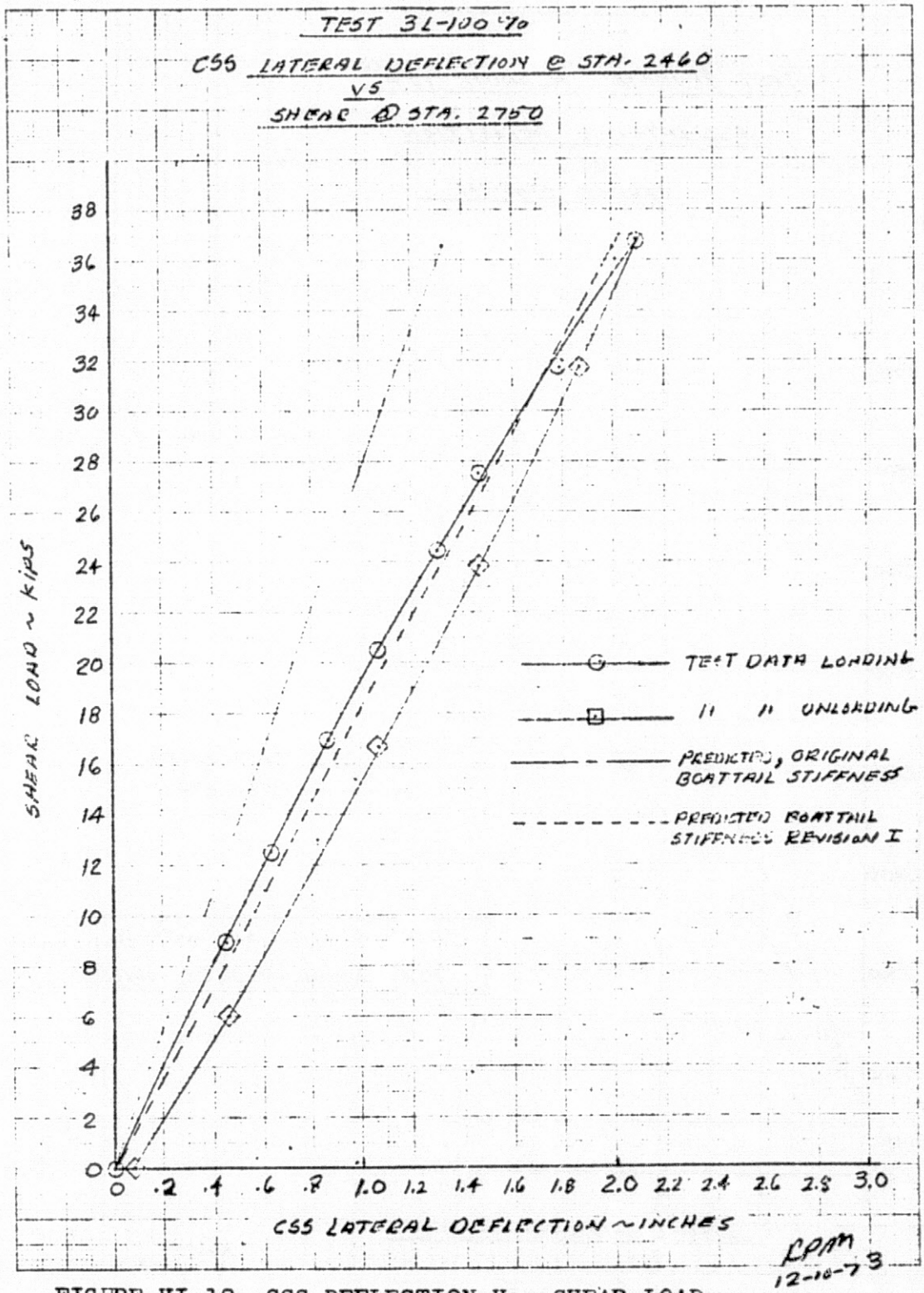

FIGURE VI-18. CSS DEFLECTION Vs. SHEAR LOAD.

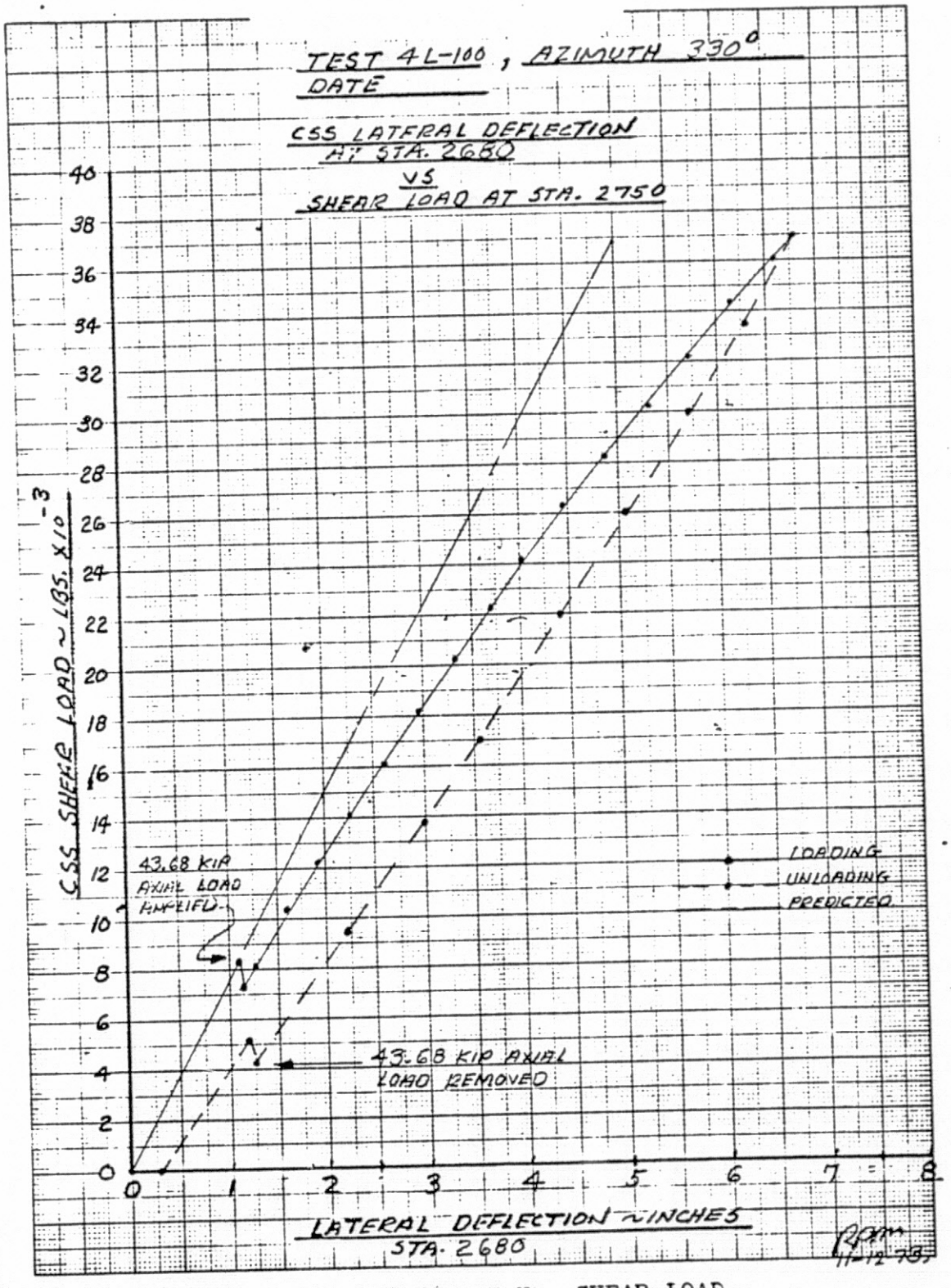

FIGURE VI-19. CSS DEFLECTION Vs. SHEAR LOAD.

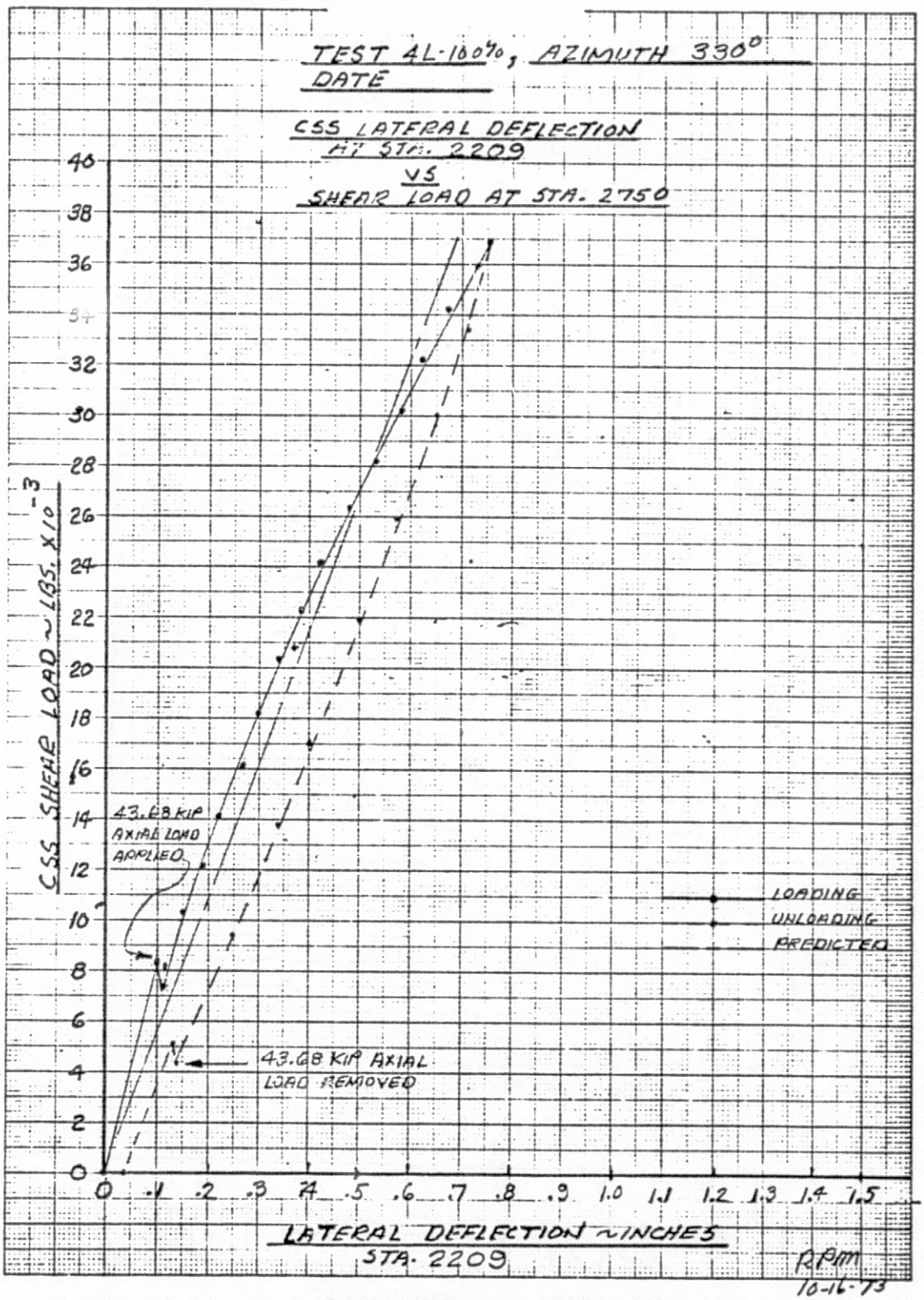

FIGURE VI-20. CSS DEFLECTION Vs. SHEAR LOAD.

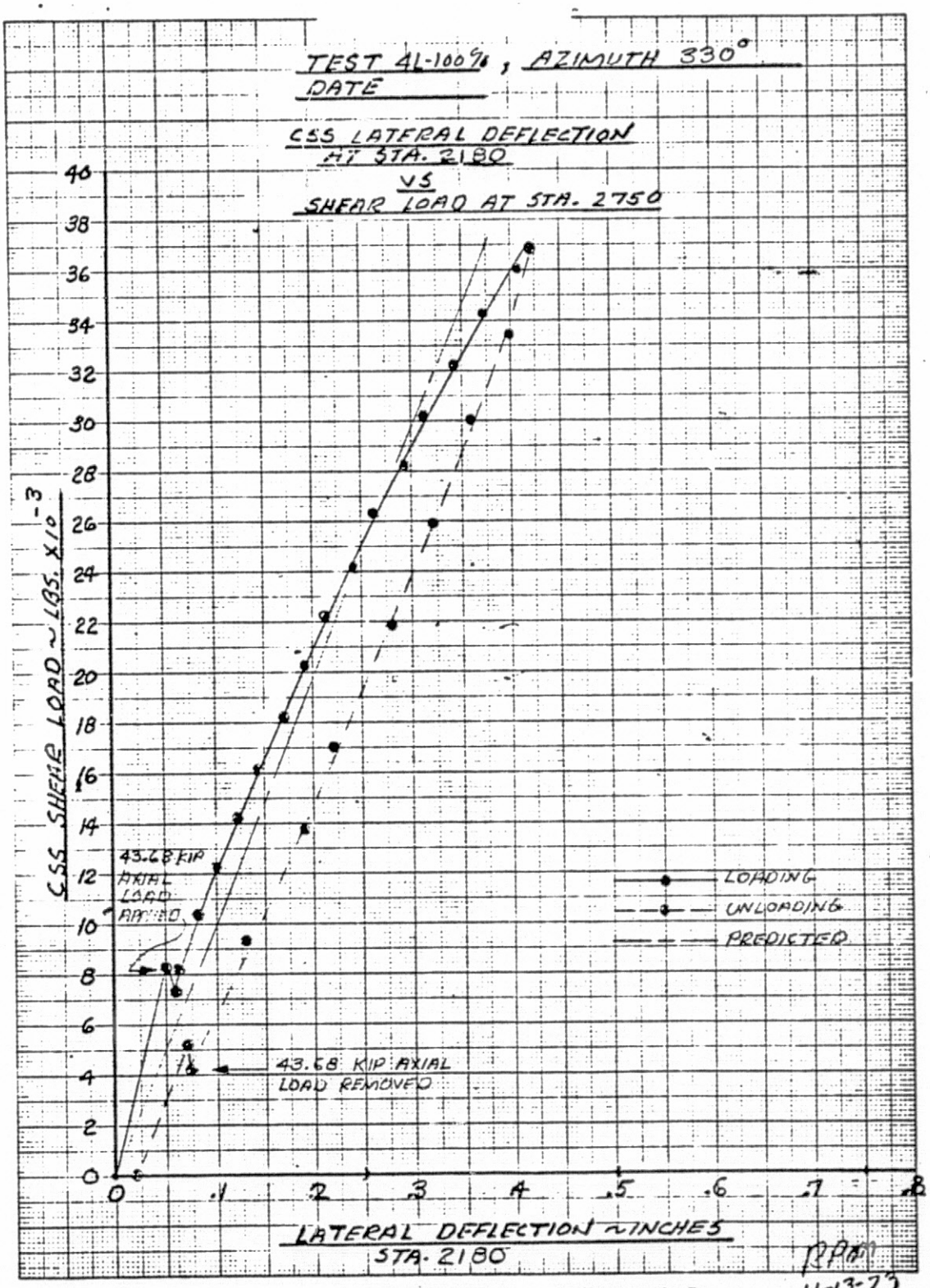

FIGURE VI-21. CSS DEFLECTION Vs. SHEAR LOAD.

ORIGINAL PAGE IS
OF POOR QUALITY

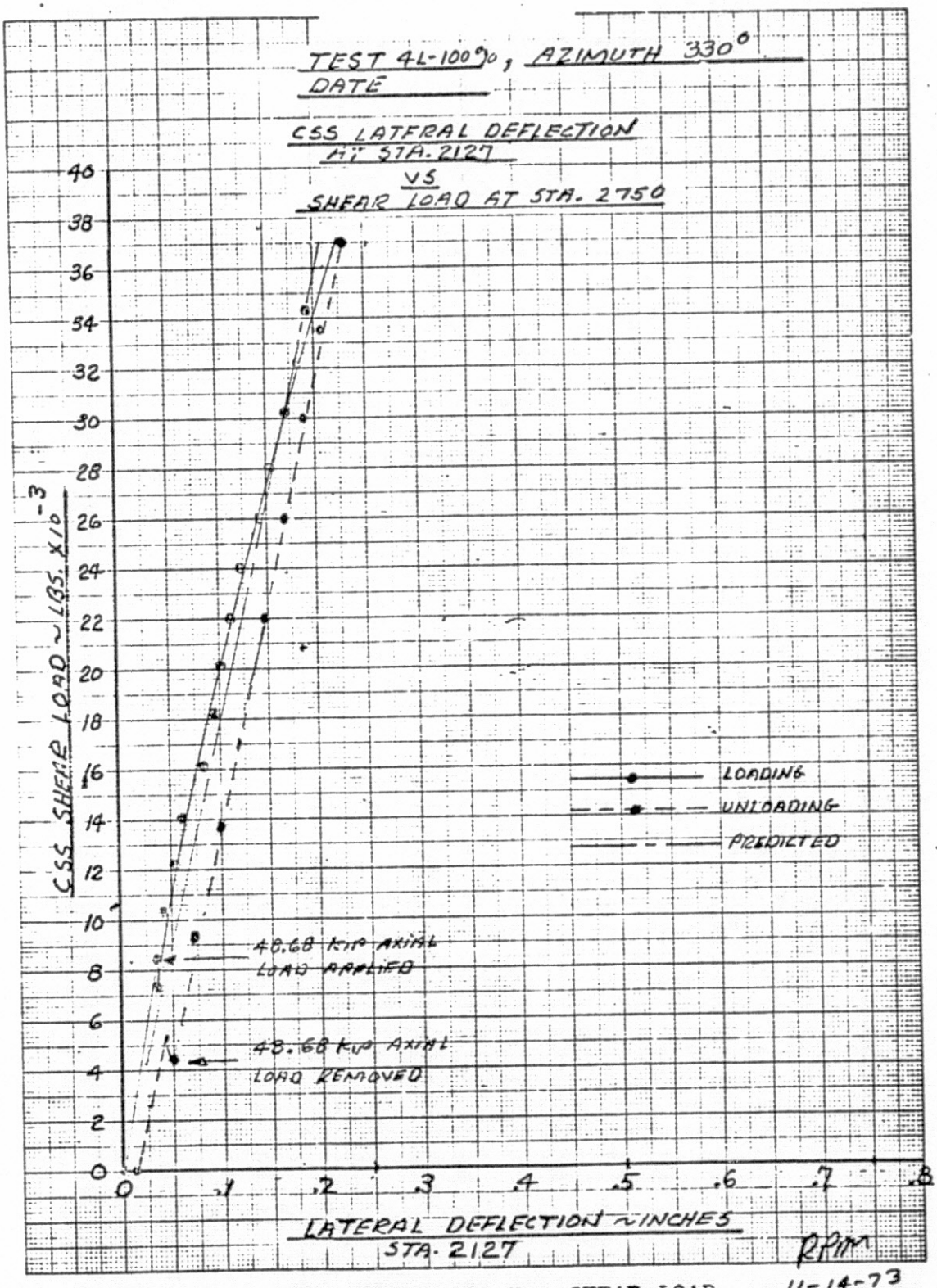

FIGURE VI-22. CSS DEFLECTION Vs. SHEAR LOAD.

ORIGINAL PAGE IS
OF POOR QUALITY

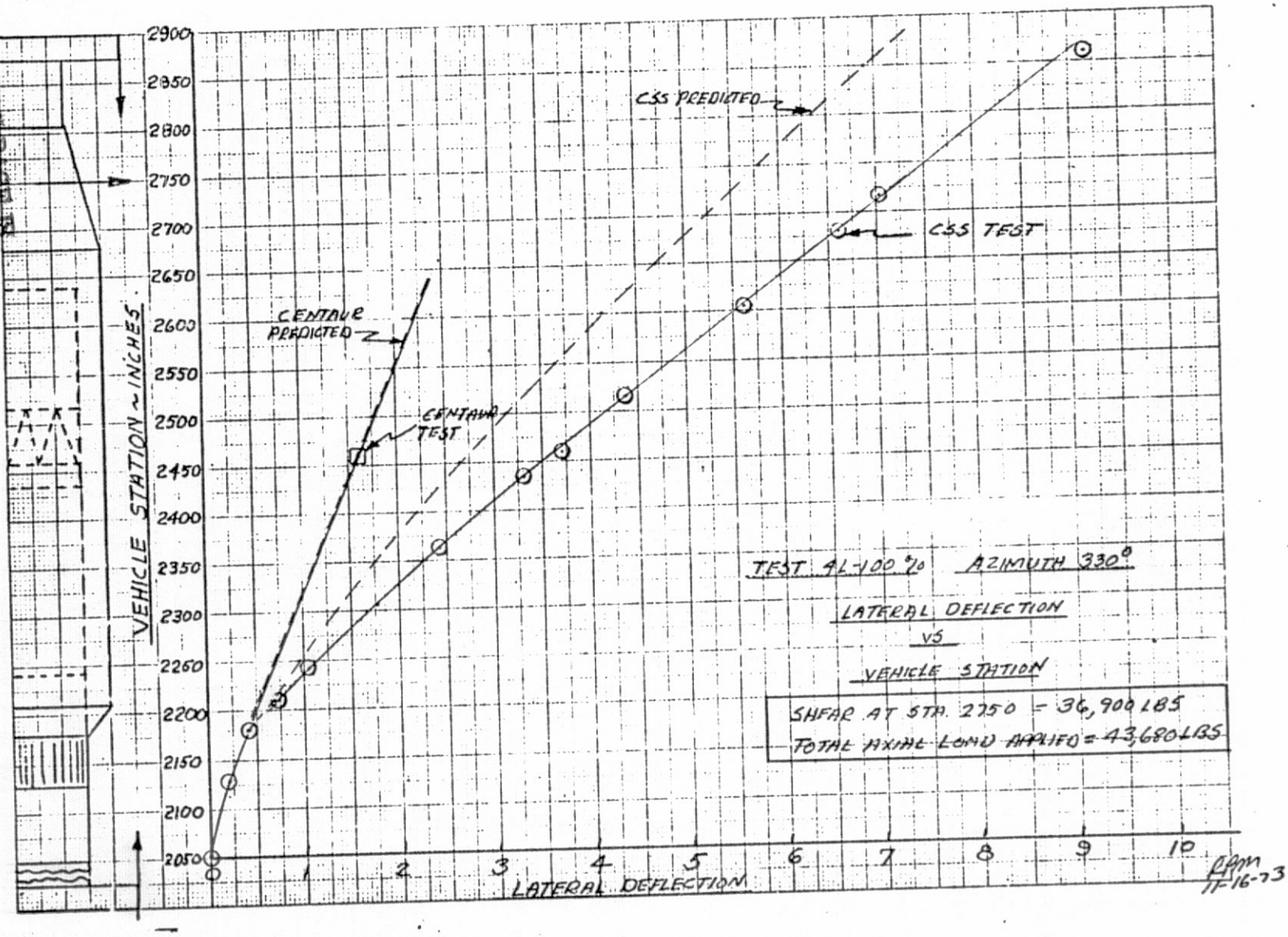

FIGURE VI-23. DEFLECTION Vs. STATION.

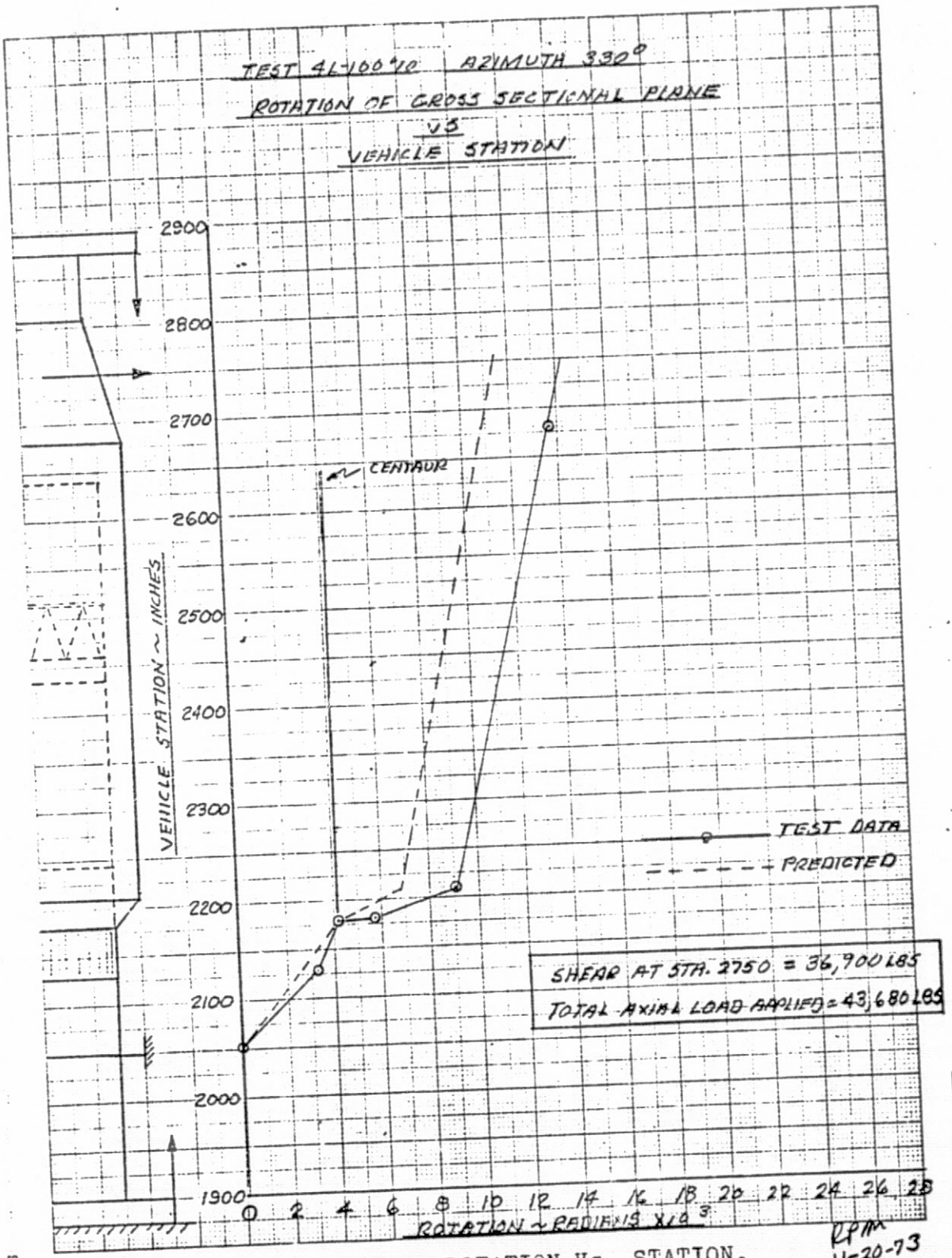

FIGURE VI-24. BENDING ROTATION Vs. STATION.

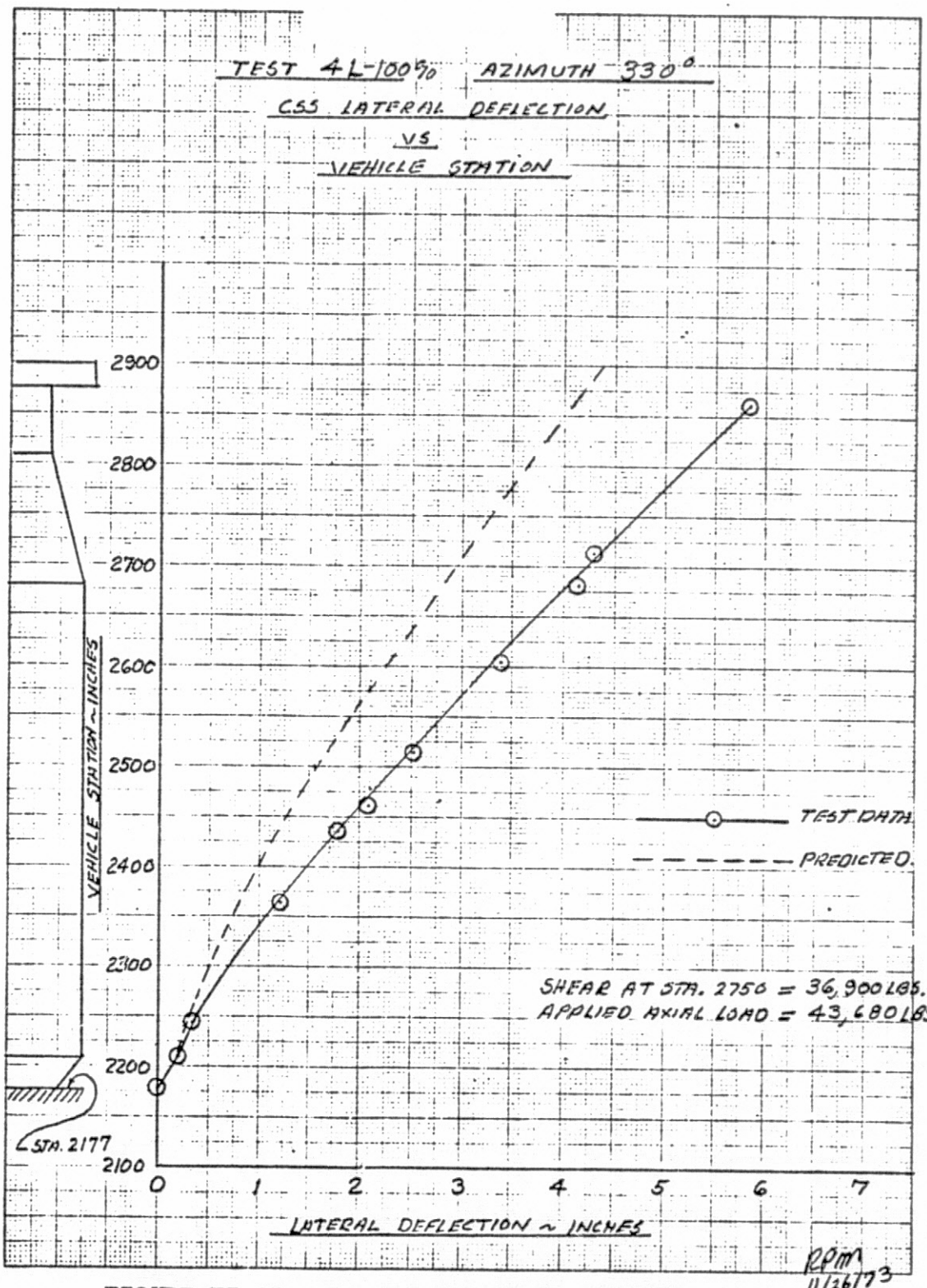

FIGURE VI-25. CSS DEFLECTION Vs. STATION.

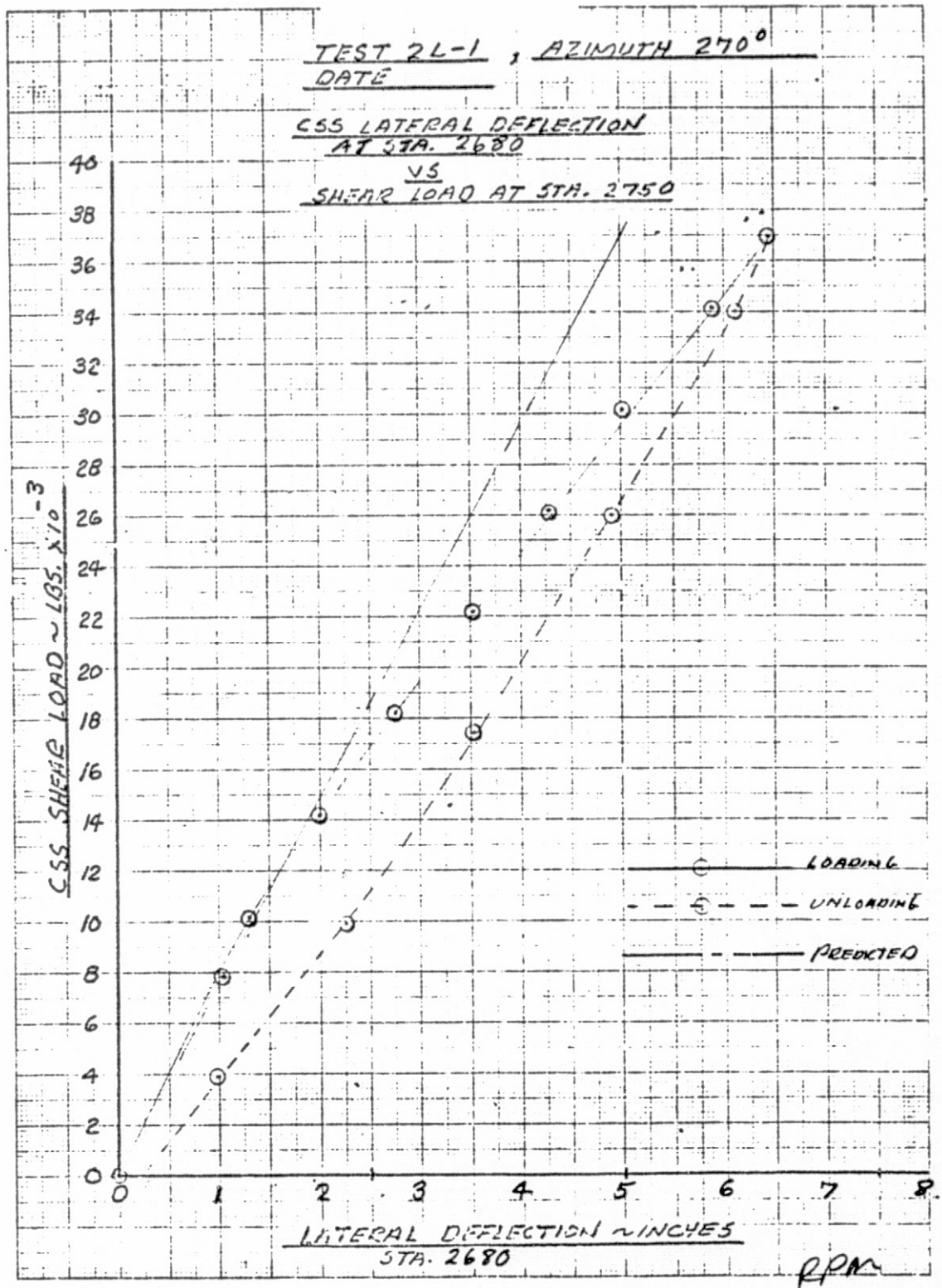

FIGURE VI-26. CSS DEFLECTION Vs. SHEAR LOAD.

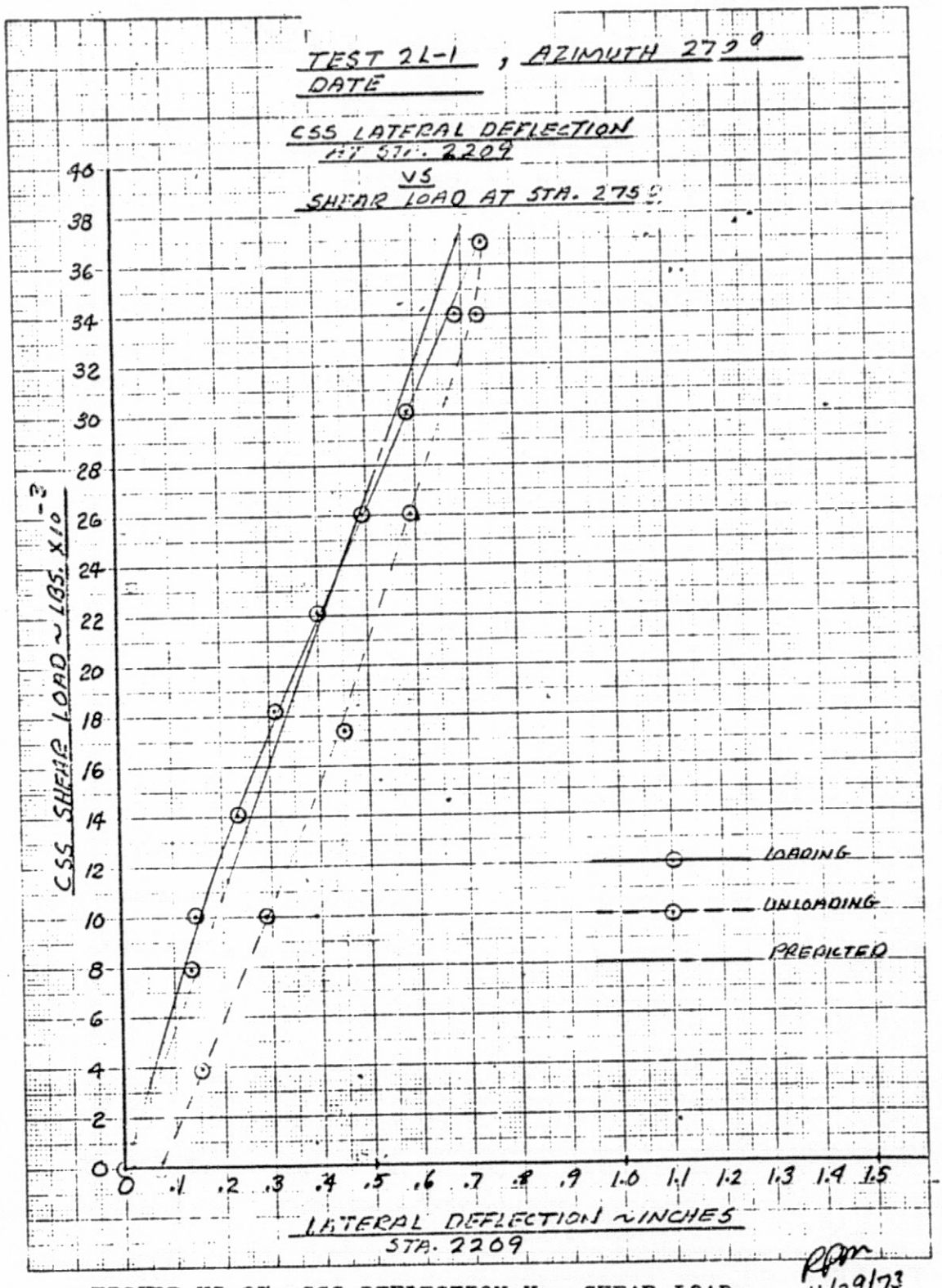

FIGURE VI-27. CSS DEFLECTION Vs. SHEAR LOAD.

ORIGINAL PAGE IS
OF POOR QUALITY

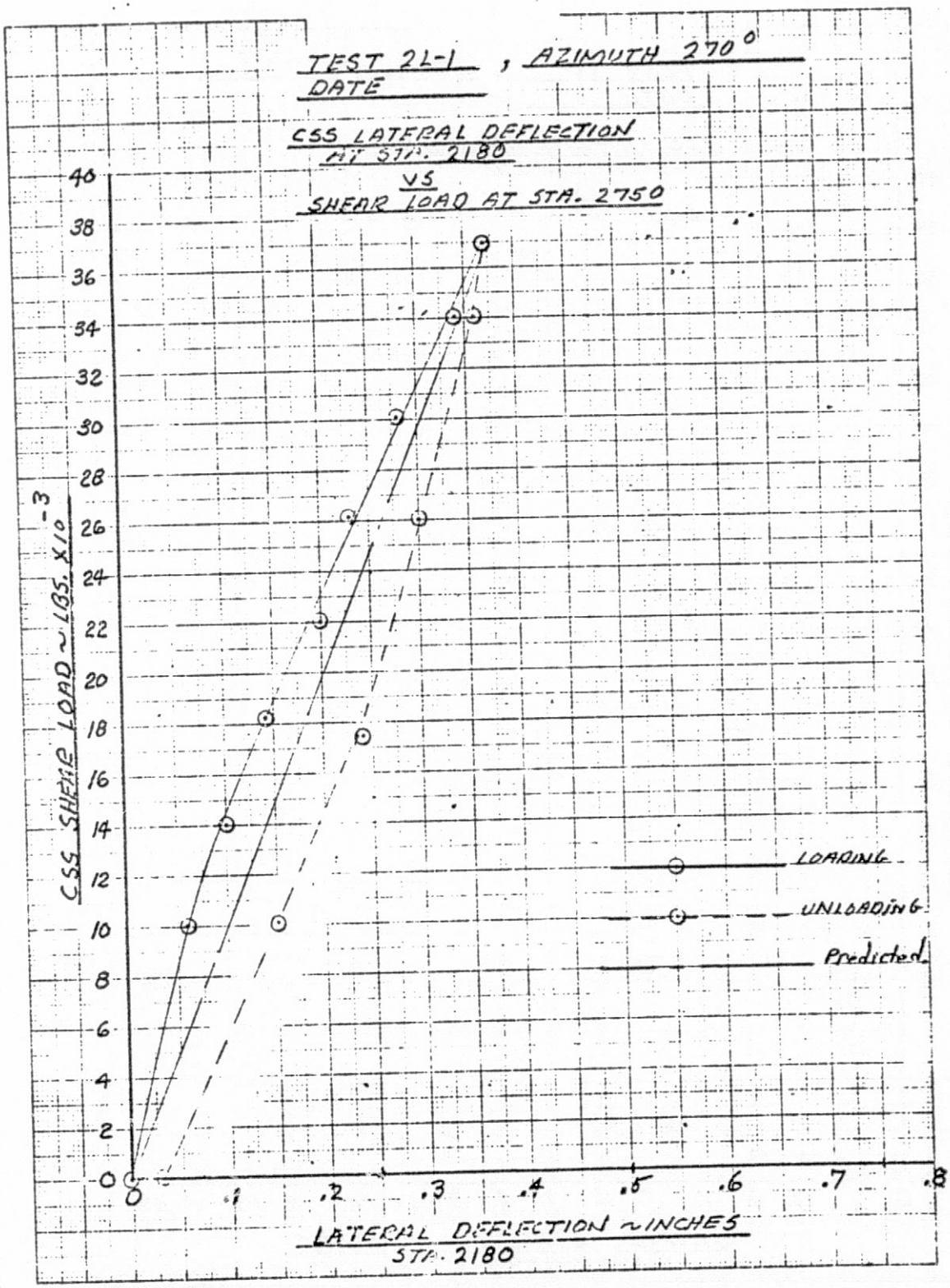

FIGURE VI-28. CSS DEFLECTION Vs. SHEAR LOAD.

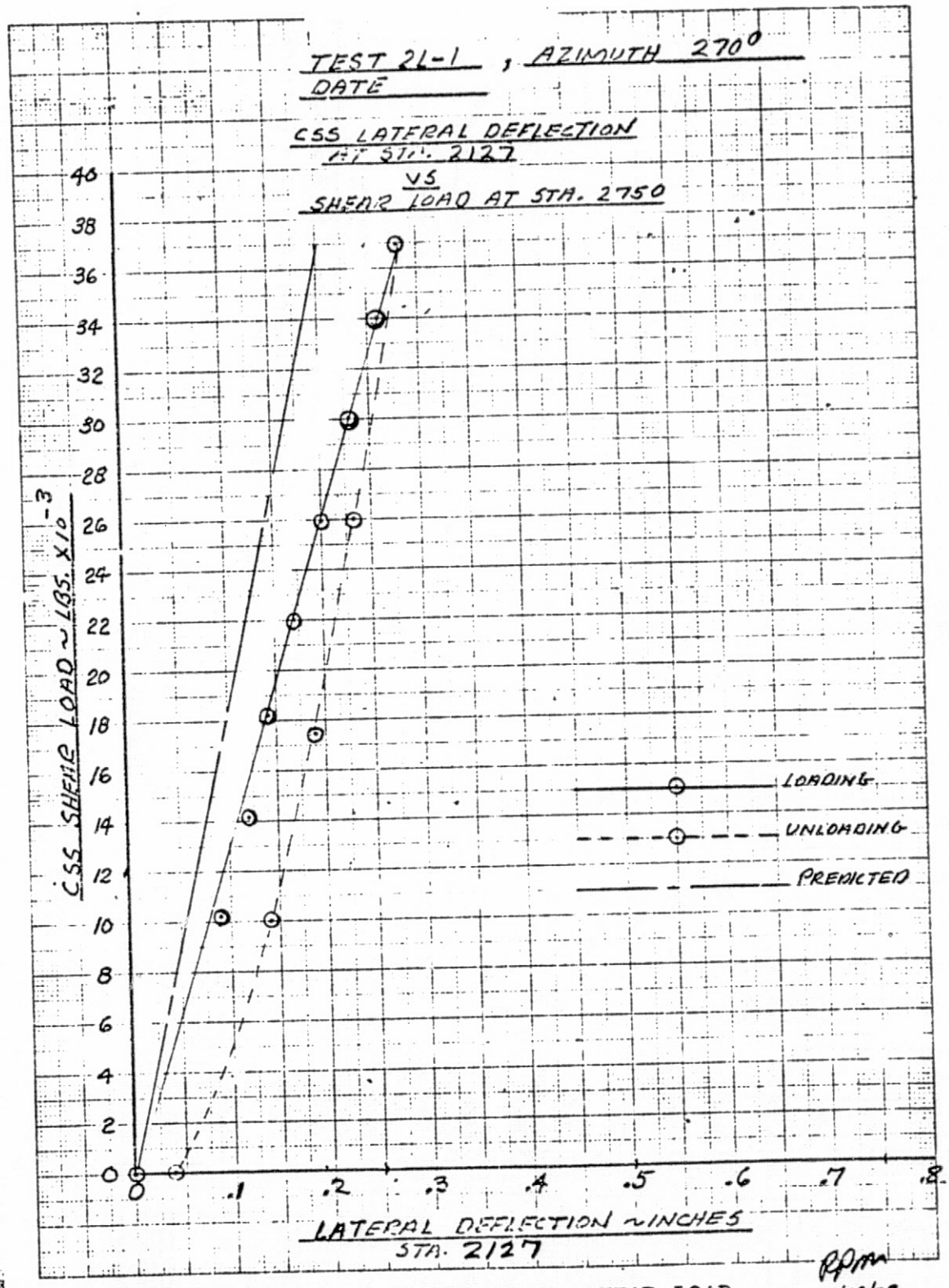

FIGURE VI-29. CSS DEFLECTION Vs. SHEAR LOAD.

RPM
11/29/73

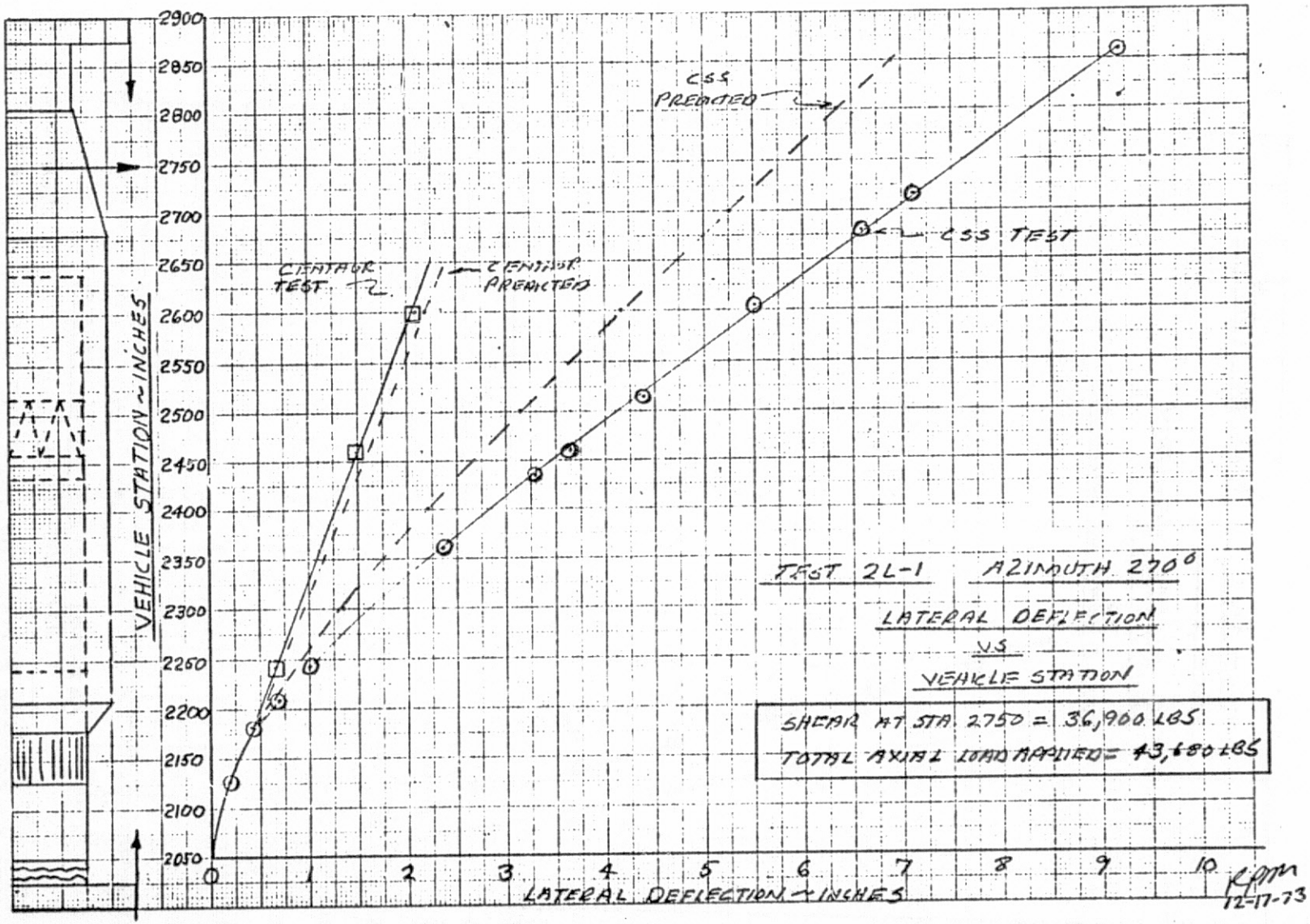

FIGURE VI-30. DEFLECTION Vs. STATION.

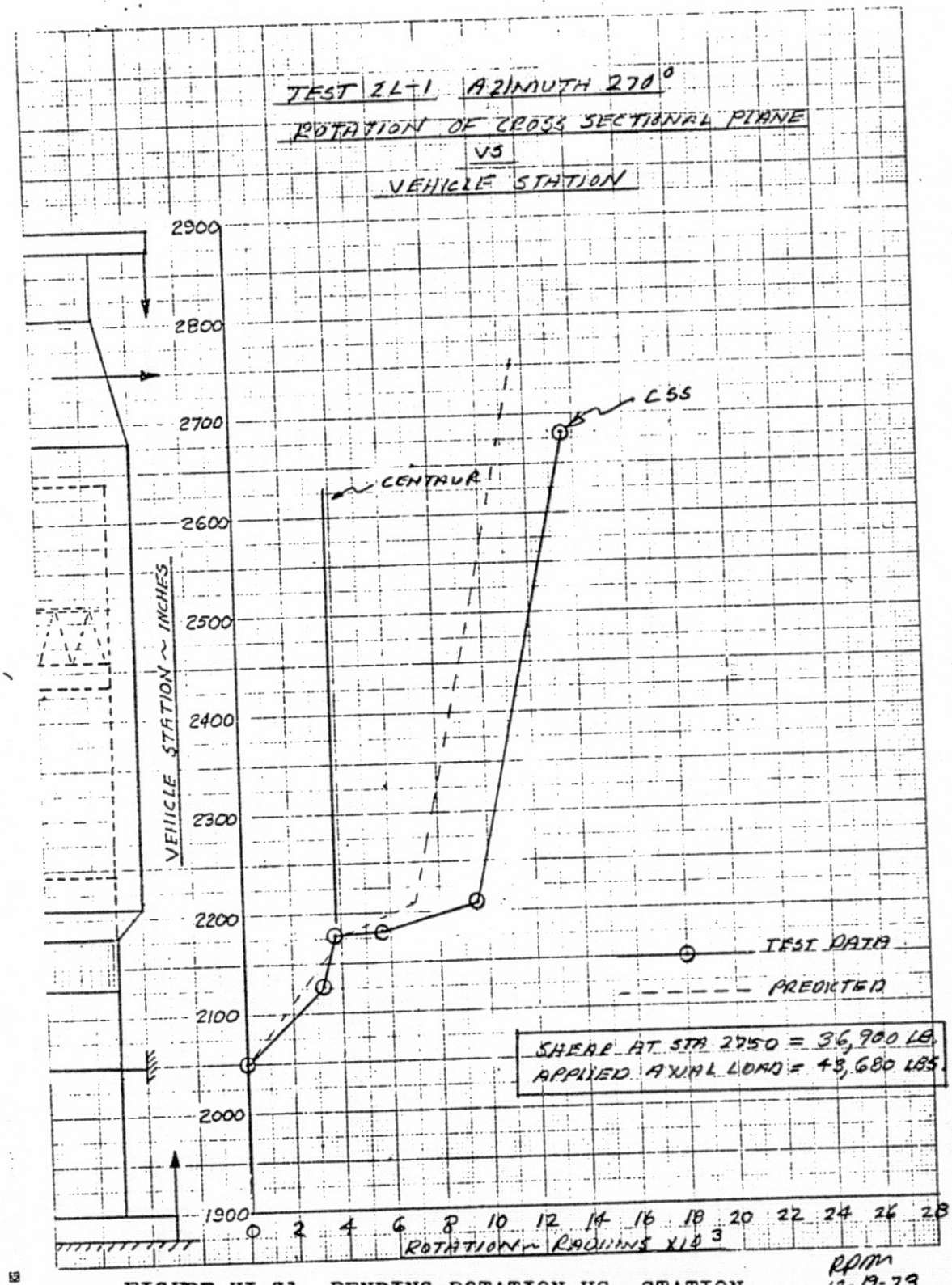

FIGURE VI-31. BENDING ROTATION VS. STATION.

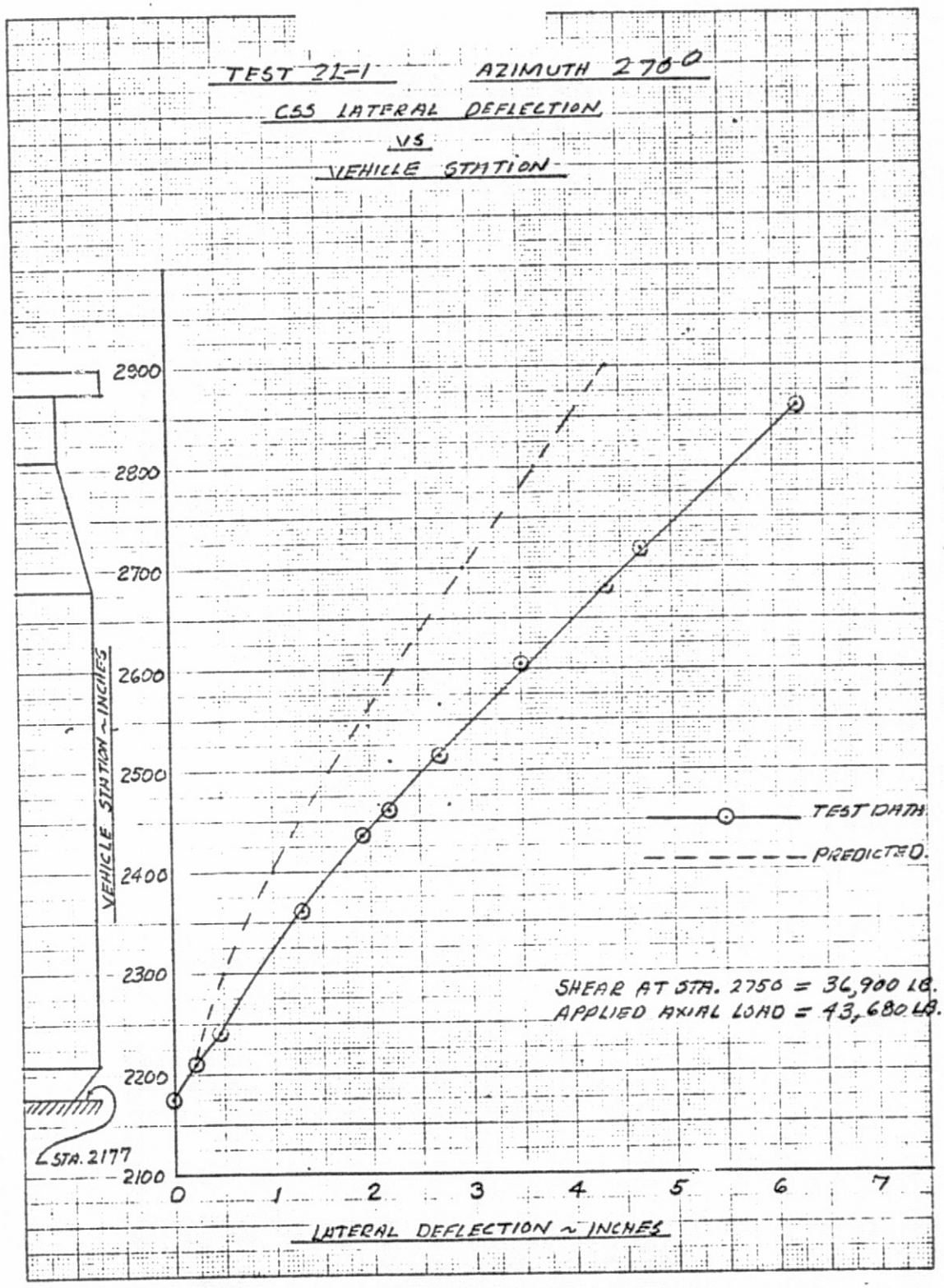

FIGURE VI-32. CSS DEFLECTION Vs. STATION.

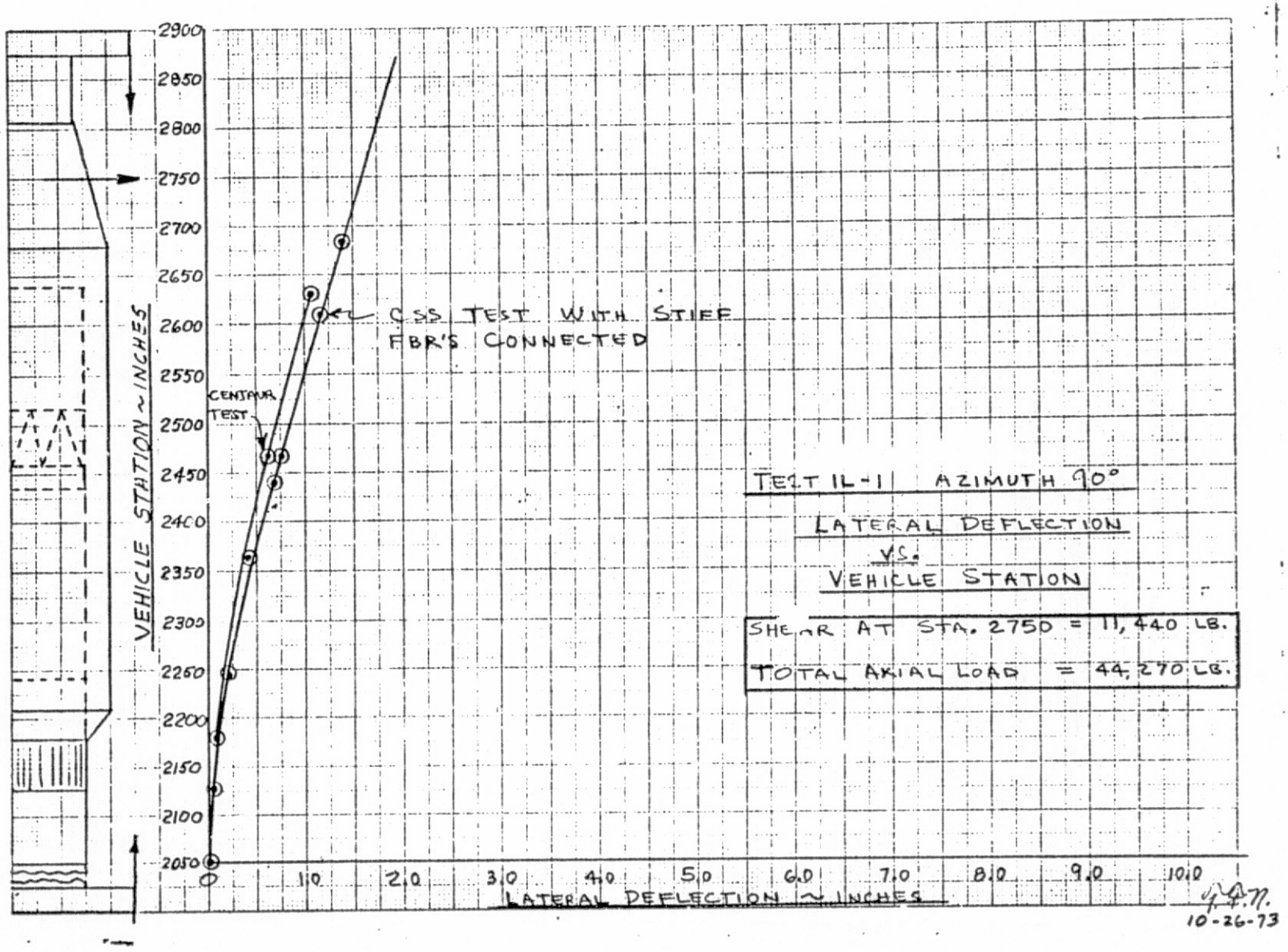

FIGURE VI-33. DEFLECTION Vs. STATION.

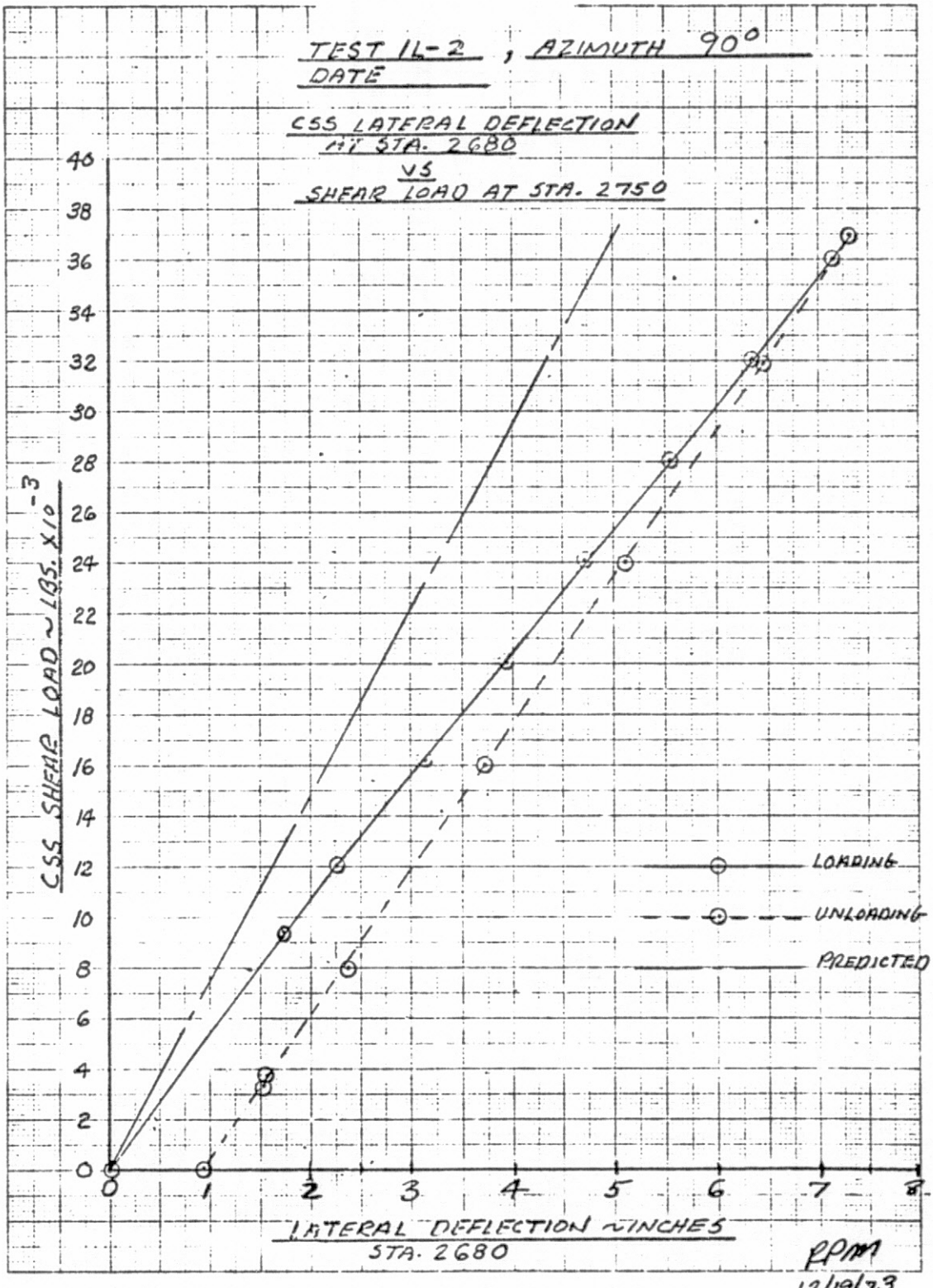

FIGURE VI-34. CSS DEFLECTION Vs. SHEAR LOAD.

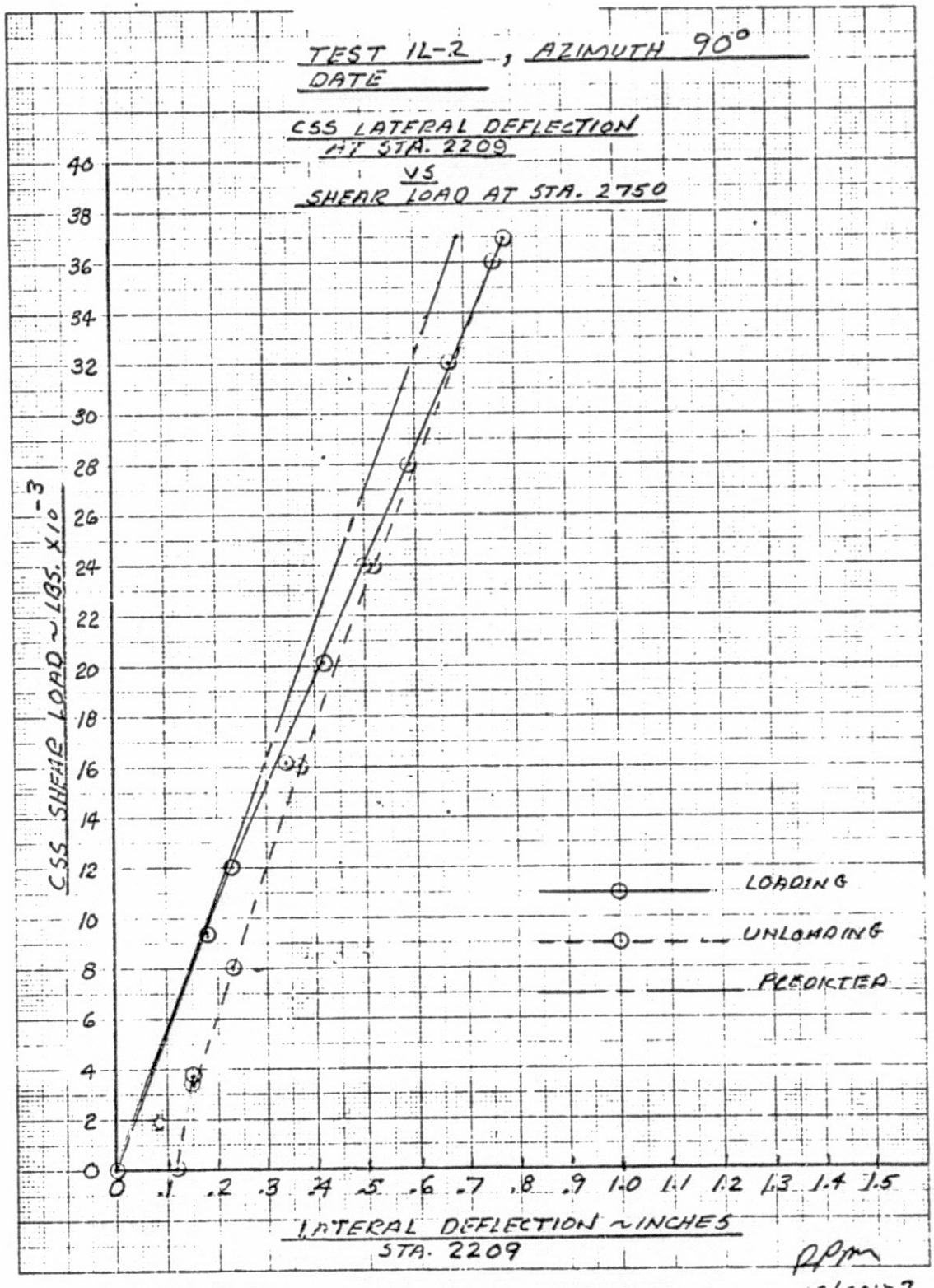

FIGURE VI-35. CSS DEFLECTION Vs. SHEAR LOAD.

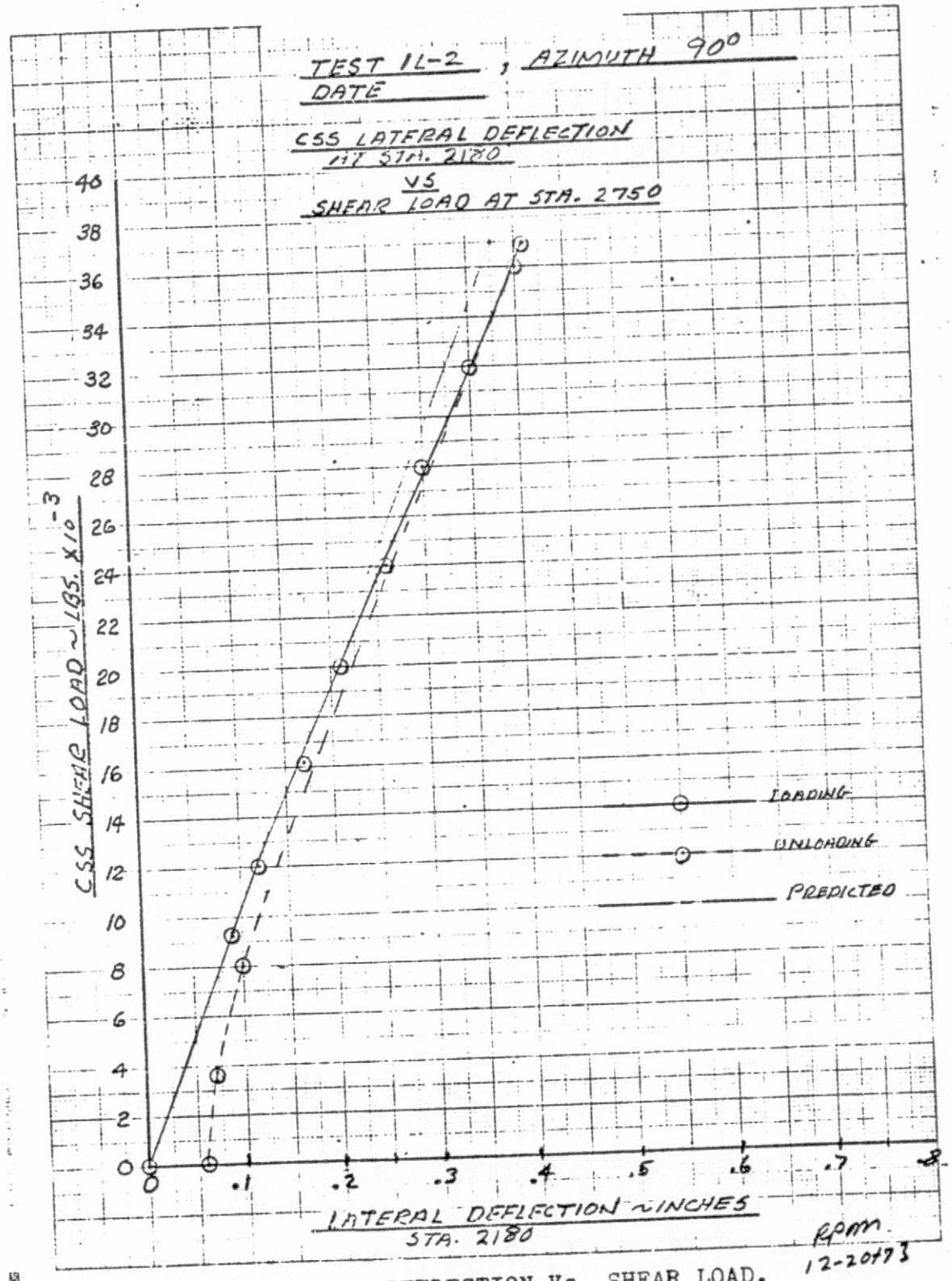

FIGURE VI-36. CSS DEFLECTION Vs. SHEAR LOAD.

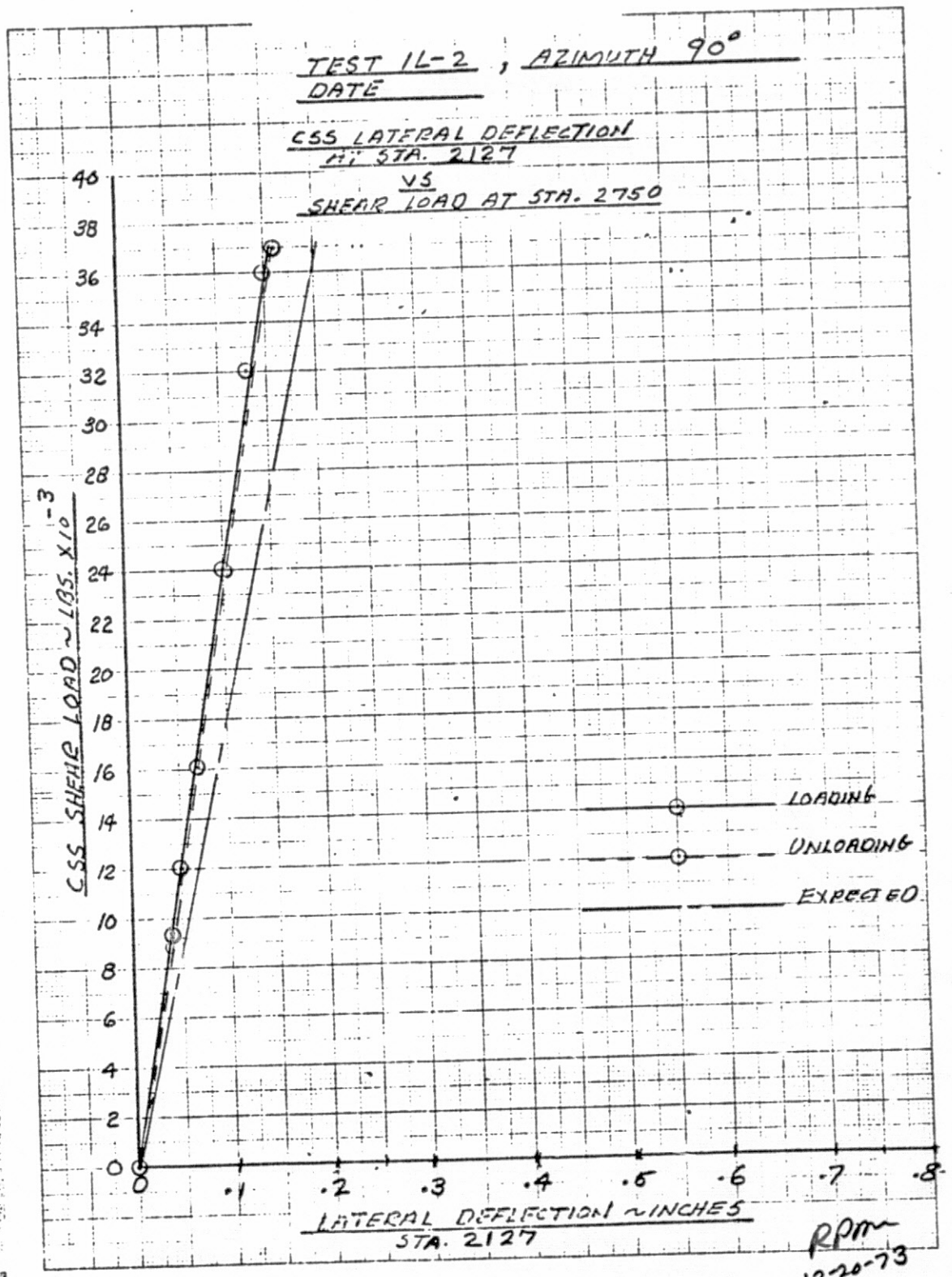

FIGURE VI-37. CSS DEFLECTION Vs. SHEAR LOAD.

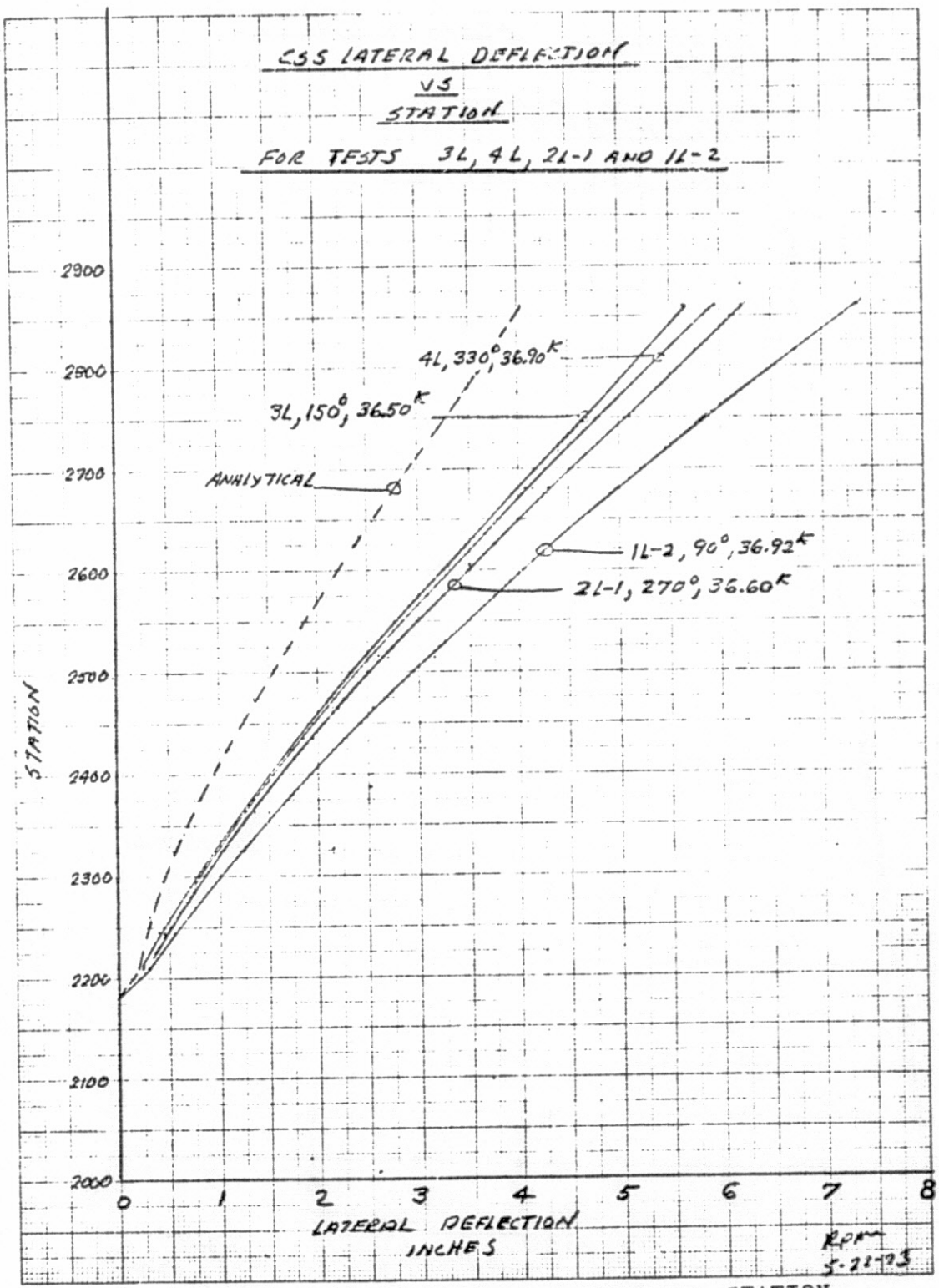

FIGURE VI-38. SUMMARY CSS DEFLECTION Vs. STATION.

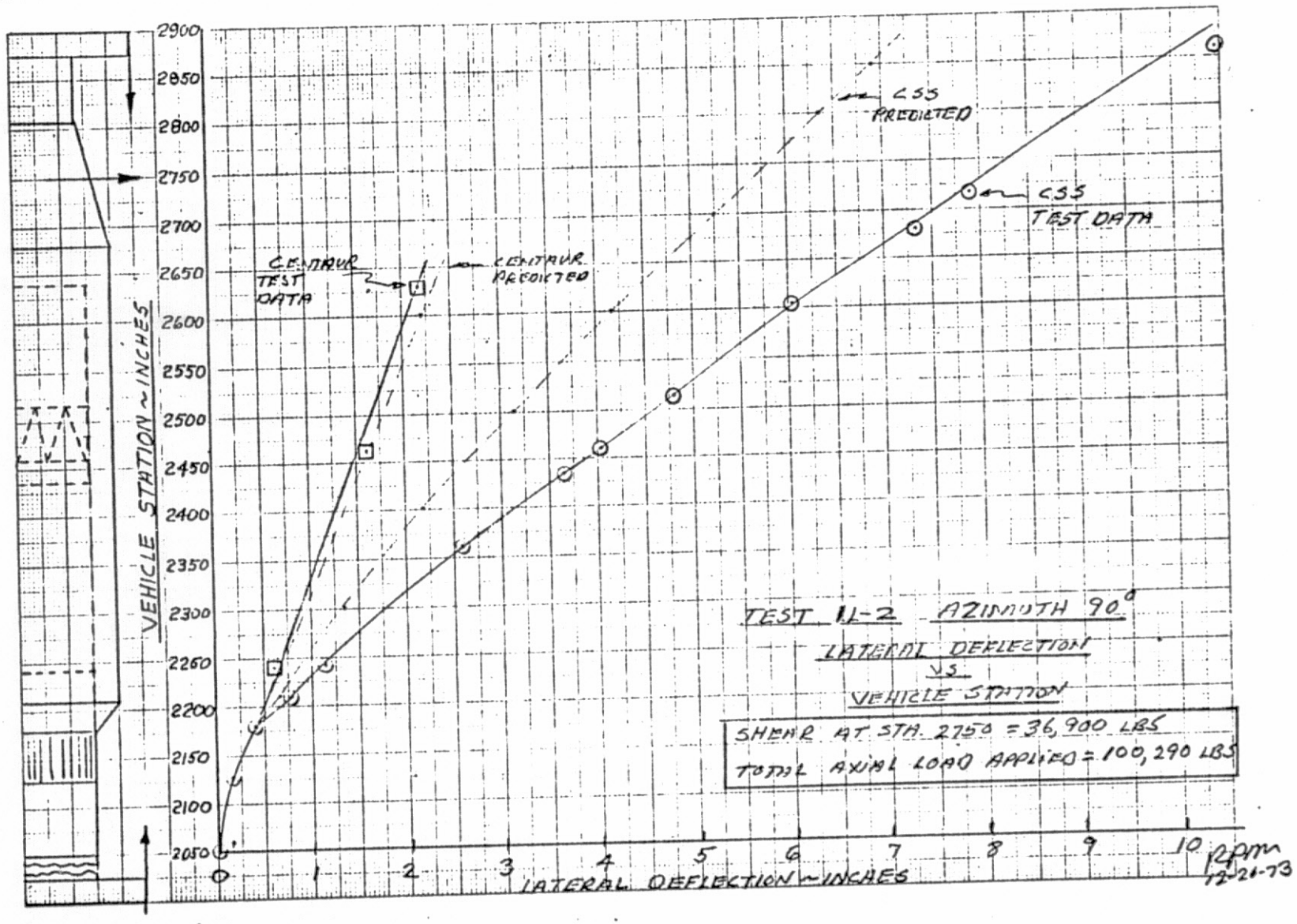

FIGURE VI-39. DEFLECTION Vs. STATION.

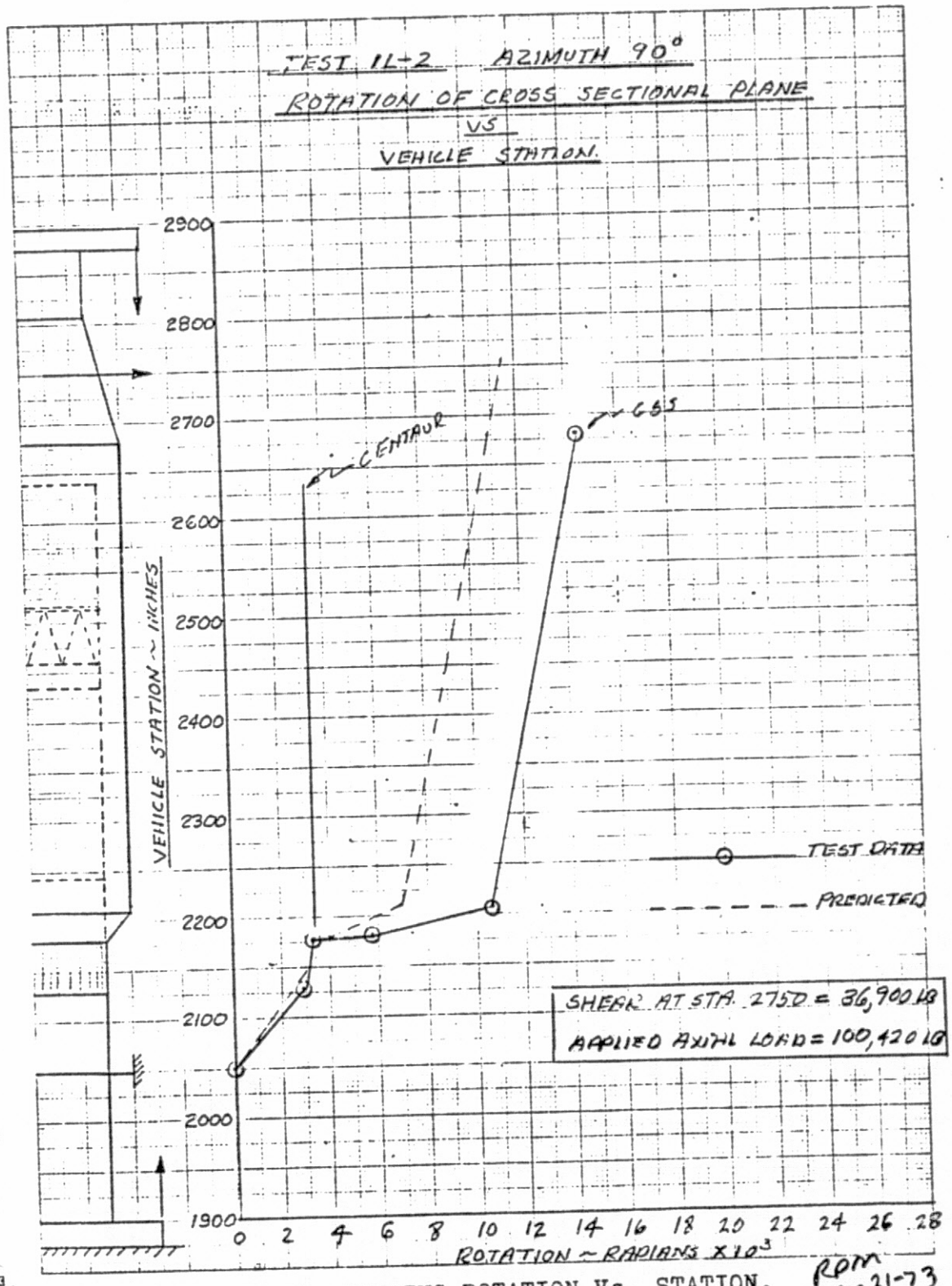

FIGURE VI-40. BENDING ROTATION Vs. STATION.

RDM
12-21-73

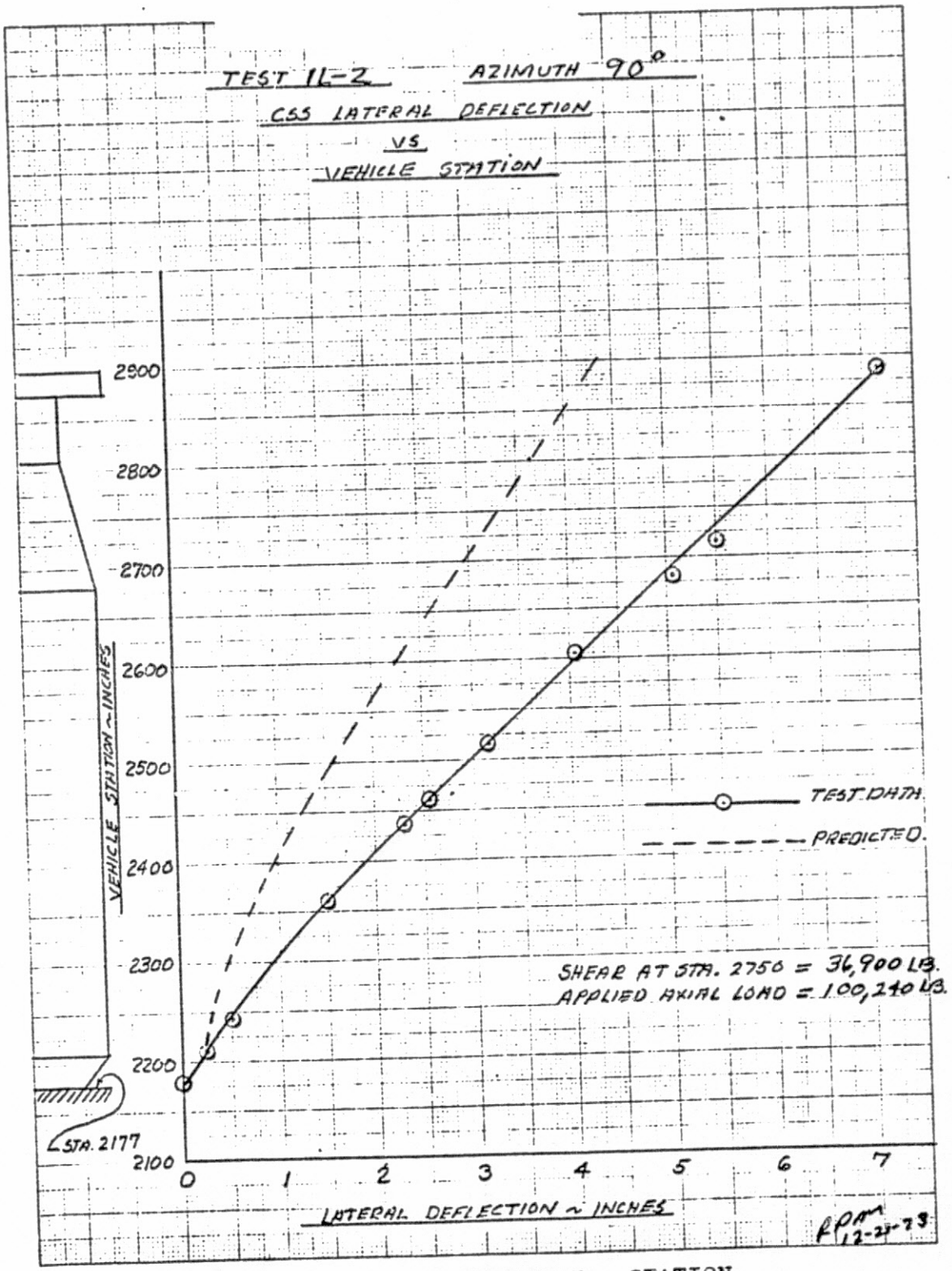

FIGURE VI-41. CSS DEFLECTION Vs. STATION.

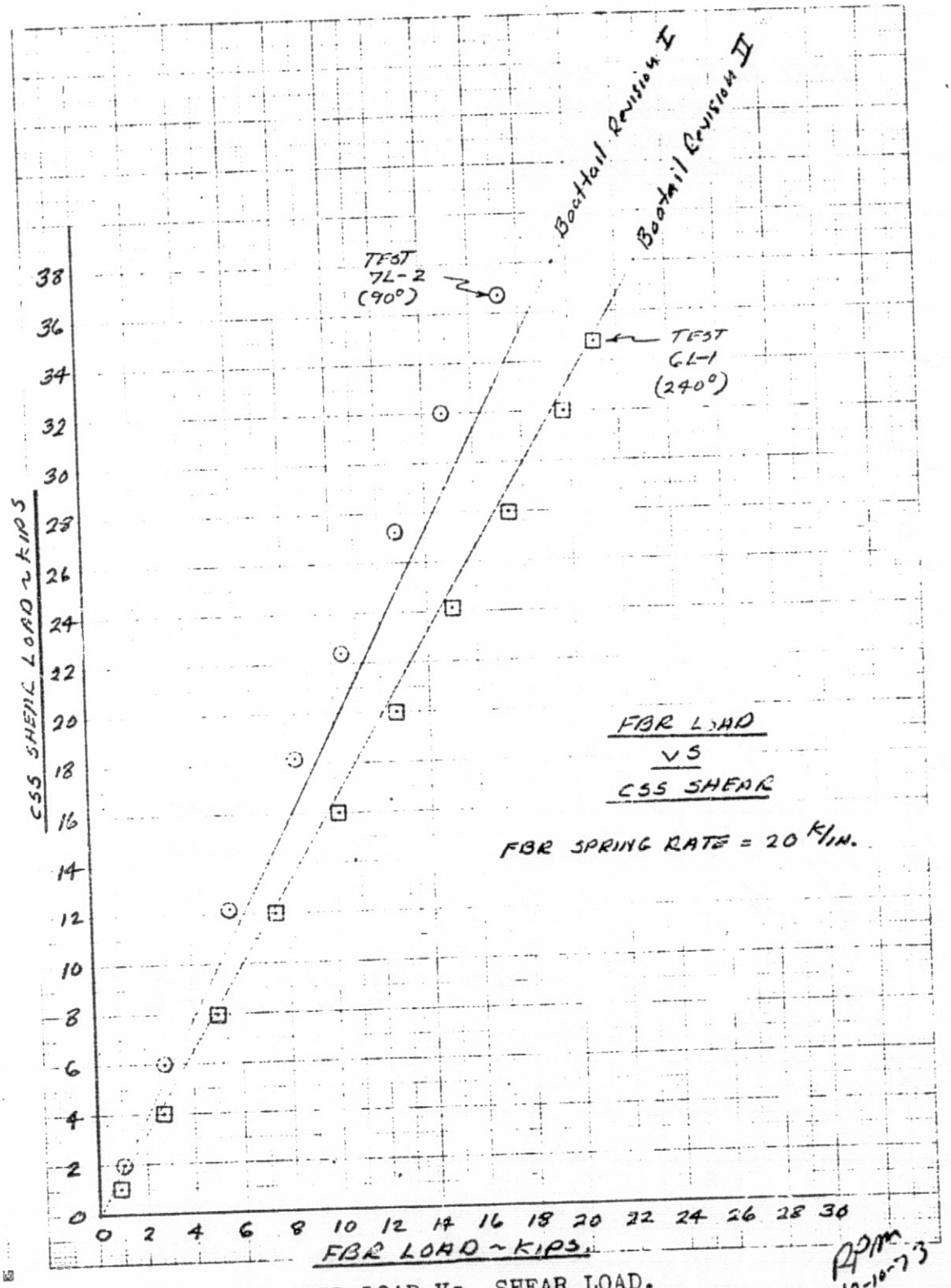

FIGURE VI-42. FBR LOAD Vs. SHEAR LOAD.

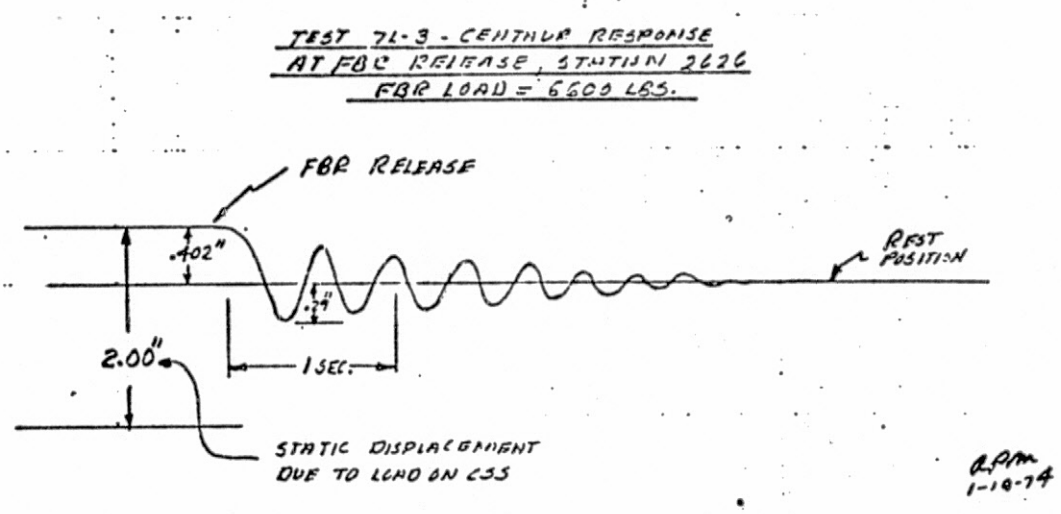

FIGURE VI-43. CENTAUR RESPONSE.

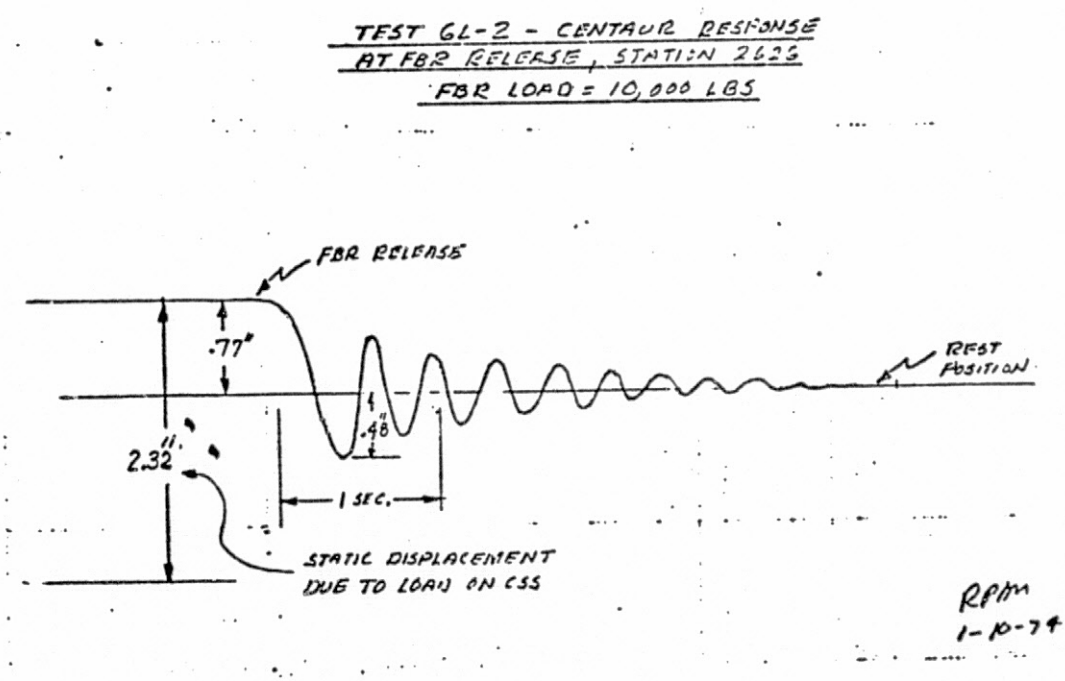

FIGURE VI-44. CENTAUR RESPONSE.

VII SIMULATED FLIGHT STRUCTURAL INSTRUMENTATION

By C. W. Eastwood

SUMMARY

Instrumentation which simulated the type to be used on Titan/Centaur flights was incorporated on the test specimen. The objectives of the flight simulated structural instruments were (1) to verify that structural instrument locations would produce usable data, (2) to obtain data to calibrate the strain measurement assemblies, and (3) to develop correlation between the test and flight specimens. Test data were successfully reduced to bending moment values on the CSS and ISA that compared favorably with the bending moments from the applied shear loads. Axial load values, which constitute only a small part of the total strains, did not compare well with the applied load values. Calibration factors were obtained from the test data so that the flight strain measurement data can be corrected from apparent to actual loads. A chart was developed correlating the bending moments calculated from the simulated flight instrument data on the CSS and ISA with the applied loads.

Use of the correlation chart with flight data will permit bending moment determination at stations along the CSS and ISA other than at the flight instrument locations.

DESCRIPTION

Strain gages were installed on the ISA in the same configuration and on the CSS in a similar configuration as those that are to be mounted on the Proof Flight vehicle. Near the aft end of the CSS four strain gage arrays were located at Station 2294 and spaced 90^{o} apart at azimuths 24^{o}, 114^{o}, 204^{o}, and 294^{o}, as shown in figure VII-1. Each array consisted of two uniaxial gages mounted on the shroud exterior skin corrugations as shown in figure VII-2(b). This connection compensated for temperature variations but also gave an augmented signal voltage output proportional to Poisson's ratio, which was corrected to true value by the data reduction equations. The strain gage arrays varied from the flight instrumentation in that the flight configuration uses 4 gages in a 4 leg active element Wheatstone bridge circuit array. The flight arrangement increases the combined output voltage by a factor of two which is corrected by the data reduction equation in determining the true strain. The test installation was modified from the flight installation for simplicity and data reduction.

PRECEDING PAGE BLANK NOT FILMED

On the forward section of the ISA 4 arrays of strain gages were installed at Station 2208 as shown in figure VII-1 and spaced at the same azimuths as those on the CSS (24^{o}, 114^{o}, 204^{o}, 294^{o}). Each array was configured identical to the flight measurements and consisted of 4 uniaxial gages. The gages were mounted on the sides of the longitudinal stringers on the exterior of the ISA as shown in figure VII-3(a). The electrical connection for each array was configured as depicted in figure VII-3(b). The circuit compensated for temperature changes and augmented the output signal by Poisson's ratio, which was corrected in the data reduction. The flight circuit is a 4-leg bridge of the same configuration as the CSS instrumentation.

The locations of the strain measurements were the same on the test specimen as on the flight vehicle. Locations on both the CSS and the ISA were selected because of the relatively clear structural areas free of doors and cutouts. On the CSS the designated station was the most aft clear area, which experiences the largest evenly distributed bending moment. The selected station on the ISA was forward of the CSS/ISA interface and experiences the largest bending moment of the Centaur/payload branch of the structure. The 90^{o} spacing at each station permitted reduction of the data readily into axial loads and bending moments.

TEST RESULTS

Tests 6L-1 and 7L-2

Of the 7 basic static load tests that were performed, Tests 6L-1 and 7L-2 included the flight configured system. Bending moments were shared between the Centaur and the CSS structures in a manner equivalent to flight conditions on these two tests only.

Bending Moments

The data from each gage array was reduced from the output signal voltage to strains and then to stresses. Since the CSS skin corrugations and the ISA stringers are axial members, the stresses were all uniaxial in nature. Using measurements diametrically opposite each other as pairs, e.g., 4901S and 4903S, the data were reduced to bending moments as follows:

Where:

S = stress, psi
P = axial load, lbs.
a = section area, sq.in.
M = bending moment, in.-lbs.
C = distance to neutral axis from gage, in.
I = moment of inertia, $in.^{4}$.
"CSS" = Centaur Standard Shroud
"ISA" = Interstage Adapter

Subscript	1	=	Measurement 4901S
"	2	=	" 4902S
"	3	=	" 4903S
"	4	=	" 4904S
"	5	=	" 4905S
"	6	=	" 4906S
"	7	=	" 4907S
"	8	=	" 4908S

Subscript	1, 3	=	axis through 4901S and 4903S
"	2, 4	=	" " 4902S and 4904S
"	5, 7	=	" " 4905S and 4907S
"	6, 8	=	" " 4906S and 4908S

$$S_2 = \frac{-P}{a} + \frac{M_{1,3}(C)}{I_{1,3}}$$

$$S_4 = \frac{-P}{a} - \frac{M_{1,3}(C)}{I_{1,3}}$$

$$M_{1,3} = \frac{(S_2 - S_4)\, I_{1,3}}{2\,C}$$

Similarly,

$$M_{2,4} = \frac{(S_3 - S_1)\, I_{2,4}}{2\,C}$$

Combining $M_{2,4}$ and $M_{1,3}$

$$M_{\text{"CSS"}} = \sqrt{(M_{2,4})^2 + (M_{1,3})^2}$$

Similarly,

$$M_{\text{"ISA"}} = \sqrt{(M_{6,8})^2 + (M_{5,7})^2}$$

A graphic representation is shown in figure VII-4.

Strain measurement data reduced to bending moments are plotted against FBR system loads in figure VII-5 from 0 to 100% limit load in 20% load increments for Tests 6L-1 and 7L-2. Figure VII-5 also includes plots of the moments for the same tests as determined from the applied loads as corrected for secondary moments created by offset of the CSS and Centaur masses including the load fixtures. In figure VII-6 the measurement data curves are averaged as are the applied load data curves. By utilizing the averaged data for the two tests 6L-1 and 7L-2, which experienced applied shear loads at 240^{o} and 90^{o} azimuth respectively, calibration factors were obtained for the moments determined by the applied loads versus the moments determined by the strain measurements. The factor for the moments on the CSS at Station 2294 was 0.99 and on the ISA at Station 2208 was 0.79. Because of averaging and instrumentation and data reduction errors, the possible error of the moments determined from the strain measurement data and corrected by the calibration factors is $\pm$ 10%.

A bending moment diagram of the average applied loads for Tests 6L-1 and 7L-2 is presented in figure VII-7. This diagram closely approximates the CSS bending moment design criteria for limit load conditions. The maximum bending moments calculated from the strain measurement test data, and corrected by the calibration factors, are plotted on the figure. Fair correlation between values from the applied and calculated loads was obtained. With this correlation of data, a method of determining the flight bending moments at various stations other than at the strain measurement locations was devised as follows:

1. The flight strain measurement data are reduced to bending moments on the CSS and ISA.

2. The ISA bending moment value is plotted as Item 1 in figure VII-7.

3. A straight line Centaur moment diagram from a zero inch-pound moment at the FBR station through Item 1 is drawn as Item 2 in the figure.

4. The bending moment value at Station 2294 on the Centaur diagram is obtained as Item 3 in the figure. This value represents the amount of bending moment load relief at Station 2294 that the CSS experiences by load transfer to the Centaur through the FBR system.

5. The CSS bending moment value is plotted as Item 4 in the figure.

6. At Station 2294, the CSS bending moment (plotted as Item 4) is increased by the value obtained at Item 3. This summed value (Items 3 and 4) represents the bending moment the CSS would have experienced without Centaur load relief.

7. A straight line total bending moment diagram from a zero-inch pound moment at Station 2750 through the summed value of Step 6 (Items 3 and 4) is drawn as Item 5 in figure VII-7.

8. The CSS tank section bending moment diagram is drawn as Item 6. Load relief on the CSS is shown by the reduction in bending moment between Item 5 and Item 6 in the figure.

Flight bending moment values at any station for the CSS and ISA can be taken from such a diagram constructed from flight data. The constructed straight line bending moment diagram will not be completely representative of the flight loading, however, the error is estimated at ± 10%.

Shear Azimuths

The azimuth of the applied shear load was calculated from the reduced strain measurement data as follows:

ω = resultant moment azimuth, deg.

θ = shear load azimuth, deg.

ψ = 24 deg.

$M_{1,3}$ = bending moment about axis joining strain measurements 4901S and 4903S, in.-lbs.

$M_{2,4}$ = bending moment about axis joining strain measurements 4902S and 4904S

$M_{5,7}$ = bending moment about axis joining strain measurements 4905S and 4907S

$M_{6,8}$ = bending moment about axis joining strain measurements 4906S and 4908S

$$\theta_{\text{"CSS"}} = \left[\psi + \tan^{-1}\left(\frac{M_{2,4}}{M_{1,3}}\right) - 90^\circ\right] = \psi + \omega_{CSS} - 90^\circ$$

$$\theta_{\text{"ISA"}} = \left[\psi + \tan^{-1}\left(\frac{M_{6,8}}{M_{5,7}}\right) - 90^\circ\right] = \psi + \omega_{ISA} - 90^\circ$$

The difference between the calculated and the applied shear load azimuth at limit load was within ± 5°. At smaller loads the difference was greater. Curves of the calculated shear load azimuths versus the percent applied shear loads are shown in figure VII-8.

Axial Loads

The strain measurement data were also reduced to obtain the axial loads by the following equation:

Where:

a = section area, sq.in.

P = compressive axial load, lbs.

S = stress, psi.

Subscripts 1 through 8 = measurements 4901S through 4908S, respectively.

$$P_{\text{"CSS"}} = \left(\frac{a}{4}\right)(S_1 + S_2 + S_3 + S_4)$$

$$P_{\text{"ISA"}} = \left(\frac{a}{4}\right)(S_5 + S_6 + S_7 + S_8)$$

The axial loads determined from the strain measurement data varied from the applied load values (including load fixture and simulated propellant weights) by large factors. The calibration factor for the CSS axial loads was 0.63 and for the ISA was 1.60 for averaged data from Tests 6L-1 and 7L-2. The large discrepancy between the strain measurement determined axial loads and the applied loads is explained by the small portion of the total strain that the axial loading created as shown in figure VII-4. The percent full scale instrument error was a large part of the instrument reading in the axial load portion of the strains developed in the test. Maximum axial load values for Tests 6L-1 and 7L-2 were:

Test No.	Structure	Applied Loads, Lbs.	Strain Determined Loads, Lb.
6L-1	CSS	19,805	29,660
7L-2	CSS	19,805	32,895
6L-1	ISA	77,469	49,840
7L-2	ISA	75,879	45,560

The axial load calibration factors as determined from the tests can be applied to the flight data determined loads to obtain actual flight loads on the CSS and ISA. A summation of the two values will be the axial load value at the Titan Skirt/ISA interface at Station 2127.

TEST RESULTS

Tests 1L through 5L

Basic Tests 1L through 5L were performed without the FBR system and, as a result, the bending moments on the two branches of the structure were not equivalent to the conditions of the planned flights during maximum loads. However, a discussion of the results is included.

Bending Moments

Bending moments were calculated from the strain measurement data of the CSS by the same method as used for tests with the FBR system installed. Moments on the ISA were only those created by the offset of the Centaur branch of the structure and were insignificant, being less than 1/4% of the limit load moment. The bending moment values on the CSS for limit load conditions as calculated from the strain measurement data compare with the applied moments as follows:

Test No.	CSS Bending Moment, In.-Lbs. Applied	Calculated
1L-2	17.03×10^6	19.1×10^6
2L-1	17.02×10^6	18.6×10^6
3L	16.98×10^6	17.5×10^6
4L	16.58×10^6	17.0×10^6
5L-2	16.90×10^6	18.1×10^6

Shear Azimuths

The azimuths also were calculated from the strain data by the same method used for the tests with the FBR system installed. Maximum difference of the calculated azimuths from the applied load azimuths was $\pm$ 5% at limit load.

Axial Loads

The axial loads on the CSS as determined from the strain measurement data varied greatly from the applied load values. Again, the low level of the strain created by the axial loading was judged to be responsible for the large differences. A summary of the maximum axial loads is as follows:

Test No.	Axial Load, Lbs. Applied	Calculated
1L-2	89,460	70,500
2L-1	32,600	10,100
3L	89,480	65,100
4L	32,190	22,900
5L-2	19,500	33,900

SUMMARY OF TEST RESULTS

The test specimen was configured the same as the flight vehicle with the FBR system installed in Tests 6L-1 and 7L-2. As a result the simulated flight strain measurement data from Tests 6L-1 and 7L-2 only are usable for calibration and correlation for flight use.

Bending moments on the CSS and ISA, as determined from the strain measurements in the two tests with the FBR system installed, differed from the actual applied bending moments by $\pm$ 10%. The difference is explained by two effects. The first is that local discontinuities in the structure caused the data to vary from that of a uniform cylindrical structure, and the second is that the full scale instrument error was a significant portion of the data readings.

The averaged measurement data for the CSS bending moments differed from the averaged applied loads by + 1% so that the calibration factor for the apparent to actual values was 0.99. For the ISA data the difference was + 21% and the calibration factor was 0.79.

Strains caused by the axial loads were only a small part (12%) of the total strain that was developed. In addition, the instrument range was twice the maximum total strain value. The possible instrument error was as great in value as the apparent axial strain value for the CSS and 25% of the value for the ISA. As a result, confidence is small in the axial loads determined from the strain measurements. Apparent axial loads, calculated from the strain data, compared with the applied values were widely dispersed and tended to confirm the inaccuracy of the axial load strains. The calibration factor for the averaged axial loads on the CSS was 0.63 and on the ISA was 1.60.

Vehicle azimuths of the shear load application that were determined from the strain measurement data compared favorably with the actual azimuths of the applied shear loads. At maximum loads the calculated shear azimuths were within $\pm$ 5% of the actual values. At lower values of shear load, the calculated shear azimuths differed more.

Flight bending moment values for the CSS and ISA at any station can be determined within $\pm$ 10% from the flight strain measurement data by construction of a straight line bending moment diagram.

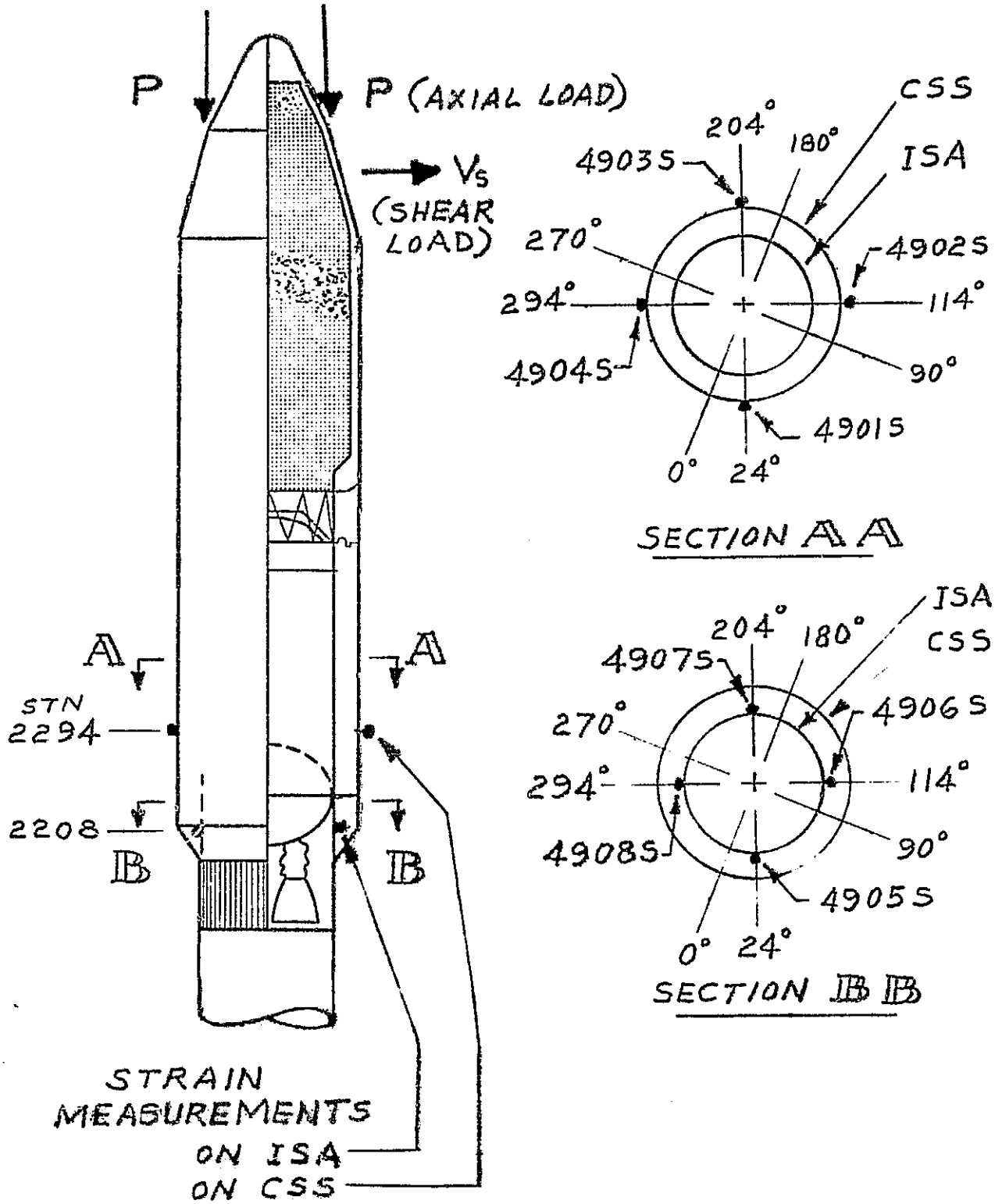

FIGURE VII-1. FLIGHT SIMULATED STRUCTURAL STRAIN MEASUREMENT LOCATIONS ON CSS AND ISA.

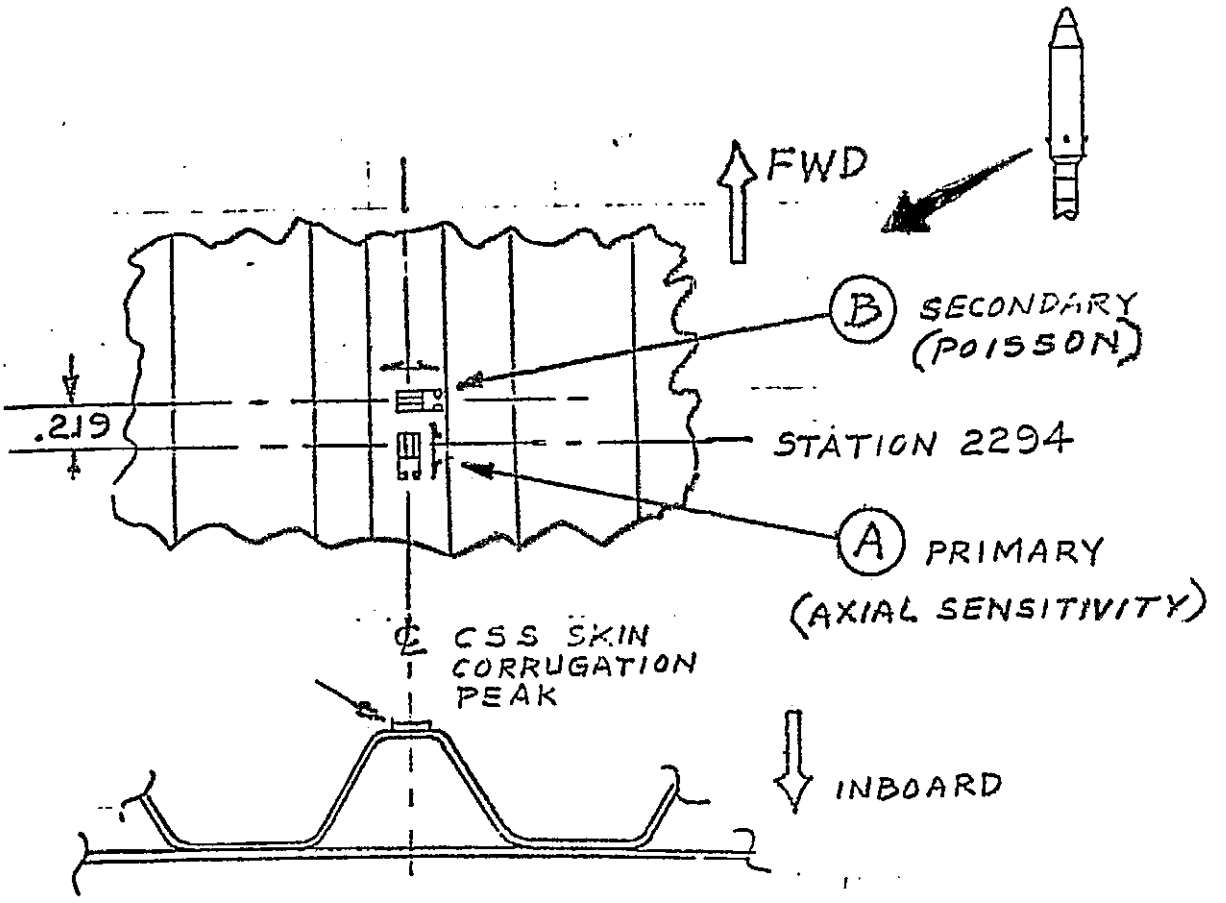

a. STRAIN GAGE MOUNTING DETAILS.

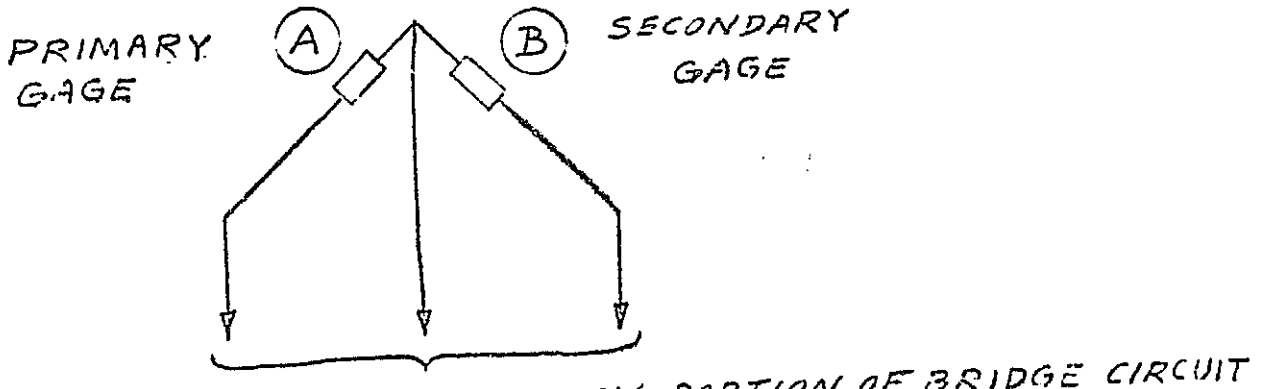

b. STRAIN GAGE WHEATSTONE BRIDGE CIRCUIT.

FIGURE VII-2. FLIGHT SIMULATED STRUCTURAL STRAIN MEASUREMENT DETAILS.

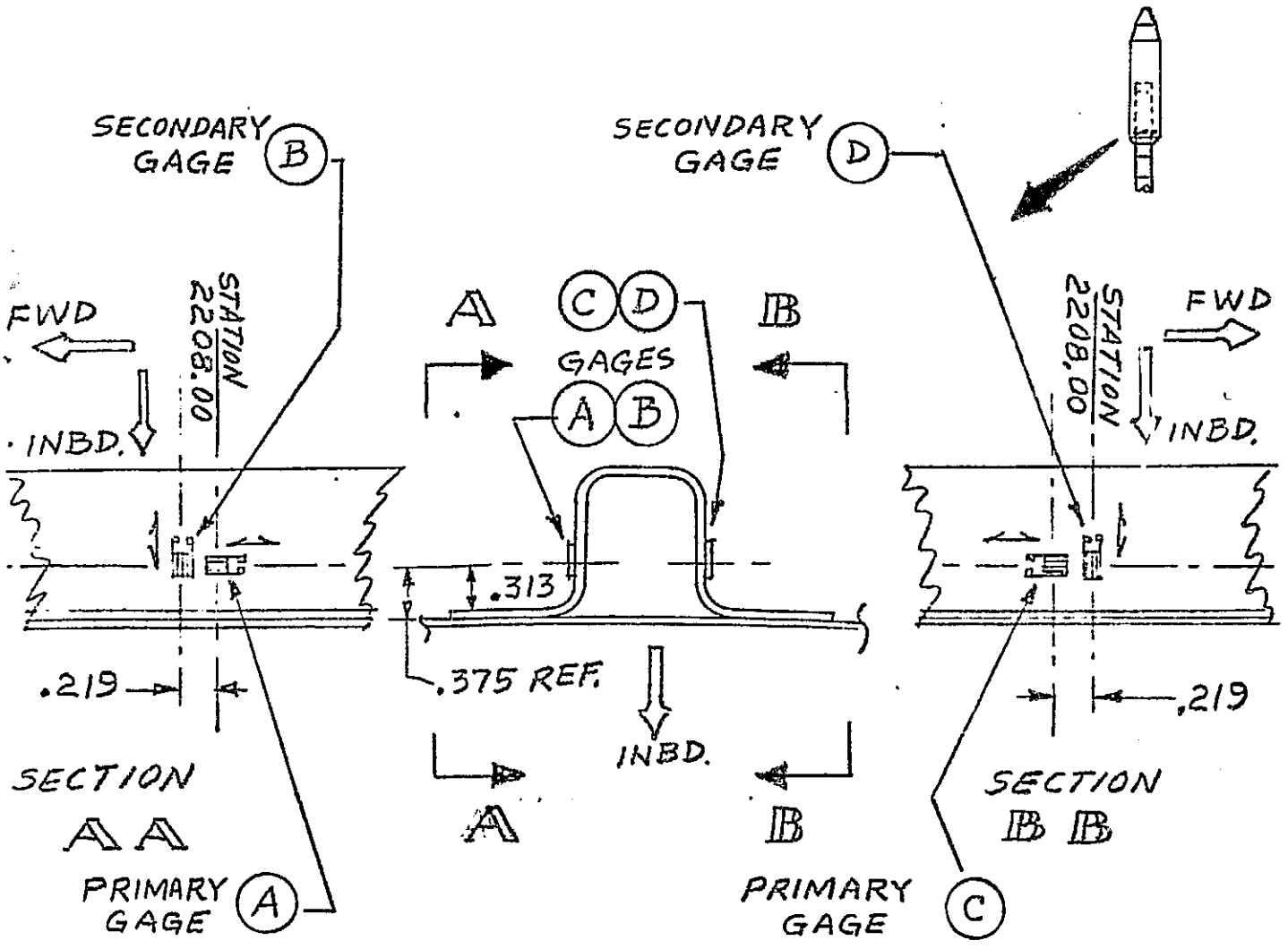

a. STRAIN GAGE MOUNTING DETAILS.

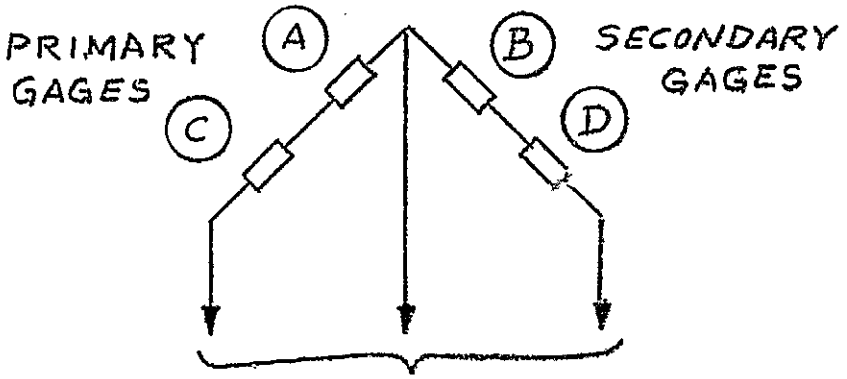

b. STRAIN GAGE WHEATSTONE BRIDGE CIRCUIT.

FIGURE VII-3. FLIGHT SIMULATED STRUCTURAL STRAIN MEASUREMENT DETAILS

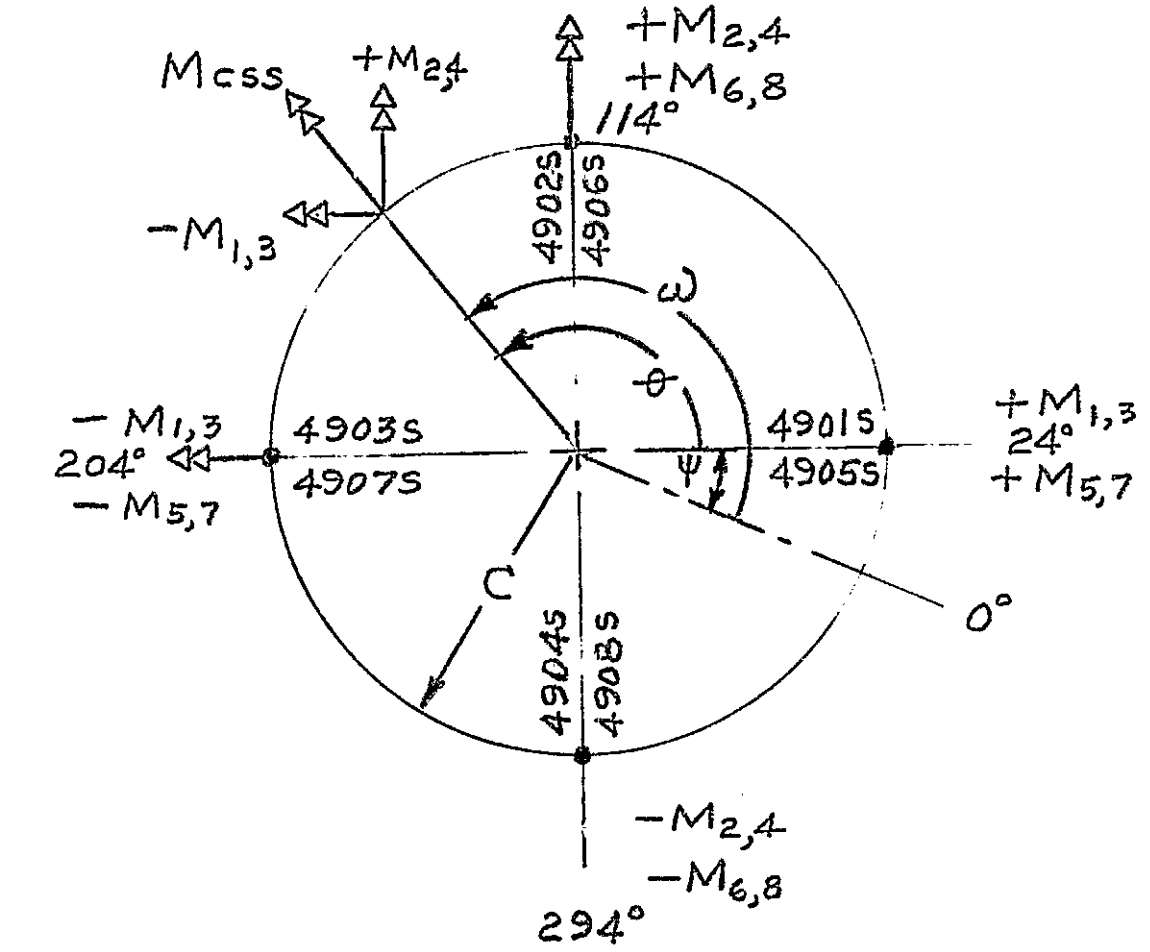

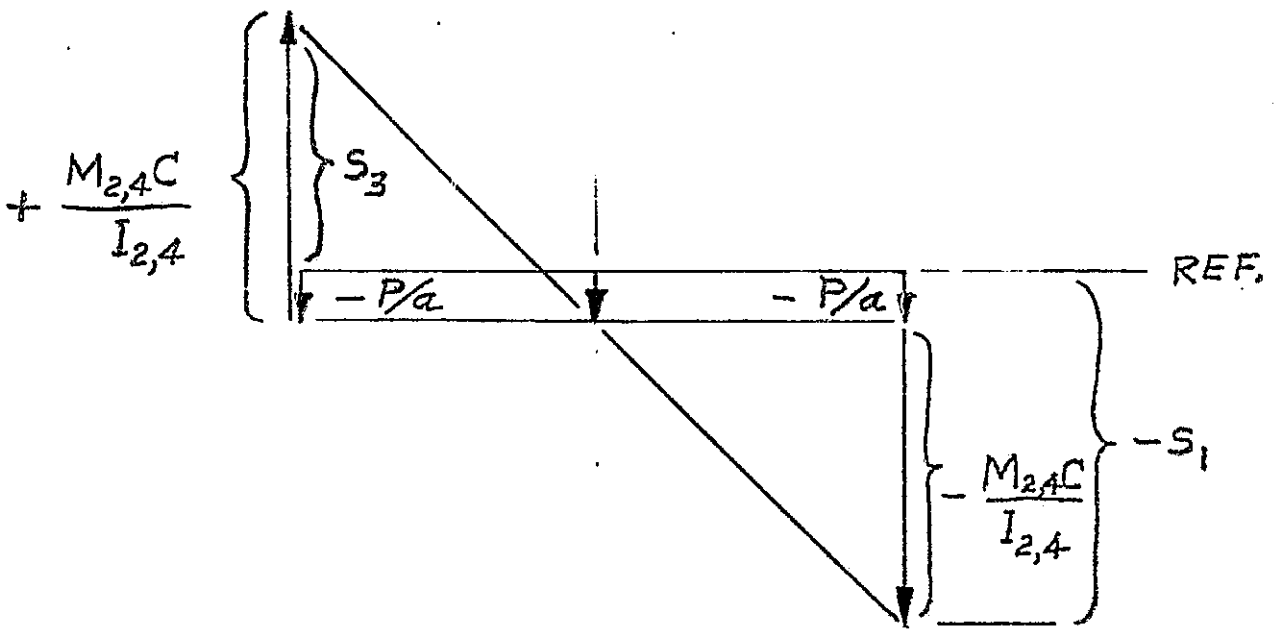

FIGURE VII-4. GRAPHIC STRESS DIAGRAM OF STRUCTURAL BENDING MOMENTS AND AXIAL LOADS.

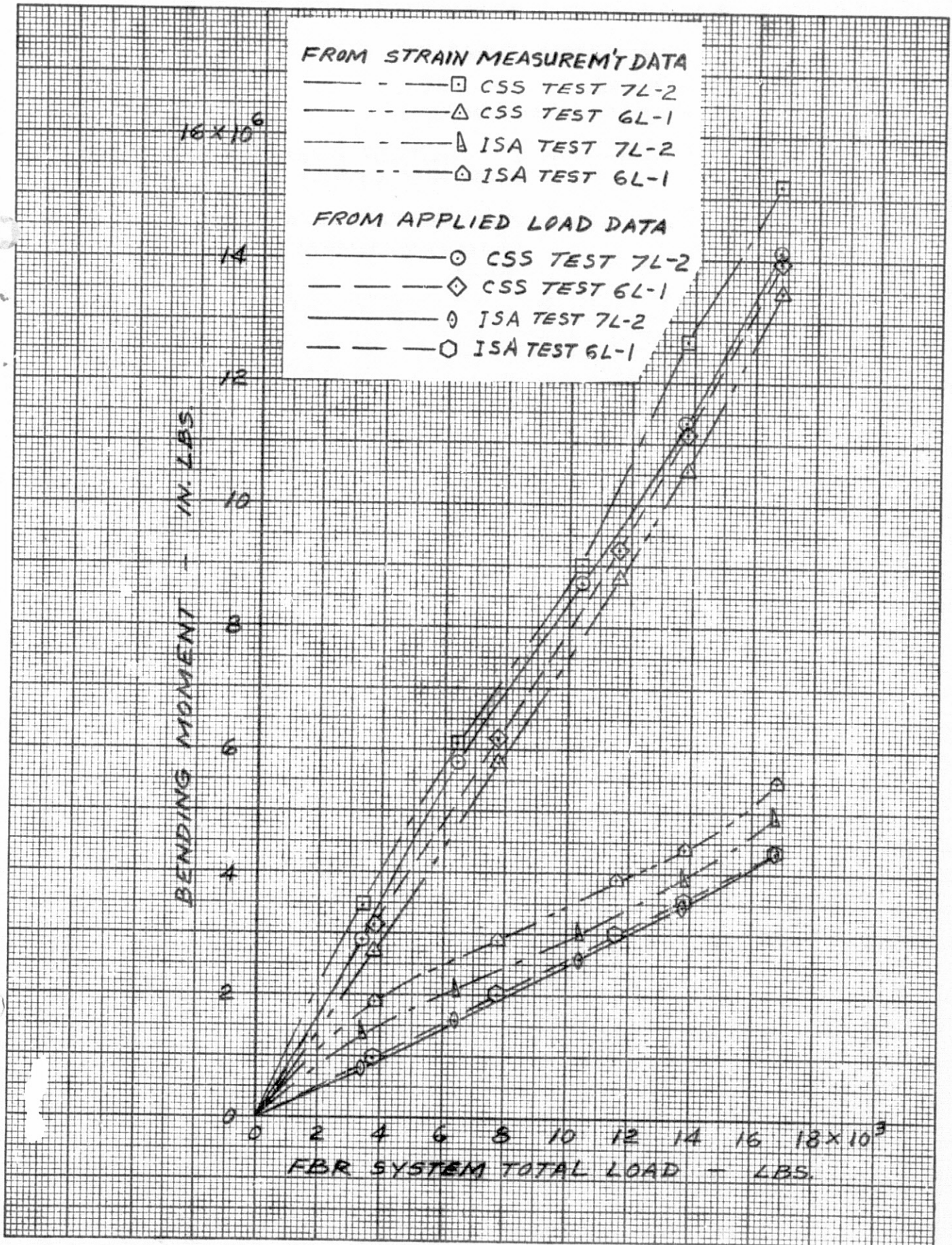

FIGURE VII-5. BENDING MOMENTS ON STRUCTURAL TEST SPECIMEN.

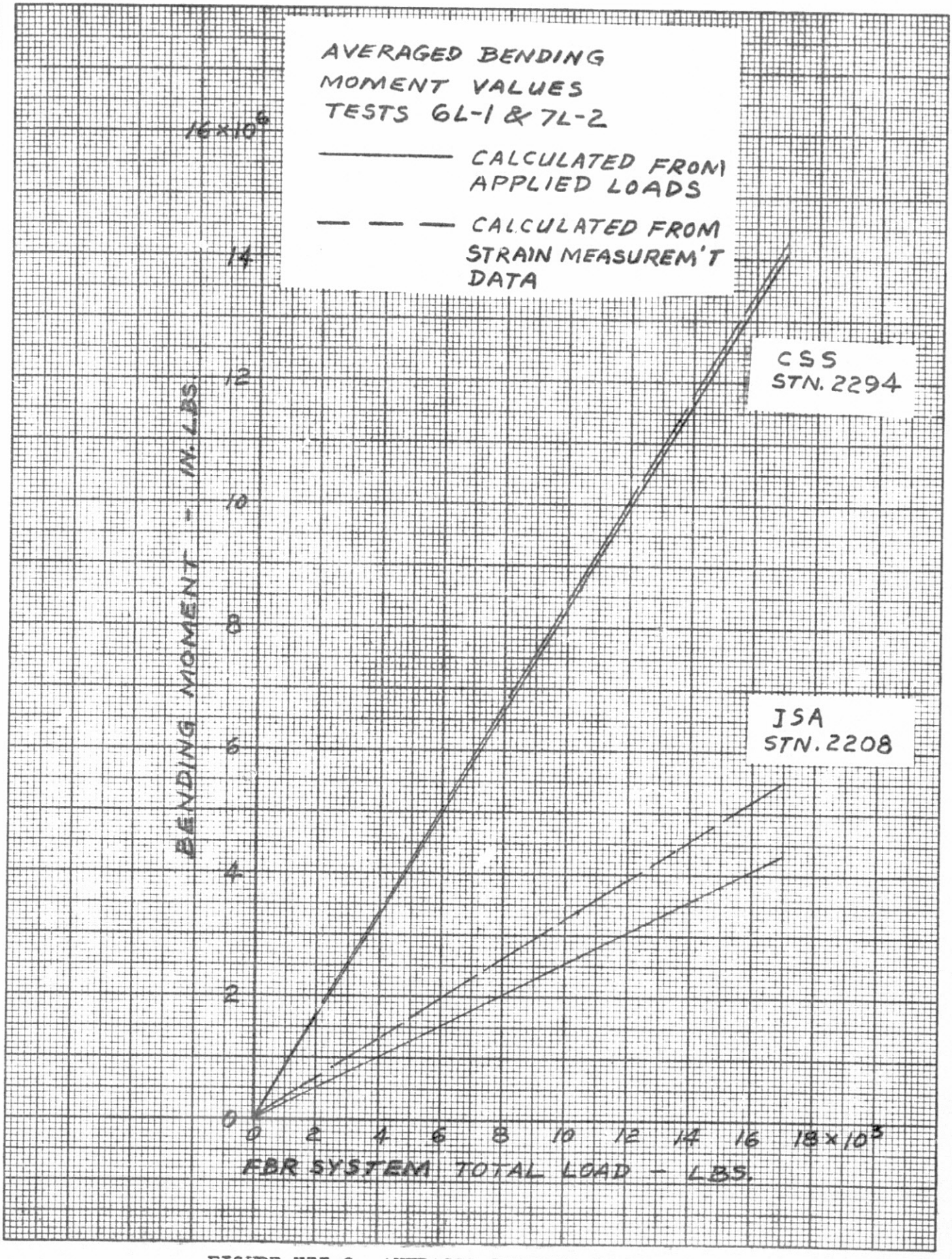

FIGURE VII-6. AVERAGED BENDING MOMENTS.

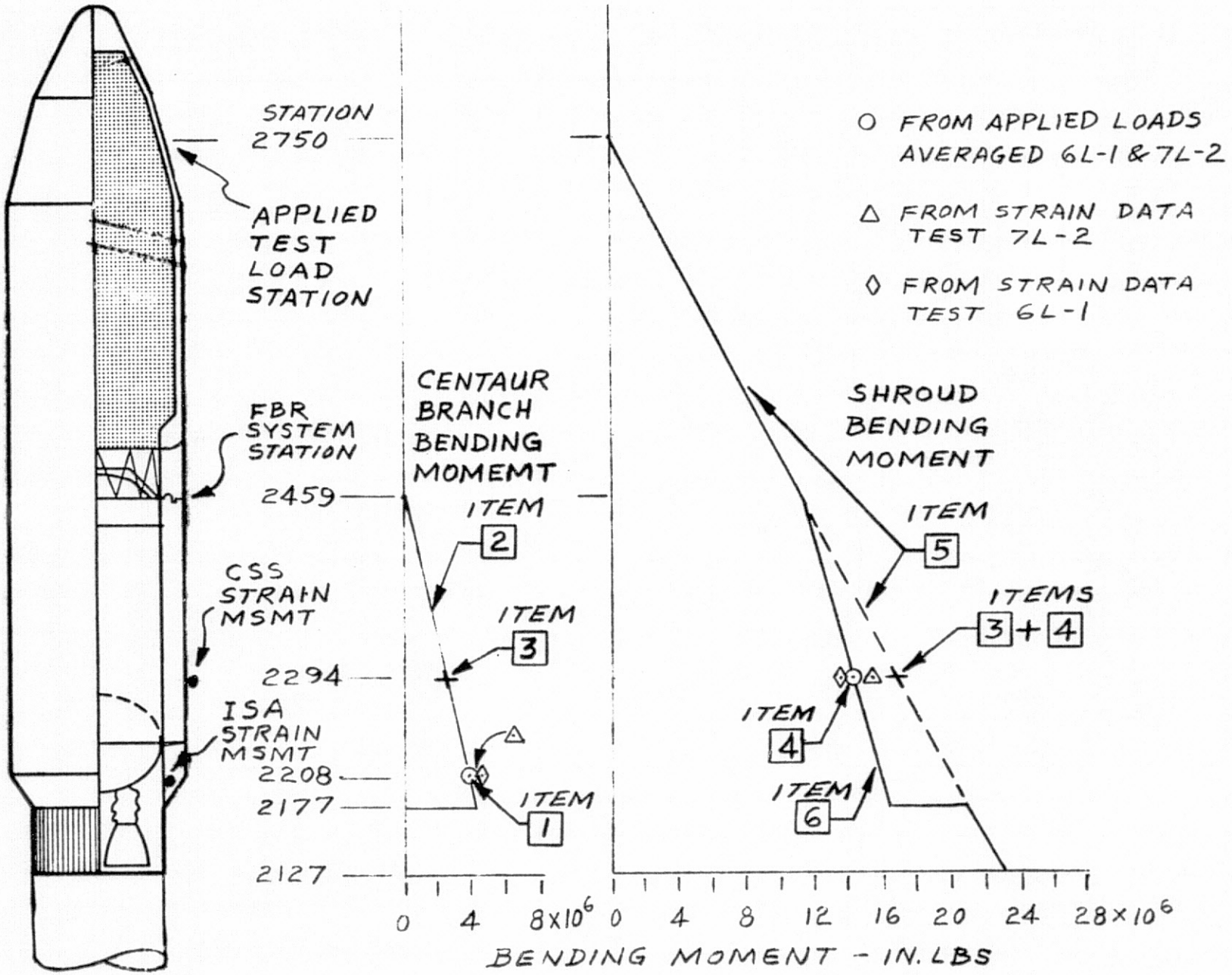

FIGURE VII-7. LIMIT LOAD BENDING MOMENT DIAGRAM (FBR SYSTEM ACTIVE).

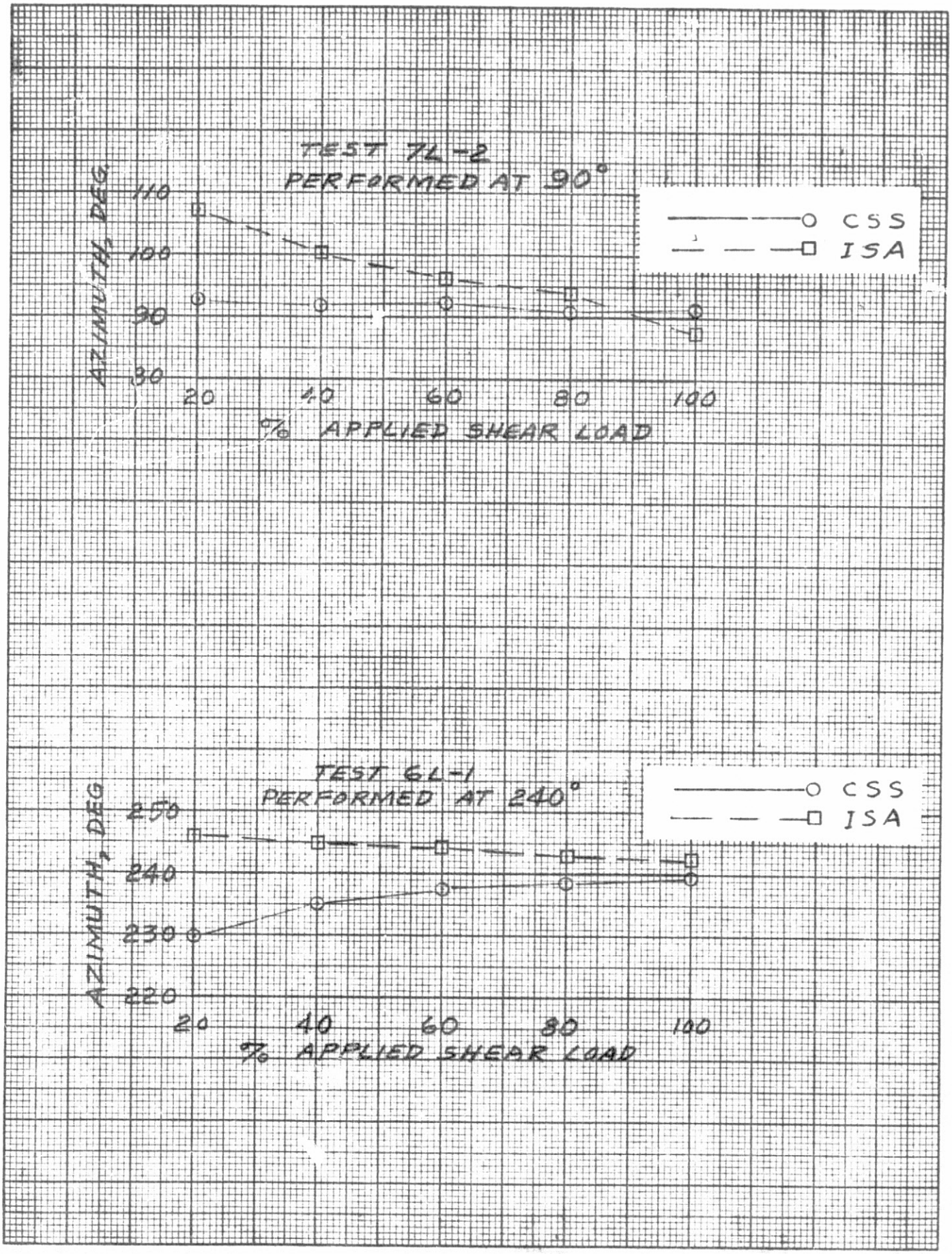

FIGURE VII-8. SHEAR LOAD AZIMUTHS FROM STRAIN DATA CALCULATIONS.

VIII BOILOFF TEST

By R. F. Lacovic

SUMMARY

A cryogenic boiloff test utilizing LN_2 in the Centaur LH_2 tank was performed in order to obtain a comparison with data obtained in similar tests that were conducted four months earlier. This would reveal any changes that might have occurred in the insulation due to aging. The difference in measured heat transfer rates indicated no appreciable change in the insulation properties of the CSS.

TEST RESULTS

The total LH_2 tank heating rate was determined over an 80-minute interval by evaluating LN_2 boiloff. The transfer rate was 83,900 BTU/Hr. When converted to LH_2 conditions the rate becomes 107,200 BTU/Hr. The previous gross heating rate was 100,300 BTU/Hr. Another indication of possible changes in the thermal system is provided by comparing the shroud annulus pressure and the weighted gas temperatures. The pressures were the same at 0.29 psig and the weighted gas temperatures were within 10^{o} of each other.

SUMMARY OF TEST RESULTS

The difference seen in the gross heat transfer rate was less than 7%; this is within the normal range of data scatter seen between similar tests. The 10^{o} difference in weighted gas temperatures indicates a close correlation between the two boiloff tests. These comparisons show that very little, if any, degradation occurred in the CSS insulation systems during the four months between tests.

PRECEDING PAGE BLANK NOT FILMED

REFERENCES

1. Stofan, A. J.: Titan/Centaur --- NASA's Newest Vehicle. NASA TMX-68249, July 1973.

2. Staff of Lewis Research Center: Centaur Standard Shroud Cryogenic Unlatch Tests. NASA TMX-71455, October 1973.

3. Nagle, T. G.: Centaur Standard Shroud Cryogenic Unlatch Test Final Report. LMSC No. D337090, April 20, 1973.

4. Jenness, J. H.: CSS/Centaur Structural Test Evaluation Report. CASD/LVP 74-069, November 1974.

5. Bauman, R. E. and Simson, S.C.: Static Structural Test Evaluation CSS - Limit Load Tests. LMSC No. D338384, September 20, 1973.

6. Zishka, W.: Test Report on the Limit Load Structural Test of the Titan IIIE Stage II Forward Oxidizer Skirt During the CSS Limit Load Structural Tests CSS Qualification Program. MMC No. MCR 73-266, September 1973.

7. Staff of Lewis Research Center: Test Requirements Document Centaur Standard Shroud Limit Load Structural Tests CSS Qualification Test Program. LeRC/TCPO-22, January 1973.

8. Anon: Test Report for Forward Bearing Reactor D-1T Centaur. GDC 55A6384, February 1973.

APPENDIX A

FACILITIES AND SUPPORTING SYSTEMS AND OPERATIONS

B-3 TEST FACILITY AND MECHANICAL SYSTEMS

By L. C. Gentile

B-3 Facility

The B-3 Facility, located at NASA Lewis Research Center's Plum Brook Station, was used to conduct the Centaur Standard Shroud (CSS) Limit Load Structural Tests. The B-3 Facility is a tower structure 50 feet square and 200 feet high as shown in figure A-1. It contains a test area at level 3 which is 74 feet above the ground floor. The test area is approximately 24 feet by 36 feet with a working height of 100 feet. An overall view of the test configuration is shown in figure A-2. Movable work platforms were installed in the test area at 5 levels for access to the test specimen. A 65 ton bridge crane serviced the test area and the ground level rail siding delivery apron adjacent to the tower. The major components of the test specimen were subassembled and prepared for the test in a building remote from B-3 tower, but serviced by a Plum Brook Station rail line.

Test Fixtures and Specimen Installation

The stackup of the fixtures and the test specimen were erected on a load application base fixture that was fastened to the tower structure at level 3. This base fixture was a heavy steel assembly which supported the test hardware and reacted the test axial loads and part of the shear loads. A lower distribution fixture was mounted on the base. The lower distribution fixture was a steel cylinder 10 feet in diameter with a 3/4 inch thick wall and was 10-1/2 feet long. It was reinforced with internal rings and was restrained at the forward end by 4 tubular steel struts attached to the tower structure. The struts acted as lateral ties which, together with the base fixture, reacted the test shear loads.

The test specimen was erected on the forward flange of the lower distribution fixture starting with the Titan skirt. As shown in figure A-2 the ISA, Centaur tank, stub adapter, equipment module, and truss adapter were mounted successively thereon using flight vehicle launch site planned procedures where applicable. The CSS boattail and tank section installation operations also were the same as the launch site proposed procedures as much as practical to verify the procedural operations for use at the vehicle launch site.

ORIGINAL PAGE IS
OF POOR QUALITY

At that stage of the assembly, the test hardware erection operation deviated from the planned procedure for the vehicle launch site. This was necessitated because the launch site operation includes a payload spacecraft and the test setup did not. In place of the payload a Centaur loading fixture was mounted on the truss adapter. The Centaur loading fixture was a 14,000 pound steel cylinder 10 feet in diameter and 10 feet 9 inches in length. The cylindrical portion of the payload section of the CSS was erected and topped off with the biconic section less the dome piece. Smaller components such as the forward and aft seals, FBR struts, LH_2 vent fin and disconnects, and other flight type subassemblies were installed as necessary for each test.

A CSS load distribution fixture was mounted on a non-flight test flange bolted on the biconic section of the CSS at the interface of the 25° and 15° cones at Station 2806.95. The CSS load distribution fixture was a 4,000 pound steel cylinder approximately 8-1/2 feet in diameter and 5 feet long. A forward load application fixture was mounted on the CSS load distribution fixture. The forward load application fixture was a heavy steel octagonal spider beam assembly to transmit the axial loads into the CSS.

Load Application System

The CSS structural load application systems allowed each test load to be applied independently. There were five systems used to simulate the flight loads: CSS axial, CSS shear, Centaur axial, Centaur shear, and LH_2 vent fin load application systems.

The CSS axial load system was used to apply and maintain a compressive load on the CSS. The basic components were the CSS load distribution fixture, forward load application fixture, 4 whiffletree beams, and 4 connecting cables to the 4 axial hydraulic load actuators. The whiffletree beams distributed the load more uniformly into the CSS load distribution fixture. The axial loading cables connected the whiffletree beams to 4 hydraulic loading actuators which were attached to the load application base. The 4 axial loading actuators could simultaneously apply loads at either of two manually selected load application rates. The system provided loading and unloading only while the appropriate control was activated manually. An event marker for data reduction purposes was issued to the data system each time the load or unload controls were activated. The system included feedback control. A counter-force system was used to alleviate as required the tare weight of the CSS axial loading system. The counter-force system used four actuators which provided a controlled upward force to the total axial load fixture assembly.

The CSS shear load system consisted of a load application strap, a shear whiffletree beam, and a linkage to a hydraulic actuator attached to the tower. The load application strap was a half-cone shaped collar of 0.075 inch thick stainless steel and was designed to fit over the 15° section of the nose cone. End fittings on the collar were attached to a shear

whiffletree beam which was connected by a link to a hydraulic loading actuator. The centerline of the load application strap and the link was located at Station 2750. The CSS shear load system could be rotated to allow application of shear loads from the several test azimuths. The assembly was counterbalanced so that the loading system exerted no more than 50 pounds shear force tare on the CSS prior to load application. The system was similar to the axial loading system except that it was position controlled instead of rate controlled. Data taking markers and loading and unloading were accomplished in the same manner as the axial system.

Centaur axial loads were applied by the Centaur loading fixture which was installed on the truss adapter and occupied the space normally allowed for the payload. The tare weight of the Centaur loading fixture was the only axial load applied to the Centaur vehicle. For zero axial load, the Centaur loading fixture was counterbalanced by the Centaur stretch assembly which is described later. Centaur shear loads were applied through the Centaur loading fixture. A cable assembly attached to the fixture at Station 2626 passed through a 5 inch diameter non-flight type hole in the CSS at 270° azimuth. This cable assembly was attached to a hydraulic load actuator assembly that was fastened to the tower structure. The Centaur shear loading actuator loaded the Centaur laterally at either of two load application rates. Except for load magnitudes and rates this system operated in the same manner as the CSS axial loading system.

The LH_2 vent fin structural loading system consisted of a modified flight vent fin fitted with a special loading fixture that was attached to 3 load actuators pinned to the facility structure. The system allowed 3 components of force (axial, radial, and tangential) to be applied to the vent fin. The vent fin loading actuators simultaneously loaded the vent fin in prescribed directions at either of two loading rates. Except for load magnitudes and rates, this system operated in the same manner as the axial loading system.

Liquid Nitrogen and Inert Gas Systems

A cryogenic system supplied liquid nitrogen (LN_2) to the test vehicle. The LN_2 was pumped via insulated lines from ground level dewars to the Centaur fuel and oxidizer sump ports for the two series of tests performed with a cryogenic environment.

Inert gas systems supplied gaseous nitrogen and helium to the test specimen. Both gases were piped from storage cylinders adjacent to the B-3 tower. The gases were used for Centaur tank pressurization, test specimen compartment purging, and facility systems operation.

Centaur Tank Protection Systems

A system of servo-operated valves and pressure relief valves was connected to each of the Centaur tanks. These systems maintained the tank pressures at the desired levels throughout the tests.

There was one oxidizer tank (LO_2) vent system that was used throughout the tests. The LO_2 flight vent valve was not installed. A facility vent system was used instead. The LO_2 vent line and the fill line also had sufficient flexibility to permit the Centaur aft bulkhead to move 1.25 inches laterally during testing. There were two vent systems on the fuel tank (LH_2). The LH_2 flight vent system was connected to a 6-inch vent line in the facility. This vent was used during the initial tank fill operation and during the boiloff test. An 8-inch facility vent system was connected to a flange in the forward door of the LH_2 tank and was sized to accommodate a large boiloff should the CSS insulation system be damaged or fail in the tank section of the CSS. The flight vent system could not accommodate the flow volume for that condition. The facility vent line was flexible enough to allow the Centaur forward bulkhead to move 4.0 inches laterally and 1.5 inches axially. The top of the CSS could move 12.0 inches laterally without interfering with the vent line.

A facility system based on Centaur tank differential pressure was used to protect the intermediate bulkhead between the oxidizer and fuel tanks. By use of pressure transducers and an automatic control system, the necessary tank pressure differential was maintained.

Another protection system for the Centaur tank, which is not self-supporting when depressurized, was a Centaur stretch system. This system consisted of a cable sling assembly connected to an actuator that was attached to the tower structure. The sling was connected to the forward end of the Centaur loading fixture. Activation of the actuator exerted sufficient force to counterbalance the fixture and all hardware mounted on the forward end of the Centaur tank and in addition support the weight of the tank. This system was required if the tank should lose pressure or when it was purposely depressurized. Also, the system could be controlled to counterbalance the tare weight of the Centaur loading fixture only, when that load was not required in a test.

Camera Systems

Four motion picture cameras were provided to record the FBR system and forward seal separation sequences. These cameras and their lighting system were activated by an automatic sequence initiated by the test conductor. Two single frame cameras were used to record the CSS and forward seal deflections at discrete steps. These cameras and their lighting system were activated manually for each frame. Four TV cameras were used to provide general views of the test hardware during the tests.

TEST INSTRUMENTATION AND DATA SYSTEMS

By R. H. Fabik, J. L. Harrold, and F. L. Manning

Instrumentation Transducers

Several types of instrumentation transducers were used to provide test data. A brief description of each type is given below.

Strain Gages - Uniaxial, biaxial (Poisson), and three-element rosette types of strain gages were used in this test program. The uniaxial gages were used with temperature compensating tab mounted dummy gages, as were each of the rosette elements. Each biaxial gage was arranged in its electrical bridge circuit to be temperature compensated. Approximately 600 strain gages were used in the total test series. A maximum of 250 were used for any single test.

Deflectometers - Most of the 250 deflection measurement locations used in the single tests were instrumented from an inventory of 150 rotary potentiometric transducers of various ranges. Connector and cabling systems allowed for rapid change of location from one test to the next. A few short stroke (± 0.1 inch) measurements employed special strain gage caliper type transducers. The B-3 tower deflections were measured with a NASA developed system which tracked a laser light source with a two axis photo detector mounted on X and Y servos to null balance tracking.

Pressure Transducers - Most of the approximately 50 pressure measurements were made by standard 8 wire strain gage transducers. Both absolute and differential types were used. Special low temperature calibrations were employed where appropriate. Two high sensitivity capacitance transducers were also used.

Temperature Transducers - Temperatures were measured with thermocouple and platinum resistance transducers. Platinum types were used where maximum accuracy was required. The chromal-constantan thermocouples provided low volume, low mass, and low heat transfer. Where thermocouple measurements were made on aluminum, a special technique was used whereby the chromal-constantan conductors were attached separately. This method incorporated the aluminum in the circuit and, if an alloy wire came loose, false temperature data were not recorded. It also provided maximum thermal transfer. Approximately 60 temperature measurements were made for these tests.

Accelerometers - The shock and vibration measurements were made with piezoelectric or piezoresistive accelerometers depending on the required sensitivity and frequency range. A total of 17 accelerometers were used.

Load Cells - Load measurements were made with standard strain gage type load cells. A total of 13 measurement locations were required. However, a maximum of 6 locations were used for each test configuration.

ORIGINAL PAGE IS OF POOR QUALITY

Liquid Level Probes - The three liquid level probes were capacitance type. The main LO_2 and LH_2 tank probes were standard coaxial types. The LH_2 tank ullage probe was a NASA designed double coaxial type. This design provided the additional accuracy and sensitivity required for heat transfer studies.

Miscellaneous - Measurements were made also of wind speed, wind direction, pyrotechnic system current and voltage, and FBR breakwire status.

Signal Conditioning and Routing

The outputs from the various transducers were conditioned at the B-3 Facility and transmitted in digital form to the data building for further processing. All signal conditioner outputs were routed to the patchboard. The 4,896 conductor board used fully shielded patchcords. This arrangement allowed random interconnection from signal conditioners to the digital data recorder, the FM recorder, the light beam oscillographs, the strip chart recorders and the panel meters. It provided also for input and output connection of amplifiers, where required. A basic overall flow schematic is shown in figure A-3.

Data Recording

The data for these tests were recorded in digital form on magnetic tape using a 400 channel multiplexer at the B-3 tower and the central recording system at the data building. Most of the data was recorded at a rate of 2,500 data points per second. A rate of 20,000 data points per second was recorded during pyrotechnic firings. This gave sample rates per channel of about 6 and 50 per second, respectively. High response data such as vibration and pyrotechnic system parameters were recorded on FM and light beam oscillographs. Ink type strip chart recorders were used to display certain critical parameters. Time was recorded on all recorders to provide precise time correlation.

Data Computer and Display System

The data computer and display system allowed immediate visual analysis of test data in engineering units. Data were displayed in real time. Post-test data was obtained from magnetic tape playback. Data were presented in tabular and graphic forms on Cathode Ray Tube (CRT) displays and digital plotters. Tabular printouts of selected parameters were available for playback. The various features of the system are described below.

Figure A-4 is a block diagram of the system components and data flow of the data computer and display system. Raw data for the tests were derived from the digital recording system in the data building for immediate display and recording on magnetic tape. The raw data were transmitted to the B-3 site control building where the data were stored

directly into the memory of the Xerox 9300 digital computer. The prime task of the digital computer was to convert raw data and special equations to engineering units for the two Xerox CF16A controllers. Raw data from the digital recording system could be recorded on magnetic tape in a simplified format. Zero adjustment of predetermined raw data was selectable. Conversion was accomplished for only those parameters requested by the display controller, Required for special equations, or necessary for selected printout. After conversion, the engineering unit data were transformed to CF16A formats for direct reading by the CF16A controllers.

Two Xerox CF16A minicomputers were direct coupled to the main computer and were used for specialized input/output control. One minicomputer was designated as the display controller and the second as the plotter controller. The display controller serviced up to three keyboard/CRT units and provided printouts on a remote digital plotter. The controller accepted remote control from switches, control keyboards, and one keyboard/CRT unit. Engineering unit data were read directly from the digital computer memory and prepared for each of the CRT individual requirements. Remote pushbutton print commands caused the program to print the associated CRT image on the remote plotter. The plotter controller accumulated engineering unit data for up to twenty XY plots and generated the plots upon request. This controller also accepted remote plot control and selection from a selector station. The program stored data points on an individual plot basis if a significant change occurred. A display console was available with multiple viewing positions. The console contained five TV units, a keyboard/CRT unit, and control panels with remote control and selection for the display and plotter controllers. The remote digital plotter was located adjacent to the display console. The data displayed on all three CRT units were displayed on four of the TV units in the console and could be paralleled to other TV units in the B-3 site Control Building.

Data Reduction Systems

A flow schematic of the digital reduction and display systems associated with the Structural Tests in the B-3 Facility is shown in figure A-5. The primary experimental data were recorded as digitized millivolt signals on magnetic tapes in the data building. Data sampling rates of 2,500 data points per second and 20,000 data points per second were used to record data. The 20,000 points per second sampling rate was used only during the FBR system firing and forward seal release system firing portions of the autosequence. All other data were recorded using the 2,500 points per second sampling rate.

The magnetic tapes containing the primary data from each test were copied and edited immediately after each test and then delivered to the Lewis

Research Center (LeRC) for data processing. The LeRC IBM 360 computer processed the tapes using a pre-programmed data retrieval program. This program was designed to retrieve preselected parameters and specific test events and produce millivolt signal levels as output. The program outputs were zero-corrected (pretest zero offsets were removed from the data), averaged and smoothed, and stored in the IBM 360 computer. After all data had been retrieved and stored, the data reduction and calibration program converted the stored signals into appropriate engineering units. These values were, in turn, stored in specific arrays in the computer. The processed data from each test were made available to the DD-250 microfilm camera system.

The data reduction and calibration program proceeded to the plotting program. The plotting program was designed so that a combination of parameters and constants could be plotted against any other combination of parameters and constants. The plotting program also had the capability of plotting up to 4 similar parameters or combination of parameters on the abscissa. The ranges on the ordinate and abscissa could either be fixed or allowed to maximize the range of available data. The plotting data also were made available to the DD-250 microfilm camera system. From the developed microfilm, printed digital data listings and data plots were reproduced. The entire process of data reduction and reproduction took less than 48 hours after completion of each test.

TEST CONTROL, ABORT, AND ALARM SYSTEMS

By E. J. Cieslewicz and W. J. Rice

Systems Description

A schematic of the test control, abort, and alarm system is shown in figure A-6. The principle components of the system are the Xerox 910 digital computer, its output relay system, the abort monitor system, the Xerox CF16 minicomputer alarm system, and the loading and positioning system which also includes the EAI model TR-48 analog computer ramp generating and error detection system. The details of the loading and positioning system are shown in figure A-7. The ramp generator and error detection portion of the above system is shown in figure A-8. The digital computer allowed the test load application and positioning system to be operated manually as long as the abort limits were not violated. The minicomputer processed the multiplexed data and exhibited on television screens those channels which exceeded the alarm limits. Once an abort limit was exceeded, as determined by the abort monitor, the manual loading capability was deactivated by the digital computer and the abort sequence was performed. Essentially it activated all hydraulic load cylinder fail-safes systems. The fail-safe feature prevented the hydraulic cylinders from developing any force by closing the hydraulic pressure supply and venting the load cylinders to the hydraulic reservoir.

Also, relief valves were on each cylinder and in the circuit at all times for use in case the other devices failed. Differential pressure relief valves were included in the load cylinder hydraulic circuits for redundant protection.

A functional block diagram of the ramp generator and error detector is shown in figure II-5. The manual ramp rate and direction command switches provided the following commands to the ramp generator:

1. Slow increase
2. Medium increase (CSS shear only)
3. Fast increase
4. Slow decrease
5. Medium decrease (CSS shear only)
6. Fast decrease
7. Hold (no switches actuated)

The ramp generator and error detector circuitry (figure A-8) was designed such that no combination of switches could produce a ramp rate greater than the fast rate. The ramp generator produced a signal which was linear with respect to time and was used as the load rate or position command to the loading system controller. This command signal was prevented from exceeding a predetermined maximum level by the maximum command limiter. The maximum command limiter also provided a locking signal which prevented the command signal from drifting with time and provided lamp indication at the command switches. The zero command limiter prevented the command signal from going negative.

A half-summing circuitry and half-summed error detector initiated an abort when the load cell signals (A and B) violated the following condition:

$$\frac{(A + B)}{2} - \text{Command} < 0.10 \text{ (Maximum Command Limit)}$$

The primary purpose for the half-summed error aborts was to detect control loop failure before a maximum load abort was reached. In addition, these aborts were designed to cause a shutdown if either or both of the load cells failed, so as to produce either zero or full scale outputs. A difference between the two load cell outputs greater than 20% of the maximum load limit would also cause an abort. This type of failure would occur if one of the load cells failed, so as to produce an intermediate value due to drift or signal conditioning failure.

The system was used for both the load rate controlled loops (axial, payload shear, and vent fin) and the position controlled loop (CSS shear). However, the system used for the CSS shear also incorporated a maximum load limit detector which prevented a command to position the CSS shear cylinder beyond the point where a predetermined maximum load was achieved. A separate lamp indication was provided at the command switches when this condition was established.

The TR-48 analog computer was also used to generate a marker pulse every 2 percent of applied load. This pulse was recorded by the digital recording system and used in the data plotting program to limit the reduced data to 100 points (50 on the increasing load ramp and 50 on the decreasing load ramp).

The operate command signal from the Xerox 910 computer was incorporated to prevent the ramping of the command signals until the proper time. In addition at the start of an abort sequence the operate command was removed forcing all commands immediately to zero. This feature provided an alternate means of removing the loads in the event of a cylinder fail-safe manifold failure.

System Performance

Figure A-9 presents the operation of the control and abort system with time. This figure is typical of most of the structural test sequences used. It lists all the relays that were operated by the computer throughout the tests. Each relay has its status represented in bar chart format. One state of the relay is shown as a single line and its opposite state is shown as a bar. The relay identification shown conforms to the bar state. Status changes from autosequence start take place in the figure from left to right as time varies. The time scale shown is in seconds. It should be noted that certain sequence holds are shown taking place during the test. The computer program essentially commands relays in an open-loop control fashion until a hold period is reached. Further sequencing of the relays does not take place during a hold until the computer has received an indication through the abort monitor of an occurrence of a desired event. Consequently, the holds shown are variable in time duration and dependent on the test configuration. The hold events and their identifications are as labeled in the figure. An illustration of the typical autosequence abort requirements and how they were varied with time is also shown in figure A-9. This figure lists all the data that were specifically examined by the abort monitor for the computer. Each of the channels has its required armed-disarmed status, as shown in the bar chart format. The bars indicate the period of time an abort channel was to be armed, and the digital notation of "one" or "zero" within them designates the desired response throughout that interval. The time-scale identification and program-hold identification are the same as those used to explain the control requirements sequencing. Table A-1 identifies each abort channel, how it was sensed, and its digital notation.

ORIGINAL PAGE IS
OF POOR QUALITY

TABLE A-I

Abort Identification, Input, Notation, and Condition

Abort Name & Function	Signal Input for Detection at Abort Monitor	Digital Notation of "1" Denotes	Notation for Abort
Data Observer Manual	Normally Open Contacts	Button Not Pushed	0
CSS Shear Load Limit	Analog Voltage	Load Above Limit	1
LH_2 Tank Low Pressure	Analog Voltage	Pressure Above Minimum Limit	0
Tank Protection Circuit	Normally Closed Contacts	Tank Protection Circuit In Operation	1
FBR Strut Load	Analog Voltage	Load Above Limit	1
FBR & FSR Arming Voltage	Analog Voltage	Voltage Above Limit	0
Payload Shear Load	Analog Voltage	Load Above Limit	1
CSS Shear Load	Analog Voltage	Load Above Limit	1
CSS Shear Position	Analog Voltage	Position Greater Than Limit	1
Payload Shear Load	Analog Voltage	Load Above Limit	1
Abort Monitor Power Supply	Analog Voltage	Voltage Above Limit	0
Test Conductor Sequenced	Normally Open Contacts	Button Not Pushed	0
Data Record Failure Permissive	Normally Closed Contacts	Data Not Recording	1
Analog Computer Permissive	Normally Open Contacts	Power Applied to Computer	0
Programmed Value Permissive	Normally Closed Contacts	Function Out of Program Mode	1

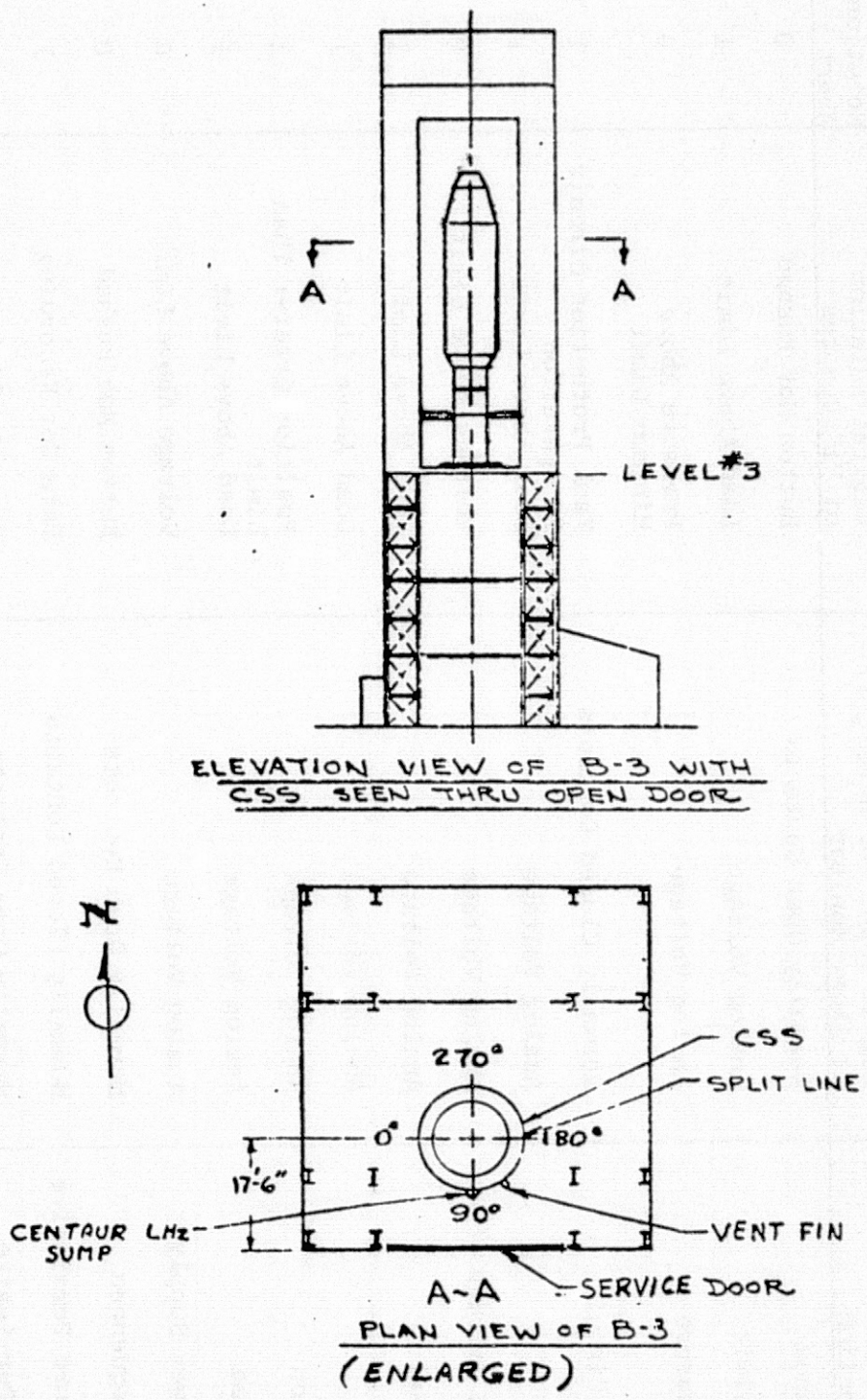

FIGURE A-1. B-3 FACILITY TOWER STRUCTURE.

Ps axil load, CSS
Vs shear load, CSS
Vpl shear load, Centaur
Pva axial load, vent fin
Pvr radial load, vent fin
Pvt tangential load, v.fin

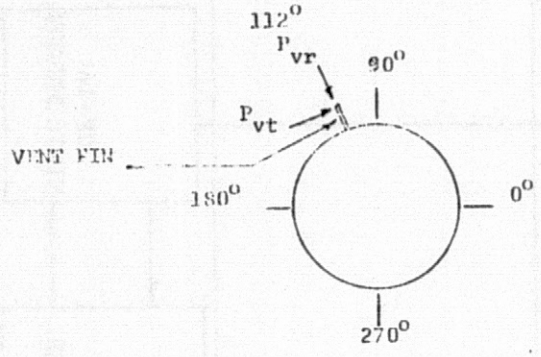

SECTION A-A

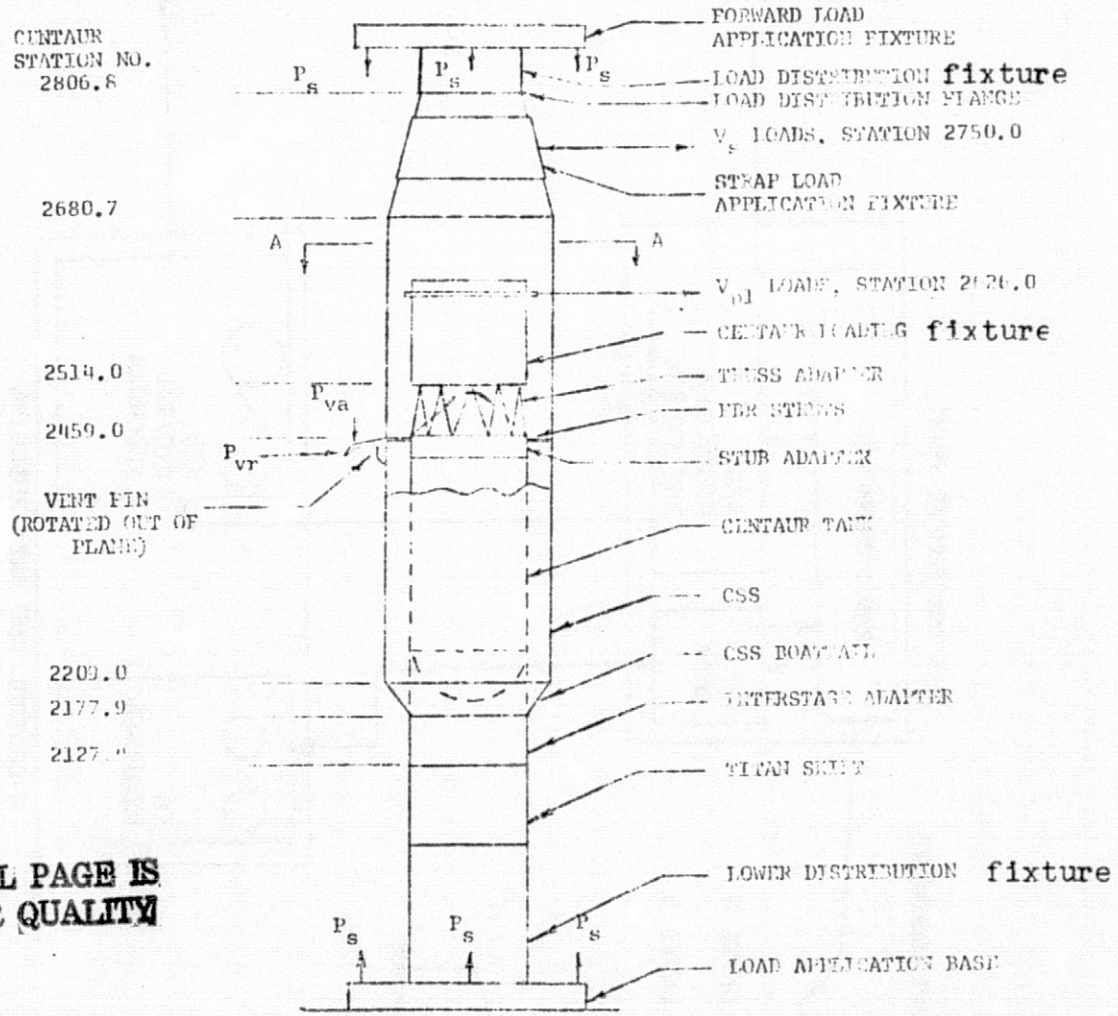

ORIGINAL PAGE IS
OF POOR QUALITY

FIGURE A-2. TEST SPECIMEN & FIXTURE ASSEMBLY IN B-3 FACILITY.

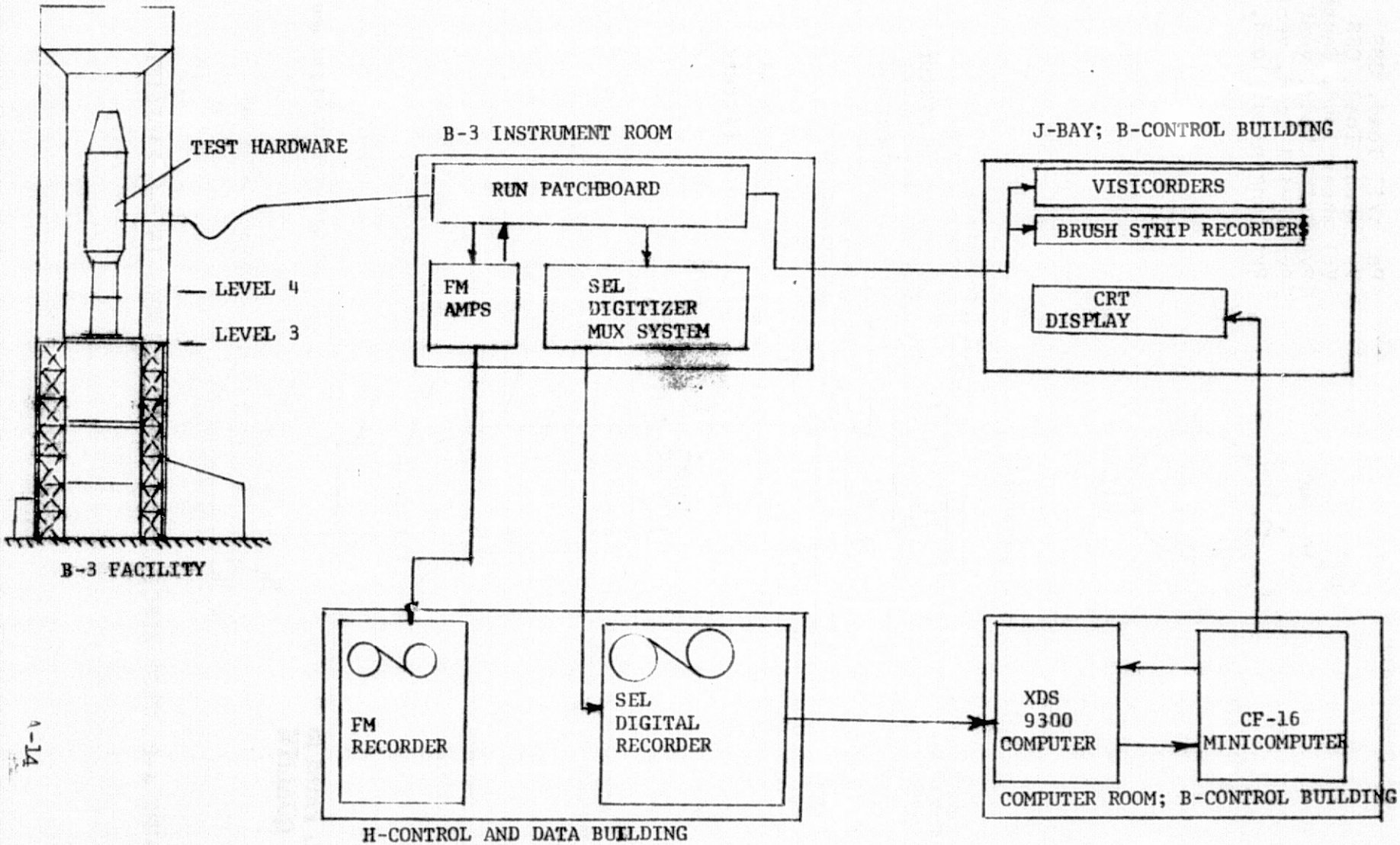

FIGURE A-3 INSTRUMENTATION AND DATA SYSTEMS FLOW SCHEMATIC FOR CSS STRUCTURAL TESTS

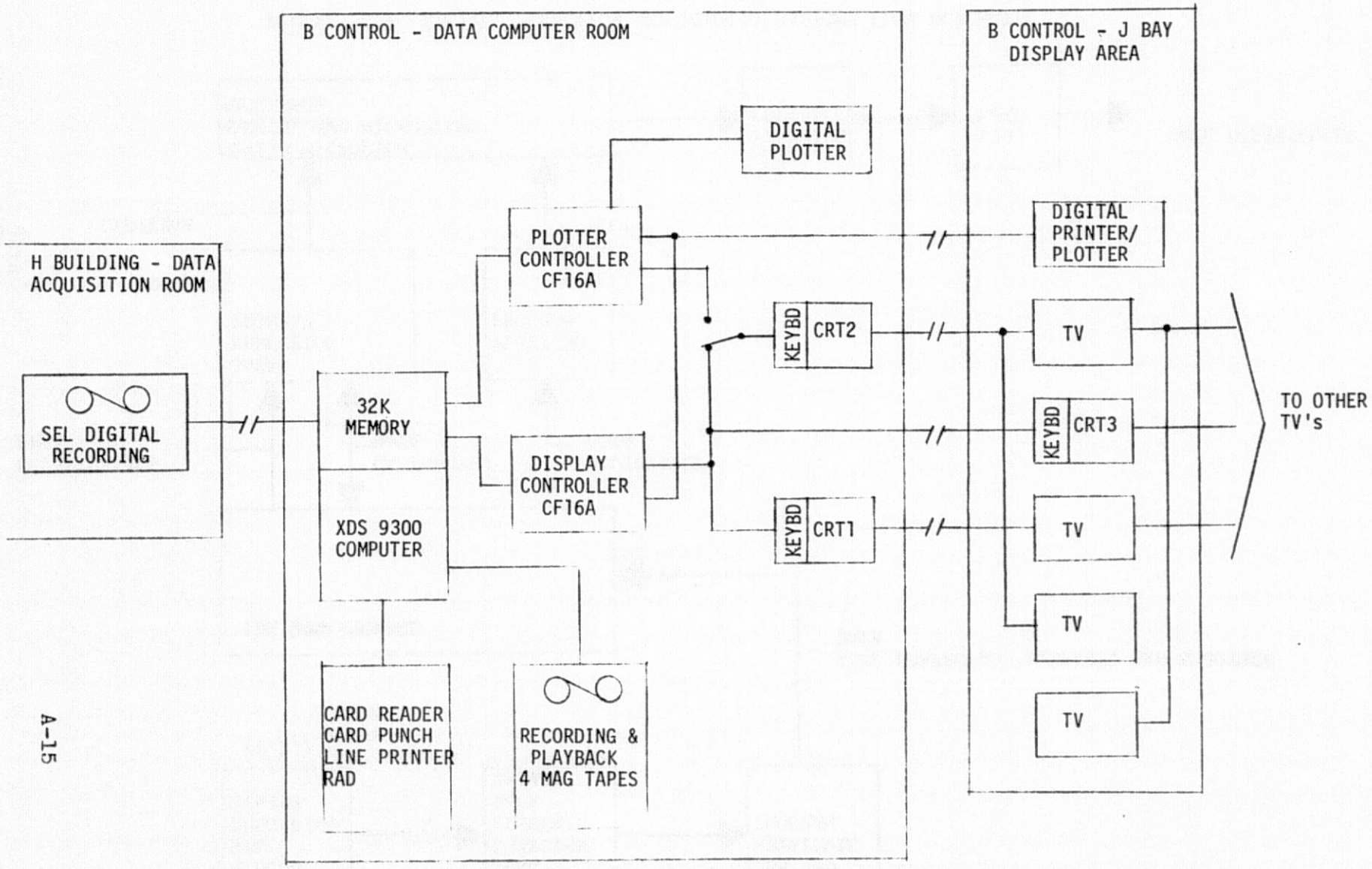

FIGURE A-4. DATA COMPUTER AND DISPLAY SYSTEM FLOW SCHEMATIC.

ORIGINAL PAGE IS
OF POOR QUALITY

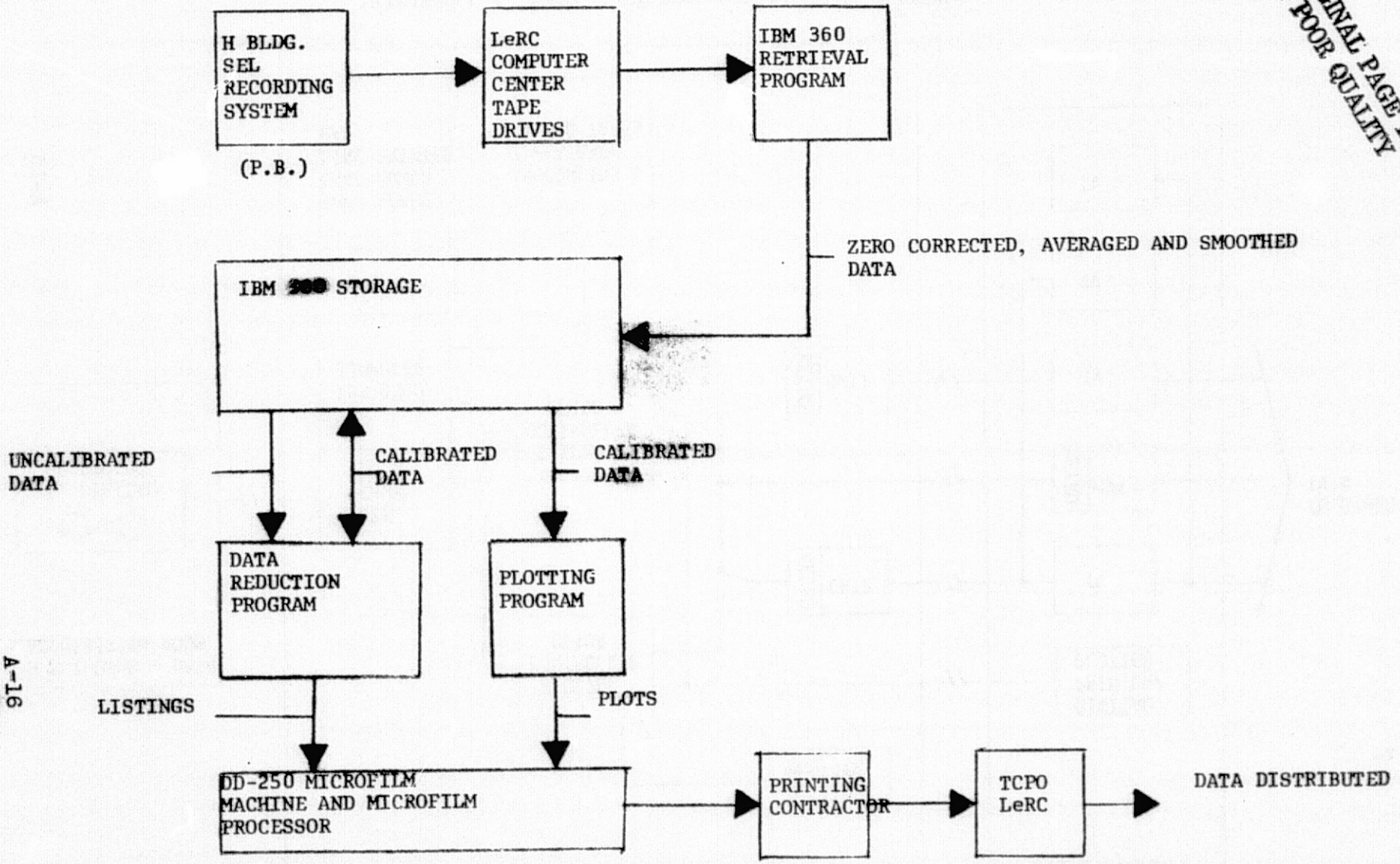

FIGURE A-5 DIGITAL REDUCTION AND DISPLAY SYSTEMS FLOW SCHEMATIC

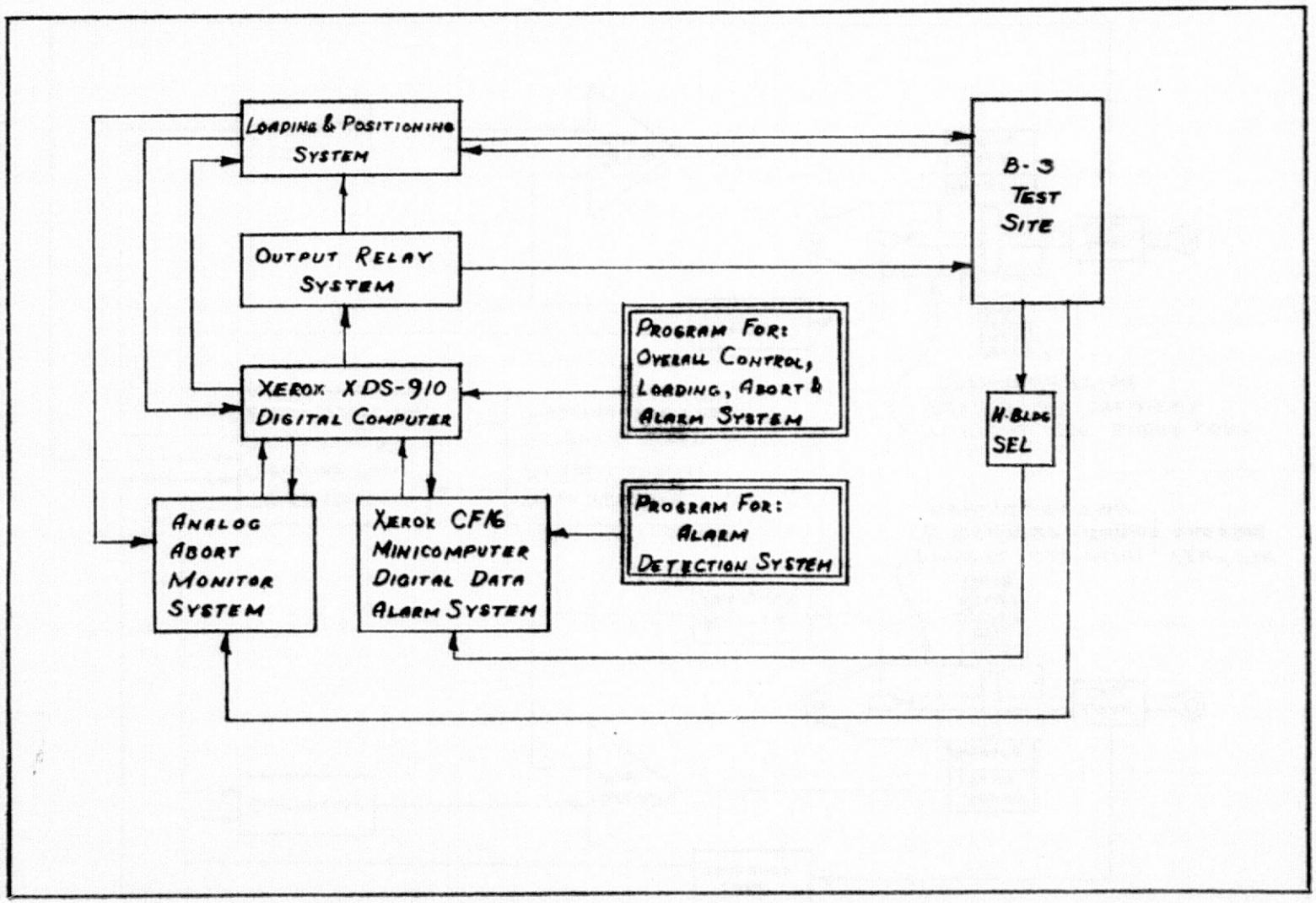

FIGURE A-6. TEST CONTROL, ABORT, AND ALARM SYSTEM SCHEMATIC.

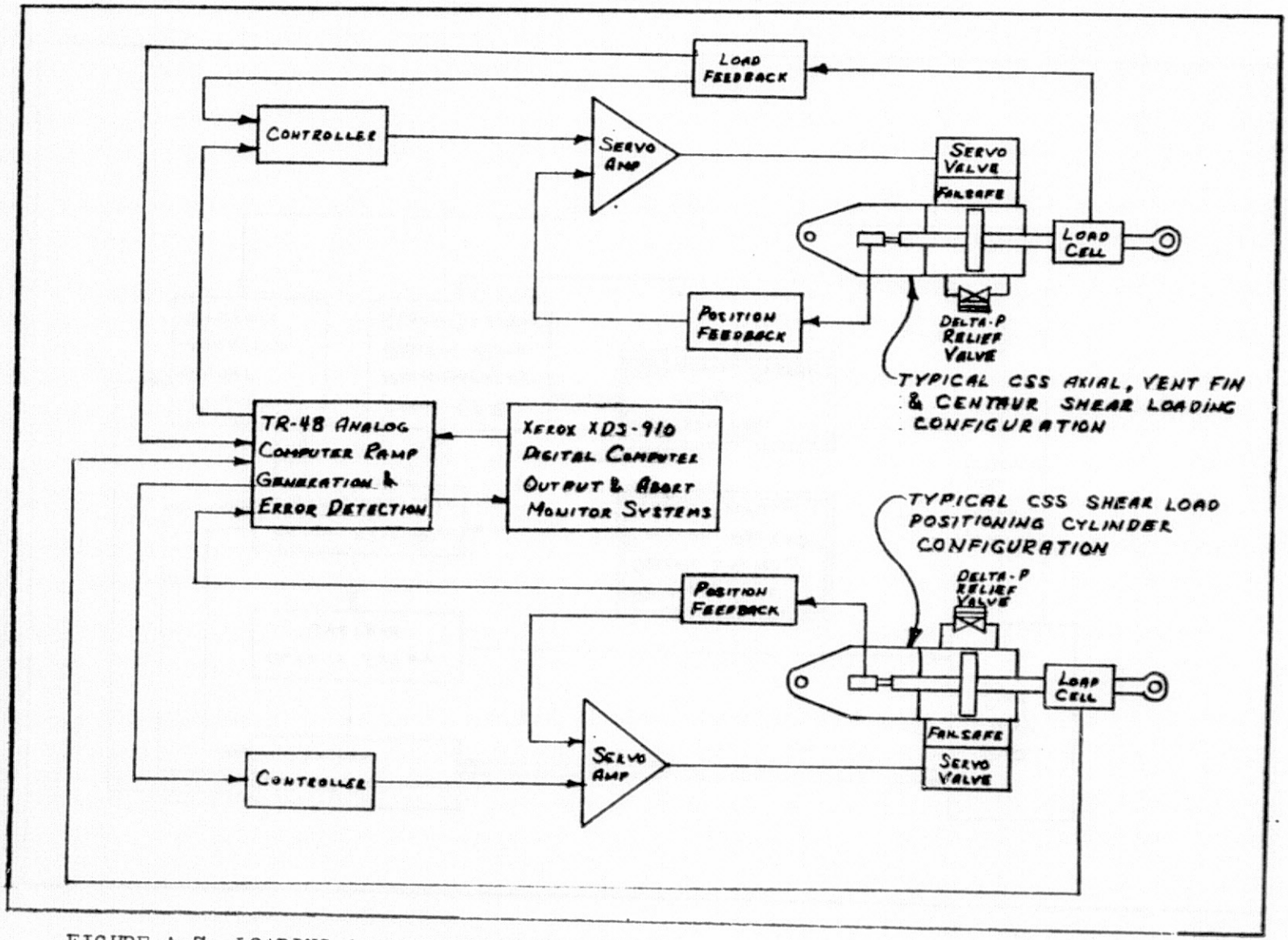

FIGURE A-7. LOADING & POSITIONING SYSTEM FOR AXIAL & SHEAR LOADS.

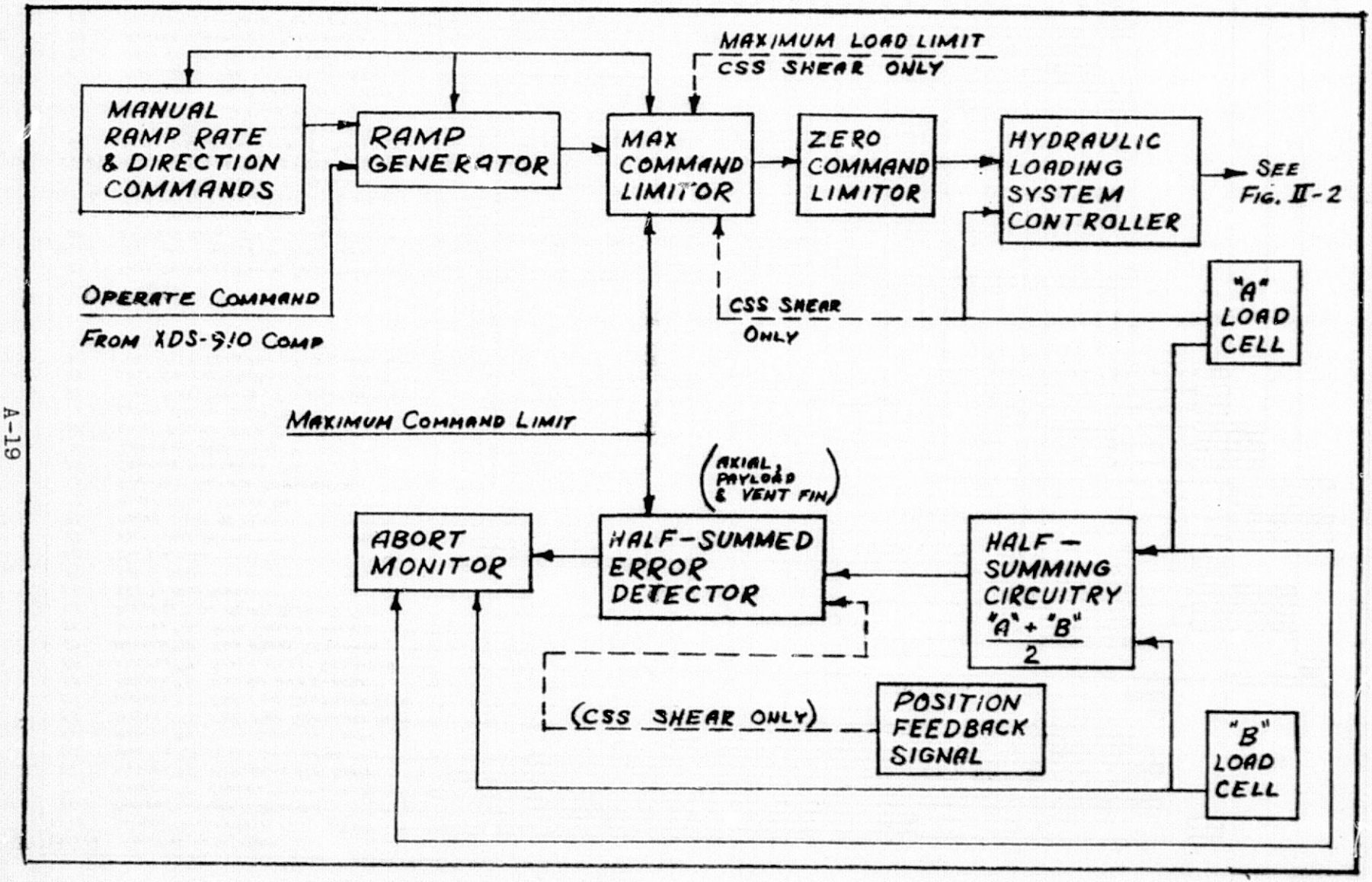

FIGURE A-8. RAMP GENERATING & ERROR DETECTION SYSTEM SCHEMATIC.

ORIGINAL PAGE IS
OF POOR QUALITY

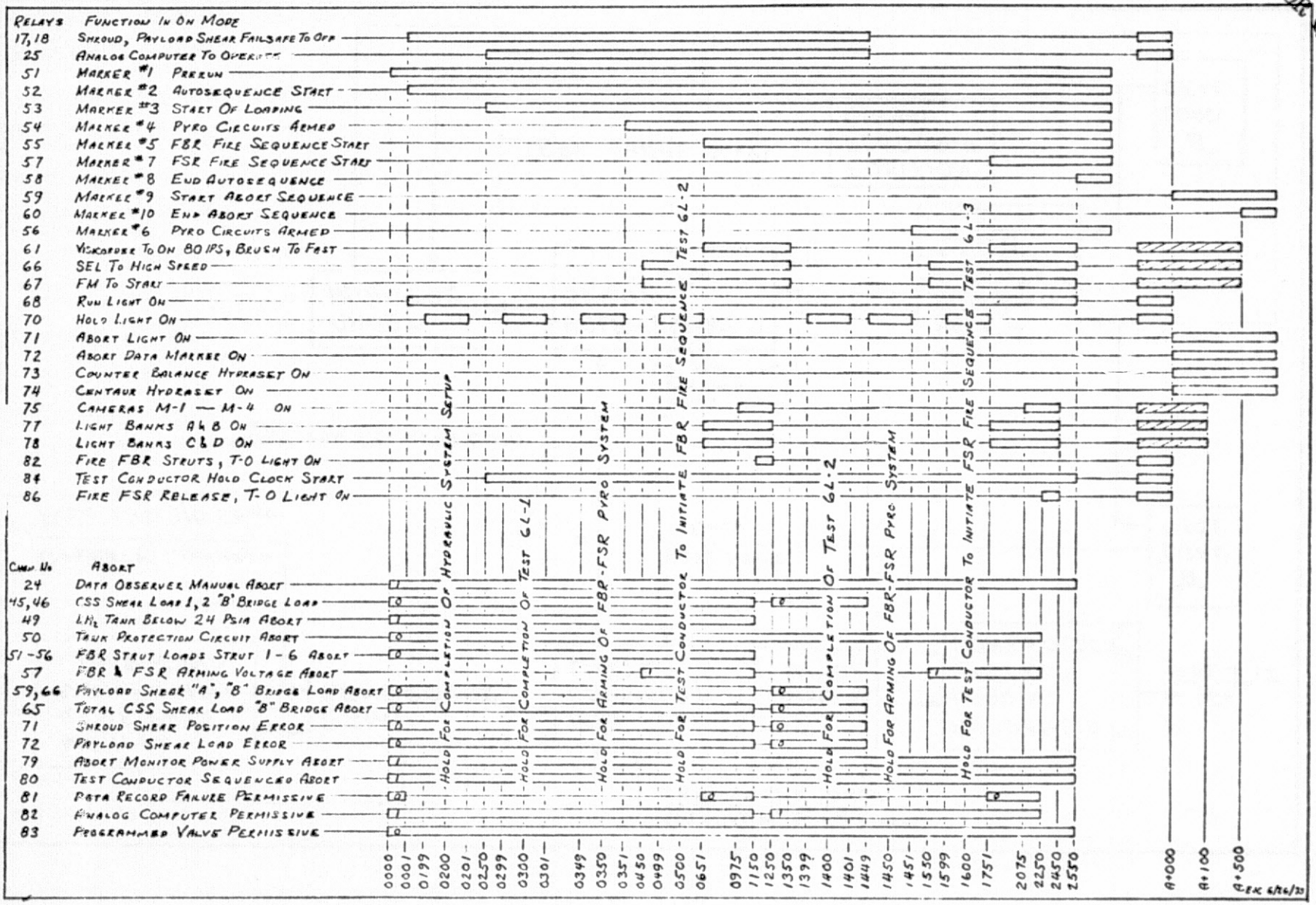

FIGURE A-9. CONTROL & ABORT SYSTEM SEQUENCE FOR TESTS 6L-1, -2, & -3.

APPENDIX B

Differences in Configuration between the Proof Flight and Test CSS

PROOF FLIGHT CSS DESIGN CHANGES NOT RETROFITTED TO TEST CSS

1. "T" section cross braces in the nose cone at Station 2867 (test CSS has angle braces).

2. Radioactive Thermionic Generator (RTG) cutout, 15" x 12" at Station 2649 to 2664, azimuth 90° (test CSS has no cutout).

3. Air conditioning door cutout at Station $2670/117^{\circ}$ - 3/8" narrower than test CSS cutout (test CSS cutout at Station $2656/131^{\circ}$).

4. 2.2" diameter encapsulation bulkhead lanyard disconnect cutouts at Station $2502/92^{\circ}$ and 54° (test CSS has no cutouts).

5. Flight vent holes - forward vents at Station 2471 and aft vents including those for the Titan skirt at Station 2221 (non-flight vent holes on the test CSS).

6. Five aft purge seal access doors, i.e., additional door at Station $2241/135^{\circ}$ (test CSS has four doors).

7. Lock bolts incorporated at the split lines, Station 2687 (test CSS has rivets).

8. Flight CSS has strengthened ring at Station 2523 and an additional ring at Station 2251.

9. Boost pump door redesigned to be solid with full length stiffeners throughout (test CSS has no door).

10. Flight CSS RTG cutout has channel stiffener on inboard surface of panel doubler.

11. Flight CSS forward and aft thermal shields have strengthened tie-down tabs.

12. FBR bearing block assembly and fitting assembly fabricated using steel (test CSS has aluminum).

13. Lock bolts at range safety command antenna splice on flight CSS (test CSS has rivets).

TEST PECULIAR FEATURES NOT ON PROOF FLIGHT CSS

1. A removable notched dome ring installed at Station 2867.

2. A removable axial load application ring installed at the transition of the 25^{o} and 15^{o} cone at Station 2806.

3. Two 3.5" diameter holes and associated doublers incorporated in the payload area at Station 2626.

4. Removable plate segments installed at three places at Stations 2732, 2753, and 2777 in the 15^{o} cone.

OTHER TEST CONFIGURATION DIFFERENCES OR CHANGES

1. The encapsulation bulkhead not installed.

2. After Test 1L-1, the FBR struts were modified to have a "softer" spring rate. New barrel assemblies (outboard) were matched with the old (inboard) cap assemblies to form struts having the same functional characteristics as the struts on the Proof Flight vehicle.

3. After Test 1L-3 the forward seal replaced with a new seal having a larger edge bead. Retract straps from the old seal installed on the new seal.

4. The T-4 panel not installed and the T-4 chute replaced with the Design Evaluation Test unit.

5. Radius blocks installed on the Centaur tank at Station 2240/219 ring.

6. The aft Titan skirt mounting ring clamped to the lower distribution cylinder rather than bolted at 12 of the 144 attachments.

7. For Test 2L-2 the hydrogen vent fin replaced with a strengthened dummy fin having load application brackets at the outboard end. Dummy fin mounted on the CSS in the same way as the flight-configuration fin.

APPENDIX C

CSS Stiffness Analysis Data

This Appendix contains the basic stiffness data used to compute the expected deflection values presented in this report. The revisions to the boattail stiffness were based upon data from Tests 3L (Revision 1) and 1L-2 (Revision II).

The original stiffness data were from the following references:

1. Kidder, R. L., Equivalent Beam Model of Centaur Standard Shroud for Dynamic Analysis. LMSC/A983875, August 18, 1971.

2. MMC, TIIID/Centaur Loads Data Book, Volume 2, Basic Data, Book 3, December 1970.

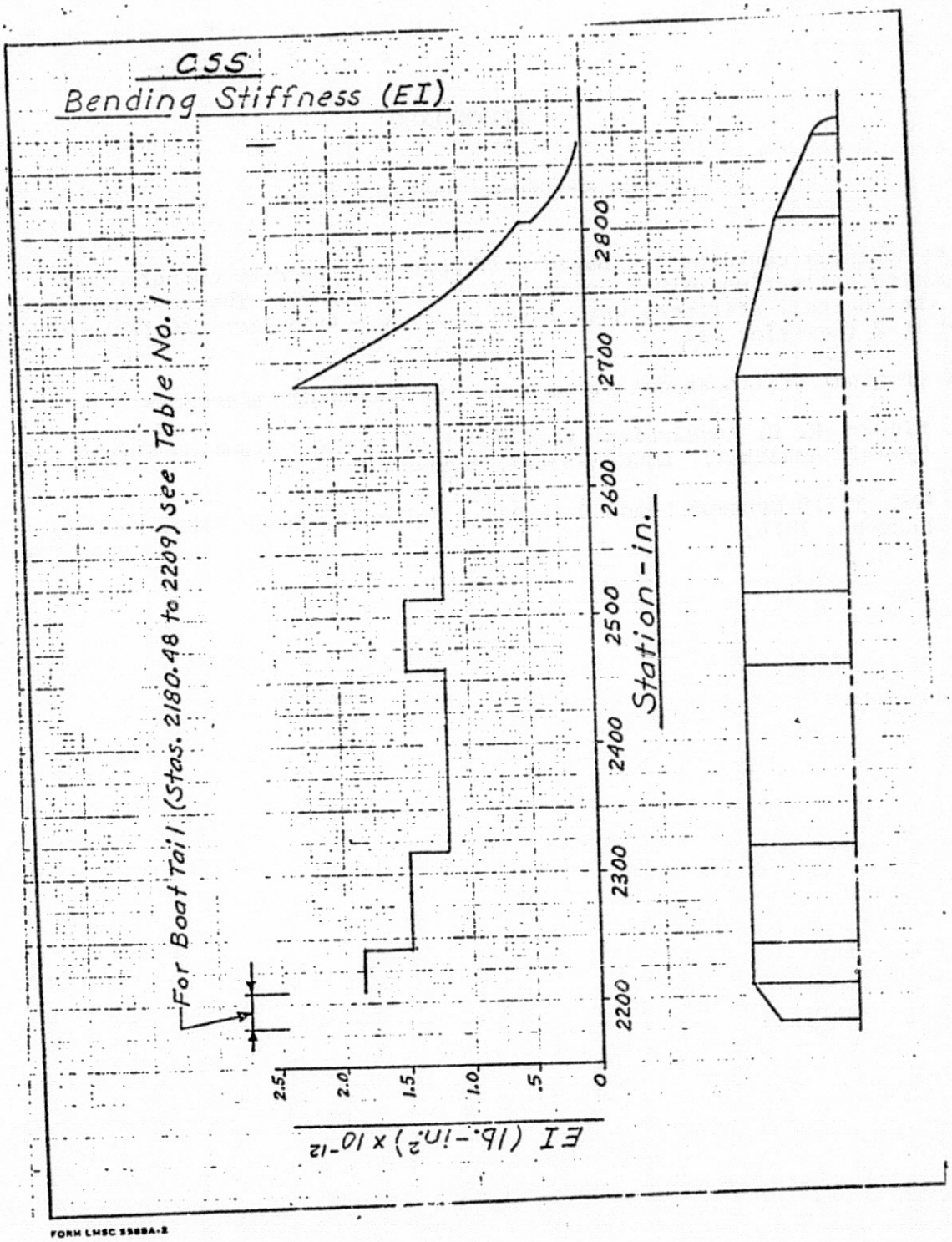

FORM LMSC 5588A-2

ORIGINAL PAGE IS
OF POOR QUALITY

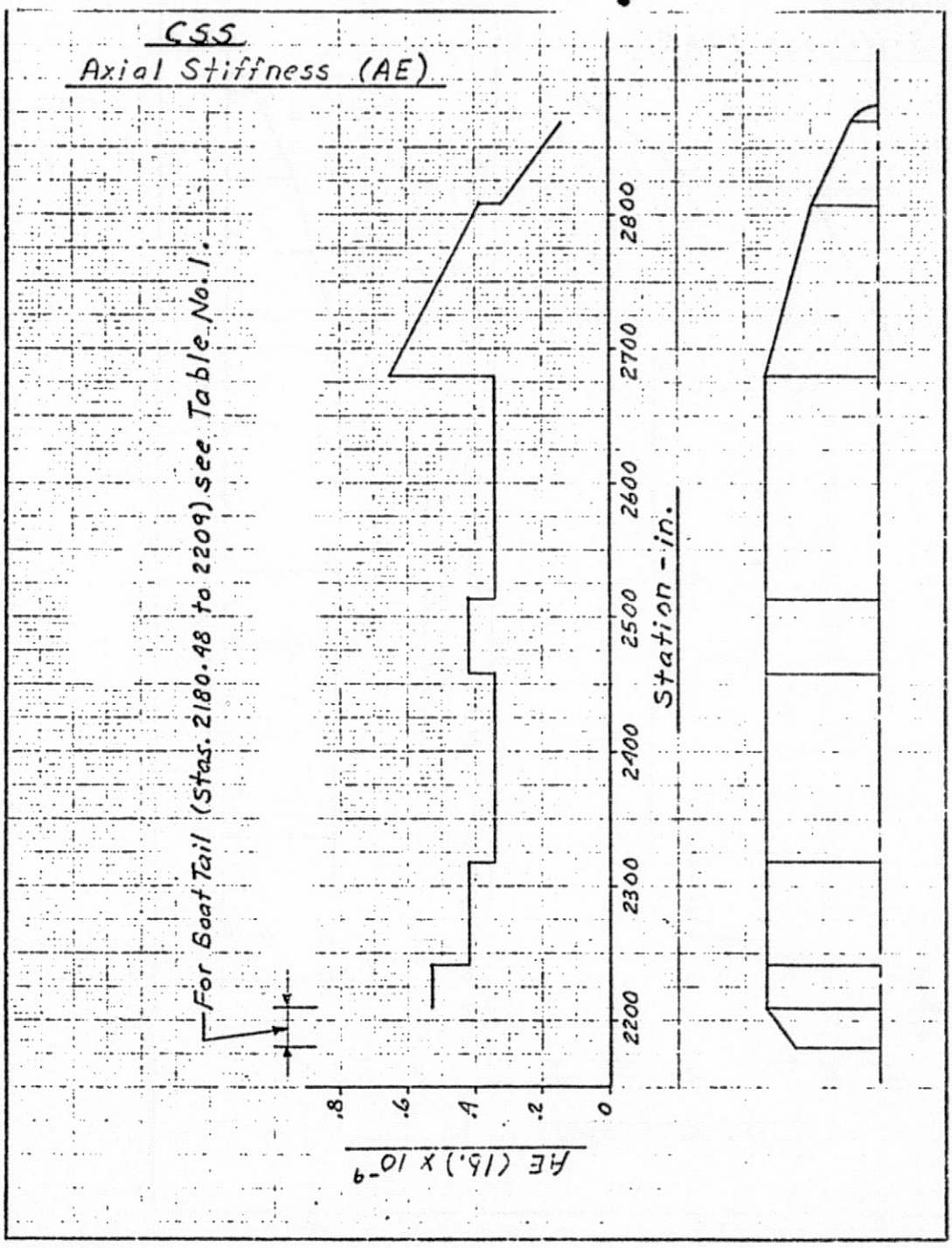

FORM LMSC 5588A-2

ORIGINAL PAGE IS
OF POOR QUALITY

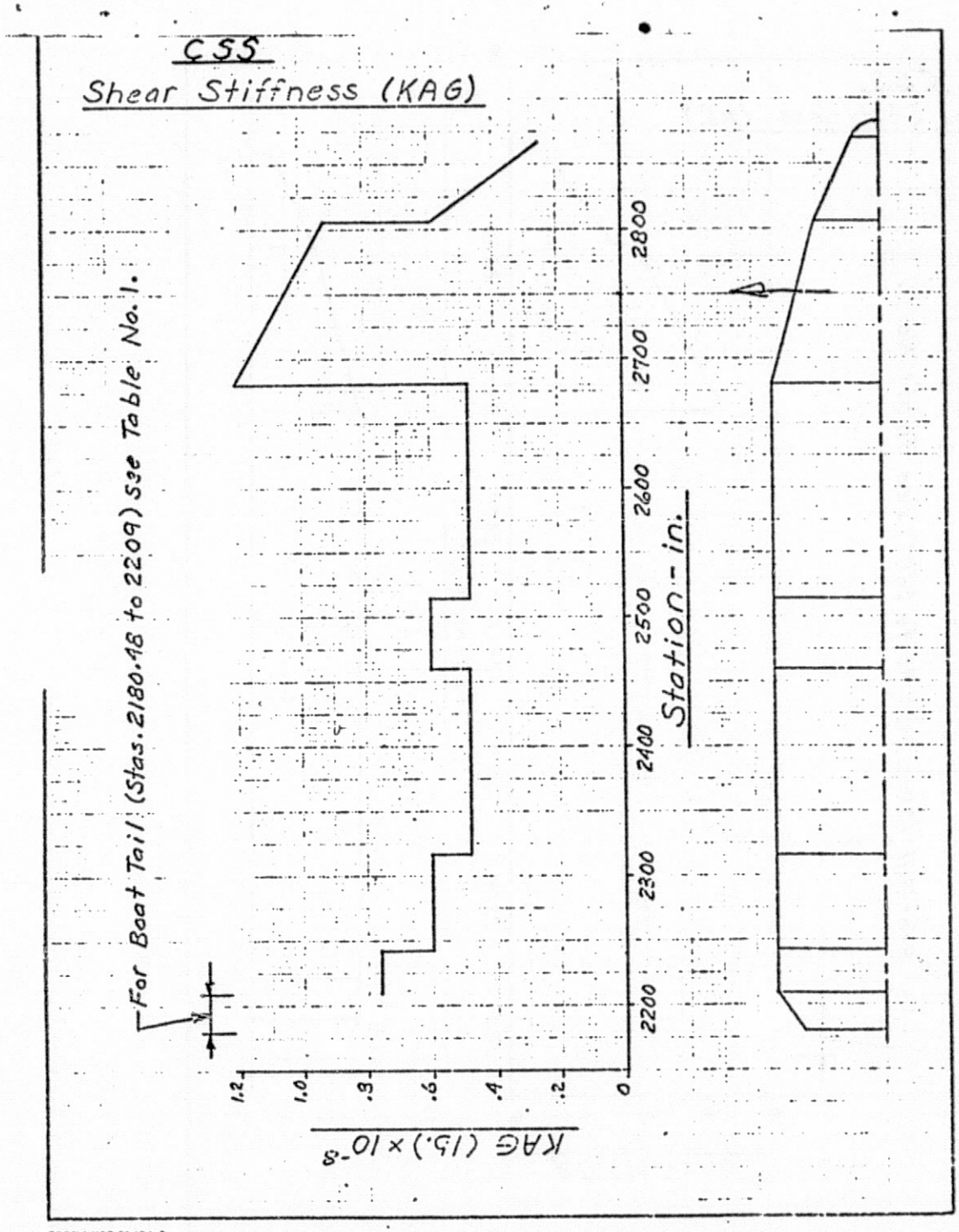

FORM LMSC 5548A-2

TABLE NO. 1

STIFFNESS MATRIX BOAT TAIL OF CENTAUR STANDARD SHROUD

①	②	③	④	⑤	⑥
2.878×10^6	0	0	-2.878×10^6	0	0
0	4.24844×10^6	-1.86830×10^8	0	-4.24844×10^6	3.08332×10^8
0	-1.86830×10^8	1.74054×10^{10}	0	~~-1.8683×10^8~~ -1.86830	-2.27486×10^{10}
-2.878×10^6	0	0	2.878×10^6	0	0
0	-4.24844×10^6	1.86830×10^8	0	4.24844×10^6	-3.08332×10^8
0	3.08332×10^8	-2.27486×10^{10}	0	-3.08332×10^8	3.15669×10^{10}

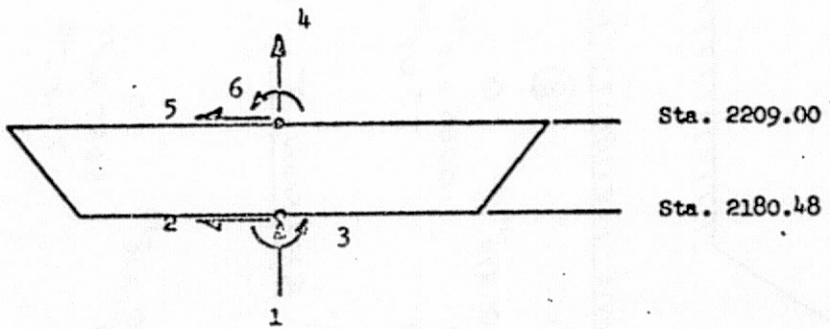

FLEXIBILITY MATRICES FOR CSS BOATTAIL

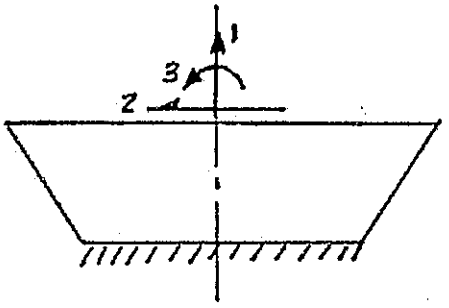

ORIGINAL FLEXIBILITY MATRIX

①	②	③
3480×10^{-10}	0	0
0	8085×10^{-10}	79×10^{-10}
0	79×10^{-10}	1.09×10^{-10}

REVISION I (Based upon Test 3L)

3480×10^{-10}	0	0
0	8085×10^{-10}	79×10^{-10}
0	79×10^{-10}	2.52×10^{-10}

REVISION II (Based upon test 1L-2)

3480×10^{-10}	0	0
0	$10,900 \times 10^{-10}$	131×10^{-10}
0	131×10^{-10}	3.21×10^{-10}

MILLIMETER
EUGENE DIETZGEN CO.

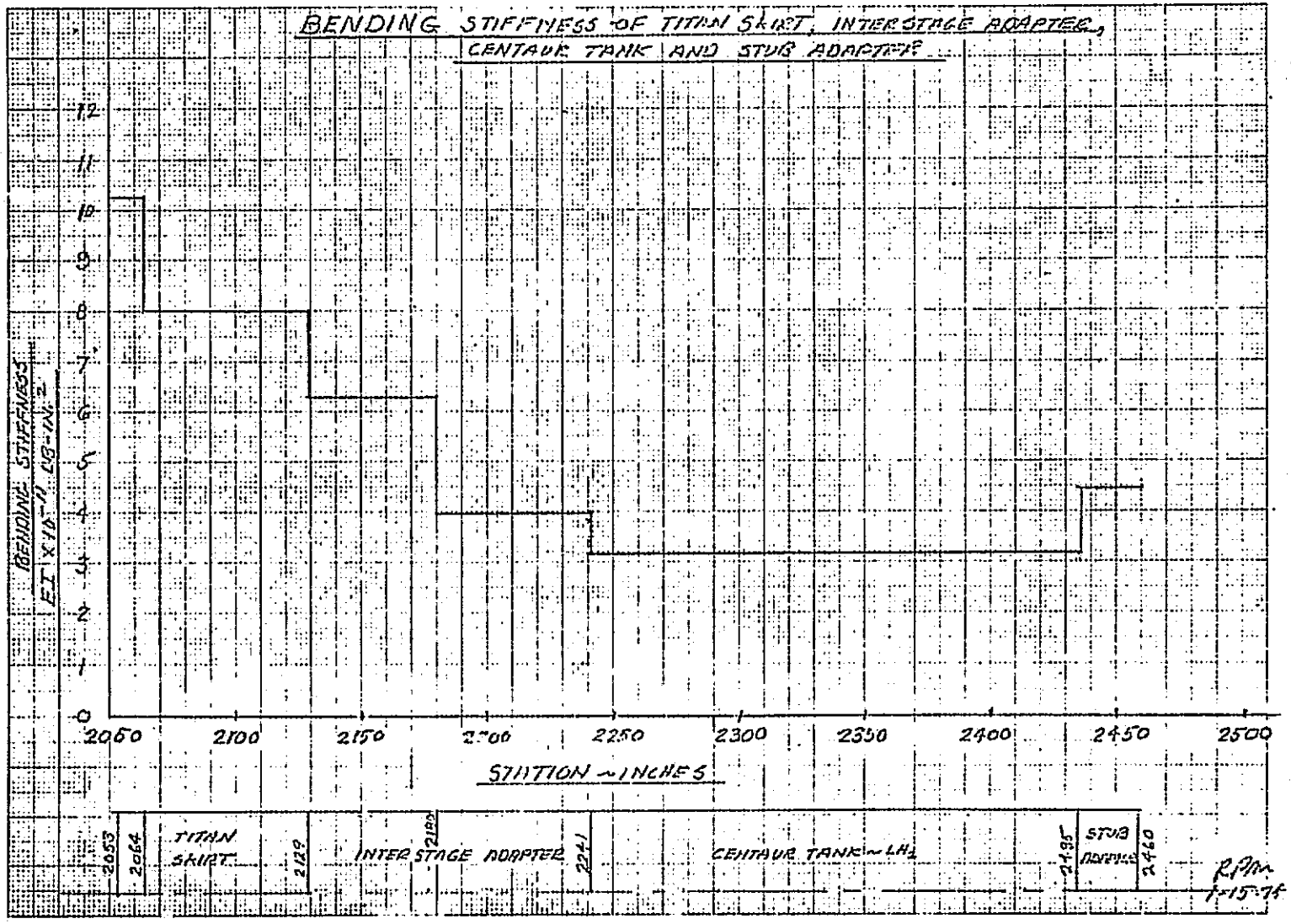

C-7

MILLIMETER

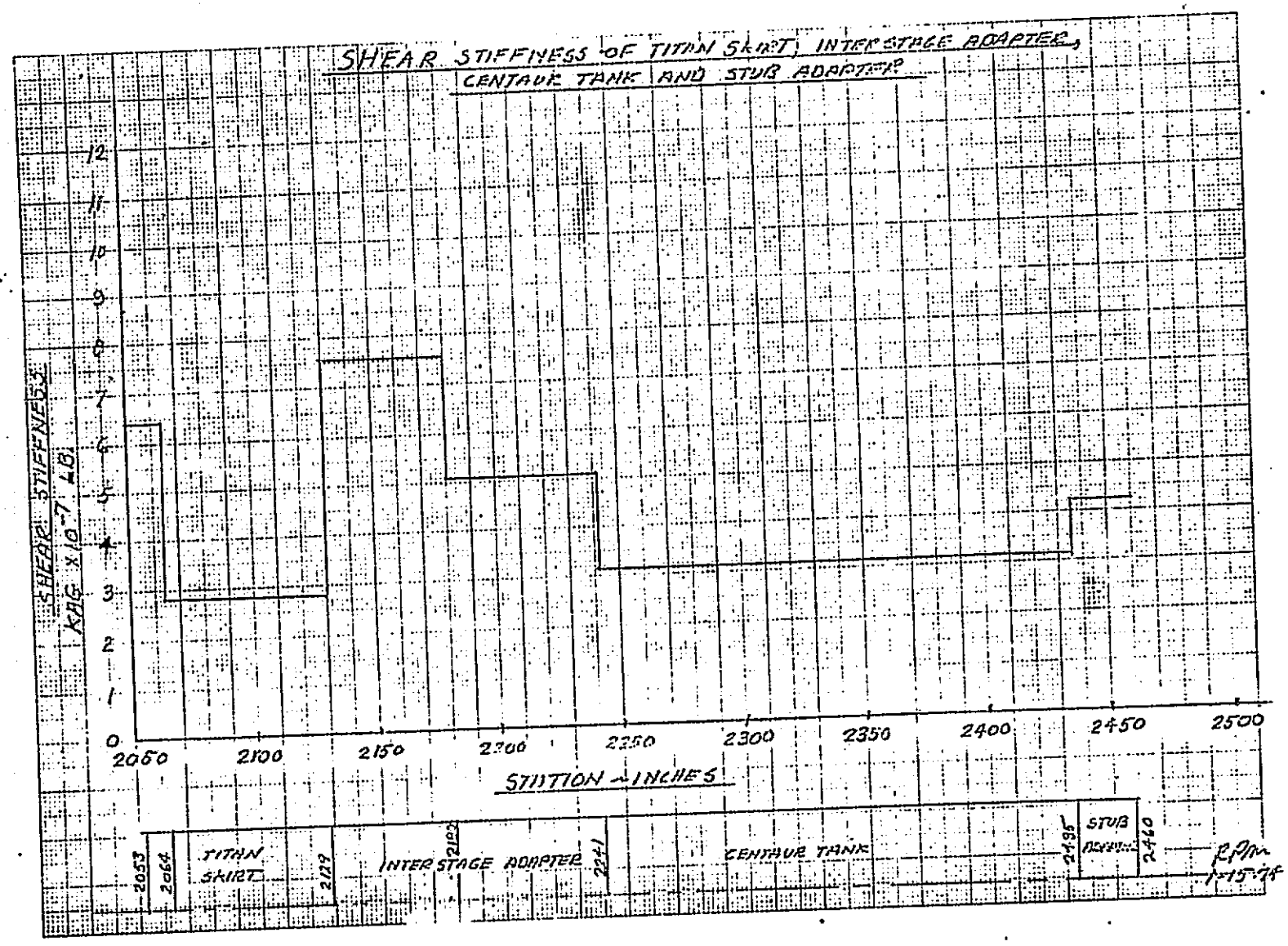

8-C

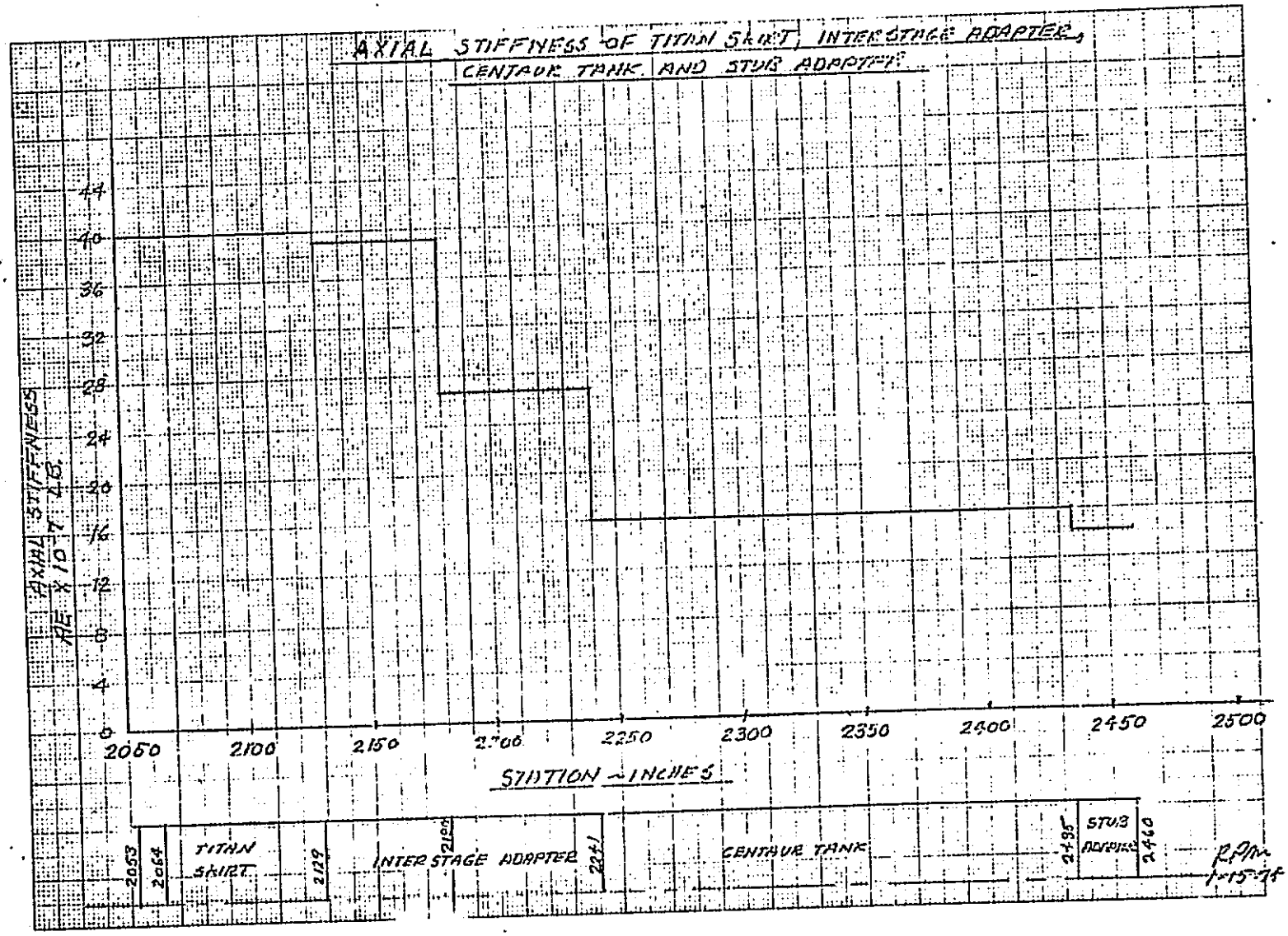
AXIAL STIFFNESS OF TITAN SKIRT, INTERSTAGE ADAPTER, CENTAUR TANK AND STUB ADAPTER
AXIAL STIFFNESS AE x 10⁻⁶ LB.
0
4
8
12
16
20
24
28
32
36
40
44
2050
2100
2150
2200
2250
2300
2350
2400
2450
2500
STATION - INCHES
2053
2064
TITAN SKIRT
2129
INTERSTAGE ADAPTER
2200
2241
CENTAUR TANK
2485
STUB ADAPTER
2460
RPM 1-15-64